Jennifer Greenhowe

Green Templeton College

Stem and Progenitor Cells in Wound Healing

D.Phil. Clinical Laboratory Sciences

Stem and Progenitor Cells in Wound Healing

Jennifer Greenhowe
Green Templeton College
D.Phil. Clinical Laboratory Sciences
Submitted Hilary Term 2014

Abstract

As more patients with large body surface area burns are surviving and requiring reconstructive surgery, there is a necessity for advances in the provision of bioengineered alternatives to autologous skin cover. The aims of this Thesis are to identify feasible source tissues of Endothelial Colony Forming Cells and Mesenchymal Stem/Stromal Cells for microvascular network formation *in vitro* with three-dimensional dermal substitute scaffolds. The working hypothesis is that pre-vascularised dermal scaffolds will result in better quality scarring when used with split thickness skin grafts.

Human umbilical cord blood, peripheral blood and adipose tissue were collected and processed with ethical approval and informed consent. Samples were cultured to form endothelial outgrowth colonies and confluent Mesenchymal Stem/Stromal Cells, which were characterised using flow cytometry and expanded *in vitro*. Mesenchymal Stem/Stromal Cell multipotency was confirmed with tri-lineage mesenchymal differentiation. Primary cells were tested in a two-dimensional tubule formation co-culture assay and differences assessed using a proangiogenic antibody array. Tubule formation was tested in four different acellular dermal substitute scaffolds; Integra® Dermal Regeneration Template, Matriderm®, Neuskin-F® and De-cellularised Human Cadaveric Dermis.

Umbilical cord blood was the most reliable source of Endothelial Colony Forming Cells, the yield of which could be predicted from placental weight. Microvasculature dissected free from adipose tissue was a reliable source of Mesenchymal Stem/Stromal Cells which supported significantly more tubule formation than Mesenchymal Stem/Stromal Cells from whole adipose tissue. Microvasculature Mesenchymal Stem/Stromal Cells secreted significantly higher levels of the proangiogenic hormone leptin, and addition of exogenous leptin to the tubule formation assay resulted in significantly increased tubule formation. Microvasculature was cultured in all four of the scaffolds tested, but depth of penetration was limited to 100µm. The artificial oxygen carrier perfluorocarbon was shown to increase two-dimensional tubule formation and may be useful in further three-dimensional scaffolds studies to improve microvascular penetration.

Declaration

The Thesis I am submitting is my own work, apart from two sections of collaborative work appropriately referenced in the text, for which I was a co-author of the resulting publications, under my maiden name, Jennifer Kean.

The collaborative work is found in the following table and figures:

- Table 3.1: Demographics of perinatal maternal, obstetric and neonatal variables.
- Figure 3.6: Correlation between placental weight and ECFC yield.

Work adapted and reproduced from Coldwell *et al.* 2011, published under the CC-BY-NC license (Coldwell KE, Lee SJ, Kean J, Khoo CP, Tsaknakis G, Smythe J, et al. Effects of obstetric factors and storage temperatures on the yield of endothelial colony forming cells from umbilical cord blood. Angiogenesis. 2011;14(3):381-92. Epub 2011/07/02.).

- Figure 6.1: Transduction efficiency and viability after GFP lentiviral transduction of UCB ECFC derived cells at different Multiplicities of Infection (MOI).
- Figure 6.2: Pre-vascularisation of Integra® and Matriderm® dermal scaffolds.
- Figure 6.3: Comparative characteristics of 3D-microvascular tubule formation on Integra® and Matriderm® using co-cultures of $2x10^4$ GFP labelled UCB ECFCs and $1x10^5$ unlabelled HDF or BM MSC.

Work prepared for and adapted from Athanassopoulos *et al.* 2012 (Athanassopoulos A, Tsaknakis G, Newey SE, Harris AL, Kean J, Tyler MP, Watt SM. Microvessel networks [corrected] pre-formed in artificial clinical grade dermal substitutes in vitro using cells from haematopoietic tissues. Burns. 2012;38(5):691-701.).

Acknowledgements

I would like to extend my thanks to Restore Burn and Wound Research for employing me as a Plastic Surgery Research Fellow and funding the work presented in this Thesis. Also, a special thank you to the patients who took part in the study, without whom this work would not have been possible. Thanks to Mrs Sandra Britt and Ms Janice Gotobed who collected the umbilical cord blood samples and the team at NHS Blood and Transplant, Liverpool for providing de-cellularised human cadaveric dermis.

Thanks to Professor Suzanne Watt and Dr Enca Martin-Rendon for supervising the project and the production of this Thesis. The many scientists, post-doctoral researchers and fellow students in the Stem Cell Research Laboratory are a credit to the department, and their advice and support on a daily basis taught me how to be a proper lab scientist and not just a surgeon with a bit of an imagination. In particular I would like to thank Dr Kate Coldwell for teaching me tissue culture techniques, Dr Lisa McRae for teaching me the ways of the flow cytometer and Dr Enca Martin-Rendon for teaching me how to safely perform viral transductions. Thanks to Dr Cheen Khoo, Dr Nita Fisher, Dr Grigorios Tsaknakis and Dr Youyi Zhang for advice regarding tubule assays. For everything else I would like to thank Mr Dominic Sweeney, who not only helped me during the three years in the lab, but was also an excellent friend and advisor after my return to clinical work when I needed data that I could not retrieve in person.

Personal thanks to my family and friends who have made it possible to spend so much time pursuing an academic career as well as a clinical one, without being disowned! My parents Valerie and David have provided years of continued personal support and encouragement; they have never let me doubt that I was making the best choices for a happy and successful life. Our family has had some difficult experiences in the past few years, but they always reassured me that we could get through.

Finally, I would like to dedicate this Thesis to my husband Mark. We met as friends just before I moved to Oxford to begin this huge undertaking and I never dreamed that a year later we would meet again and become inseparable. Even after the Incan mountains almost had you as a sacrifice and I had to look after you for a while, you were still looking after me. You are the strongest, kindest and most thoughtful person I have known and your patience and support are immeasurable. Thank you for everything- ‘best supporting husband’.

Nequiquam non propter…

List of Abbreviations

ABC	Avidin and Biotinylated horseradish peroxidase macromolecular Complex
ADAMTS 1	A Disintegrin And Metalloproteinase with ThromboSpondin motifs 1
α-SMA	alpha Smooth Muscle Actin
AT	Adipose Tissue
BM-MSC	Bone Marrow Mesenchymal Stromal Cells
ddH_2O	Double Distilled water
BSA	Bovine Serum Albumin
CAIM	Complete Adipogenic Induction Medium
CAMM	Complete Adipogenic Maintenance Medium
CCIM	Complete Chondrogenic Induction Medium
CEA	Cultured Epithelial Autografts
COIM	Complete Osteogenic Induction Medium
CXCL16	C-X-C motif Ligand 16
DAB	3,3'-diaminobenzidine
DAPI	4',6-diamidino-2-phenylindole
DHCD	De-cellularised Human Cadaveric Dermis
DIEP	Deep Inferior Epigastric artery Perforator
DMEM	Dulbecco's Modified Eagle Medium
DMSO	Dimethyl Sulfoxide
DNA	Deoxyribonucleic Acid
DPBS	Dulbecco's Phosphate Buffered Saline
DPP IV	Dipeptidyl peptidase 4
DSRed	Discosoma Red
ECFC	Endothelial Colony Forming Cell
EDTA	Ethylenediaminetetraacetic Acid
EGF	Endothelial Growth Factor
EGM-2	Endothelial Growth Medium-2
EG-VEGF	Endocrine Gland derived Vascular Endothelial Growth Factor
ELISA	Enzyme-Linked ImmunoSorbent Assays
EPC	Endothelial Progenitor Cell
FACS	Fluorescence Activated Cell Sorting
FcR	Fc Receptor
FCS	Fetal Calf Serum
FGF	Fibroblast Growth Factor
FTSG	Full Thickness Skin Graft
GAG	Glycosaminoglycans
GDNF	Glial cell Derived Neurotrophic Factor
GFP	Green Fluorescent Protein
GM-CSF	Granulocyte-Macrophage Colony-Stimulating Factor
GMP	Good Manufacturing Practice
HB-EGF	Heparin Binding Endothelial growth factor like Growth Factor
HBSS	Hank's Balanced Salt Solution
HDF	Human Dermal Fibroblasts
HEK293FT	Human Embryonic Kidney cells from the 293FT cell line
HGF	Hepatocyte Growth Factor
HLA-DR	Human Leukocyte Antigen D Related
HRP	Horse Radish Protein
HUVEC	Human Umbilical Vein Endothelial Cells
IBMX	3-isobutyl-methyl-xanthine

ICIM	Incomplete Chondrogenic Induction Medium
IGF BP	Insulin-like Growth Factor Binding Protein
IgG	Immunoglobulin G
IL	Interleukin
ISCT	International Society for Cellular Therapy
LAP(TGF-β1)	Latency Associated Peptide Transforming Growth Factor Beta 1
LB	Luria Broth
MCGS	Mesenchymal Cell Growth Supplement
MCP-1	Monocyte Chemoattractant Protein 1
MFI	Mean Fluorescence Intensity
MIP-1α	Macrophage Inflammatory Protein 1 alpha
MMP	Matrix Metalloproteinase
MNC	Mononuclear Cells
MOI	Multiplicity of Infection
MSC	Mesenchymal Stem/Stromal Cell
MSCGM	Mesenchymal Stem Cell Growth Medium
MTT	(3-(4,5-Dimethylthiazol-2-yl)-2,5-diphenyltetrazolium bromide
MV	Microvasculature
NHS	National Health Service
NHSBT	National Health Service Blood and Transplant
NRG1-β1	Neuregulin – 1 Beta 1
O.C.T.	Optimal Cutting Temperature
PB	Peripheral Blood
PBS	Phosphate Buffered Saline
PD-ECGF	Platelet Derived Endothelial Cell Growth Factor
PDGF	Platelet Derived Growth Factor
PECAM-1	Platelet/Endothelial Cell Adhesion Molecule 1
PFA	Paraformaldehyde
PFC	Perfluorocarbon
PLGA	PolyLactic co-Glycolic Acid
PlGF	Placental Growth Factor
PTPRC	Protein Tyrosine Phosphatase Receptor type C
REC	Research Ethics Committee
SCRL	Stem Cell Research Laboratory
SEM	Standard Error of the Mean
S.O.C.	Super Optimal Broth with Catabolite repression
SSG	Split thickness skin graft
SVF	Stromal Vascular Fraction
TGFβ	Transforming Growth Factor Beta
TIE2	Tyrosine kinase with Immunoglobulin and EGF homology domains 2
TIMP	Tissue Inhibitor of Metalloproteinase
Tris-HCl	Tris(hydroxymethyl)aminomethane-hydrochloride
TU	Transducing Units
UCB	Umbilical Cord Blood
uPA	Urokinase-type Plasminogen Activator
UV	Ultraviolet
VEGF	Vascular Endothelial Growth Factor
VEGFR2	Vascular Endothelial Growth Factor Receptor 2
WBC	White Blood Cell

Table of Contents

List of Figures

List of Tables

Chapter 1 Introduction

One of the greatest challenges for plastic and reconstructive surgeons is the provision of autologous skin cover in large body surface area burns. A large systematic review of burns aetiology and mortality in Europe by Brusselaers *et al.* showed a clear reduction in burns mortality over the past two decades (1), which means more large body surface area burns patients are surviving and requiring reconstructive surgery. Burn wound excision and replacement skin cover must be achieved as soon as possible in order to restore the physiological functions of the skin which include fluid balance, electrolyte homeostasis, thermal regulation and bacterial defence (2). The current gold standard treatment of full thickness burns is early tangential excision of the burn wound and reconstruction with split thickness skin grafting (3-5), and it is obvious that the larger the burn wound, the more scarce the remaining undamaged area of skin from which to harvest autologous skin grafts. Thus there is a necessity for advances in the provision of alternative skin cover (5-7).

A second group of patients which may benefit from advanced skin cover alternatives are those with large chronic wounds, refractory to conservative management (7). In a similar fashion to burns patient survival, the incidence of chronic wounds is also increasing in the UK, mainly due to improvements in the management of medical co-morbidities and an ageing population (8, 9). Faster healing of chronic wounds is not only beneficial for patients due to reduced morbidity, but also for the National Health Service as continued wound care provision is costly in both consumables and staff hours (8-10).

1.1 Wound healing and scarring

Cutaneous wounds can vary from a superficial scratch in the epidermis to large, deep defects with loss of various tissue layers (11). Burn wounds can be classified as superficial, superficial dermal, deep dermal or full thickness depending on the depth of the burn injury through the dermis (12). Regardless of wound severity, the purpose of the healing process in cutaneous wounds is to maintain homeostasis by restoring the structure and function of the skin (2). Ideally, healthy tissue architecture would be restored by regeneration of the constituent cells, but this is rarely possible in full thickness human wounds (13, 14). Where repair by regeneration is not possible, such as in full thickness burns or deep chronic wounds involving all layers of the skin, the wound healing process allows for repair by replacement with scar tissue (15).

1.1.1 Full thickness cutaneous wounds

Full thickness cutaneous wound healing is a complex process with many interacting and overlapping stages of cellular activity (16), the main phases of which have been widely accepted as haemostasis, inflammation, proliferation and remodelling (11). In the proliferative phase there is production of granulation tissue, extracellular matrix, new microvascular networks and finally an outer layer of keratinocytes to form the new epidermis (17). As the healing wound remodels, there is a decrease in cellularity and vascularity and an increase in tensile strength, eventually resulting in a stable scar (13).

The main stages of normal wound healing are outlined in Figure 1.1.

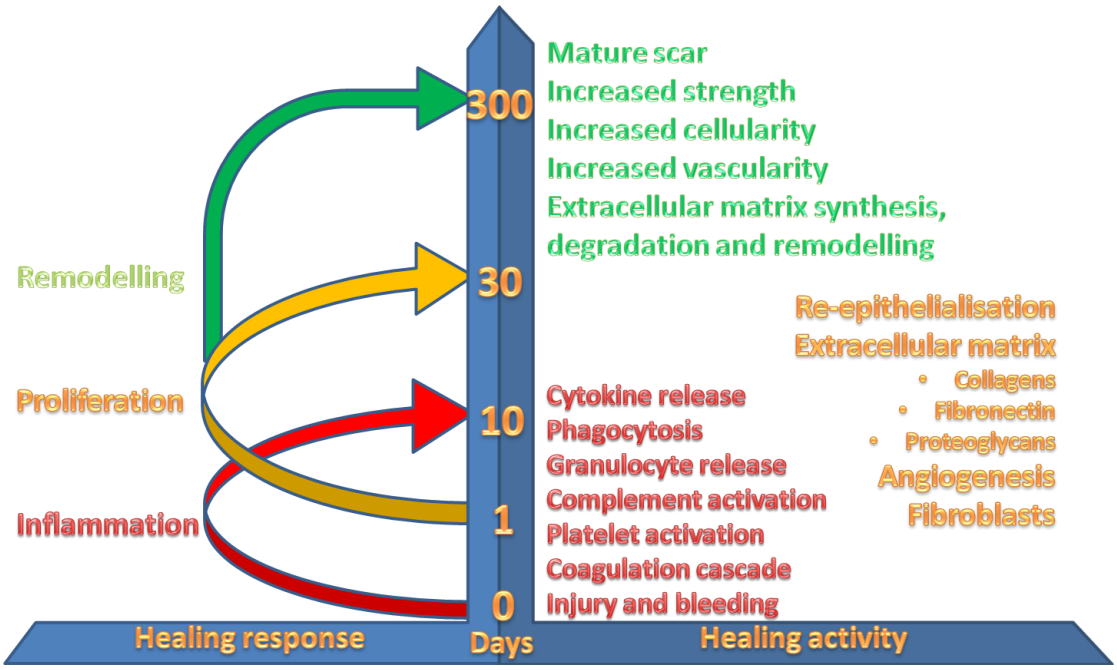

Figure 1.1: Phases of normal wound healing. The inflammatory phase begins at the time of injury and bleeding and continues until around day 10. Proliferation begins at around 24 hours and will continue for around 30 days. During the proliferative phase fibroblasts migrate to the wound, the extracellular matrix is formed and angiogenesis takes place. The remodelling phase begins around day 20 and will continue for almost a year, eventually forming a mature, stable scar with gradually increased strength and improved appearance.

1.1.2 Cutaneous scarring

Scarring is the permanent and unavoidable end-point of full thickness wound healing (18, 19). The quality of scarring can be influenced by many aspects such as underlying pathology, patient co-morbidities, type of wound healing, and, in the case of surgical wounds, operative technique and tissue handling (20, 21). As well as psychological distress due to aesthetic considerations, poor scarring can cause functional problems and physical symptoms (18, 22, 23). Scar contractures can limit the functional range of movement in the affected area and are common in burns scars where wounds have healed by secondary intention (24-26). They are also more common in split thickness skin grafting than full thickness skin grafts or healing by primary intention (27). Hypertrophic or keloid scars result from excess fibroproliferation and form thick, raised scars (28) which have been shown to have excess microvasculature that is disorganised and often occluded (29).

1.2 Burn wound pathophysiology

The acute burn wound results in both cutaneous thermal injury and a systemic inflammatory response (30). The cutaneous wound may extend within the first few days from the central coagulation zone with definite ischaemia and devitalised tissue, through a zone of stasis which may be re-perfused with optimal medical management. A final peripheral zone of hyperaemia displays an inflammatory response without any structural damage to the tissue (31). The zone of stasis can only be saved if revascularisation is achieved in the first few days (30).

Significant burn injury results in systemic effects on multiple organ systems, in part due to release of inflammatory mediators and cytokines (30). Intravascular hypovolaemia can result in poor organ perfusion, therefore adequate fluid resuscitation and avoidance of anaemia are key to acute management (32).

1.3 Skin grafting and skin substitutes

The gold standard treatment of full thickness burn wounds is early tangential excision of the burn tissue and cover of the resulting deficit with autologous split thickness skin grafting (4). However, in patients where the wound is so large that there is not enough undamaged skin from which to harvest autologous split thickness skin grafts, alternative cover must be provided in order to maintain normal skin physiology (33).

1.3.1 Split thickness and full thickness skin grafting

Split thickness skin grafts (SSG) are harvested from areas of undamaged skin (5). Variable depths of SSG can be harvested, with different clinical properties depending on the amount of dermis taken in the graft and left in situ at the donor site (27). The thicker the graft the better the cosmetic result and the lower the risk of scar contracture at the recipient wound bed, but

the slower the donor site healing and greater risk of donor site scar formation (34). Donor sites heal by re-epithelialisation from epidermal remnants within hair follicles and from the wound edges. Grafts can be harvested from most anatomical sites, and once healed can be re-used to harvest further SSG (27, 34).

Full thickness skin grafts (FTSG) are excised with the full structure of epidermis and dermis intact (34). Full thickness donor sites are closed directly and heal by primary intention. Although FTSG have better cosmetic properties, their availability is limited since they must be harvested from an area of skin laxity where a linear scar is unobtrusive, and once harvested the area can usually not be re-used (5, 27, 34-36).

1.3.2 Skin graft vascularisation

Skin grafts heal by a process of fibrin adhesion to the wound bed, plasmatic imbibition of nutrients from the wound bed, inosculation of vessels in the wound bed and the graft, and neovascularisation across the wound bed into the graft (34). During vessel inosculation, remnants of vasculature within the graft align with vasculature in the wound bed (37), allowing perfusion of graft vasculature within 48 hours (38). As the graft matures the vessels re-organise into a functional network, but areas of unfavourable hypertrophic or keloid scarring have been shown to contain a disorganised vascular network entangled around dense bundles of fibroblasts (19, 28). In addition to the re-organisation of the existing vessels, new vessels sprout from the wound bed and become the primary vascular supply of the graft tissue, replacing original graft pericytes (39).

Full thickness skin grafts contain the full extent of the dermis, including the existing dermal vasculature, and have consistently better quality scarring than split thickness skin grafting (34, 35). Whereas split thickness grafts scar throughout the entire surface of the graft, full

thickness grafts tend to have a linear scar around the periphery of the graft, whilst the central graft remains soft and pliable as it was at the donor site (35).

Where dermal substitutes are used, there is no inherent graft microvasculature and the wound bed granulation tissue must proliferate through the scaffold to provide a neo-vascularised surface for later split skin graft take (40, 41). We theorise that, by pre-vascularising the dermal scaffold, we could provide a more organised dermal microvascular network, with less need for remodelling and better quality resultant scarring.

1.3.3 Alternative skin cover

A variety of alternatives to autologous split thickness skin grafting already exist, but as yet none offer permanent, functional replacement skin with acceptable levels of scarring (42). In cases of large burn wounds, the properties of even temporary replacement skin or dressings are highly important (43). A fully physiological man made skin alternative does not yet exist, though modern dressings or cadaveric donor skin allografting can offer temporary management of the wound, and dermal substitutes can be combined with autologous skin grafts either at initial surgery or in a two-step procedure when donor sites have healed and can be re-used (33, 43-45).

Cultured Epithelial Autografts (CEA) were developed in the 1970s and first reported in 1981 as an alternative skin cover option in the absence of sufficient area donor skin (46). A small skin biopsy is harvested and either processed to obtain a cellular solution of single keratinocytes which can be sprayed over the wound bed, or which can be cultured for up to four weeks in the laboratory to form confluent sheets of cultured epithelium (47). Although CEA are a useful life-saving measure to achieve wound coverage (47), the lack of dermal structure means that cosmesis and functional stability are poor and infection rates are high (48). A review of the outcomes of patients managed with CEA for large burns over an 18 year period in Indiana

found that 66% of these patients developed wound contractures, almost half of whom required further reconstruction (49). Revision surgery is commonly required to replace the delicate and friable resulting grafts or release scar contractures (46-49).

Dermal substitutes based on collagen networks such as Integra® and Matriderm® have been shown to improve scar quality in two staged procedures which allow initial vascularisation of the dermal substitute prior to application of split thickness skin grafts (50-52). By providing a pre-vascularised dermal scaffold to the wound bed we predict an improvement in scar quality similar to full thickness skin graft results which can be achieved in a single operative procedure without the donor site limitations experienced with full thickness skin grafting (35, 53).

The working hypothesis underlying this research is that clinical application of a skin substitute with a pre-formed vascular network plus split thickness skin grafting may result in improved scarring compared with split thickness skin grafting alone or on top of non-vascularised dermal substitute.

1.4 Cells involved in vessel formation

1.4.1 Endothelial cells

Endothelial cells form the internal luminal layer of every blood and lymphatic vessel in the human circulatory system (54). During embryonic development the vasculature forms from the mesoderm and this primitive organ system provides oxygen and nutrients to the developing foetus. The vasculature later remodels and specialises into arteries, veins and capillaries, with different subsets of endothelial cells differentiating from endothelial stem and progenitor cells (54). In the post-natal circulatory system, numbers of freely circulating mature endothelial cells increase with age and are considered a marker of vascular injury (55). However, endothelial progenitor cells capable of repairing and expanding the existing vasculature are released from

bone marrow or other peripheral vascular niches in response to trauma or ischaemia, and may also be found in circulation (56-58). This concept is illustrated in Figure 1.2.

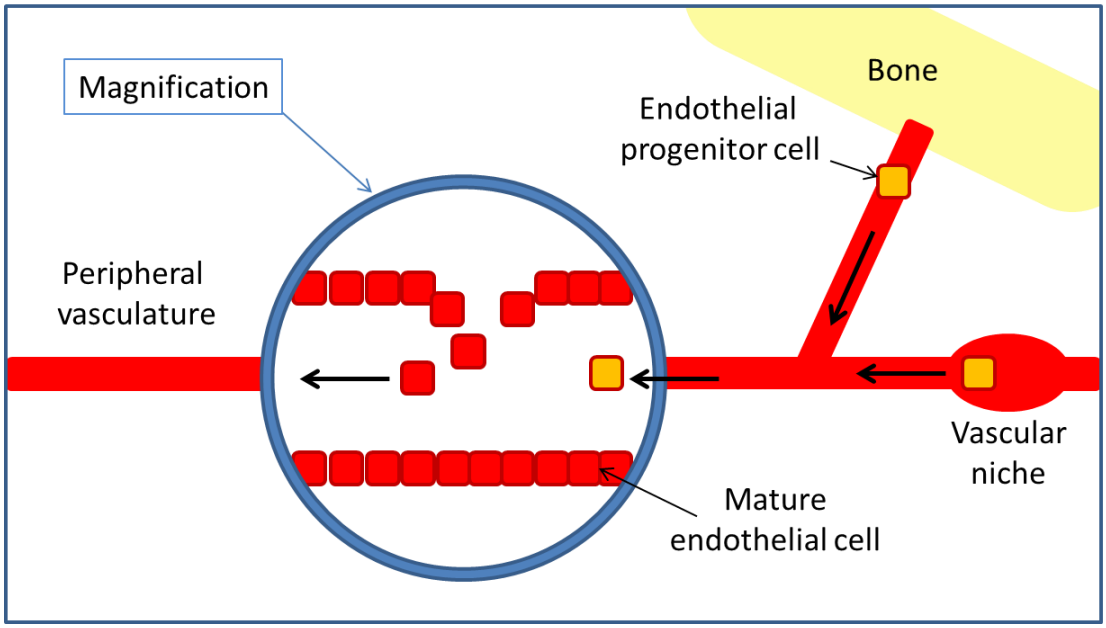

Figure 1.2: Schematic representation of the source of mature endothelial cells and endothelial progenitor cells in peripheral vasculature. Mature endothelial cells line the entirety of the post-natal vascular system. These cells may be disrupted due to minor injury and are released into circulating peripheral blood. Endothelial progenitor cells are released from bone marrow and peripheral vascular niches in response to vascular injury. These cells home to the site of injury in order to repair damage by the process of vasculogenesis.

The post-natal vascular system is in frequent need of repair from minor internal injury and expansion to accommodate growth, and this is achieved by three main physiological processes of neovascularisation (59). Vasculogenesis is the process whereby vascular networks are created by progenitor cell migration, differentiation and coalescence, in contrast to angiogenesis in which existing vasculature sprouts and remodels new vascular buds, or arteriogenesis in which existing blood vessels remodel to change flow rates (59-61). Excess neovascularisation may occur in disease states such as neoplasia, arthritis and diabetic retinopathy (62, 63) whereas insufficient neovascularisation or vascular repair may result in cardiovascular disease or impaired wound healing (58, 59, 64).

Much controversy exists over the classification of endothelial cells and their precursors or progenitors (65-69), but it is necessary to identify cells with the potential for vasculogenesis in order to harvest and expand them for clinical use (59). The term 'endothelial progenitor cell' (EPC) is now considered to describe a group of different cells from the haematopoietic lineage, and the term has been discontinued due to lack of clarity (67). As such, cell surface markers found on endothelial cell subsets are not unique to EPCs (65-70). Estes *et al.* used polychromatic flow cytometry to define the population of cells with the greatest vasculogenic potential as $CD45^{dim}$, $CD31^{+}$, $CD34^{+}$ and with variable expression of AC133 (70), but these markers may also be found on various leucocytes, platelets and haematopoietic stem cells (71-75). Mund *et al.* further defined the phenotype of the EPCs most likely to form vasculature with the addition of $CD146^{+}$ cell surface marker (76). CD146 alone is not specific for endothelial cells as it is an endothelial cell to cell adhesion molecule which is also present on activated T cells (77, 78), but it may be considered in combination with the rest of the phenotype to improve characterisation (76). The simplest measure of the vasculogenic potential of endothelial cells is the ability to form endothelial colonies in culture, and thus cells with vasculogenic potential cultured in this manner are referred to as endothelial colony forming cell (ECFC) derived cells (59, 76).

1.4.2 Mesenchymal cells

Endothelial cells require a mesenchymal stem or stromal cell (MSC) source to support the formation of vasculature (79). In addition to formation of the vascular system, embryonic mesoderm is the source of other mesenchymal tissues which differentiate and mature into the connective tissue and internal architecture of the human body (80). As such, several sources of human MSC harvest have been described including bone marrow (81-86), skin (87, 88), skeletal muscle (89-92) and adipose tissue (93-98). The basic requirements for characterising MSC are

adherence to plastic, consistent minimum phenotyping ($CD73^+$, $CD90^+$, $CD105^+$, $CD14^-$, $CD34^-$ and $CD45^-$) and the ability to differentiate into three different mesenchymal lineages; adipose, cartilage and bone (82, 95, 98-102).

In human skin the dominant differentiated mesenchymal cells are dermal fibroblasts, which are mature, spindle-shaped stromal cells (95, 103). In considering a suitable MSC source to harvest and expand for clinical use in patients with large burn injuries, it is clear that autologous dermal fibroblasts may be in short supply and other sources should be considered.

1.4.3 Autologous cell sources

Endothelial and mesenchymal cells can be harvested from a number of potential autologous tissues (81-98, 104-108). The proposed recipient patients of pre-vascularised dermal substitutes may be those suffering from acute, severe burn injuries, and this limits the autologous tissues which may be available for harvest and *in vitro* culture. For example, many patients with large body surface area burns require blood transfusions due to blood loss and fluid compartment shift, making venesection of large volumes of peripheral blood impractical (109, 110). However, previous work in our research laboratory suggested that there was a peak concentration of proangiogenic cells in peripheral blood at 24 hours post burn injury, as these cells are mobilised from bone marrow (56), and it remains unclear if appropriate timing of venesection may allow culture of endothelial cells from a relatively small volume of peripheral blood.

As these severe burn patients mount a systemic response to their injuries by mobilising cells from bone marrow (32), this too may be an unacceptable source tissue to harvest. Additionally, undamaged skin may be in short supply, thus obtaining skin biopsies to culture dermal fibroblasts as an autologous stromal cell source is also unlikely to be feasible, although in mixed thickness burns there may be areas of healthy dermis which could be harvested.

Adipose tissue is a well-established source of mesenchymal stromal cells, and some recent work has also shown that endothelial cells may be cultured from the same source (111).

Even in patients with acute, large body surface area burns there should be an availability of adipose tissue which could be harvested without difficulty from directly underneath the burn eschar or by minimally invasive liposuction at an undamaged anatomical site. This could be harvested under general anaesthesia at the first burn wound debridement in the operating theatre, which should be performed within 24 to 48 hours of injury(3).

Adipose tissue is a mesenchymal derivative and is again a clinical feasible potential source of autologous supportive stromal cells for microvasculature formation. Recently, Natesan *et al.* demonstrated that subcutaneous tissue debrided along with burned skin was capable of yielding up to $2.5x10^5$ cells per millilitre of tissue in culture, including a population of viable stem cells (112). Adipose tissue derived stem cells have been described by several authors and many potential clinical uses are currently being investigated, including enhancing tendon and nerve repair and improving perfusion in ischaemic limbs and traumatic brain injury (97, 113-118).

Within current plastic surgery practice, fat transfer is an established technique whereby adipose tissue aspirated from a suitable donor site using liposuction is then re-injected at other anatomical sites (119-122). The technique was standardised by Coleman who showed optimal yield of viable adipocytes by manual liposuction with a large bore cannula and syringe, followed by a short period of centrifugation (120). Pu *et al.* demonstrated a statistically significant difference in viable adipocyte yield when using the Coleman technique compared with traditional mechanically assisted liposuction to harvest lipoaspirate (123). Recently the fat transfer procedure has been improved by introducing a closed system of adipose digestion and separation for use intra-operatively in order to boost the ratio of adipose derived MSCs within the re-injected solution. Results have shown better survival of free fat transfers which are

boosted with additional cells from the stromal vascular fraction, and so there is already a clinical precedence for autologous use of these cells *in vivo* (118, 124-129).

1.4.4 Allogeneic cell sources

Where it is not feasible to use autologous cell sources, allogeneic cells may be utilised. Allogeneic cells must be typed and matched to the patient to minimise the risks of rejection (130-132), and despite thorough screening there is still a risk of transmission of infection from donor to patient (133, 134). These risks are mostly eliminated with the use of autologous cells, although there is such a risk of infection if cells are cultured prior to transplant.

1.5 *In vitro* vasculogenesis

Co-culture of endothelial and stromal cells at an appropriate ratio results in microvascular tubule formation *in vitro* (135). This is most representative of *in vivo* vasculogenesis, which recruits new endothelial and stromal cells from the vascular or bone marrow niche for neovascularisation (61, 136). New microvasculature cultured in this manner has been shown to have a functional lumen (137) which is important for future clinical applications of this research.

Whilst supportive stromal cells are relatively abundant and easily obtained from many human tissue sources such as skin, blood, bone marrow and adipose tissue (138), human adult ECFC derived cells are less readily available (139). In order to produce a pre-vascularised skin substitute which is feasible for clinical use, the endothelial and stromal cells used in co-culture should be human and preferably autologous to avoid immune reactions (131). Feasible sources of autologous ECFC derived cells require sufficient proliferative potential for *in vitro* expansion

and stromal cell sources must be capable of supporting microvascular network formation (140).

1.5.1 Proangiogenic factors

In vitro vasculogenesis requires cells to be cultured in an appropriate combination of pro-angiogenic factors. Proangiogenic factors are not only supplied to the co-cultures via growth media, but are also expressed by the endothelial and stromal cells (59, 141, 142). Different sources of endothelial and stromal cells may therefore provide different proangiogenic factors for vasculogenesis, and it may be possible to directly provide further exogenous proangiogenic factors to optimise *in vitro* vasculogenesis. The sequence of angiogenic factor signalling is best understood in angiogenesis where Vascular Endothelial Growth Factor (VEGF), Fibroblast Growth Factor (FGF) and angiopoietin-2 are the main triggers for the sprouting of new blood vessels (143). VEGF also leads migration and proliferation of endothelial cells, then maturation of the vessels and their lumens is led by Transforming Growth Factor beta (TGF-β), Platelet Derived Growth Factor B (PDGF-B), Ephrin-B2 and NOTCH signalling (143). Recent trials of topical proangiogenic growth factors have showed potential to improve angiogenesis and chronic wound healing *in vivo* (144-149), and this may support our proposed application of pre-vascularised dermal substitutes.

1.6 Three dimensional vascularisation

In order to produce a pre-vascularised dermal substitute with properties similar to a full thickness skin graft, it would be necessary for the vasculature to grow in three dimensions to populate the depth of the dermal scaffold (34). Vessels should cross from one side of the scaffold to the other in order to provide vessel ends for inosculation (37) with both the wound bed inferiorly and the split thickness skin graft superiorly.

1.6.1 Scaffolds

Dermal substitute scaffolds have different mechanical and biological properties and can broadly be classified as natural biological scaffolds, biological constructs or synthetic constructs (7). For the purpose of *in vitro* vascularisation prior to proposed clinical use in burn wound cover, scaffolds considered for use in this Thesis had to be non-immunogenic, capable of *in vivo* absorption or integration, and mechanically able to withstand culture and transfer from plates to the wound bed. Four different scaffolds were chosen for use in this Thesis; Integra® Dermal Regeneration Template (Integra LifeSciences Corporation, Plainsboro, NJ, U.S.A.) and Matriderm® (Eurosurgical Ltd., Guildford, UK) which are currently used in reconstructive procedures in the UK (150), and Neuskin-F® (Medira Ltd., Sandy, UK) and De-cellularised Human Cadaveric Dermis (DHCD, NHS Blood and Transplant, Liverpool, UK) which are two scaffolds not yet in established clinical use but which meet the criteria outlined above.

1.6.1.1 Integra® Dermal Regeneration Template

Integra® is a biological construct of bovine cross-linked collagen and shark glycosaminoglycans (GAG) with pores of 70-200µm designed to allow migration of cells from the wound bed (151). Cross-links and GAGs provide mechanical structure to the scaffold without antigens (42), but the structure is not comparable with human dermis (42, 152). When used clinically, there is an outer silicone layer which acts as a barrier to organisms, fluid and electrolytes whilst the collagen scaffold fills with granulation tissue from the wound bed (152), which may take up to three weeks (153). This silicone layer is removed prior to split skin graft (SSG) application as a secondary procedure (152). Integra® is the most commonly used dermal substitute in the UK (150) and many small clinical trials have shown an improvement in scar quality with two stage use of Integra® and SSG compared with SSG alone (50-52, 154, 155).

1.6.1.2 Matriderm®

Matriderm® is a biological construct of bovine collagen types I, III and V, and bovine elastin fibres (156). Early investigation of the effect of bovine collagen and elastin matrices with SSG in a porcine wound model by Lamme *et al*. showed improved angiogenesis and faster wound healing than with SSG alone (157). It may be the faster vascularisation of the collagen and elastin scaffold which has allowed clinicians to use Matriderm® and SSG in single stage reconstructive procedures with reliable, if delayed, graft take (158-162). However, Matriderm® is available in different thickness sheets and direct comparison of 2mm Matriderm® with similar depth Integra® in an animal *in vivo* wound model with immune-incompetent neonatal rats showed no difference in neovascularisation or subsequent take of SSG (163). A more recent study by Bottcher-Haberzeth *et al.* using a rat wounding model to compare 1mm Matriderm® and a new thinner 1.3mm product called Integra® Single Layer found no difference between the matrices when used in a single stage procedure with SSG (158). Case series of single stage Matriderm® and SSG reconstructive procedures have shown good results with regard to scar stability, pliability and function (159-162), but no control trials exist to compare results with SSG alone.

1.6.1.3 Neuskin-F®

Neuskin-F® (Medira Ltd., Sandy, UK) is a biological construct of intact type I piscine collagen (164). It was selected for use in this Thesis because it is thinner than the Integra® and Matriderm® scaffolds, but still maintains stability in culture. No peer-reviewed literature exists on this scaffold as it is not yet in clinical use; however, Lin *et al*. have reported successful *in vitro* corneal regeneration on a similar, thin fish scale collagen scaffold (165) and Neuskin-F® has been shown to be fully biodegradeable and biocompatible (164). Shiratsuchi *et al.* have shown that piscine elastin peptides enhance human fibroblast migration and proliferation

(166), but such effects with piscine collagen have not been documented. Type I collagen can be extracted from fish skin, scales, bone and fins, which are abundant as discarded waste in the food industry, and may prove to be both safer than other mammalian sources due to the absence of prion disease and also more acceptable to a wider range of patient cultures (167, 168).

1.6.1.4 De-cellularised Human Cadaveric Dermis

De-cellularised Human Cadaveric Dermis (DHCD) is a natural biological scaffold which has been treated with a series of lysis, detergent and nuclease steps to remove any cellular content (169). Donor human cadaveric skin is collected by NHS Blood and Transplant in the UK as part of the organ donation scheme with informed consent under the Human Tissue Act of 1961 (170). Cadaveric skin can be used to provide temporary skin cover in large body surface areas burns without de-cellularisation, but once the patient is well enough to mount an immune response the donor skin is rejected (171-174). The purpose of the de-cellularisation process is to remove any cellular material from the tissue which may trigger an immune response, whist maintaining the existing architecture and stability of the original structure (175-177). The de-cellularisation protocol used by NHS Blood and Transplant (Liverpool, UK), who provided the DHCD for use in this Thesis, was adapted from a technique used to de-cellularise heart valves (169). The existing literature on de-cellularised allogeneic and xenogeneic matrices for tissue engineering for heart valve replacement is well established, and in that context the scaffolds have been shown to be capable of re-cellularisation, integration and long-term growth (178-181).

DHCD retains the negative impression of the original donor vasculature (182) and it was hypothesised that engineered vasculature may follow these impressions through the depth of the dermis. Barnes *et al.* used a rat model to investigate de-cellularised scaffold extra-cellular

matrix components and found residual molecular surface markers which they hypothesise may help guide seeded or repopulating cells throughout the tissue (183). It is hypothesised that *in vitro* microvascular networks may therefore receive molecular cues as to where the endothelial and mesenchymal cells should migrate and attach, as well as being able to follow pre-existing donor vasculature channels within the scaffold.

1.6.2 Oxygen

Three-dimensional vessel growth is a limiting factor in many tissue engineering applications and is thought to be restricted due to poor oxygen diffusion into the tissue construct (63, 184-190). Various methods to improve oxygenation of three dimensional *in vitro* cultures have been attempted by other researchers, including fabrication of culture scaffolds with channels or pores to improve oxygen transport (191-193), incorporating proangiogenic growth factors into scaffold material to increase neovascularisation (186, 194), use of bioreactors to improve flow of fresh media (188, 189, 195, 196), and use of perfluorocarbon additives to increase to oxygen carrying capacity of the culture media (197, 198). In this Thesis, there was no scope to develop a bespoke scaffold or perfusion bioreactor and so it was decided to try addition of an artificial oxygen carrier perfluorocarbon compound to the culture media in order to increase the oxygen content of the media in which the available scaffolds were suspended. Perfluorocarbon has been shown to significantly increase the oxygen uptake rate of hepatocytes in three dimensional *in vitro* culture (197) and to improve epithelial metabolism and partial tissue oxygen tension in a tissue engineered tracheal construct (198).

1.7 Aims of this Thesis

The aims of this Thesis are:

- To identify feasible source tissues of Endothelial Colony Forming Cells (ECFCs) for use in clinical applications
- To identify feasible source tissues for stromal cell isolation and culture, for use in clinical applications
- To establish the best conditions for forming microvascular networks *in vitro* using primary human endothelial and mesenchymal stromal cells
- To apply microvasculature formation techniques with our chosen primary cells to three dimensional dermal substitute scaffolds which are currently used as acellular matrices for wound repair

Chapter 2 Methods and Materials

2.1 Materials

Table 2.1 lists the reagents used in this Thesis, with company details, and Table 2.2 lists equipment and software used. The test and control antibodies used for cell surface marker analysis and their suppliers are listed in Table 2.4 alongside the individual volumes and concentrations used in the method.

Table 2.1: List of reagents used in this Thesis.

Reagents	Company
Accutase® cell detatchment solution	PAA Laboratories Ltd., Yeovil, UK
Agarose	Lonza Biologics, Slough, UK
Amersham™ ECL™ Prime Western blotting detection reagent	GE Healthcare Life Sciences, Buckinghamshire, UK
Amersham™ Hyperfilm™	GE Healthcare Life Sciences, Buckinghamshire, UK
Ammonium Chloride Solution (0.8%)	Stem Cell Technologies, Grenoble, France
BM-MSC (Human Bone Marrow Mesenchymal Stromal Cells)	Lonza Biologics, Slough, UK
BSA (Bovine Serum Albumin)	Sigma Aldrich Ltd., Gillingham, UK
Chloramphenicol	Sigma Aldrich Ltd., Gillingham, UK
Collagenase A	Roche Diagnostics, Basel, Switzerland
CAIM (Complete Adipogenic Induction Medium)	Cambrex Bio Science, Walkersville, Inc., Maryland, U.S.A.
CAMM (Complete Adipogenic Maintenance Medium)	Cambrex Bio Science, Walkersville, Inc., Maryland, U.S.A.
CCIM (Complete Chondrogenic Induction Medium)	Cambrex Bio Science, Walkersville, Inc., Maryland, U.S.A.
COIM (Complete Osteogenic Induction Medium)	Cambrex Bio Science, Walkersville, Inc., Maryland, U.S.A.
DAB substrate kit (3,3'-diaminobenzidine)	Vector Labs, Burlingame, CA U.S.A.
DAPI (4',6-diamidino-2-phenylindole)	Invitrogen Ltd., Paisley, UK
DHCD (Decellularised Human Cadaveric	NHS Blood and Transplant, Liverpool, UK

Dermis)	
Dimethyformamide	Sigma Aldrich Ltd., Gillingham, UK
DMEM (Dulbecco's Modified Eagle Medium)	Lonza Biologics, Slough, UK
DMSO (dimethyl sulfoxide)	Sigma Aldrich Ltd., Gillingham, UK
DPBS (Dulbecco's Phosphate Buffered Saline)	PAA Laboratories Ltd., Yeovil, UK
E. coli JM109 competent bacteria	Stratagene, Agilent Technologies UK Ltd., Wokingham, UK
EcoR1 endonuclease enzyme	New England BioLabs, Hertfordshire, UK
EGM-2 (Endothelial Growth Medium 2)	Lonza Biologics, Slough, UK
Ethanol	VWR International Ltd., Leicestershire, UK
Fast Red	Sigma Aldrich Ltd., Gillingham, UK
FcR blocking reagent	Miltenyi Biotec, Gladbach, Germany
Geneticin	Invitrogen Ltd., Paisley, UK
Goat anti-collagen II test antibody	ABcam, Cambridge, UK
Goat IgG isotype control	R&D Systems, Abingdon, UK
Haematoxylin	VWR International Ltd., Leicestershire, UK
HBSS (Hank's Balanced Salt Solution)	Lonza Biologics, Slough, UK
HDF (Human Dermal Fibroblasts)	Lonza Biologics, Slough, UK
HEK293FT (Human Embryonic Kidney cells from the 293FT cell line)	Invitrogen Ltd., Paisley, UK
HEK293FT culture media	Invitrogen Ltd., Paisley, UK
HMSC Differentiation Basal Medium – Chondrogenic	Cambrex Bio Science, Walkersville, Inc., Maryland, U.S.A.
HMSC Differentiation Basal Medium – Osteogenic	Cambrex Bio Science, Walkersville, Inc., Maryland, U.S.A.
Hyclone FCS (Fetal Calf Serum)	Thermo Scientific, Loughborough, UK
Hydrochloric acid (0.1M)	VWR International Ltd., Leicestershire, UK
Hydrogen Chloride (HCl)	Sigma Aldrich Ltd., Gillingham, UK
HyperLadder™ 1kb	Bioline Reagents Limited, London, UK
ICIM (Incomplete Chondrogenic Induction Medium)	Cambrex Bio Science, Walkersville, Inc., Maryland, U.S.A.
Integra® Dermal Regeneration Template	Integra LifeSciences Corporation, Plainsboro, NJ, U.S.A.
Isopropanol	Sigma Aldrich Ltd., Gillingham, UK
LB (Luria Broth)	Sigma Aldrich Ltd., Gillingham, UK
Lipofectamine™ 2000	Invitrogen Ltd., Paisley, UK
Loading buffer	New England BioLabs, Hertfordshire, UK

Lyophilised TGF-β3	Cambrex Bio Science, Walkersville, Inc., Maryland, U.S.A.
Matriderm®	Eurosurgical Ltd., Guildford, UK
Matrigel™ solution	BD Biosciences, Franklin Lakes, NJ, U.S.A.
MSCGM (Mesenchymal Stem Cell Growth Medium)	Lonza Biologics, Slough, UK
Methanol	Sigma Aldrich Ltd., Gillingham, UK
MTT (3-(4,5-Dimethylthiazol-2-yl)-2,5-diphenyltetrazolium bromide)	Sigma Aldrich Ltd., Gillingham, UK
Naphthol AS-mx	Sigma Aldrich Ltd., Gillingham, UK
Neuskin-F®	Medira Ltd., Sandy, UK
Nuclease free water	Invitrogen Ltd., Paisley, UK
Oil Red	Sigma Aldrich Ltd., Gillingham, UK
OptiMEM medium	Invitrogen Ltd., Paisley, UK
PFA (paraformaldehyde)	Sigma Aldrich Ltd., Gillingham, UK
Penicillin/Streptomycin	PAA Laboratories Ltd., Yeovil, UK
Pluronic® F-68 (Polyoxyethylene-polyoxypropylene block copolymer)	Sigma Aldrich Ltd., Gillingham, UK
Polybrene® (1,5-dimethyl-1,5-diazaundecamethylene)	Sigma Aldrich Ltd., Gillingham, UK
Primary mouse anti-human CD31 (Clone WM59)	AbD Serotec, Kidlington, UK
Proteome Profiler™ Antibody Array – Human Angiogenesis Array Kit	R&D Systems, Abingdon, UK
pUC18 control plasmid	Stratagene, Agilent Technologies UK Ltd., Wokingham, UK
PureLink™ HiPure Plasmid Filter Purification Kit for Maxi Preparation of Plasmid DNA	Invitrogen Ltd., Paisley, UK
PureLink™ HiPure Plasmid DNA Purification Kit for Mini Preparation of Plasmid DNA	Invitrogen Ltd., Paisley, UK
Rabbit anti-goat AlexaFluor® 488-conjugated antibody	Invitrogen Ltd., Paisley, UK
Recombinant Human Leptin	R&D Systems, Abingdon, UK
RNase H Reaction Buffer	New England BioLabs, Hertfordshire, UK
Secondary goat anti-mouse IgG (H+L) biotinylated	Vector Labs, Burlingame, CA U.S.A.
Silver nitrate	Sigma Aldrich Ltd., Gillingham, UK
S.O.C. (Super Optimal Broth with Catabolite repression) media	Invitrogen Ltd., Paisley, UK
Sodium thiosulphate	Sigma Aldrich Ltd., Gillingham, UK

SYPRO® Red Protein Gel Stain	Lonza Biologics, Slough, UK
TAE Buffer (Tris Acetate-EDTA)	Lonza Biologics, Slough, UK
Tissue-Tek® O.C.T™ (Optimal Cutting Temperature) Compound	Sakura, Alphen aan den Rijn, The Netherlands
Tris-HCl (tris(hydroxymethyl)aminomethane-hydrochloride)	Sigma Aldrich Ltd., Gillingham, UK
Trisodium citrate	VWR International Ltd., Lutterworth, UK
Triton	Sigma Aldrich Ltd., Gillingham, UK
Trypan Blue stain 0.4% (w/v)	Invitrogen Ltd., Paisley, UK
Trypsin EDTA	PAA Laboratories Ltd., Yeovil, UK
Vectashield mounting media with DAPI	Vector Labs, Burlingame, CA U.S.A.
Vectastain® Universal Elite® ABC Kit (Avidin and Biotinylated horseradish peroxidase macromolecular Complex)	Vector Labs, Burlingame, CA U.S.A.

Table 2.2: List of equipment and software used.

Equipment and Software	**Company**
Accuspin tubes	Sigma Aldrich Ltd., Gillingham, UK
Adobe® Photoshop® CS Version 8.0 imaging software	Adobe Systems Incorporated, San Jose, CA, U.S.A.
AngioSys Image Analysis Software	Cellworks, Buckingham, UK
Biopsy punch (6mm)	Stiefel Laboratories, Durham, NC, U.S.A.
Blood bag containing 21ml citrate anticoagulant	MacoPharma Ltd., Twickenham, UK
Cloning rings	Sigma Aldrich Ltd., Gillingham, UK
Cryogenic vials (2ml)	Corning B.V. Life Sciences, Schiphol-Rijk, The Netherlands
Eppendorf tubes (1.5ml)	Eppendorf UK Limited, Stevenage, UK
Exposure cassette	Bio-Rad Laboratories Ltd., Hertfordshire, UK
Falcon tubes (15ml, 50ml)	BD Biosciences, Franklin Lakes, NJ, U.S.A.
Gel running dock with electrode assembly and power supply	Bio-Rad Laboratories Ltd., Hertfordshire, UK
Glass microscope slides	Thermo Scientific, Loughborough, UK
Heraeus Megafuge 1.0S centrifuge	DJB Labcare, Newport Pagnell, UK
Hettich Rotina 46R centrifuge	DJB Labcare, Newport Pagnell, UK
Imaris Version 6.4	Bitplane AG, Zurich, Switzerland

ImmEdge™ hydrophobic barrier pen	Vector Labs, Burlingame, CA U.S.A.
Innova 4200 incubator (5% CO_2)	New Brunswick Scientific, Enfield, CT, U.S.A.
Leica CM3050S cryostat	Leica Biosystems Ltd., Newcastle Upon Tyne, UK
Leica RM2135 rotary microtome	Leica Biosystems Ltd., Newcastle Upon Tyne, UK
LSM 5 Image Browser Version 3.2 SP2	Carl Zeiss Ltd., Cambridge, UK
Microsoft Excel 2010	Microsoft Corporation, Redmond, WA, U.S.A.
Model 680 microplate reader	Bio-Rad Laboratories Ltd., Hertfordshire, UK
NanoDrop Microvolume UV-Vis Spectrophotometer	Thermo Fisher Scientific Inc., Wilmington, DE, U.S.A.
NEBcutter Version 2 online software	New England BioLabs, Hertfordshire, UK
Nikon DS-L2 control unit	Nikon Corporation, Tokyo, Japan
Nikon TS100 inverted microscope	Nikon Corporation, Tokyo, Japan
Nuaire DH autoflow incubator (5% CO_2)	Nuaire, Plymouth, MN, U.S.A.
Polypropylene conical bottom centrifuge tubes (15ml, 250ml)	Corning B.V. Life Sciences, Schiphol-Rijk, The Netherlands
Quantity One® 1-D Analysis Software	Bio-Rad Laboratories Ltd., Hertfordshire, UK
Rat tail collagen I coated 6-well, 12-well, 24-well, 48-well and 96-well plates	BD Biosciences, Franklin Lakes, NJ, U.S.A.
Round plastic culture dishes (10cm)	Corning B.V. Life Sciences, Schiphol-Rijk, The Netherlands
SUB Aqua Pro 5 water bath	Grant Instruments Ltd., Cambridgeshire, UK
Sysmex XE-2100 (haematology blood analyser)	Sysmex UK Ltd., Milton Keynes, UK
Tissue culture flasks (T25, T75 and T150)	Corning B.V. Life Sciences, Schiphol-Rijk, The Netherlands
Whatman® filter (0.22µm)	Sigma Aldrich Ltd., Gillingham, UK
Zeiss LSM-510 inverted confocal microscope	Carl Zeiss Ltd., Cambridge, UK

2.2 Ethics

Human umbilical cord blood (UCB) units were collected with written informed maternal consent and ethical approval from the Oxford Radcliffe Research Ethics Committee (REC Reference Number 07/H0606/68). The donor subjects were expectant mothers over the age of 18 with uncomplicated pregnancies delivering at term (>36 weeks gestation) at the John Radcliffe Hospital, Oxford. Exclusion criteria were the presence of blood borne infection, known genetic disease in the foetus and the use of illicit drugs. This ethical approval was already in place at the outset of the current research project and the Stem Cell Research Laboratory (SCRL) holds a licence for handling and storage of human cells for research purposes under the Human Tissue Act 2004 (UK) (License number 11042). UCB units were collected from fresh placentae by SCRL research nurses and delivered directly to the SCRL in citrate anticoagulant blood bags (MacoPharma Ltd., Twickenham, UK) for processing and/or storage.

Human adult peripheral blood (PB) and adipose tissue (AT) were collected with written patient informed consent and ethical approval from the Southampton and South West Hampshire Research Ethics Committee (A) (REC Reference Number 09/H0502/120). This was a new ethical application obtained by the primary researcher specifically for this project. The target subjects were plastic surgery patients at Stoke Mandeville Hospital undergoing operative procedures under general anaesthesia, during which they would have removal of adipose tissue which would normally be discarded such as deep inferior epigastric artery perforator (DIEP) flap breast reconstruction. The only additional inclusion criteria were age ≥ 16 years, and exclusion criteria presence of blood borne infection. Patient information sheets are shown in Appendix 1 and consent forms in Appendix 2.

2.3 Cells and cell culture

Human Dermal Fibroblasts (HDF) and Human Bone Marrow Mesenchymal Stromal Cells (BM-MSC) were purchased from Lonza Biologics (Slough, UK) and cultured in Dulbecco's Modified Eagle Medium (DMEM) (Lonza Biologics, Slough, UK) with 10% (v/v) Hyclone Fetal Calf Serum (FCS) (Thermo Scientific, Loughborough, UK).

Human Umbilical Vein Endothelial Cells (HUVEC) were obtained from Emma Pepperell in the Stem Cell Research Laboratory (SCRL), Oxford, and cultured in complete Endothelial Growth Medium-2 (EGM-2) (Lonza Biologics, Slough, UK), which included the SingleQuot Bullet kit of ascorbic acid, 2% (v/v) FCS, gentamicin, heparin, human epidermal growth factor (EGF), human basic fibroblast growth factor (FGF), hydrocortisone, insulin-like growth factor-1 (ILGF-1) and vascular endothelial growth factor (VEGF), with additional 10% (v/v) Hyclone FCS (Thermo Scientific, Loughborough, UK) and 1% (v/v) Penicillin/Streptomycin (PAA Laboratories Ltd., Yeovil, UK), as described by Zhang *et al.* (135).

Human Embryonic Kidney cells from the 293FT cell line (HEK293FT) were purchased from Invitrogen Ltd. (Paisley, UK) and cultured in complete HEK293FT culture media (DMEM with 10% (v/v) Fetal Bovine Serum (FBS), 0.1mM MEM Non-Essential Amino Acids (NEAA), 6mM L-glutamine and 1mM MEM Sodium Pyruvate) (Invitrogen Ltd., Paisley, UK).

2.4 Isolation of endothelial outgrowth colonies

2.4.1 Umbilical cord blood (UCB)

Mononuclear cells (MNC) were isolated from UCB units via serial centrifugation on Accuspin tubes (Sigma Aldrich Ltd., Gillingham, UK) containing 1.077g/ml Ficoll-Hypaque as a density separation medium. Each UCB unit was initially diluted in wash buffer prepared as 500ml Hank's Balanced Salt Solution (HBSS) without calcium and magnesium (Lonza Biologics, Slough,

UK) with 12ml 125g/l trisodium citrate (VWR International Ltd., Lutterworth, UK) and 2.5ml Hyclone FCS (Thermo Scientific, Loughborough, UK). The dilution ratio was 1:1 for units with a white blood cell (WBC) count ≤$7x10^6$ cells/ml measured on a haematology total blood analyser (Sysmex XE-2100, Sysmex UK Ltd., Milton Keynes, UK) and the ratio was 1:2 for units with >$7x10^6$ WBC/ml.

The diluted UCB was layered into Accuspin tubes (Sigma Aldrich Ltd., Gillingham, UK) pre-spun at 1000g for 2 minutes, and the filled tubes were centrifuged at 1000g for 10 minutes at 22°C in a Hettich Rotina 46R centrifuge (DJB Labcare, Newport Pagnell, UK). The upper clear plasma layer was aspirated from the tubes and discarded. White MNC layers were then aspirated gently with a pastette and transferred into 50ml Falcon tubes (BD Biosciences, Franklin Lakes, NJ, U.S.A.), two layers per tube. Tubes were topped up to 50ml with wash buffer, then centrifuged at 400g for 10 minutes at 22°C. The supernatants were removed and discarded, then cell pellets were resuspended in 10ml wash buffer, transferred into one tube and topped up to 50ml. This final tube was centrifuged at 200g for 5 minutes at 22°C, and then the supernatant was removed and discarded. The final cell pellet was resuspended in 10ml complete EGM-2 (Lonza Biologics, Slough, UK), and 0.3ml was transferred to a 1.5ml Eppendorf tube (Eppendorf UK Limited, Stevenage, UK) for analysis using the Sysmex haematology blood analyser (Sysmex XE-2100, Sysmex UK Ltd., Milton Keynes, UK). Centrifugation steps are summarised in Table 2.3.

Using the haematology analyser results, the isolated MNCs were plated at a concentration of $2x10^6$ per well on rat tail collagen I coated 6-well plates (BD Biosciences, Franklin Lakes, NJ, U.S.A.) and cultured in 4ml/well complete EGM-2 (Lonza Biologics, Slough, UK) in a 5% CO_2 Nuaire DH autoflow incubator (Nuaire, Plymouth, MN, U.S.A.) at 37°C. On day one, wells were washed twice with HBSS (Lonza Biologics, Slough, UK) to remove non-adherent cells, the media

was replaced and the plates put back into the incubator. Complete media change was performed every 2-3 days for 2 weeks.

Table 2.3: Centrifuge settings for staged processing of Umbilical Cord Blood (UCB) units.

Centrifugation step	Speed (g)	Time (mins)	Acceleration grade (0-9)	Deceleration grade (0-9)	Temp. (°C)
Pre-spinning of Accuspin tubes	1000	2	9	0	22
Whole blood in wash buffer layered on Accuspin tubes	1000	10	9	1	22
Paired MNC layers in wash buffer in 50ml Falcon tubes	400	10	9	9	22
Collated cell pellets in wash buffer in 50ml Falcon tube	200	5	9	9	22

Mononuclear cells (MNC) were isolated from umbilical cord blood units via serial washing and centrifugation, firstly on Accuspin tubes, then in 50ml Falcon tubes.

After 2 weeks, endothelial colonies were identified, marked by outlining the colonies on the inferior surface of the culture plate with a marker pen, and counted under a Nikon TS100 inverted microscope (Nikon Corporation, Tokyo, Japan). The colonies were then isolated using plastic cloning rings (Sigma Aldrich Ltd., Gillingham, UK) to enable targeted cell passage as follows. Colonies were washed twice with HBSS (Lonza Biologics, Slough, UK), then 0.1-0.5ml 0.5mg/ml Trypsin EDTA (PAA Laboratories Ltd., Yeovil, UK) was added inside the cloning ring to coat the cell layer. Plates were placed in the 5% CO_2 Nuaire DH autoflow incubator (Nuaire, Plymouth, MN, U.S.A.) for 5 minutes at 37°C then removed, and the trypsin cell solution was aspirated from each cloning ring and added to 7ml complete EGM-2 (Lonza Biologics, Slough, UK) in T25 tissue culture flasks (Corning B.V. Life Sciences, Schiphol-Rijk, The Netherlands). Multiple colonies from the same well were combined in one T25 tissue culture flask (Corning B.V. Life Sciences, Schiphol-Rijk, The Netherlands). The cells in the T25 flasks were cultured in

the 5% CO_2 Nuaire DH autoflow incubator (Nuaire, Plymouth, MN, U.S.A.) at 37°C, with complete media change every 2-3 days until ≥80% confluence. This was termed passage 0 or P0. Expansion then continued until experimental use or storage of cells. Cells were used at passage 2-4.

2.4.2 Adult peripheral blood

Fifty millilitres per sample of human adult peripheral blood (PB) was collected by the primary researcher. Each blood sample was injected into a 500ml blood bag containing 21ml citrate anticoagulant (MacoPharma Ltd., Twickenham, UK) for transport to the laboratory. A 0.3ml sample was taken from the blood bag and analysed using the Sysmex haematology total blood analyser (Sysmex XE-2100, Sysmex UK Ltd., Milton Keynes, UK). MNCs were isolated and cultured as per UCB processing described in section 2.4.1, but culture continued for 4 weeks prior to marking, counting and expanding the colonies as cell proliferation was slower than UCB-derived cells, and as detailed above.

2.4.3 Adipose tissue

Human adult adipose tissue (AT) samples were collected by the primary researcher directly from the operating theatre. AT was excised from the patient in continuity with overlying skin, and the tissue block was transported to the laboratory in a 500ml container with 200ml HBSS without calcium and magnesium (Lonza Biologics, Slough, UK) at room temperature. Following excision of skin, AT was finely cut with a scalpel into approximately 2x2x2mm cubes, then 25ml of mechanically processed AT was added to a 50ml Falcon tube (BD Biosciences, Franklin Lakes, NJ, U.S.A.) and chemically dissociated in either 5ml 0.5mg/ml Trypsin EDTA (PAA Laboratories Ltd., Yeovil, UK) or 1.0mg/ml Collagenase A (Roche Diagnostics, Basel, Switzerland) in a 5% CO2 Nuaire DH autoflow incubator (Nuaire, Plymouth, MN, U.S.A.) at 37°C

for 40 minutes. Following incubation, the tube was topped up to 40ml with complete EGM-2 (Lonza Biologics, Slough, UK), then centrifuged at 1000g for 10 minutes in a Hettich Rotina 46R centrifuge (DJB Labcare, Newport Pagnell, UK) at 22°C. Centrifugation resulted in four distinct layers, as seen in Figure 2.1.

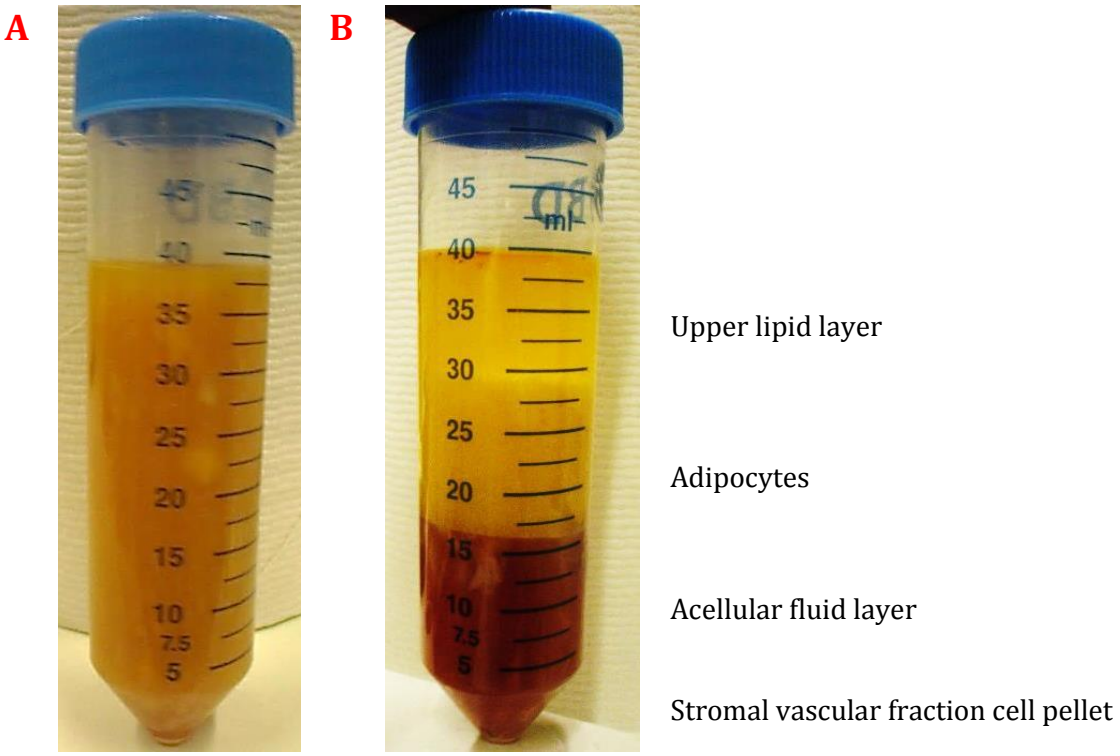

Figure 2.1: Processing of adipose tissue to isolate the stromal vascular fraction. A- Mechanically and chemically dissociated tissue prior to centrifugation B- Dissociated tissue post centrifugation showing distinct layers of free lipid, adipocytes, acellular fluid and the stromal vascular fraction cell pellet.

The cell pellet containing the stromal vascular fraction (SVF) was aspirated from the bottom of the tube by passing a 5ml pipette down the side of the tube and was resuspended in 50ml complete EGM-2 (Lonza Biologics, Slough, UK). A 25µl sample of the cell solution was added to 25µl Trypan Blue stain 0.4% (w/v) (Invitrogen Ltd., Paisley, UK) and viable cells were counted using a haemocytometer under light microscopy (Nikon TS100 inverted microscope (Nikon Corporation, Tokyo, Japan)). Viable cells without uptake of Trypan Blue stain were counted

manually in four large squares of the haemocytometer grid and the number of cells in each original cell solution was calculated using the formula:

$$\textit{Total cell count} = ((N1+N2+N3+N4)/4)HDV$$

Where ***N***=number of cells per counted square, ***H***=haemocytometer value (10000), ***D***= dilution factor (2) and ***V***=volume of original cell solution.

The SVF cell suspension was added to rat tail collagen I coated 6 well plates (BD Biosciences, Franklin Lakes, NJ, U.S.A.) at a concentration of $2x10^6$ cells per well and each well was topped up to a total of 4ml per well complete EGM-2 (Lonza Biologics, Slough, UK). Plates were placed in the 5% CO_2 Nuaire DH autoflow incubator (Nuaire, Plymouth, MN, U.S.A.) at 37°C with complete media change on day 1 and every 2-3 days until cell layer confluence.

After initial growth of only stromal cells using the above protocol, the process was adapted to separate out microvasculature from whole adipose tissue in an attempt to improve endothelial cell yield. AT was divided and either had microvasculature (MV) dissected from the tissue using sterile scissors under 3.5x loupe magnification, or remained as whole AT (Figure 2.2). These samples were then processed separately with the same stages as before. In addition, larger sections of AT veins and arteries were collected directly from the patient in theatre and cultured as tissue explants in complete EGM-2 (Lonza Biologics, Slough, UK) on rat tail collagen I coated 6-well plates (BD Biosciences, Franklin Lakes, NJ, U.S.A.) without further processing.

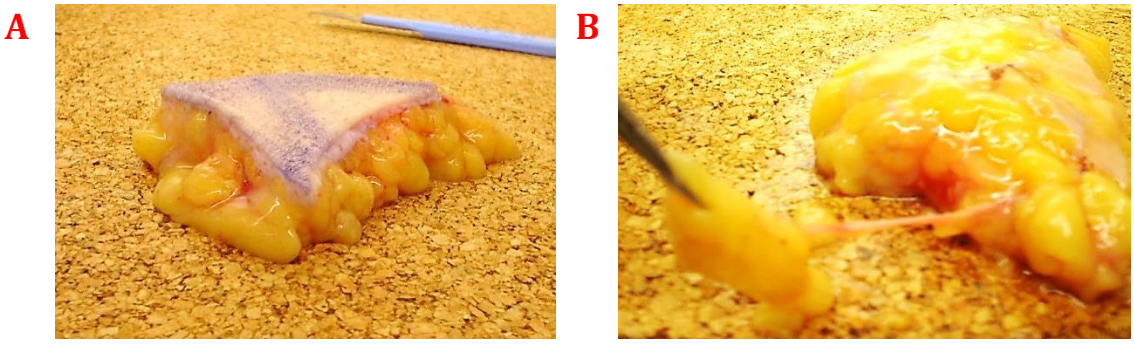

Figure 2.2: Macroscopic processing of adipose tissue. A- Whole AT with attached skin as collected from the operating theatre. B- Dissection of microvasculature from within the tissue was performed using 3.5x operating loupe magnification.

Two distinct cell types were isolated from the above culture process; endothelial-like cells and MSC-like cells. Endothelial-like cells, described as Endothelial Colony Forming Cell (ECFC) derived cells, were marked, counted and expanded using cloning rings (Sigma Aldrich Ltd., Gillingham, UK) as described for UCB in section 2.4.1, and MSC-like cells achieved confluence in the 6-well plates and were harvested using 0.5mg/ml Trypsin EDTA (PAA Laboratories Ltd., Yeovil, UK) and directly seeded into T150 tissue culture flasks (Corning B.V. Life Sciences, Schiphol-Rijk, The Netherlands) with 30ml complete EGM-2 (Lonza Biologics, Slough, UK) for continued culture and expansion in the 5% CO_2 Nuaire DH autoflow incubator (Nuaire, Plymouth, MN, U.S.A.) at 37°C. Complete media change was performed every 2-3 days until ≥80% confluence, termed P0. Expansion continued until experimental use or storage of cells at P2-4.

A summary of the adult tissue samples collected and processed from each subject is shown in Figure 2.3.

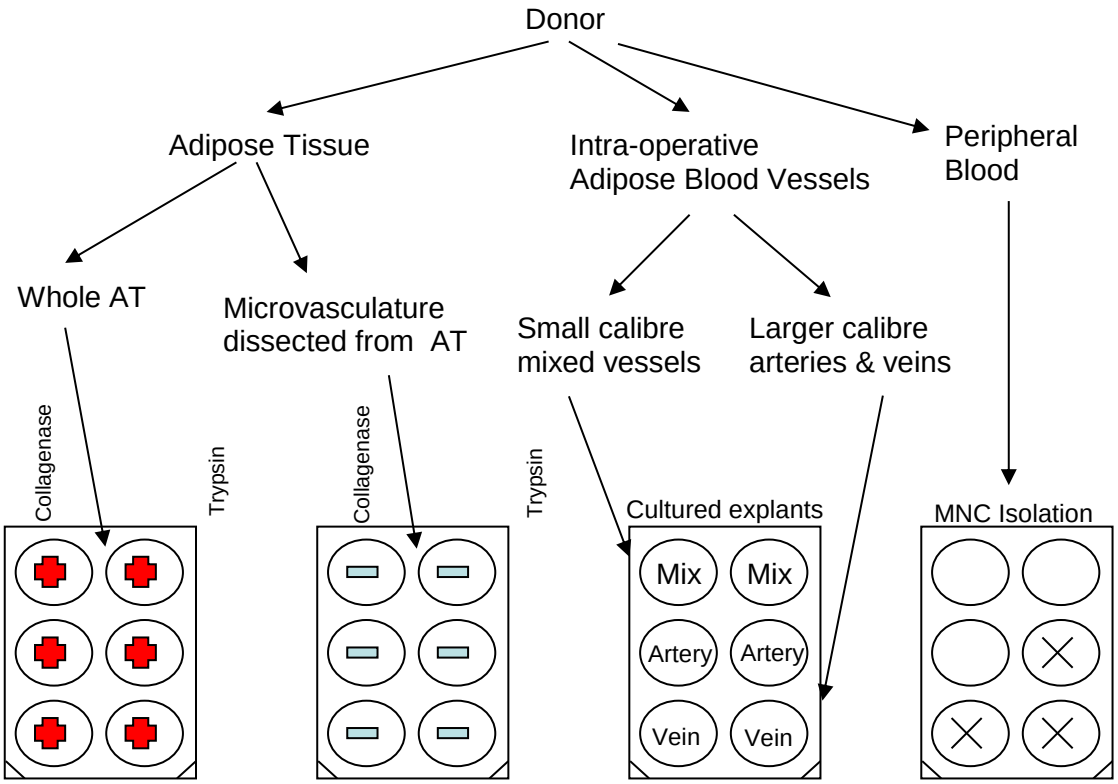

Figure 2.3: Processing of adult donor samples. Each patient enrolled in the study consented to donation of Adipose Tissue (AT) and Peripheral Blood (PB) samples. AT was divided into two halves; one half of the sample was processed as whole AT and the other had microvasculature dissected free from the AT for separate processing. Mechanically and chemically dissociated and centrifuged AT and microvasculature (MV) samples were cultured in EGM-2 (Lonza Biologics, Slough, UK) on rat tail collagen I coated 6-well plates (BD Biosciences, Franklin Lakes, NJ, U.S.A.). Adipose blood vessels identified intra-operatively at time of tissue excision were plated as explants in EGM-2 (Lonza Biologics, Slough, UK) on rat tail collagen I coated 6-well plates (BD Biosciences, Franklin Lakes, NJ, U.S.A.). PB underwent serial washing and centrifugation to isolate mononuclear cells which were cultured in EGM-2 (Lonza Biologics, Slough, UK) on rat tail collagen I coated 6-well plates (BD Biosciences, Franklin Lakes, NJ, U.S.A.). All plates were cultured in a 5% CO_2 Nuaire DH autoflow incubator (Nuaire, Plymouth, MN, U.S.A.) at 37°C with media change every 2-3 days until cell colonies were identified for isolation and expansion.

2.5 Cell surface marker analyses

Cell surface marker analysis was performed on Endothelial Colony Forming Cell (ECFC) derived cells from UCB (as per section 2.4.1), HUVEC (from Emma Pepperell at the SCRL, Oxford), PB (as per section 2.4.2) and AT (as per section 2.4.3), dissociated cells from fresh AT (as per section 2.4.3), dermal fibroblasts (from Lonza Biologics, Slough, UK), and MSC from AT and microvasculature (MV) (as per section 2.4.3) by flow cytometry.

2.5.1 Single colour surface marker analysis

Cultured cells were washed twice with HBSS (Lonza Biologics, Slough, UK) then harvested with Accutase® cell detatchment solution (Accutase® enzymes in PBS with 0.5mM EDTA) (PAA Laboratories Ltd., Yeovil, UK), just covering the cell layer. Following five minutes of incubation at 37°C in the 5% CO_2 Nuaire DH autoflow incubator (Nuaire, Plymouth, MN, U.S.A.), the cells were washed in Fluorescence Activated Cell Sorting (FACS) Buffer (Dulbecco's Phosphate Buffered Saline (DPBS) without Calcium and Magnesium (PAA Laboratories Ltd., Yeovil, UK) containing 1% (w/v) Bovine Serum Albumin (BSA) (Sigma Aldrich Ltd., Gillingham, UK)), then resuspended in 2ml of this buffer, kept on ice.

Uncultured cells dissociated from fresh AT were chemically and mechanically processed as described in section 2.4.3, and the aspirated SVF cell pellet was resuspended in 10ml 0.8% (v/v) Ammonium Chloride Solution (Stem Cell Technologies, Grenoble, France) for ten minutes at room temperature to lyse any remaining red blood cells. This solution was centrifuged at 1200rpm for 5 minutes at 22°C in a Hettich Rotina 46R centrifuge (DJB Labcare, Newport Pagnell, UK), the supernatant discarded, and the cells resuspended in 10ml FACS buffer. This cell suspension was centrifuged again at 1200rpm for 5 minutes at 22°C, the resulting supernatant was discarded and the cells were resuspended in 2ml FACS buffer and kept on ice.

From this step, cultured and uncultured cells were treated identically. A 25µl sample of the cell suspension was added to 25µl Trypan Blue stain 0.4% (w/v) (Invitrogen Ltd., Paisley, UK) and viable cells were counted using a haemocytometer under light microscopy (Nikon TS100 inverted microscope (Nikon Corporation, Tokyo, Japan)) as described in section 2.4.3. For each test or isotype control antibody used, 5-15 $x10^4$ cells from each sample in 100µl FACS buffer were placed in a FACS tube and blocked with 10% (v/v) FcR blocking reagent (Miltenyi Biotec, Gladbach, Germany) whilst incubated on ice for 10 minutes. The cell suspension was then mixed with the relevant antibody or isotype control using light vortexing, and then incubated

for 30 minutes on ice and protected from the light. The test and control antibodies used and their individual volumes and concentrations are shown in Table 2.4. An additional tube of FcR blocked cells was prepared without test antibody or isotype control staining for setting the flow cytometer parameters.

Following incubation with the relevant antibodies, cells were then washed by adding 500µl FACS buffer/tube, spinning the tubes at 1200rpm for 5 minutes at 4°C in a Heraeus Megafuge 1.0S centrifuge (DJB Labcare, Newport Pagnell, UK) and discarding the supernatant. Cell pellets were then resuspended in 400µl FACS buffer and kept on ice protected from the light until processing on the flow cytometer.

Samples were analysed on a BD LSR II flow cytometer (BD Biosciences, Franklin Lakes, NJ, U.S.A.) using BD FACSDiva 6 software. Unstained cells were analysed first to set values for forward and side scatter. Cell viability was assessed using either 1nM To-Pro-3 (Invitrogen Ltd., Carlsbad, CA, U.S.A.) or 1mg/ml Propidium Iodide (Sigma Aldrich Ltd., Gillingham, UK) for APC labelled samples, added at 1µl per tube prior to analysis. Relevant isotype control staining was used to set the median fluorescence intensity (MFI) at approximately 10^2 by adjusting voltage values in the flow cytometer. Resulting histograms from each sample had MFI of the peak recorded, as well as comparing the number of cells on the antibody stained samples which fell within an arbitrary gate set on the isotype controls.

Table 2.4: Summary of test antibodies and isotype controls used for flow cytometry*.

Antibody / Isotype control	Clone name	Volume per tube in microlitres [concentration]	Company
CD14 PECy7	M5E2	5 [0.625µg/ml]	BD Biosciences, Franklin Lakes, NJ, U.S.A.
CD31 PE	WM59	10 [6.25ng/ml]	BD Biosciences, Franklin Lakes, NJ, U.S.A.
CD 34 APC	AC136	11 [1.1µg/ml]	Miltenyi Biotec, Gladbach, Germany
CD45 PerCP	2D1	5 [1.25µg/ml]	BD Biosciences, Franklin Lakes, NJ, U.S.A.
CD49d PE	7.2R	10 [10µg/ml]	R&D Systems, Abingdon, UK
CD 73 PE	AD2	10 [1.25µg/ml]	BD Biosciences, Franklin Lakes, NJ, U.S.A.
CD 90 FITC	5E10	2 [50µg/ml]	BD Biosciences, Franklin Lakes, NJ, U.S.A.
CD 105 FITC	166707	10 [5µg/ml]	R&D Systems, Abingdon, UK
CD133 APC	293C3	11 [0.825µg/ml]	Miltenyi Biotec, Gladbach, Germany
CD146 FITC	P1H12	5 [5µg/ml] (1st diluted 1:20)	Merck Millipore, Billerica, MA, U.S.A.
VEGFR2 PE	89106	40 [50µg/ml]	R&D Systems, Abingdon, UK
TIE2 PE	33.1	20 [50µg/ml]	BioLegend, San Diego, CA, U.S.A.
IgG1 PE	MOPC-21	10 [5µg/ml]	BD Biosciences, Franklin Lakes, NJ, U.S.A.
IgG1 PE	11711	40 [5µg/ml]	R&D Systems, Abingdon, UK
IgG2a APC	S43.10	11 [11µg/ml]	Miltenyi Biotec, Gladbach, Germany
IgG1 FITC	MOPC-21	10 [20µg/ml]	BD Biosciences, Franklin Lakes, NJ, U.S.A.
IgG1 PerCP	MOPC-21	1 [5µg/ml]	BD Biosciences, Franklin Lakes, NJ, U.S.A.
IgG2a PECy7	MOPC-173	1.25 [200µg/ml]	BD Biosciences, Franklin Lakes, NJ, U.S.A.
IgG2b APC	IS6-11E5.11	11 [22µg/ml]	Miltenyi Biotec, Gladbach, Germany

*Test antibodies and isotype controls with corresponding fluorophores were used at pre-titrated volumes. Fluorophore abbreviations: PE-Cy7 = PhycoErythrin-Cyanine 7, PE = PhycoErythrin, APC = AlloPhycoCyanin, PerCP = Peridinin Chlorophyll Protein, FITC = Fluorescein IsoThioCyanate.

2.5.2 Multiple colour surface marker analysis

Small numbers of adult PB and AT derived endothelial-like cells were analysed using a multi-colour flow cytometry assay. This assay is normally used in our laboratory as part of a clinical research trial involving small blood samples from patients with cancer to assess to effect of an anti-angiogenic drug. Cells were initially prepared and blocked as per section 2.5.1, then two tubes of 200µl cell solution at a concentration of $10x10^6$ cells/ml FACS buffer were prepared with the cocktail of test antibodies and isotype controls shown in Table 2.5. Unstained tubes were prepared to set the analysis voltages and samples were analysed on a BD LSR II flow cytometer (BD Biosciences, Franklin Lakes, NJ, U.S.A.) using BD FACSDiva 6 software as per section 2.5.1.

Table 2.5: Antibody cocktails for multiple colour cell surface marker analysis.

Test antibodies (volume)	Control antibodies (volume)
CD144 PE (5µl)	IgG1 PE (20µl)
CD90 FITC (4µl)	IgG1 FITC (20µl)
CD45 PerCP (5µl)	IgG1 PerCP (5µl)
CD34 APC (5µl)	IgG1 APC (5µl)
UV activated Live Dead dye (1µl)	UV activated Live Dead dye (1µl)

Fluorophore abbreviations: PE = PhycoErythrin, FITC = Fluorescein IsoThioCyanate, PerCP = Peridinin Chlorophyll Protein, APC = AlloPhycoCyanin.

2.6 Adipose tissue histology

One centimetre cube sections of human adult AT were fixed in 4% (w/v) Paraformaldehyde (PFA) (Sigma Aldrich Ltd., Gillingham, UK) and then embedded in paraffin by staff at the John Radcliffe Hospital, Department of Pathology. The received paraffin embedded samples were cut into multiple 5-10µm sections using a Leica RM2135 rotary microtome (Leica Biosystems Ltd., Newcastle Upon Tyne, UK), collected on glass slides (Thermo Scientific, Loughborough, UK) and air dried overnight. Slides were then deparaffinised, rehydrated and stained using

serial immersions in Citroclear (TCS Biosciences, Buckingham, UK), various concentrations of ethanol (VWR International Ltd., Leicestershire, UK), haematoxylin (VWR International Ltd., Leicestershire, UK), 0.1M hydrochloric acid (VWR International Ltd., Leicestershire, UK) and eosin Y-solution (VWR International Ltd., Leicestershire, UK). The concentrations of reagents and timing of the serial immersions are shown in Table 2.6.

On completion of the serial immersions, the haematoxylin and eosin stained sections were sealed on the glass slides (Thermo Scientific, Loughborough, UK) with glass coverslips and examined using a Nikon TS100 inverted microscope (Nikon Corporation, Tokyo, Japan).

Table 2.6: Process of haematoxylin and eosin staining of paraffin embedded Adipose Tissue (AT) samples.

Stage	Chemical	Duration of immersion
Deparaffinise	Citroclear 1	5 minutes
	Citroclear 2	5 minutes
Rehydrate	100% ethanol (1)	3 minutes
	100% ethanol (2)	3 minutes
	95% ethanol (1)	3 minutes
	95% ethanol (2)	3 minutes
	75% ethanol	3 minutes
	Distilled water	3 minutes
Stain nucleus	Haematoxylin	3 minutes
	0.1% Hydrogen Chloride	2 seconds
	Tap water	3 minutes (running water)
Stain cytoplasm	0.5% Eosin Y solution	3 minutes
	Tap water	3 minutes (running water)
Fixation	95% ethanol (1)	3 minutes
	95% ethanol (2)	3 minutes
	100% ethanol (1)	3 minutes
	100% ethanol (2)	3 minutes
	Citroclear 1	5 minutes
	Citroclear 2	5 minutes

One centimetre cube sections of human adult AT were fixed in 4% (w/v) PFA, embedded in paraffin, and cut into multiple 5-10µm sections using a rotary microtome. Air dried sections on glass slides were deparaffinised, rehydrated and stained using serial immersions in Citroclear, ethanol, haematoxylin, 0.1M hydrochloric acid and eosin Y-solution for histological examination.

2.7 Differentiation of adipose derived Mesenchymal Stem/Stromal Cells

In order to determine the differentiation potential of AT and MV MSCs cultured in this study, cells were induced to give rise to three mesenchymal lineages: adipogenic, osteogenic and chondrogenic. The assays were performed with paired AT and MV MSC, and BM-MSC, known to be capable of differentiation into the three lineages, were used as a positive control.

2.7.1 Adipogenesis

Complete adipogenic induction medium (CAIM) (Cambrex Bio Science, Walkersville, Inc., Maryland, U.S.A.) was prepared by defrosting the Singlequots® (recombinant h-Insulin, L-Glutamine, Mesenchymal Cell Growth Supplement (MCGS), Dexamethasone, Indomethacin, 3-isobutyl-methyl-xanthine (IBMX) and Pen/Strep) and adding them to basic hMSC Adipogenic Induction medium. Complete adipogenic maintenance medium (CAMM) (Cambrex Bio Science, Walkersville, Inc., Maryland, U.S.A.) was prepared by defrosting the Singlequots® (recombinant h-Insulin, L-Glutamine, MCGS and Pen/Strep) and adding them to basic hMSC Adipogenic Maintenance medium.

MSC were cultured to passage 4, washed with DPBS (PAA Laboratories Ltd., Yeovil, UK), harvested with 0.5mg/ml Trypsin EDTA (PAA Laboratories Ltd., Yeovil, UK) and counted using Trypan Blue stain 0.4% (w/v) (Invitrogen Ltd., Paisley, UK) and a haemocytometer, as discussed in section 2.4.3. Six wells of each cell type were plated as follows: $2x10^5$ MSC in 2ml Mesenchymal Stem Cell Growth Medium (MSCGM) (Lonza Biologics, Slough, UK) per well of a 6 well plate. Plates were incubated at 37°C in the 5% CO_2 Nuaire DH autoflow incubator (Nuaire, Plymouth, MN, U.S.A.) and had complete media change every 2-3 days until 100% confluent. Once confluent, the adipogenic induced cells underwent three cycles of three days of culture in CAIM (Cambrex Bio Science, Walkersville, Inc., Maryland, U.S.A.) followed by one to three days of culture in CAMM (Cambrex Bio Science, Walkersville, Inc., Maryland, U.S.A.). Non-induced control wells were fed only with CAMM (Cambrex Bio Science, Walkersville, Inc., Maryland, U.S.A.) on the same schedule. After the three cycles of feeding both induced and non-induced control wells were kept in culture for a further seven days in CAMM (Cambrex Bio Science, Walkersville, Inc., Maryland, U.S.A.), replaced every 2-3 days.

At the end of the culture period, wells were fixed and stained to identify the presence or absence of adipocytes. Wells were washed twice with DPBS (PAA Laboratories Ltd., Yeovil, UK)

and 1ml methanol (Sigma Aldrich Ltd., Gillingham, UK) pre-cooled to -20°C was added per well and incubated at -20°C for five minutes. The methanol was removed and wells were washed twice with double distilled water (ddH_2O). Oil Red stock solution was prepared by adding 150mg Oil Red (Sigma Aldrich Ltd., Gillingham, UK) to 50ml isopropanol (Sigma Aldrich Ltd., Gillingham, UK). Oil Red working solution was prepared by diluting Oil Red stock solution 3:2 with ddH_2O. The working solution was then filtered through a 0.22µm Whatman® filter (Sigma Aldrich Ltd., Gillingham, UK) and left to stand for five minutes before applying 0.5ml Oil Red stain per well. Plates were then incubated for 20 minutes on a shaker platform at room temperature. The staining solution was removed and wells washed twice with ddH_20. Each well had 200µl ddH_2O added prior to viewing and photographing under a Nikon TS100 inverted microscope (Nikon Corporation, Tokyo, Japan). The Oil Red stain colours lipid droplets within adipocytes and allowed identification of the differentiated cells.

2.7.2 Osteogenesis

Complete osteogenic induction medium (COIM) (Cambrex Bio Science, Walkersville, Inc., Maryland, U.S.A.) was prepared by defrosting the Singlequots® (L-Glutamine, MCGS, Dexamethasone, Ascorbate, β-Glycerophosphate and Pen/Strep) and adding them to hMSC Differentiation Basal Medium – Osteogenic (Cambrex Bio Science, Walkersville, Inc., Maryland, U.S.A.).

MSC were cultured to passage 4, washed with DPBS (PAA Laboratories Ltd., Yeovil, UK), harvested with 0.5mg/ml Trypsin EDTA (PAA Laboratories Ltd., Yeovil, UK) and counted using Trypan Blue stain 0.4% (w/v) (Invitrogen Ltd., Paisley, UK) and a haemocytometer, as described in section 2.4.3. Six wells of each cell type were plated as follows: $3x10^4$ MSC in 2ml MSCGM (Lonza Biologics, Slough, UK) per well of a 6 well plate. Plates were incubated at 37°C in the 5% CO_2 Nuaire DH autoflow incubator (Nuaire, Plymouth, MN, U.S.A.) for 24 hours until adherent.

Induced cells then had media changed to COIM (Cambrex Bio Science, Walkersville, Inc., Maryland, U.S.A.), and incubated, with complete media change every 3-4 days, for up to three weeks. Non-induced control wells were fed with MSCGM (Lonza Biologics, Slough, UK) on the same schedule. Once osteogenic induced cells showed changes in morphology by becoming cuboidal and forming gaps in the mineralised post-confluent cell layer, cultures were fixed and stained.

Osteogenic stain, which stains for alkaline phosphatase, was prepared by combining 1ml dimethyformamide (Sigma Aldrich Ltd., Gillingham, UK), 4mg naphthol AS-mx (Sigma Aldrich Ltd., Gillingham, UK), 20mg Fast Red (Sigma Aldrich Ltd., Gillingham, UK) and 19ml 0.1M Tris-HCl (Sigma Aldrich Ltd., Gillingham, UK) at pH 9.2. The plates were washed once with 1ml DPBS (PAA Laboratories Ltd., Yeovil, UK) per well then 1ml osteogenic staining solution per well was applied and incubated at room temperature for 30 minutes. The staining solution was then removed and wells were washed once with 1ml DPBS (PAA Laboratories Ltd., Yeovil, UK) per well before fixation with 1ml per well 4% (w/v) paraformaldehyde (PFA) (Sigma Aldrich Ltd., Gillingham, UK) in DPBS (PAA Laboratories Ltd., Yeovil, UK) and incubation at room temperature for ten minutes.

During this incubation, von Kossa staining solution was prepared by adding 200mg silver nitrate (Sigma Aldrich Ltd., Gillingham, UK) to 20ml ddH_2O. Plates were washed once with 1ml ddH_2O per well then had 1ml von Kossa stain added per well and were incubated in strong light, at room temperature for one hour. Following the von Kossa stain, plates were washed three times with 1ml ddH_2O per well then had 1ml 5% (w/v) sodium thiosulphate (Sigma Aldrich Ltd., Gillingham, UK) per well added for 5 minutes. Plates were washed two further times with 1ml ddH_2O per well then viewed and photographed under the Nikon TS100 inverted microscope (Nikon Corporation, Tokyo, Japan). Osteocytes had a background fast red stain (alkaline phosphatase positive staining) and brown von Kossa staining of calcium deposits.

2.7.3 Chondrogenesis

Incomplete chondrogenic induction medium (ICIM) (Cambrex Bio Science, Walkersville, Inc., Maryland, U.S.A.) was prepared by defrosting the Singlequots® (L-Glutamine, Dexamethasone, Ascorbate, ITS+ supplement, Sodium Pyruvate, Proline and Pen/Strep) and adding them to hMSC Differentiation Basal Medium – Chondrogenic (Cambrex Bio Science, Walkersville, Inc., Maryland, U.S.A.). Lyophilised TGF-β3 (Cambrex Bio Science, Walkersville, Inc., Maryland, U.S.A.) was resuspended in 4mM Hydrogen Chloride (HCl) (Sigma Aldrich Ltd., Gillingham, UK) with 1mg/ml BSA (Sigma Aldrich Ltd., Gillingham, UK) at a concentration of 20µg/ml then divided into 5µl aliquots and frozen at -80°C. Complete chondrogenic induction medium (CCIM) (Cambrex Bio Science, Walkersville, Inc., Maryland, U.S.A.) was prepared immediately before each use by adding defrosted TGF-β3 (Cambrex Bio Science, Walkersville, Inc., Maryland, U.S.A.) to ICIM (Cambrex Bio Science, Walkersville, Inc., Maryland, U.S.A.) at a concentration of 10ng/ml (i.e. one 5µl TGF-β3 aliquot per 10ml ICIM).

MSC were cultured to passage 4, washed with DPBS (PAA Laboratories Ltd., Yeovil, UK), harvested with 0.5mg/ml Trypsin EDTA (PAA Laboratories Ltd., Yeovil, UK) and counted using Trypan Blue stain 0.4% (w/v) (Invitrogen Ltd., Paisley, UK) and a haemocytometer, as described in section 2.4.3. A tube containing $1x10^6$ MSC in 1.5ml ICIM (Cambrex Bio Science, Walkersville, Inc., Maryland, U.S.A.) was prepared for each cell type. The cells were centrifuged in a Hettich Rotina 46R centrifuge (DJB Labcare, Newport Pagnell, UK) at 150g for five minutes at 22°C, the supernatant discarded and the cell pellet resuspended in 1.5ml ICIM (Cambrex Bio Science, Walkersville, Inc., Maryland, U.S.A.). The centrifugation was repeated and the cell pellet then resuspended in 2ml CCIM (Cambrex Bio Science, Walkersville, Inc., Maryland, U.S.A.). For each cell type, 0.5ml cell solution ($2.5x10^5$ cells) was added to each of four separate 15ml polypropylene conical bottom centrifuge tubes (Corning B.V. Life Sciences, Schiphol-Rijk, The Netherlands). These tubes were centrifuged in a Hettich Rotina 46R centrifuge (DJB Labcare, Newport Pagnell, UK) at 150g for five minutes at 22°C to form cell pellets, the caps were

loosened to allow gas exchange and the tubes were placed upright in the 5% CO_2 Nuaire DH autoflow incubator (Nuaire, Plymouth, MN, U.S.A.) at 37°C for 24 hours. The cell pellets had a complete media change every 2-3 days, ensuring that the pellet remained free floating after every change by flicking the bottoms of the tubes (0.5ml CCIM (Cambrex Bio Science, Walkersville, Inc., Maryland, U.S.A.) for induced pellets and 0.5ml ICIM (Cambrex Bio Science, Walkersville, Inc., Maryland, U.S.A.) for non-induced controls). Culture continued for 28 days until preparation for frozen sectioning.

The cultured pellets were washed in DPBS (PAA Laboratories Ltd., Yeovil, UK) and duplicate condition pellets were placed in the centre of tin foil boats. The paired pellets were covered with a 2mm layer of Tissue-Tek® O.C.T™ Compound (Sakura, Alphen aan den Rijn, The Netherlands) (10.24% (w/w) polyvinyl alcohol, 4.26% (w/w) polyethylene glycol, 85.5% (w/w) non-reactive ingredients) then snap frozen by immersion in liquid nitrogen. The frozen specimens were stored at -20°C until cryosectioning and staining.

A Leica CM3050S cryostat (Leica Biosystems Ltd., Newcastle Upon Tyne, UK) was used to cut 10µm sections through the specimens and these were mounted on glass microscope slides (Thermo Scientific, Loughborough, UK). A well was created surrounding the samples with an ImmEdge™ hydrophobic barrier pen (Vector Laboratories Inc., Burlingame, CA, USA) and the samples were treated with a drop of permeablisation buffer (DPBS (PAA Laboratories Ltd., Yeovil, UK) with 5% (w/v) BSA (Sigma Aldrich Ltd., Gillingham, UK) and 0.2% Triton (Sigma-Aldrich Ltd., Gillingham, UK)) for one hour at room temperature to remove the residual mounting medium. The buffer was removed and samples had either 100µl of 0.1mg/ml goat anti-collagen II test antibody (ABcam, Cambridge, UK) or 100µl of 0.1mg/ml goat IgG isotype control (R&D Systems, Abingdon, UK) applied and incubated for one hour at room temperature. The antibody and isotype control were removed and the samples washed three times with DPBS (PAA Laboratories Ltd., Yeovil, UK). Next, 100µl rabbit anti-goat AlexaFluor®

488-conjugated antibody (Invitrogen Ltd., Paisley, UK) diluted 1 in 1000 in DPBS (PAA Laboratories Ltd., Yeovil, UK) was applied to each sample and the samples were incubated protected from the light at room temperature for 30 minutes. This antibody was removed, the samples washed three times with DPBS (PAA Laboratories Ltd., Yeovil, UK) and a drop of Vectashield mounting media with DAPI (Vector Laboratories Inc., Burlingame, CA, USA) was added to each sample to stain the nuclei. Samples were covered with glass cover slips and sealed with clear nail varnish for examination with a Nikon Eclipse TS100 light microscope (Nikon Corporation, Tokyo, Japan), under UV light. Chondrogenic differentiated pellets demonstrated collagen stained green and nuclei stained blue.

2.8 Tubule assays

Three different types of tubule assay were performed. The Matrigel™ assay was used to determine if monocultured cells were capable of lining up into linear tubules. The two-dimensional sandwich co-culture assay was used to measure the amount of tubule formation achieved under different culture conditions. Various permutations of the three-dimensional co-culture assay in scaffolds were trialled to optimise microvascular growth for potential clinical applications.

2.8.1 Matrigel™ assay

Cultured cells were washed twice with HBSS (Lonza Biologics, Slough, UK) then lifted with trypsin as decribed in section 2.4.3 and neutralised with complete EGM-2 (Lonza Biologics, Slough, UK). The solution was centrifuged at 1200rpm for 5 minutes in a Hettich Rotina 46R centrifuge (DJB Labcare, Newport Pagnell, UK) at 22°C, the supernatant was discarded and the cells were resuspended in 10ml complete EGM-2 (Lonza Biologics, Slough, UK). Cells were counted using Trypan Blue stain 0.4% (w/v) (Invitrogen Ltd., Paisley, UK) and a

haemocytometer, as discussed in section 2.4.3, and diluted to a concentration of $6x10^4$ cells in 400µl complete EGM-2 (Lonza Biologics, Slough, UK).

Matrigel™ solution (BD Biosciences, Franklin Lakes, NJ, U.S.A.) was kept on ice overnight then loaded into rat tail collagen I coated 96-well plates (BD Biosciences, Franklin Lakes, NJ, U.S.A.) at 50µl per well, avoiding air bubbles with careful use of the pipette. The Matrigel™ solution (BD Biosciences, Franklin Lakes, NJ, U.S.A.) was polymerised by incubating the plate at 37°C in the 5% CO_2 Nuaire DH autoflow incubator (Nuaire, Plymouth, MN, U.S.A.) for 30 minutes.

Cells were added on top of the polymerised Matrigel™ (BD Biosciences, Franklin Lakes, NJ, U.S.A.) in a circular motion at 1.5 $x10^4$ cells per well in 100µl complete EGM-2 (Lonza Biologics, Slough, UK). Plates were incubated at 37°C in the 5% CO_2 Nuaire DH autoflow incubator (Nuaire, Plymouth, MN, U.S.A.) for 20 hours then wells were photographed under the Nikon TS100 inverted microscope (Nikon Corporation, Tokyo, Japan) before fixing and staining.

Media were aspirated from each well and the Matrigel™ (BD Biosciences, Franklin Lakes, NJ, U.S.A.) was washed with 100µl DPBS (PAA Laboratories Ltd., Yeovil, UK) per well and fixed with 100µl -20°C methanol (Sigma Aldrich Ltd., Gillingham, UK) per well for 30 seconds at room temperature. The methanol (Sigma Aldrich Ltd., Gillingham, UK) was aspirated from each well and the Matrigel™ (BD Biosciences, Franklin Lakes, NJ, U.S.A.) was washed with 100µl double distilled water (ddH_2O). The Matrigel™ (BD Biosciences, Franklin Lakes, NJ, U.S.A.) was then stained with 100µl per well 50% (v/v) haematoxylin (VWR International Ltd., Leicestershire, UK) diluted in DPBS (PAA Laboratories Ltd., Yeovil, UK), incubated for 10 seconds at room temperature. The Matrigel™ (BD Biosciences, Franklin Lakes, NJ, U.S.A.) wells were again washed with 100µl ddH_2O then covered with 200µl DPBS without Calcium and Magnesium (PAA Laboratories Ltd., Yeovil, UK) before they were examined under the Nikon TS100 inverted microscope (Nikon Corporation, Tokyo, Japan) and photographed for analysis using the Nikon DS-L2 control unit (Nikon Corporation, Tokyo, Japan).

Images were processed using Adobe® Photoshop® CS Version 8.0 imaging software (Adobe Systems Incorporated, San Jose, CA, U.S.A.) to prepare them for use with the AngioSys Image Analysis Software (Cellworks, Buckingham, UK). Using Photoshop®, the brightfield microscopy images were transformed to grayscale and inverted to ensure that the tubules appeared darker than the background, and then set to optimal brightness. The optimised images were loaded into the AngioSys Image Analysis Software (Cellworks, Buckingham, UK) and set to skeletonise and measure the number of tubules, tubule lengths and number of tubule junctions. The output data was transferred to Microsoft Excel 2010 (Microsoft Corporation, Redmond, WA, U.S.A.) for statistical analysis and values were compared using the two tailed Student's T Test for independent samples.

2.8.2 Two-dimensional sandwich co-culture tubule assay

Multiple variations of the two-dimensional sandwich co-culture tubule assay were set in order to test different cell types and concentrations, ratios of cell concentrations and additives to the media. The basic assay is outlined here and variations are specified in the appropriate results sections.

Stromal cells (AT MSC, MV MSC, BM MSC and HDF) cultured in a T75 tissue culture flask (Corning B.V. Life Sciences, Schiphol-Rijk, The Netherlands) were washed twice with HBSS (Lonza Biologics, Slough, UK) and harvested with 0.5mg/ml Trypsin EDTA (PAA Laboratories Ltd., Yeovil, UK) as described in section 2.4.3. Cells were resuspended in 10ml complete EGM-2 (Lonza Biologics, Slough, UK). A 25µl sample of the cell solution was added to 25µl Trypan Blue stain 0.4% (w/v) (Invitrogen Ltd., Paisley, UK) and viable cells were counted using a haemocytometer under light microscopy (Nikon TS100 inverted microscope (Nikon Corporation, Tokyo, Japan)) as described in section 2.4.3. Stromal cells were then diluted to a concentration of $5x10^4$/ml in complete EGM-2 (Lonza Biologics, Slough, UK) and seeded at

three different volumes into rat tail collagen I coated 48-well plates (BD Biosciences, Franklin Lakes, NJ, U.S.A.); 12 wells of 100µl ($5x10^3$ cells), 12 wells of 200µl ($1x10^4$ cells), and 12 wells of 400µl ($2x10^4$ cells). The plate was then incubated at 37°C in the 5% CO_2 Nuaire DH autoflow incubator (Nuaire, Plymouth, MN, U.S.A.) for 2 hours.

Cultured endothelial cells cultured in at least T25 tissue culture flasks (Corning B.V. Life Sciences, Schiphol-Rijk, The Netherlands) were washed twice with HBSS (Lonza Biologics, Slough, UK) and harvested with 0.5mg/ml Trypsin EDTA (PAA Laboratories Ltd., Yeovil, UK) as described in section 2.4.3. Cells were resuspended in 10ml complete EGM-2 (Lonza Biologics, Slough, UK). A 25µl sample of the cell solution was added to 25µl Trypan Blue stain 0.4% (w/v) (Invitrogen Ltd., Paisley, UK) and viable cells were counted using a haemocytometer under light microscopy (Nikon TS100 inverted microscope (Nikon Corporation, Tokyo, Japan)) as described in section 2.4.3. Endothelial cells were then diluted to a concentration of $1x10^4$/ml in complete EGM-2 (Lonza Biologics, Slough, UK) and seeded at four different volumes into the wells containing the stromal cells in culture to give 12 different cell concentration combinations in triplicate. These were 9 wells of 100µl ($1x10^3$ cells), 9 wells of 150µl ($1.5x10^3$ cells), 9 wells of 200µl ($2x10^3$ cells), and 9 wells of 300µl ($3x10^3$ cells). The plating arrangement is demonstrated in Figure 2.4.

The plate was then placed back in the 5% CO_2 Nuaire DH autoflow incubator (Nuaire, Plymouth, MN, U.S.A.) at 37°C for 2 weeks, with complete change of media every 2-3 days. After 2 weeks, cells were fixed by removing the media, washing the wells with 1ml/well DPBS (PAA Laboratories Ltd., Yeovil, UK) then incubating each well with 300µl 70% (v/v) ethanol (VWR International Ltd., Leicestershire, UK) in ddH_2O for 30 minutes at room temperature. The wells were then washed three times with 1ml/well DPBS (PAA Laboratories Ltd., Yeovil, UK) and stored with 500µl/well DPBS (PAA Laboratories Ltd., Yeovil, UK) until ready to stain.

$1x10^3$ Endothelial	$1.5x10^3$ Endothelial	$2x10^3$ Endothelial	$3x10^3$ Endothelial	$1x10^3$ Endothelial	$1.5x10^3$ Endothelial	$2x10^3$ Endothelial	$3x10^3$ Endothelial
$5x10^3$ Stromal	$5x10^3$ Stromal	$5x10^3$ Stromal	$5x10^3$ Stromal	$1x10^4$ Stromal	$1x10^4$ Stromal	$1x10^4$ Stromal	$1x10^4$ Stromal
$5x10^3$ Stromal	$5x10^3$ Stromal	$5x10^3$ Stromal	$5x10^3$ Stromal	$1x10^4$ Stromal	$1x10^4$ Stromal	$1x10^4$ Stromal	$1x10^4$ Stromal
$5x10^3$ Stromal	$5x10^3$ Stromal	$5x10^3$ Stromal	$5x10^3$ Stromal	$1x10^4$ Stromal	$1x10^4$ Stromal	$1x10^4$ Stromal	$1x10^4$ Stromal
$2x10^4$ Stromal	$2x10^4$ Stromal	$2x10^4$ Stromal	$2x10^4$ Stromal	x	x	x	x
$2x10^4$ Stromal	$2x10^4$ Stromal	$2x10^4$ Stromal	$2x10^4$ Stromal	x	x	x	x
$2x10^4$ Stromal	$2x10^4$ Stromal	$2x10^4$ Stromal	$2x10^4$ Stromal	x	x	x	x

Figure 2.4: Representation of stromal cell and endothelial cell co-culture combinations. Three different stromal cell concentrations and four different endothelial cell concentrations were combined to provide 12 different cell concentration combinations. Each combination was repeated in triplicate.

Tubule staining was achieved with primary mouse anti-human CD31 (Clone WM59) (AbD Serotec, Kidlington, UK) and secondary goat anti-mouse IgG (H+L) biotinylated (Vector Laboratories Inc., Burlingame, CA, U.S.A.) antibodies, Vectastain® Universal Elite® ABC Kit (Avidin and Biotinylated horseradish peroxidase macromolecular Complex) (Vector Labs, Burlingame, CA U.S.A.) and 3,3'-diaminobenzidine (DAB) substrate kit (Vector Laboratories Inc., Burlingame, CA, U.S.A.). The sequence of staining is detailed in Table 2.7.

Table 2.7: Protocol for two-dimensional sandwich co-culture tubule assay staining.

Staining stage	Volume	Incubation
2% (w/v) BSA in DPBS (Block)	500µl/well	30 minutes, room temperature
Primary mouse anti-human CD31 (Clone WM59) 1:4000 (w/v) in DPBS with 2% (w/v) BSA (Primary antibody)	250µl/well	Overnight, 4°C
Secondary goat anti-mouse IgG (H+L) biotinylated 1:200 (w/v) in DPBS with 2% (w/v) BSA (Secondary antibody)	250µl/well	60 minutes, room temperature
Peroxidase Vectastain® Universal Elite® ABC solution (10ml DPBS + 4 drops buffer A + 4 drops buffer B)	250µl/well	60 minutes, room temperature
DAB substrate solution (10ml ddH_2O + 4 drops buffer + 8 drops DAB + 4 drops hydrogen peroxide + 4 drops nickel solution)	250µl/well	5 minutes, room temperature

Tubule staining was achieved with primary mouse anti-human CD31 (Clone WM59) (AbD Serotec, Kidlington, UK) and secondary goat anti-mouse IgG (H+L) biotinylated (Vector Laboratories Inc., Burlingame, CA, U.S.A.) antibodies, Vectastain® Universal Elite® ABC Kit (Avidin and Biotinylated horseradish peroxidase macromolecular Complex) (Vector Labs, Burlingame, CA U.S.A.) and 3,3'-diaminobenzidine (DAB) substrate kit (Vector Laboratories Inc., Burlingame, CA, U.S.A.).

Between each stage the wells were washed three times with 500µl DPBS (PAA Laboratories Ltd., Yeovil, UK) for ten minutes per wash. After the final DAB stage the wells were washed three times with 500µl ddH_2O for ten minutes per wash then left exposed to air dry. Stained tubules were examined under the Nikon TS100 inverted microscope (Nikon Corporation, Tokyo, Japan) and photographed with the Nikon DS-L2 control unit (Nikon Corporation, Tokyo, Japan) for analysis using Adobe® Photoshop® CS Version 8.0 imaging software (Adobe Systems Incorporated, San Jose, CA, U.S.A.) and AngioSys Image Analysis Software (Cellworks, Buckingham, UK) as described in section 2.8.1.

Where Green Fluorescent Protein (GFP) labelled endothelial cells were used (immunofluorescent transductions described in section 2.11), the staining procedure was

omitted and tubules were examined under fluorescent microscopy using a Nikon Eclipse TS100 light microscope (Nikon Corporation, Tokyo, Japan).

The different test conditions compared using two-dimensional sandwich co-culture tubule assays are outlined in Table 2.8.

Table 2.8: Two-dimensional sandwich co-culture tubule assay test conditions.

Stromal cells	Endothelial cells	Media	Purpose
AT MSC	UCB ECFC derived cells	Complete EGM-2	Variable concentration ratios
AT MSC MV MSC HDF	UCB ECFC derived cells	Complete EGM-2	Variable concentration ratios and stromal cell source
AT MSC	UCB ECFC derived cells	Complete EGM-2 Complete EGM-2 with 25ng/ml leptin per well Complete EGM-2 with 100ng/ml leptin per well	Variable concentration ratios and addition of leptin to media
AT MSC MV MSC	UCB ECFC derived cells	Complete EGM-2 Complete EGM-2 with 25ng/ml leptin per well	Variable concentration ratios, stromal cell source and addition of leptin to media
AT MSC MV MSC	UCB ECFC derived cells	Complete EGM-2 Complete EGM-2 0.05% (w/v) perfluorocarbon Complete EGM-2 0.5% (w/v) perfluorocarbon	Variable concentration ratios, stromal cell source and addition of Pluronic® F-68 perfluorocarbon to media

Multiple variations of the two-dimensional sandwich co-culture tubule assay were set in order to test different cell types and concentrations, ratios of cell concentrations and additives to the media; Recombinant Human Leptin (R&D Systems, Abingdon, UK) and Pluronic® F-68 (Sigma Aldrich Ltd., Gillingham, UK) perfluorocarbon.

2.8.3 Three-dimensional scaffold based co-culture assay

Multiple variations of the three-dimensional scaffold based co-culture tubule assay were set up in order to test different scaffolds, cell concentrations, ratios of cell concentrations and additives to the media. The different scaffolds used and their preparation methods are outlined in Table 2.9.

Table 2.9: Scaffolds used in the three-dimensional scaffold based tubule assay.

Scaffold	Company	Preparation
Integra® Dermal Regeneration Template	Integra LifeSciences Corporation, Plainsboro, NJ, U.S.A.	Silicone 'epidermal' layer removed Punch biopsy sectioning
Matriderm®	Eurosurgical Ltd., Guildford, UK	Punch biopsy sectioning
Neuskin-F®	Medira Ltd., Sandy, UK	6mm diameter sections cut with sterile scissors
Decellularised Human Cadaveric Dermis (DHCD)	NHS Blood and Transplant, Liverpool, UK	Frozen DHCD thawed and washed by intermittent agitation in HBSS for 20 minutes 6mm diameter sections cut with sterile scissors

Four different scaffolds were used the three-dimensional scaffold based co-culture tubule assay: Integra® Dermal Regeneration Template, Matriderm®, Neuskin-F® and Decellularised Human Cadaveric Dermis (DHCD). Integra® and Matriderm® were sectioned using a 6mm biopsy punch but Neuskin-F® and DHCD sections were hand cut using sterile scissors as sections cut with the punch were too easily damaged on removal.

For each basic assay, 6mm diameter circles of scaffold were cut using a 6mm biopsy punch (Stiefel Laboratories, Durham, NC, U.S.A.) or sterile scissors depending on the scaffold properties, then placed on the bases of 36 wells of a rat tail collagen I coated 48-well plate (BD Biosciences, Franklin Lakes, NJ, U.S.A.). Stromal cells were harvested, counted and seeded onto the scaffolds in complete EGM-2 (Lonza Biologics, Slough, UK) as described for the two-dimensional sandwich assay in section 2.8.2. The plate was incubated for two hours at 37°C in the 5% CO_2 Nuaire DH autoflow incubator (Nuaire, Plymouth, MN, U.S.A.).

Endothelial cells labelled with a lentiviral vector expressing GFP (immunofluorescent transductions described in section 2.11) were then added on top of the stromal layers as described in section 2.8.2. Plates were incubated at 37°C in the 5% CO_2 Nuaire DH autoflow incubator (Nuaire, Plymouth, MN, U.S.A.) for 2 weeks, with complete change of media every 2-3 days. After 2 weeks, wells were fixed by removing the media, washing the wells with 1ml/well DPBS (PAA Laboratories Ltd., Yeovil, UK) then incubating each well with 500µl 4% (w/v) PFA (Sigma Aldrich Ltd., Gillingham, UK) for 30 minutes at room temperature. The wells were then washed three times with 1ml/well DPBS (PAA Laboratories Ltd., Yeovil, UK) and stored with 500µl/well DPBS (PAA Laboratories Ltd., Yeovil, UK) until microscopy, imaging and analysis.

Variation from the basic assay for Integra®, Matriderm® and Neuskin-F® scaffolds are discussed in the relevant results chapters and a summary of the DHCD culture variations is presented in Table 2.10.

Integra® and Matriderm® scaffolds were examined using the Zeiss LSM-510 inverted confocal microscope (Carl Zeiss Ltd., Cambridge, UK) with the LSM 5 Image Browser Version 3.2 SP2 (Carl Zeiss Ltd., Cambridge, UK). High resolution 3D images were reconstructed using Imaris Version 6.4 software (Bitplane AG, Zurich, Switzerland) and analysed using AngioSys Image Analysis Software (Cellworks, Buckingham, UK) as described in section 2.8.1.

Table 2.10: DHCD three-dimensional scaffold based co-culture tubule assay culture variations.

Variation	Stromal cells per well	GFP UCB ECFC derived cells per well	Media Additives per well
Stromal cells only	$5x10^3$ GFP AT MSC	None	None
	$1x10^4$ GFP AT MSC	None	None
	$5x10^3$ GFP MV MSC	None	None
	$1x10^4$ GFP MV MSC	None	None
	$5x10^3$ GFP HDF	None	None
	$1x10^4$ GFP HDF	None	None
Control co-cultures	$5x10^3$ AT MSC	$1x10^3$	None
	$1x10^4$ AT MSC	$1x10^3$	None
	$5x10^3$ MV MSC	$1x10^3$	None
	$1x10^4$ MV MSC	$1x10^3$	None
Leptin co-cultures	$5x10^3$ AT MSC	$1x10^3$	25ng Leptin
	$1x10^4$ AT MSC	$1x10^3$	25ng Leptin
	$5x10^3$ MV MSC	$1x10^3$	25ng Leptin
	$1x10^4$ MV MSC	$1x10^3$	25ng Leptin
Pluronic® F-68 co-cultures	$5x10^3$ AT MSC	$1x10^3$	0.05% (w/v) Perfluorocarbon
	$1x10^4$ AT MSC	$1x10^3$	0.05% (w/v) Perfluorocarbon
	$5x10^3$ MV MSC	$1x10^3$	0.05% (w/v) Perfluorocarbon
	$1x10^4$ MV MSC	$1x10^3$	0.05% (w/v) Perfluorocarbon

Four groups of culture conditions were set using the DHCD scaffold; stromal cells only, control co-cultures of AT or MV MSC with UCB ECFC derived cells, co-cultures with 25ng leptin (Invitrogen Ltd., Paisley, UK) per well and co-cultures with 0.05% (w/v) Pluronic® F-68 (Sigma Aldrich Ltd., Gillingham, UK) perfluorocarbon additive. Within each group of conditions there were different subgroups of stromal cell concentrations, and each individual condition was repeated in triplicate.

Neuskin-F® scaffolds were examined using a Nikon TS100 inverted microscope (Nikon Corporation, Tokyo, Japan) under UV light and photographed with the Nikon DS-L2 control unit (Nikon Corporation, Tokyo, Japan). Quantification using the AngioSys Image Analysis Software (Cellworks, Buckingham, UK) was not possible due to areas of endothelial cell clumping, a tendency for the vessels to wrap around the periphery of the scaffold, and detection of the scaffold background by the software. As such, a four point qualitative grading scale was developed in order to analyse the results of this assay. Grade 0 was awarded for images with

sparse or absent tubule formation, Grade 1 for images where the predominant feature was clumps of endothelial cells with or without minimal tubule formation, Grade 2 for images with mainly short individual tubules or limited patchy networks, and Grade 3 for images with longer tubules forming identifiable networks.

DHCD scaffolds were examined using the Zeiss LSM-510 inverted confocal microscope (Carl Zeiss Ltd., Cambridge, UK) with the LSM 5 Image Browser Version 3.2 SP2 (Carl Zeiss Ltd., Cambridge, UK), but image quality was limited by DHCD autofluorescence. Due to difficulties regarding quantification of three-dimensional confocal imaging, DHCD were fixed with 4% (v/v) PFA (Sigma Aldrich Ltd., Gillingham, UK) and snap frozen by immersion in liquid nitrogen. A Leica CM3050S cryostat (Leica Biosystems Ltd., Newcastle Upon Tyne, UK) was used to cut 10µm sections through the specimens and up to ten sections per scaffold were mounted on glass microscope slides (Thermo Scientific, Loughborough, UK) then examined using the Nikon TS100 inverted microscope (Nikon Corporation, Tokyo, Japan) under UV light.

2.9 Antibody array of tubule assay supernatant

A commercially available angiogenesis antibody array (Proteome Profiler™ Antibody Array – Human Angiogenesis Array Kit, R&D Systems, Abingdon, UK) designed to capture 55 different angiogenesis related proteins (Table 2.11) was used to compare expression of angiogenic factors in tubule assay co-cultures with AT versus MV MSC as the supportive stromal cell source.

Two-dimensional sandwich co-culture tubule assays with either AT or MV MSCs at $1x10^4$ per well and UCB ECFC derived cells at $1x10^3$ per well were set as per the standard assay protocol described in section 2.8.2, with three paired MSC samples and each condition repeated in duplicate. The supernatant was collected at every media change and was stored at -80°C for later analysis. Control media collected from wells without any cells was also stored at each

stage. Day 7 samples were selected for analysis since at this stage of the assay there is active tubule formation and maturation.

The nitrocellulose membranes with the capture antibodies were prepared by incubating each membrane in a well of the 4-well multi-dish with 2ml Array Buffer 7 (R&D Systems, Abingdon, UK) for one hour on a rocking platform. Each co-culture supernatant or control media sample was defrosted and 1ml of each sample was added to 0.5ml Array Buffer 4 and incubated with 15µl reconstituted Detection Antibody Cocktail (R&D Systems, Abingdon, UK) at room temperature for one hour. Array Buffer 7 (R&D Systems, Abingdon, UK) was then aspirated from each well of the 4-well multi-dish and the prepared sample/antibody mixtures were applied to the individual membranes. Lids were placed on the 4-well multi-dishes and these were incubated overnight at 4°C on a rocking platform.

Table 2.11: Proteins detected using the Proteome Profiler™ Antibody Array - Human Angiogenesis Array Kit (R&D Systems, Abingdon, UK).

Proteome Profiler™ Antibody Array – Human Angiogenesis Array Proteins (Membrane co-ordinates)				
Activin A (A5, A6)	EGF (B7, B8)	HB-EGF (C5, C6)	MMP-8 (D3, D4)	Serpin B5 (E1, E2)
ADAMTS-1 (A7, A8)	EG-VEGF (B9, B10)	HGF (C7, C8)	MMP-9 (D5, D6)	Serpin E1 (E3, E4)
Angiogenin (A9, A10)	Endoglin (B11, B12)	IGF BP-1 (C9, C10)	NRG1-β1 (D7, D8)	Serpin F1 (E5, E6)
Angiopoietin-1 (A11, A12)	Endostatin (B13, B14)	IGF BP-2 (C11, C12)	Pentraxin3 (D9, D10)	TIMP-1 (E7, E8)
Angiopoietin-2 (A13, A14)	Endothelin-1 (B15, B16)	IGF BP-3 (C13, C14)	PD-ECGF (D11, D12)	TIMP-4 (E9, E10)
Angiostatin (A15, A16)	FGF acidic (B17, B18)	IL-1 β (C15, C16)	PDGF-AA (D13, D14)	Trombospondin-1 (E11, E12)
Amphiregulin (A17, A18)	FGF basic (B19, B20)	IL-8 (C17, C18)	PDGF-AB/PDGF-BB (D15, D16)	Trombospondin-2 (E13, E14)
Artemin (A19, A20)	FGF-4 (B21, B22)	LAP(TGF-β1) (C19, C20)	Persephin (D17, D18)	uPA (E15, E16)
Coagulation Factor III (B1, B2)	FGF-7 (B23, B24)	Leptin (C21, C22)	Platelet Factor 4 (D19, D20)	Vasohibin (E17, E18)
CXCL16 (B3, B4)	GDNF (C1, C2)	MCP-1 (C23, C24)	PlGF (D21, D22)	VEGF (E19, E20)
DPP IV (B5, B6)	GM-CSF (C3, C4)	MIP-1α (D1, D2)	Prolactin (D23, D24)	VEGF-C (E21, E22)

Detectable angiogenic proteins are listed with the co-ordinates of the corresponding membrane location in brackets. Membranes also contain six positive control (A1, A2, A23, A24, F1, F2) and two negative control (F23, F24) spots on the membrane to facilitate normalisation of expression.

Following overnight incubation, each membrane was removed from the multi-dish wells and placed in an individual plastic dish with 20ml wash buffer (R&D Systems, Abingdon, UK) for ten minutes on a rocking platform. Wash buffer was replaced and the ten minute rocking repeated for a total of three washes. Streptavidin-Horse Radish Protein (HRP) was diluted in Array Buffer

5 (R&D Systems, Abingdon, UK) at a variable concentration determined on the Streptavidin-HRP vial label (Approximately 1:1000), and 1.5ml of this solution was added to each well of the cleaned and dried 4-well multi-dishes. Each membrane was removed from its wash dish, blotted and placed in a well with the diluted Streptavidin-HRP (R&D Systems, Abingdon, UK) for 30 minutes at room temperature on a rocking platform. The three times wash in 20ml wash buffer (R&D Systems, Abingdon, UK) for ten minutes was repeated, and the membranes were then blotted dry and placed on a sheet of cling film.

Chemiluminescent detection reagents (Amersham™ ECL™ Prime Western blotting detection reagent, GE Healthcare Life Sciences, Buckinghamshire, UK), which react with the Streptavidin-HRP bound to the capture antibodies, were applied to just cover the membranes, as a working solution of 50% (v/v) solution A (luminol) and 50% (v/v) solution B (peroxide) mixed immediately prior to use. The membranes were incubated at room temperature for five minutes, then the excess solution was tipped off and the edge of the membrane blotted against a tissue. Treated membranes were then sealed with another layer of cling film, the sealed package of membranes was placed in an exposure cassette (Bio-Rad Laboratories Ltd., Hertfordshire, UK) against an Amersham™ Hyperfilm™ (GE Healthcare Life Sciences, Buckinghamshire, UK) and the film was developed in the laboratory dark room. An example of the developed film is shown in Figure 2.5.

Developed films were scanned to obtain a digital image, and the intensity of the developed membrane spots was then compared using the Quantity One® 1-D Analysis Software (Bio-Rad Laboratories Ltd., Hertfordshire, UK). Relative pixel density was first corrected by subtracting the value for the negative control from each other value on the membrane. Secondary normalisation was performed against the highest value mean positive control in the series of membranes by finding the multiplication factor for each membrane mean positive control to reach the highest positive control value, and then using this multiplication factor against all

other spots on each membrane. This removed the effect of differences in developing the membranes and allowed more thorough comparisons to be made.

Media control

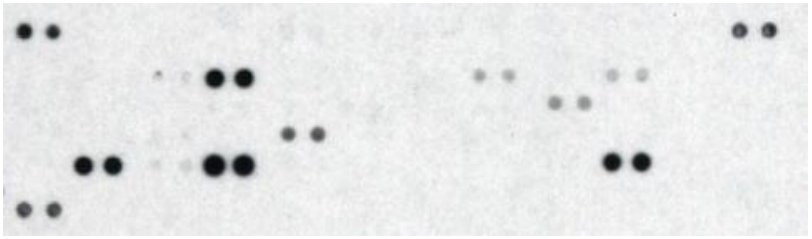

AT MSC and UCB ECFC co-culture supernatant

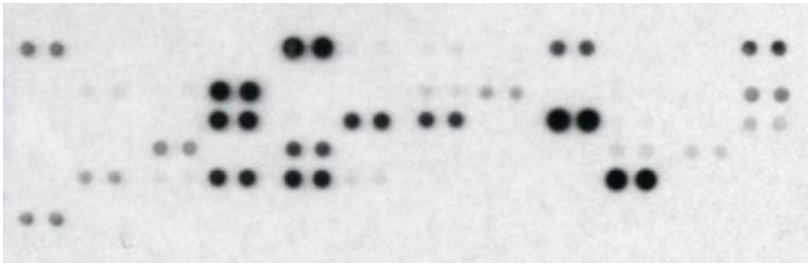

MV MSC and UCB ECFC co-culture supernatant

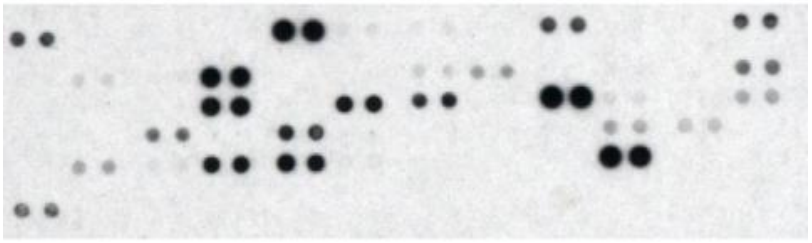

Figure 2.5: Example of developed films showing three membranes from the Proteome Profiler™ Antibody Array – Human Angiogenesis Array Kit. The variable intensity spots were developed following five minutes of exposure in the dark room, and the digital images were analysed using Quantity One® 1-D Analysis Software (Bio-Rad Laboratories Ltd., Hertfordshire, UK).

2.10 MTT cell proliferation assay

MTT (3-(4,5-Dimethylthiazol-2-yl)-2,5-diphenyltetrazolium bromide), a compound metabolised by viable cells in growth phase, was used in a colorimetric assay which determined the comparative proliferation of different cell types under different culture conditions. A summary of the different test conditions is shown in Table 2.12.

Table 2.12: Test conditions used with the MTT assay.

MTT test conditions	Cell seeding densities/well
AT versus MV MSC	500, 1000 and 2000
UCB ECFC derived cells with and without 100ng/ml leptin	250, 500 and 1000
HUVEC with and without 100ng/ml leptin	250, 500 and 1000
AT MSC with and without 100ng/ml leptin	500 and 1000
MV MSC with and without 100ng/ml leptin	500 and 1000

The MTT assay determined the comparative proliferation of different endothelial and stromal cell types with and without the addition of 100ng/ml leptin. Different cell seeding densities were chosen to optimise the range of final MTT colorimetric output.

Cells cultured to passage 5 in a T25 tissue culture flask (Corning B.V. Life Sciences, Schiphol-Rijk, The Netherlands) were washed twice with HBSS (Lonza Biologics, Slough, UK) and harvested with 0.5mg/ml Trypsin EDTA (PAA Laboratories Ltd., Yeovil, UK) as described in section 2.4.3. Cells were resuspended in 10ml complete EGM-2 (Lonza Biologics, Slough, UK). A 25µl sample of the cell solution was added to 25µl Trypan Blue stain 0.4% (w/v) (Invitrogen Ltd., Paisley, UK) and viable cells were counted using a haemocytometer under light microscopy (Nikon TS100 inverted microscope (Nikon Corporation, Tokyo, Japan)) as described in section 2.4.3. Cells were seeded at the densities recorded in Table 2.11 in triplicate wells of a rat tail collagen I coated 96-well plates (BD Biosciences, Franklin Lakes, NJ, U.S.A.) in 200µl complete EGM-2 (Lonza Biologics, Slough, UK). Triplicate media only wells were included as controls for later colorimetric analysis. Plates were incubated overnight at 37°C in the 5% CO_2 Nuaire DH autoflow incubator (Nuaire, Plymouth, MN, U.S.A.). On day one, wells set to test the effect of the pro-angiogenic protein leptin had 10µl of 1mg/ml Recombinant Human Leptin (R&D Systems, Abingdon, UK) added to the media, and the plate was returned to the 5% CO_2 Nuaire DH autoflow incubator (Nuaire, Plymouth, MN, U.S.A.) at 37°C.

On day four, 50µl 2mg/ml MTT (Sigma Aldrich Ltd., St Louis, MO, U.S.A.) in HBSS (Lonza Biologics, Slough, UK) was added to each well and the plate placed back in the 5% CO_2 Nuaire

DH autoflow incubator (Nuaire, Plymouth, MN, U.S.A.) at 37°C for 4 hours. Media was then aspirated and 100µl 10% dimethyl sulfoxide (DMSO) (Sigma Aldrich Ltd., Gillingham, UK) was added to each well with gentle shaking to dissolve the formazan crystals. The light absorbance through the dye in each well was then measured on a Model 680 microplate reader (Bio-Rad Laboratories Ltd., Hertfordshire, UK), using a wavelength of A_{570} to provide comparative data for quantification.

2.11 GFP and DSRed labelling of endothelial and mesenchymal cells

Lentiviral vector particles expressing either green fluorescent protein (GFP) or DSRed fluorescent protein (DSRed) were prepared to label endothelial and mesenchymal cells in order to monitor tubule formation in the three dimensional (3D) co-cultures. The plasmid containing the DSRed expressing lentiviral vector genome was kindly provided by Antoine A.F. de Vries (Department of Molecular Cell Biology, Leiden University Medical Center, Wassenaarseweg 72, 2333 AL Leiden, the Netherlands). The plasmid containing the GFP-expressing lentiviral vector genome, together with the lentiviral vector packaging and envelope constructs were kindly provided by Professor Adrian Thrasher (University College London, UK) and had been prepared as described by Demaison *et al*. (199). The procedures for the production of these lentiviral constructs are described below.

2.11.1 Transformation of JM109 *E. coli* competent cells with plasmid DNA

Luria Broth (LB) agar plates were prepared by filling 10cm round plastic culture dishes (Corning B.V. Life Sciences, Schiphol-Rijk, The Netherlands) with approximately 25ml tepid liquid sterile LB agar (1l distilled water, 10g Tryptone, 15g Agar, 5g Yeast extract, 10g NaCl) (Sigma Aldrich Ltd., Gillingham, UK) in the vicinity of a blue Bunsen burner flame. Chloramphenicol (Sigma

Aldrich Ltd., Gillingham, UK) was added to each dish at a concentration of 1µg/ml and the plates were stored upside down at room temperature for one hour to set.

E. coli JM109 competent bacteria (Stratagene, Agilent Technologies UK Ltd., Wokingham, UK) and pUC18 control plasmid (0.1ng/µl in TE buffer) (Stratagene, Agilent Technologies UK Ltd., Wokingham, UK) were retrieved from -80°C storage and kept on ice to thaw along with the DSRed plasmid DNA from -20°C storage. Three pre-chilled 1.5ml Eppendorf tubes (Eppendorf UK Limited, Stevenage, UK) were prepared as per Table 2.13.

Table 2.13: Preparation of bacteria for plasmid DNA amplification.

Tube number	Contents	Role
1	100µl JM109 + 1µl PUC18 at 0.1ng/µl	Positive control
2	100µl JM109 + 0.5µl DSRed at 1.85µg/ml	Plasmid DNA amplification
3	50µl JM109	Negative control

Pre-chilled Eppendorf tubes were prepared with E. coli JM109 competent bacteria with either pUC18 positive control plasmid or DSRed lentivirus, or with no additional additives as a negative control.

The prepared tubes were kept on ice for 20 minutes, immersed in the SUB Aqua Pro 5 water bath (Grant Instruments Ltd., Cambridgeshire, UK) at 42°C for 1 minute, and then immediately placed back in ice for 10 minutes to induce heat shock. S.O.C. media (2% (w/v) tryptone, 0.5% (w/v) yeast extract, 10mM/l sodium chloride, 2.5mM/l potassium chloride, 10mM/l magnesium chloride, 10mM/l magnesium sulphate, 20mM/l glucose) (Invitrogen Ltd., Paisley, UK), pre-heated to 37°C in a 5% CO_2 Innova 4200 incubator (New Brunswick Scientific, Enfield, CT, U.S.A.), was added at 900µl per tube. The bacterial cell suspensions were transferred to 50ml Falcon tubes (BD Biosciences, Franklin Lakes, NJ, U.S.A.) and incubated for one hour at 37°C in a 5% CO_2 Innova 4200 incubator (New Brunswick Scientific, Enfield, CT, U.S.A.) with agitation at 215rpm. Eight chloramphenicol agar plates were then plated with the transformed bacteria – four for each of the JM109 with DSRed and the JM109 cells with PUC18 bacteria

using volumes of 150µl, 100µl, 50µl and 25µl. A ninth agar plate had the JM109 cells alone applied as the negative control. Bacteria were pipetted onto the centre of the plate then spread with a sterile metal spreader in three directions, sterilising the spreader with ethanol (VWR International Ltd., Leicestershire, UK) and the Bunsen flame three times between plates. The bacterial plates were incubated overnight in the 37°C 5% CO_2 Innova 4200 incubator (New Brunswick Scientific, Enfield, CT, U.S.A.).

The next day, the agar plate seeded with bacteria transformed with 25µl of DSRed plasmid DNA had the best distribution of Chloramphenicol-resistant bacterial colonies and ten of these were lifted with a pipette tip and suspended in 3ml LB (500ml distilled water, 5g Tryptone, 2.5g Yeast extract, 5g NaCl) (Sigma Aldrich Ltd., Gillingham, UK) in individual 15ml Falcon tubes (BD Biosciences, Franklin Lakes, NJ, U.S.A.). The tubes were then incubated overnight in the 37°C 5% CO_2 Innova 4200 incubator (New Brunswick Scientific, Enfield, CT, U.S.A.) with agitation at 215rpm. The bacterial plate was wrapped and stored in the 4°C cold room and all other plates were discarded.

Following overnight incubation, all ten of the bacterial cultures had become cloudy, signalling bacterial growth. Three tubes were randomly selected for plasmid DNA isolation and preparation.

2.11.2 Mini preparation of DSRed plasmid DNA

The Invitrogen PureLink™ HiPure Plasmid DNA Purification Kit for Mini Preparation of Plasmid DNA (Invitrogen Ltd., Paisley, UK) was used as per manufacturers' instructions to elute and precipitate the plasmid DNA for DNA gel electrophoresis analysis.

Firstly, the PureLink™ HiPure Mini column was placed on the PureLink™ Nucleic Acid Purification Rack. The column was equilibrated by adding 2ml Equilibration Buffer (EQ1) to the column and allowing it to drain by gravity.

The cell lysate was prepared by centrifuging the 15ml Falcon tube containing *E. coli* JM109 transformed with DSRed plasmid at 4000g for 10 minutes at room temperature in a Heraeus Megafuge 1.0S centrifuge (DJB Labcare, Newport Pagnell, UK). The supernatant was discarded and the cell pellet resuspended in 0.4ml Resuspension Buffer (R3) with RNase A until homogenous. This solution was transferred to a microcentrifuge tube and 0.4ml Lysis Buffer (L7) was added before mixing by gentle inversion of the capped tube. The mixed solution was incubated at room temperature for 5 minutes. After 5 minutes, 0.4ml Precipitation Buffer (N3) was added and mixed by gentle inversion until homogenous. The lysate was then centrifuged at 12000g for 10 minutes at room temperature in the Heraeus Megafuge 1.0S centrifuge (DJB Labcare, Newport Pagnell, UK).

The final cell lysate supernatant was loaded onto the equilibrated HiPure Mini column and allowed to drain under gravity. The column was then washed twice by loading 2.5ml wash buffer (W8) onto the column and allowing it to drain under gravity. The flow-through from the supernatant and both washes were discarded. Next a microcentrifuge tube was placed under the column and 0.9ml Elution Buffer (E4) was loaded on top. The solution was allowed to drain under gravity and the column was discarded. The tube containing the eluted, purified plasmid DNA had 0.63ml isopropanol (Sigma Aldrich Ltd., Gillingham, UK) added, was mixed by inversion, then centrifuged at 12000g for 30 minutes at 4°C in the Heraeus Megafuge 1.0S centrifuge (DJB Labcare, Newport Pagnell, UK). The resultant supernatant was discarded and the DNA pellet was resuspended in 1ml 70% ethanol (VWR International Ltd., Leicestershire, UK) and centrifuged under the same conditions. Again the resultant supernatant was discarded, the pellet was allowed to air dry for 10 minutes, and then the DNA pellet was

washed in 50µl TE Buffer (10mM Tris-Cl, pH 7.5 with 1mM EDTA) ready for analysis by gel electrophoresis.

2.11.3 DNA gel electrophoresis of DSRed vector

DNA gel electrophoresis was performed on digested and non-digested plasmid DNA samples to confirm the identity of the plasmid DNA isolated from *E. coli* transformed cells (Stratagene, Agilent Technologies UK Ltd., Wokingham, UK).

A 1% (w/v) agarose DNA running gel was prepared using 1g agarose (Lonza Biologics, Slough, UK), 100ml Tris Acetate-EDTA (TAE) Buffer (Lonza Biologics, Slough, UK) and 100µl SYPRO® Red Protein Gel Stain (Lonza Biologics, Slough, UK), heated in a microwave until homogenous then set in a gel dock (Bio-Rad Laboratories Ltd., Hertfordshire, UK) with a comb to create a row of wells.

Plasmid DNA digestion was performed to confirm its identity by selecting restriction endonucleases known to have cleavage sites (sequences) in the plasmid DNA. The full plasmid DNA sequence was entered into the NEBcutter Version 2 online software (New England BioLabs, Hertfordshire, UK [available at http://tools.neb.com/NEBcutter]) as described by Vince *et al.* (200), and this provided a restriction enzyme map and theoretical digest using the endonuclease enzyme EcoR1 (New England BioLabs, Hertfordshire, UK). The map and digest are shown in Figure 2.6, which would digest the 9186db sequence into two fragments of 6562db and 2624db.

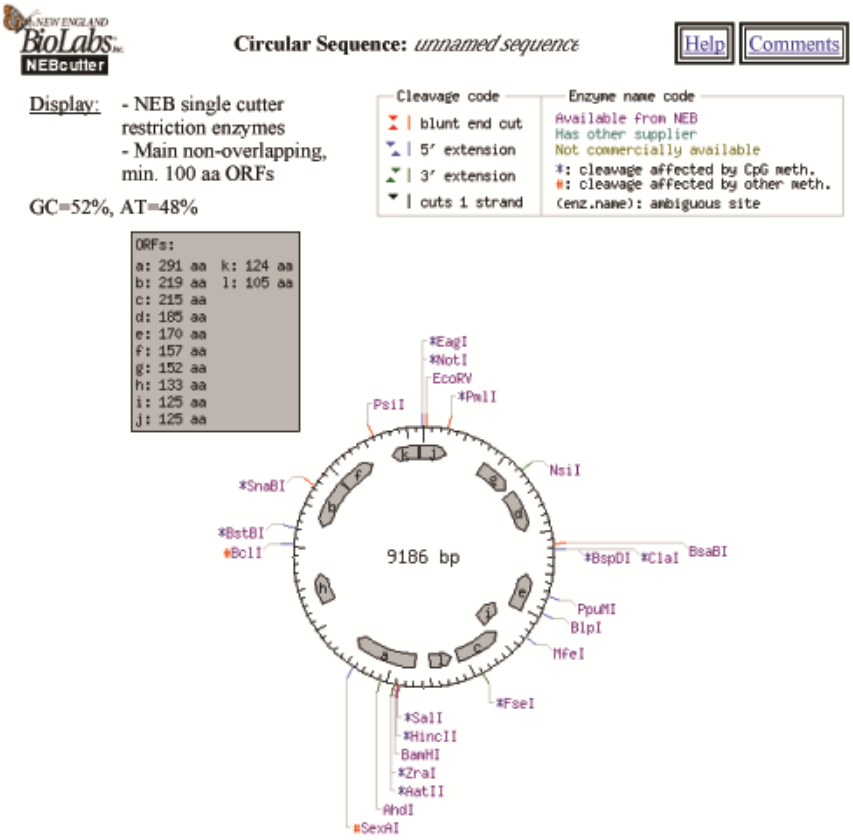

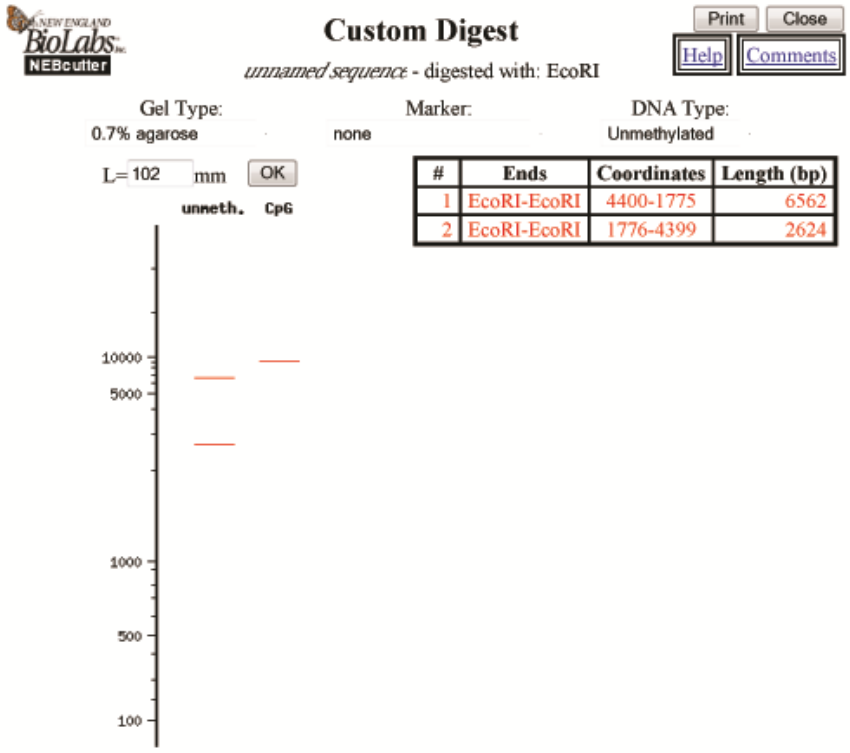

Figure 2.6: Restriction enzyme map of the DSRed plasmid and theoretical digest using the endonuclease enzyme EcoR1. Images are screenshots from the NEBcutter Version 2 online software.

Non-digested DNA was prepared to run in the agarose gel by adding 1µl DNA (1µl/ml) to 19µl nuclease free water (Invitrogen Ltd., Paisley, UK) in a 1.5ml Eppendorf tube (Eppendorf UK Limited, Stevenage, UK). Restriction endonuclease digestion was prepared by adding 1µl DNA (1µl/ml), 2.5µl RNase H Reaction Buffer (50mM Tris-HCl, 75mM KCl, 3mM $MgCl_2$, 10mM DTT, pH 8.3) (New England BioLabs, Hertfordshire, UK) and 1µl EcoR1 enzyme (New England BioLabs, Hertfordshire, UK) to 19µl nuclease free water (Invitrogen Ltd., Paisley, UK) in a 1.5ml Eppendorf tube (Eppendorf UK Limited, Stevenage, UK). Both tubes were incubated for one hour at 37°C in the SUB Aqua Pro 5 water bath (Grant Instruments Ltd., Cambridgeshire, UK).

Loading buffer (New England BioLabs, Hertfordshire, UK) was added to each sample at 5µl per tube and each sample was added to a well in the pre-prepared 1% agarose gel. An additional well was loaded with HyperLadder™ 1kb (Bioline Reagents Limited, London, UK), a molecular weight marker which produces 14 regularly spaced bands ranging from 200bp to 10037bp. The gel dock (Bio-Rad Laboratories Ltd., Hertfordshire, UK) was connected to a power supply (Bio-Rad Laboratories Ltd., Hertfordshire, UK) and run at 115 volts for 45 minutes. The gel was then disconnected from the electricity and placed in a UV box to develop the DNA gel electrophoresis image. An example is shown in Figure 2.7. Comparison with the HyperLadder™ 1kB molecular weight marker (Bioline Reagents Limited, London, UK) allowed identification of the 9186bp DNA band in all three undigested samples and two fragments of 6562bp and 2624bp in the three corresponding digested samples. Sample number 6 was selected for further amplification of the DSRed plasmid DNA for mammalian cell transfection.

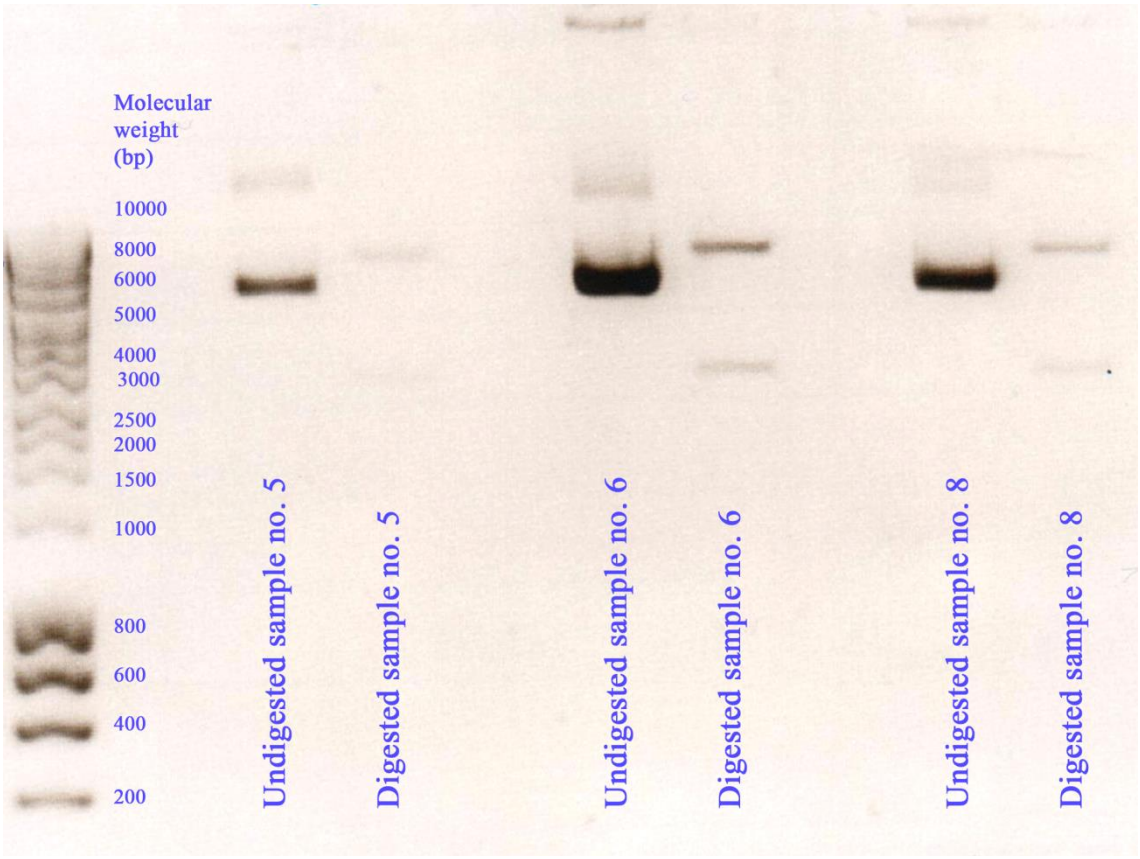

Figure 2.7: Developed gel electrophoresis image for plasmid DNA eluted from three different bacterial cultures. The HyperLadder™ 1kB molecular weight marker is on the left hand side of the image and allowed identification of the 9186bp DNA band in the undigested samples and two bands of 6562bp and 2624bp in the digested samples.

2.11.4 Maxi preparation of DSRed plasmid DNA

The process of transforming *E. coli* JM109 competent cells with the DSRed plasmid DNA was repeated as described in section 2.11.1 on a fresh chloramphenicol agar plate (10cm round plastic culture dish (Corning B.V. Life Sciences, Schiphol-Rijk, The Netherlands) with approximately 25ml tepid liquid Luria agar (1% (w/v) Tryptone, 1.5% (w/v) Agar, 0.5% (w/v) Yeast extract, 1% (w/v) NaCl in distilled water) (Sigma Aldrich Ltd., Gillingham, UK) with 1µg/ml Chloramphenicol (Sigma Aldrich Ltd., Gillingham, UK)). One colony was expanded in 3ml LB (1% (w/v) Tryptone, 0.5% (w/v) Yeast extract, 1%NaCl (w/v) in distilled water) (Sigma Aldrich Ltd., Gillingham, UK) in a 15ml Falcon tube (BD Biosciences, Franklin Lakes, NJ, U.S.A.) incubated at 37°C in the 5% CO_2 Innova 4200 incubator (New Brunswick Scientific, Enfield, CT, U.S.A.) with

agitation at 215rpm for 6 hours. The resulting bacterial culture was then divided between two large conical flasks filled with 200ml Luria broth (1% (w/v) Tryptone, 0.5% (w/v) Yeast extract, 1%NaCl (w/v) in distilled water) (Sigma Aldrich Ltd., Gillingham, UK) and incubated with agitation at 215rpm overnight in the 5% CO_2 Innova 4200 incubator (New Brunswick Scientific, Enfield, CT, U.S.A.) at 37°C. The next day the flask contents were each transferred to a 250ml polypropylene conical bottom centrifuge tube (Corning B.V. Life Sciences, Schiphol-Rijk, The Netherlands), centrifuged at 4000g for ten minutes in the Heraeus Megafuge 1.0S centrifuge (DJB Labcare, Newport Pagnell, UK) at room temperature, and the supernatants discarded.

The Invitrogen PureLink™ HiPure Plasmid Filter Purification Kit for Maxi Preparation of Plasmid DNA (Invitrogen Ltd., Paisley, UK) was used as per manufacturers' instructions to elute and precipitate the DSRed plasmid DNA for lentiviral particle production.

Firstly, the PureLink™ HiPure Filter Maxi column was placed on the PureLink™ Nucleic Acid Purification Rack. The column was equilibrated by adding 30ml Equilibration Buffer (EQ1) directly into the filtration cartridge within the column and allowing it to drain by gravity.

The cell pellets from both of the centrifuged 250ml polypropylene conical bottom centrifuge tubes (Corning B.V. Life Sciences, Schiphol-Rijk, The Netherlands) were resuspended together in 10ml Resuspension Buffer (R3) with RNase A until homogenous, then 10ml Lysis Buffer (L7) was added before mixing by gentle inversion of the capped tube. The mixed solution was incubated at room temperature for 5 minutes. After 5 minutes, 10ml Precipitation Buffer (N3) was added and mixed by gentle inversion until homogenous.

The precipitated lysate was loaded onto the equilibrated HiPure Filter Maxi column and allowed to drain under gravity. The column was then washed by loading 10ml wash buffer (W8) onto the column and allowing it to drain under gravity. The flow-through from the precipitated lysate and wash were discarded. Next a 50ml centrifuge tube was placed under the column and 15ml Elution Buffer (E4) was loaded on top. The solution was allowed to drain

under gravity and the column was discarded. The tube containing the eluted, purified DNA had 10.5ml isopropanol (Sigma Aldrich Ltd., Gillingham, UK) added, was mixed by hand, then centrifuged at 12000g for 30 minutes at 4°C in the Heraeus Megafuge 1.0S centrifuge (DJB Labcare, Newport Pagnell, UK). The resultant supernatant was discarded and the DNA pellet was resuspended in 5ml 70% ethanol (VWR International Ltd., Leicestershire, UK). Again the resultant supernatant was discarded, the pellet was allowed to air dry for 10 minutes, and then the DNA pellet of the DSRed plasmid was resuspended in 200µl TE Buffer (10mM Tris-Cl, pH 7.5 with 1mM EDTA).

2.11.5 Lentiviral vector particle production

Eight T150 tissue culture flasks (Corning B.V. Life Sciences, Schiphol-Rijk, The Netherlands) were seeded with $1x10^7$ HEK293FT cells (Invitrogen Ltd., Paisley, UK) in 30ml complete HEK293FT culture media (DMEM with 10% (v/v) FBS, 0.1mM MEM NEAA, 6mM L-glutamine and 1mM MEM Sodium Pyruvate) (Invitrogen Ltd., Paisley, UK) and cultured overnight at 37°C in the 5% CO_2 Nuaire DH autoflow incubator (Nuaire, Plymouth, MN, U.S.A.). The next day the media was replaced with 30ml complete HEK293FT culture media (DMEM with 10% (v/v) FBS, 0.1mM MEM NEAA, 6mM L-glutamine and 1mM MEM Sodium Pyruvate) (Invitrogen Ltd., Paisley, UK) containing 500µg/ml Geneticin (Invitrogen Ltd., Paisley, UK).

The DSRed plasmid eluted and purified in section 2.11.4 was analysed using a NanoDrop Microvolume UV-Vis Spectrophotometer (Thermo Fisher Scientific Inc., Wilmington, DE, U.S.A.) in order to measure the concentration and purity. The spectrophotometer was calibrated using 1µl nuclease free water (Invitrogen Ltd., Paisley, UK) then 1µl DNA was applied to the sensor. The initial concentration of the sample was 4977.4ng/µl and further dilution in TE Buffer (10mM Tris-Cl, pH 7.5 with 1mM EDTA) (Invitrogen Ltd., Paisley, UK) and re-testing achieved a concentration of 1167.6ng/µl (target 1µg/µl). Absorbance of the sample at 230nm, 260nm and

280nm was measured and used to determine DNA purity. The absorbance ratios were 1.87 for 260/280 and 2.29 for 260/230.

Lentiviral vector particle production was achieved by three plasmid co-transfection in HEK293TF. The three plasmids are the lentiviral vector genome expression plasmid (DSRed plasmid), the packaging plasmid and the envelope plasmid. Eight pairs of two separate 15ml Falcon tubes (BD Biosciences, Franklin Lakes, NJ, U.S.A.) were prepared with reagents as per Table 2.14.

Table 2.14: Preparation of reagents for transfection of HEK293FT cells.

Tube 1		**Tube 2**	
Reagent	**Role**	**Reagent**	**Role**
3.75ml OptiMEM® I medium (Invitrogen Ltd., Paisley, UK)	Reduced serum medium	3.75ml OptiMEM® I medium (Invitrogen Ltd., Paisley, UK)	Reduced serum medium
50µg DSRed plasmid (Antoine A. F. de Vries, Leiden University Medical Centre, the Netherlands)	Lentiviral vector genome expressing DSRed fluorescent protein	200µl Lipofectamine™ 2000 (Invitrogen Ltd., Paisley, UK)	Lipid-based transfection reagent
17.5µg pVSV-G (Adrian Thrasher, University College London, UK)	Plasmid expressing the envelope glycoprotein		
32.5µg pΔ8.91 (gag/pol) (Adrian Thrasher, University College London, UK)	Plasmid expressing the HIV-gag/pol protein for vector packaging		

OptiMEM® I medium with DSRed plasmid, pVSV-G envelope construct and pΔ8.91 (gag/pol) packaging construct in tube 1 was combined with OptiMEM® I medium with Lipofectamine™ 2000 in tube 2 and incubated for 20 minutes at room temperature immediately prior to addition to 70% confluent HEK293FT cells in complete HEK293FT culture media with Geneticin.

Each paired tube 1 solution was added to tube 2 and the solutions were mixed gently by inverting the tubes 5 times. The solutions were then incubated at room temperature for 20 minutes to allow the lipid-DNA complexes to form, and one each added to the T150 tissue culture flasks (Corning B.V. Life Sciences, Schiphol-Rijk, The Netherlands) of 70% confluent HEK293FT cells (Invitrogen Ltd., Paisley, UK) in 30ml complete HEK293FT culture media (DMEM with 10% (v/v) FBS, 0.1mM MEM NEAA, 6mM L-glutamine and 1mM MEM Sodium Pyruvate) (Invitrogen Ltd., Paisley, UK) containing 500µg/ml Geneticin (Invitrogen Ltd., Paisley, UK). The flasks were labelled as biohazardous and incubated overnight at 37°C in a 5% CO_2 Nuaire DH autoflow incubator (Nuaire, Plymouth, MN, U.S.A.) dedicated for use with genetically modified cells. The next morning the media was changed for 15ml fresh complete HEK293FT culture media (DMEM with 10% (v/v) FBS, 0.1mM MEM NEAA, 6mM L-glutamine and 1mM MEM Sodium Pyruvate) (Invitrogen Ltd., Paisley, UK) containing 500µg/ml Geneticin (Invitrogen Ltd., Paisley, UK) and placed back in the 5% CO_2 Nuaire DH autoflow incubator (Nuaire, Plymouth, MN, U.S.A.) dedicated for use with viral samples at 37°C for 48 hours.

2.11.6 Harvest and titration of DSRed lentiviral particles

After 48 hours of incubation post transfection, media were aspirated from the T150 tissue culture flasks (Corning B.V. Life Sciences, Schiphol-Rijk, The Netherlands), transferred to 50ml Falcon tubes (BD Biosciences, Franklin Lakes, NJ, U.S.A.) and centrifuged at 1200rpm for five minutes at room temperature in a Hettich Rotina 46R centrifuge (DJB Labcare, Newport Pagnell, UK) to remove any cell debris. The supernatant was then decanted into fresh 50ml Falcon tubes (BD Biosciences, Franklin Lakes, NJ, U.S.A.) and aliquots of 1ml lentiviral particles containing media were transferred to 2ml cryogenic vials (Corning B.V. Life Sciences, Schiphol-Rijk, The Netherlands) and frozen at -80°C.

HEK293FT cells (Invitrogen Ltd., Paisley, UK) were transduced with the DSRed lentiviral particles in order to determine their viral titre. Twelve wells of $4x10^4$ and 12 wells of $8x10^4$ HEK293FT cells (Invitrogen Ltd., Paisley, UK) were plated in 12-well plates (BD Biosciences, Franklin Lakes, NJ, U.S.A.) in 1ml complete HEK293FT culture media (DMEM with 10% (v/v) FBS, 0.1mM MEM NEAA, 6mM L-glutamine and 1mM MEM Sodium Pyruvate) (Invitrogen Ltd., Paisley, UK) containing 500µg/ml Geneticin (Invitrogen Ltd., Paisley, UK) per well. The plates were incubated overnight at 37°C in a 5% CO_2 Nuaire DH autoflow incubator (Nuaire, Plymouth, MN, U.S.A.). One vial of DSRed lentiviral particle containing media was defrosted at 37°C in the 5% CO_2 Nuaire DH autoflow incubator (Nuaire, Plymouth, MN, U.S.A.) dedicated for use with viral samples. The lentiviral media underwent serial dilution with complete HEK293FT culture media (DMEM with 10% (v/v) FBS, 0.1mM MEM NEAA, 6mM L-glutamine and 1mM MEM Sodium Pyruvate) (Invitrogen Ltd., Paisley, UK) containing 500µg/ml Geneticin (Invitrogen Ltd., Paisley, UK) to obtain different dilution factors for transduction. Lentiviral particles at dilutions of $1x10^{-3}$, $1x10^{-4}$, $1x10^{-5}$ and $1x10^{-6}$ were applied to triplicate wells of each 12-well plate (BD Biosciences, Franklin Lakes, NJ, U.S.A.) with cultured HEK293FT cells (Invitrogen Ltd., Paisley, UK). The plates were then incubated at 37°C in the 5% CO_2 Nuaire DH autoflow incubator (Nuaire, Plymouth, MN, U.S.A.) dedicated for use with genetically modified cells for a further 24 hours. After 24 hours, the number of transduced cells or colonies in each well was counted using the Nikon TS100 inverted microscope (Nikon Corporation, Tokyo, Japan) under UV light.

The viral titre was based on the most consistent triplicate wells and calculated using the equation:

Titre = Number of transduced cell or colonies per well / Dilution factor

= Transducing Units (TU)/ml

The viral titre for DSRed lentivirus was approximately $7x10^4$ TU/ml.

2.11.7 GFP lentiviral vector particle production

GFP-expressing lentiviral genome construct as well as the packaging and envelope constructs were provided by Professor Adrian Thrasher of University College London and had been prepared as described by Demaison *et al*. (199). Tranfection of eight T150 tissue culture flasks (Corning B.V. Life Sciences, Schiphol-Rijk, The Netherlands) seeded with $1x10^7$ HEK293FT cells (Invitrogen Ltd., Paisley, UK) was performed as per section 2.11.5, substituting 50µg GFP lentiviral vector plasmid for the DSRed plasmid when the reagents were prepared as per Table 2.13. GFP lentiviral particles were harvested, stored and titrated to calculate their viral titre as per section 2.11.6. The viral titre of GFP lentiviral vector particles was estimated as $3x10^6$ TU/ml.

2.11.8 Transduction of stromal and endothelial cells with GFP and DSRed lentiviral particles

AT MSC were plated in 12 wells of a 24 well plate at $1.2x10^4$ cells per well of a rat tail collagen I coated 24-well plate (BD Biosciences, Franklin Lakes, NJ, U.S.A.) in 2ml per well complete EGM-2 (Lonza Biologics, Slough, UK). Plates were placed in the 5% CO_2 Nuaire DH autoflow incubator (Nuaire, Plymouth, MN, U.S.A.) at 37°C and incubated overnight. The next morning, GFP lentiviral particles were applied to the wells at various multiplicity of infection (MOI). The MOI is the number of viral particles applied per cell, and the values selected were two wells each of MOI 0, 1, 2, 3, 4 and 5. Plates were returned to the 5% CO_2 Nuaire DH autoflow incubator (Nuaire, Plymouth, MN, U.S.A.) dedicated for use with genetically modified cells for a further 24 hours at 37°C. After 24 hours the media was replaced with 2ml per well complete EGM-2 (Lonza Biologics, Slough, UK), and following 48 hours further incubation in the 5% CO_2 Nuaire DH autoflow incubator (Nuaire, Plymouth, MN, U.S.A.) at 37°C, the number of transduced cells

or colonies in each well was counted using the Nikon TS100 inverted microscope (Nikon Corporation, Tokyo, Japan) under UV light.

Transduction of AT MSC, MV MSC, ECFC derived cells and HUVEC was then performed at an MOI 3, as these wells showed approximately or >75% of the cells were transduced at 72 hours without significant loss of viability. GFP expressing cells were transduced as required by adding 1ml GFP lentivirus per 10^6 cells (viral titre=$3x10^6$ TU/ml) cultured overnight in a T150 tissue culture flask (Corning B.V. Life Sciences, Schiphol-Rijk, The Netherlands) with 30ml complete EGM-2 (Lonza Biologics, Slough, UK) in the 5% CO_2 Nuaire DH autoflow incubator (Nuaire, Plymouth, MN, U.S.A.) at 37°C. After 24 hours the lentiviral media was discarded and replaced with 30ml fresh complete EGM-2 (Lonza Biologics, Slough, UK) and culture was continued in the 5% CO_2 Nuaire DH autoflow incubator (Nuaire, Plymouth, MN, U.S.A.) at 37°C until cells were confluent for storage, further passage or experimental use.

MOI was determined for DSRed lentiviral particles using AT MSC plated in 16 wells of a 24 well plate at $1.2x10^4$ cells per well of a rat tail collagen I coated 24-well plate (BD Biosciences, Franklin Lakes, NJ, U.S.A.) in 2ml per well complete EGM-2 (Lonza Biologics, Slough, UK). Plates were placed in the 5% CO_2 Nuaire DH autoflow incubator (Nuaire, Plymouth, MN, U.S.A.) at 37°C and incubated overnight. The next morning, DSRed lentiviral particles were applied to the wells in duplicate at MOI of 0, 5, 10 and 15, and then again in duplicate at the same MOIs with the addition of 1µl/well 100mg/ml Polybrene® (1,5-dimethyl-1,5-diazaundecamethylene) (Sigma Aldrich Ltd., Gillingham, UK), a cationic polymer which decreases electrostatic repulsion of the viral particles from the cell surface as described by Lin *et al.* (201). Plates were returned to the 5% CO_2 Nuaire DH autoflow incubator (Nuaire, Plymouth, MN, U.S.A.) dedicated for use with genetically modified cells for a further 24 hours at 37°C. After 24 hours the media were replaced with 2ml per well complete EGM-2 (Lonza Biologics, Slough, UK), and following 48 hours further incubation in the 5% CO_2 Nuaire DH autoflow incubator (Nuaire, Plymouth, MN,

U.S.A.) at 37°C, the number of transduced cells or colonies in each well was counted using a Nikon TS100 inverted microscope (Nikon Corporation, Tokyo, Japan) under UV light.

Transduction of AT MSC and MV MSC was then performed at MOI 5 with 1µl 100mg/ml Polybrene® (Sigma Aldrich Ltd., Gillingham, UK), as this was the lowest MOI to achieve approximately 70% transduction efficiency. Without the addition of Polybrene® (Sigma Aldrich Ltd., Gillingham, UK), no transduction was achieved for AT MSC and MV MSC. DSRed expressing cells were transduced as required by adding 7ml DSRed lentiviral vector particles and 1µl 100mg/ml Polybrene® (Sigma Aldrich Ltd., Gillingham, UK) per 10^5 cells (viral titre=$7x10^4$ TU/ml) cultured overnight in a T25 tissue culture flask (Corning B.V. Life Sciences, Schiphol-Rijk, The Netherlands) with 5ml complete EGM-2 (Lonza Biologics, Slough, UK) in the 5% CO_2 Nuaire DH autoflow incubator (Nuaire, Plymouth, MN, U.S.A.) at 37°C. After 24 hours the lentiviral particle containing media was discarded and replaced with 7ml fresh complete EGM-2 (Lonza Biologics, Slough, UK) and culture was continued in the 5% CO_2 Nuaire DH autoflow incubator (Nuaire, Plymouth, MN, U.S.A.) at 37°C until cells were confluent for storage, further passage or experimental use.

2.12 Statistical analysis

Data were described as mean ± standard error of the mean for continuous values in order to show the standard deviation of the sample distribution. Each condition in each assay was repeated in triplicate unless otherwise stated in order to provide mean values for each data set.

Correlation between number of MNC plated from UCB and PB and yield of ECFC colonies was analysed using the Spearman rank correlation coefficient, which is a nonparametric test of dependence between two variables which allows for strong outliers. The correlation between placental weight and yield of ECFC colonies from UCB units was analysed using a linear model

regression, which is a test of dependence between a single scalar variable (colony yield) and an explanatory variable (placental weight). Units with zero colony yield were excluded, then the remaining data were transformed by Box-Cox transformation in order to achieve a normal distribution whilst maintaining data rank. This stabilised the variance and allowed the linear model regression to be applied.

The two-tailed Student's T Test was used to determine the significance of differences between normally distributed data against a t distribution. Data from cultures under different conditions such as total tubule length or number of tubule junctions in the two-dimensional sandwich co-culture tubule assay were compared as independent samples, whereas analysis of differences between AT MSC and MV MSC were compared as paired samples since the cultured cells originated from the same donor tissue.

Chapter 3 Endothelial Colony Forming Cell Sources for Clinical Applications

3.1 Background

Both endothelial and mesenchymal stromal cell sources are required for the creation of microvascular networks *in vitro* (135). The ideal cell sources for clinical applications are autologous, easily obtainable and reliably reproducible in culture.

Allogeneic cells must be typed and matched to the patient to minimise the risks of rejection (130-132, 202), and despite thorough screening there is still a risk of transmission of infection from donor to patient (133, 134, 203). These risks are mostly eliminated with the use of autologous cells, although there is still a risk of infection if cells are cultured prior to transplant. The proposed recipient patients of pre-vascularised dermal substitutes may be those suffering from acute, severe burn injuries, and this limits the autologous tissues which may be available for harvest and *in vitro* culture. For example, many patients with large body surface area burns require blood transfusions due to blood loss and fluid compartment shift, making venesection of large volumes of peripheral blood impractical (109, 110). However, previous work in our research laboratory suggested that there was a peak concentration of proangiogenic cells in peripheral blood at 24 hours post burn injury, as these cells are mobilised from bone marrow (56), and it remains unclear if appropriate timing of venesection may allow culture of endothelial cells from a relatively small volume of peripheral blood.

As these severe burn patients mount a systemic response to their injuries by mobilising cells from bone marrow (32), this too may be an unacceptable source tissue to harvest, as it is needed *in vivo* for patient survival.

Adipose tissue is a well-established source of mesenchymal stromal cells, and some recent work has also shown that endothelial cells may be cultured from the same source (111). Even in patients with acute, large body surface area burns there should be an availability of adipose tissue which could be harvested without difficulty from directly underneath the burn eschar or by minimally invasive liposuction at an undamaged anatomical site. This could be harvested under general anaesthesia at the first burn wound debridement in the operating theatre, which should be performed within 24 to 48 hours of injury (3).

3.2 Aim and objectives

The aim in this chapter was to identify feasible source tissues of Endothelial Colony Forming Cells (ECFCs) for use in clinical applications.

Objectives:

- To isolate and culture ECFC derived colonies from Umbilical Cord Blood (UCB), defining colony numbers per UCB unit
- To establish methods for phenotyping ECFC derived cells generated in this research by analysing cell surface markers on Human Umbilical Vein Endothelial Cells (HUVEC) and UCB ECFC derived cells previously used within this research laboratory and known to form *in vitro* microvascular tubule networks
- To investigate potential autologous sources of ECFC containing tissues collected from plastic surgery and burns patients
    - Peripheral Blood (PB) from breast reconstruction patient donors
    - Adipose Tissue (AT) from breast reconstruction patient donors

3.3 Results

3.3.1 Umbilical cord blood Endothelial Colony Forming Cell derived cells

3.3.1.1 Culturing ECFC from UCB

Units of UCB were collected by NHS Blood and Transplant research nurses, with ethical approval and fully informed written consent. A unit refers to the total volume of blood collected from a single placenta and umbilical cord, and as such had variable volume. The mononuclear cell fraction of the UCB was isolated on Accuspin tubes (Sigma Aldrich Ltd., Gillingham, UK) and cultured in complete EGM-2 medium (Lonza Biologics, Slough, UK) for 2 weeks. Cultured UCB generated cobblestone colonies with a typical morphology (Figure 3.1) characteristic of endothelial cells.

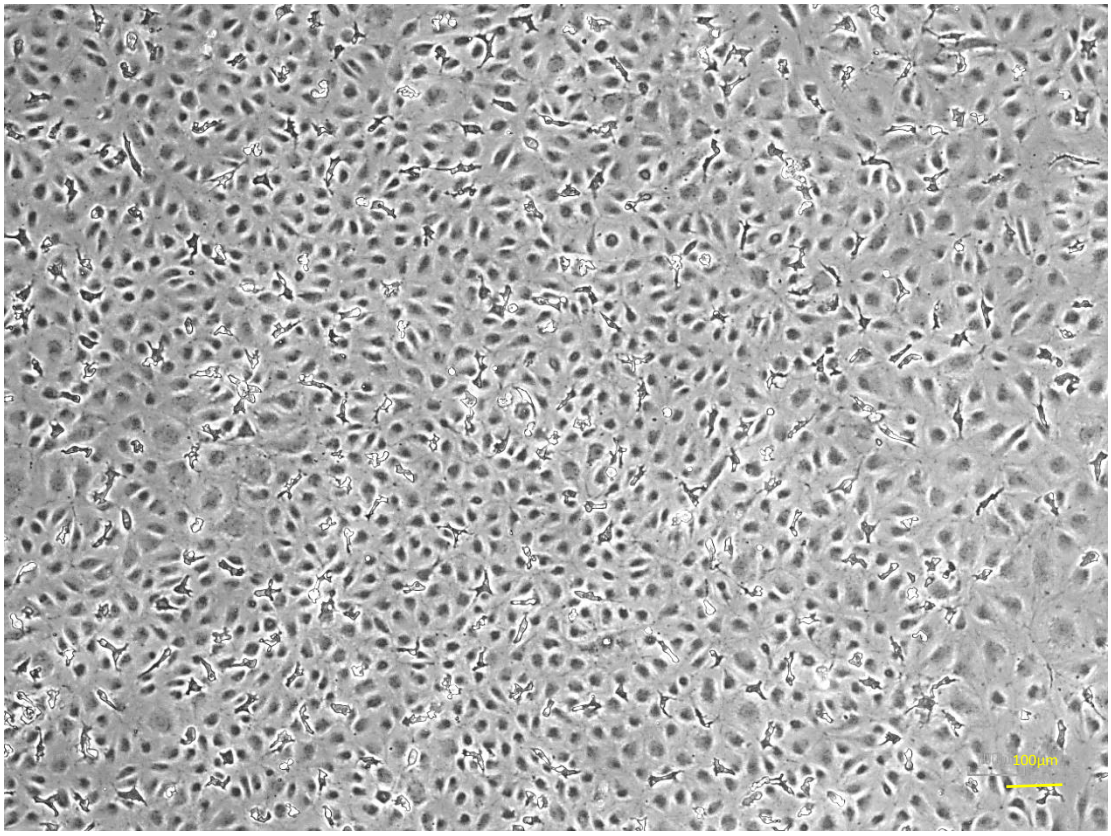

Figure 3.1: Passage 0 Umbilical Cord Blood Endothelial Colony Forming Cell (UCB ECFC) derived cells. These cells were cultured in complete Endothelial Growth Medium 2 (EGM-2) for 2 weeks from mononuclear cells separated from a single whole umbilical cord blood unit. (Phase contrast image, 100µm scale bar)

ECFCs formed characteristic round colonies (Figure 3.2) and these were selected with cloning rings to separate them from mesenchymal or mixed morphology colonies within the wells. As the colonies grew, the initial round shape was lost and colonies expanded to fill the culture surface available. A schematic to represent the colonies grown from each unit was developed (Figure 3.3), and was used to record the number and morphology of cultures at day 14. The colonies were individually drawn within the wells and labelled with dimensions to the nearest millimetre. Each colony was colour coded according to cell morphology; blue for endothelial colonies, pink for mesenchymal colonies and green for mixed morphology colonies. Where there was no cell growth, the well was marked with a cross and empty wells within the plates were labelled as 'not plated'. This figure demonstrates that populations of cultured cells vary greatly between the UCB units, but the use of cloning rings allowed the ECFC derived cells of interest to be isolated and expanded. The data are summarised in Table 3.1, with further details in Table 3.5, Table 3.6 and section 3.3.4.

A

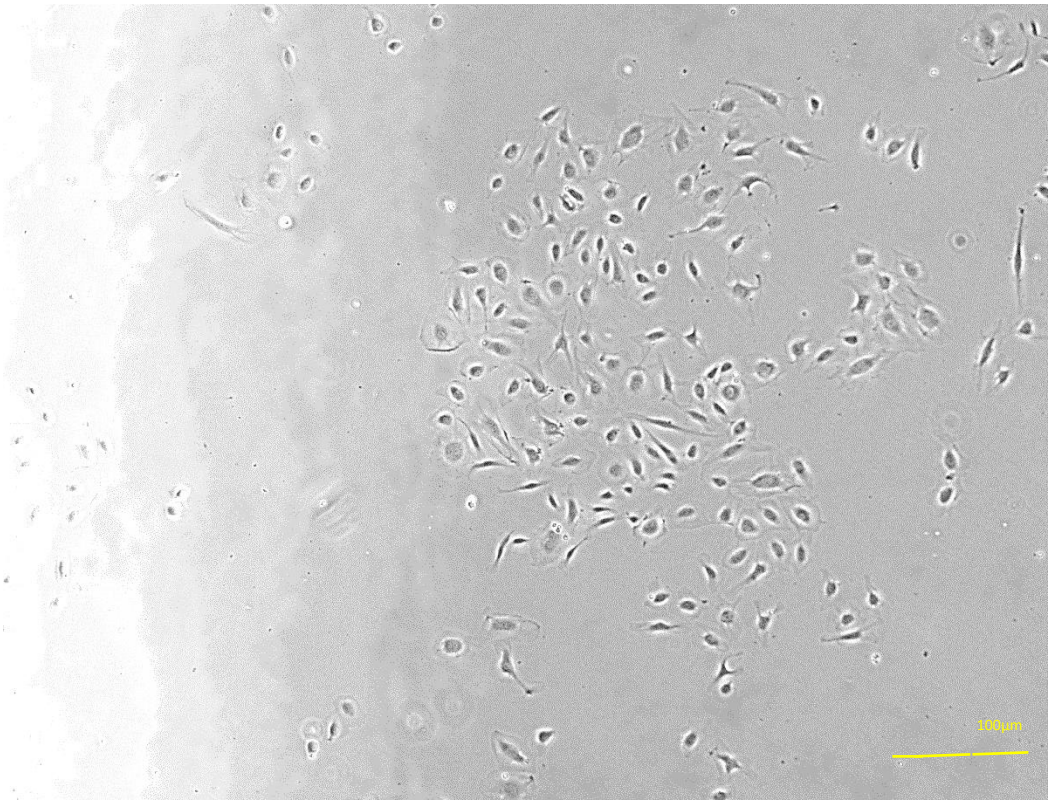

B

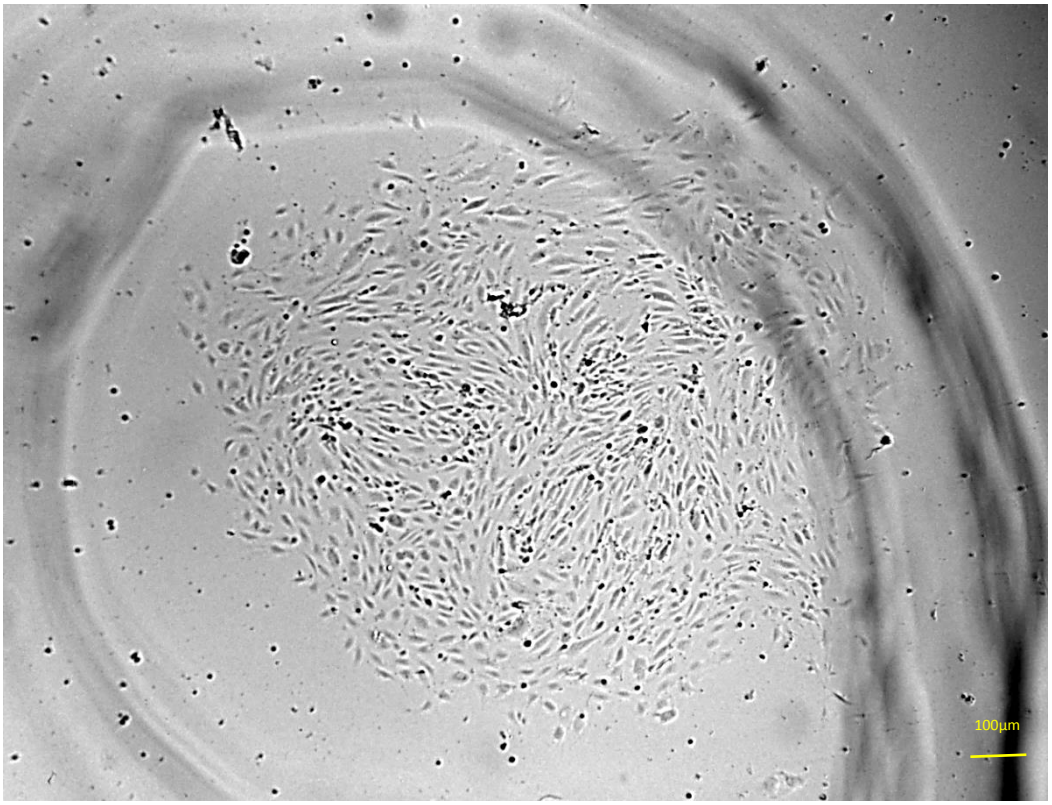

Figure 3.2: Colony formation of passage 0 Umbilical Cord Blood Endothelial Colony Forming Cell (UCB ECFC) derived cells. Image A shows early growth of a colony (day 7). Image B shows a more established colony (day 14) which has been marked with a marker pen on the underlying plastic to target with a cloning ring. (Phase contrast images, 100µm scale bars)

A

Key to 6 well plate digrams:

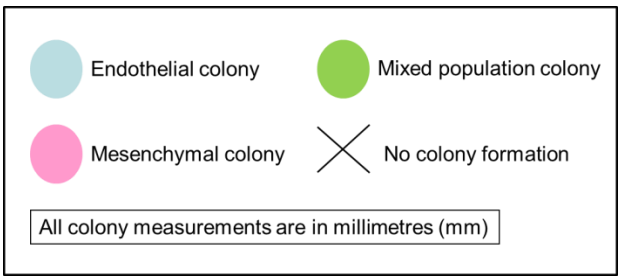

B

UCB 1

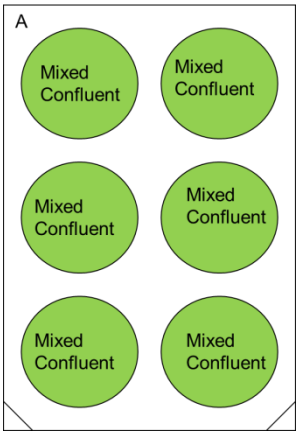

UCB 2

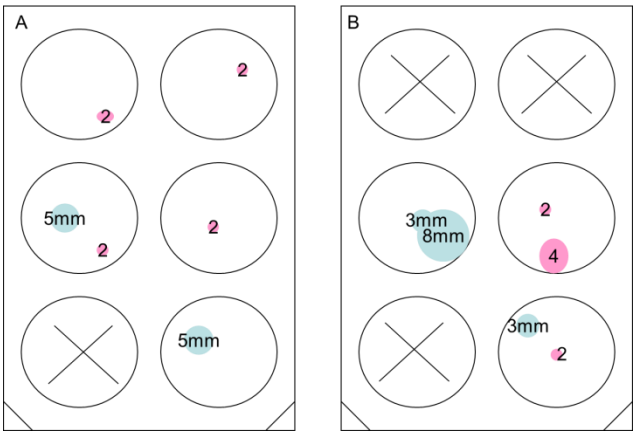

Figure continues on next page.

UCB 3

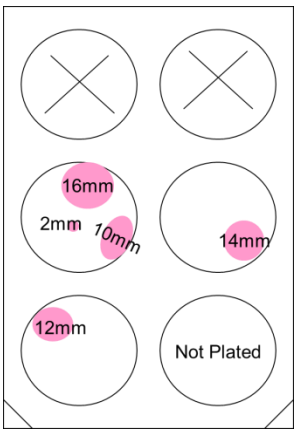

UCB 4

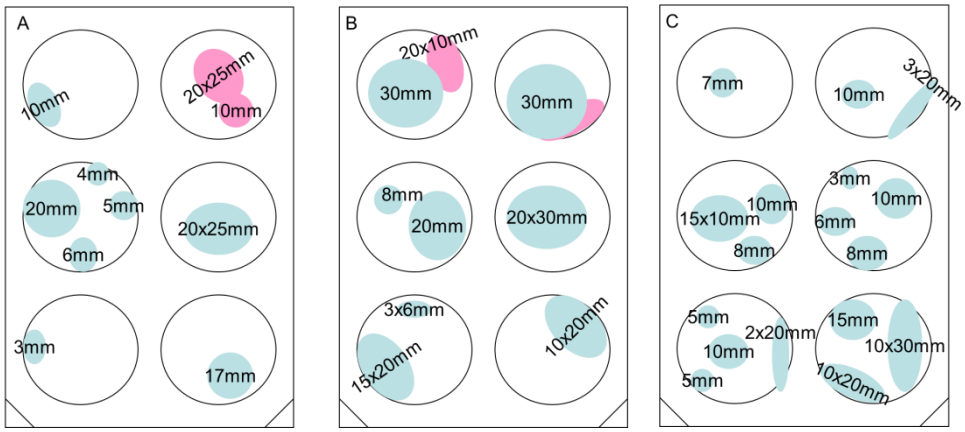

UCB 5

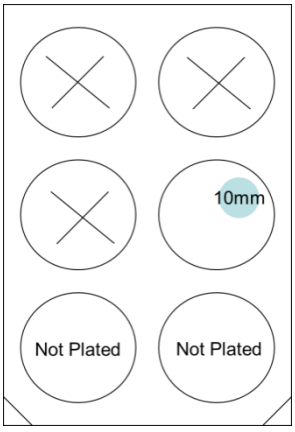

Figure continues on next page.

UCB 6

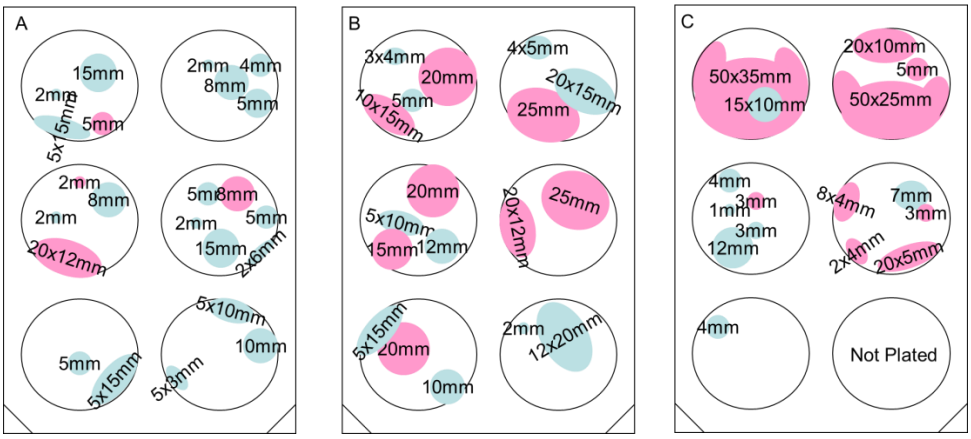

UCB 7

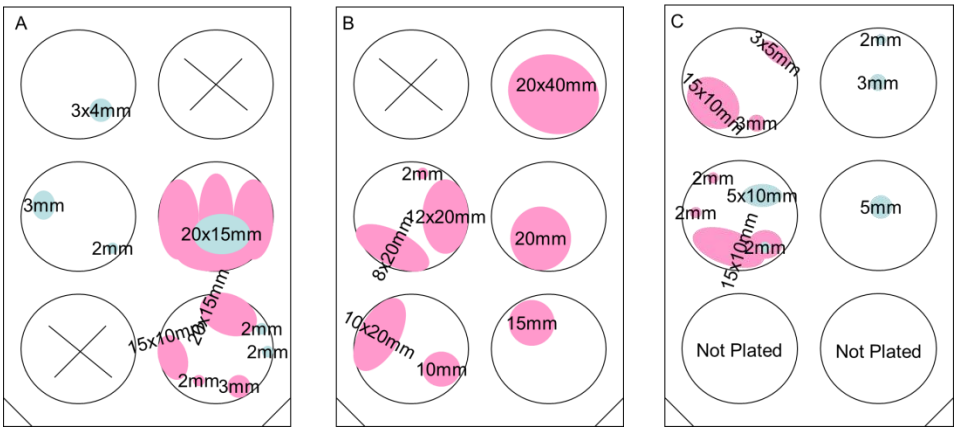

UCB 8

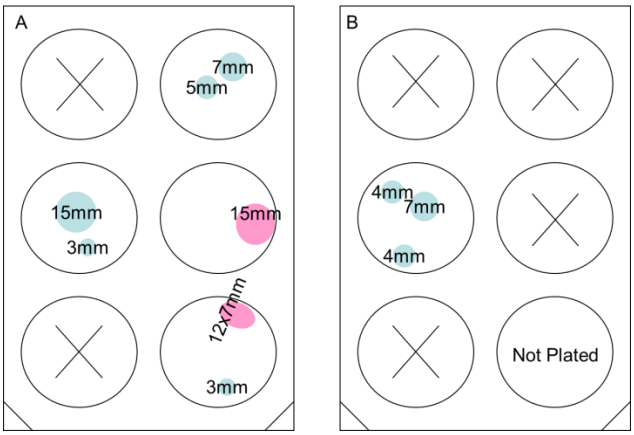

Figure continues on next page.

UCB 9

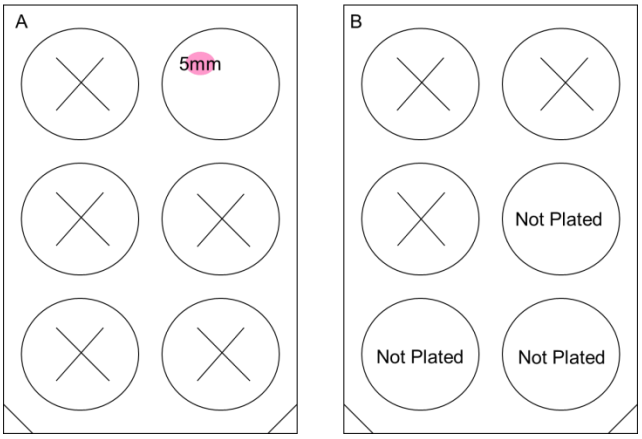

UCB 10

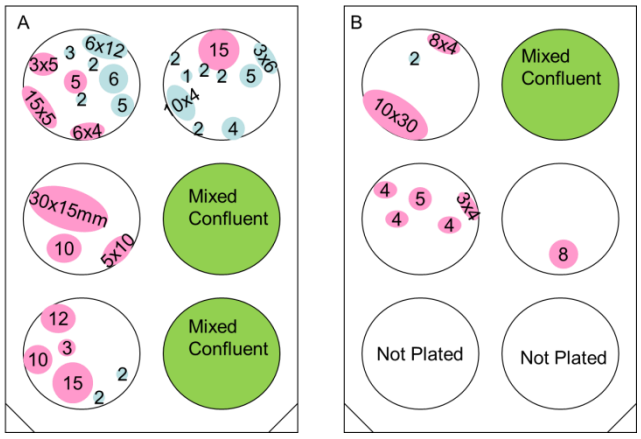

UCB 11

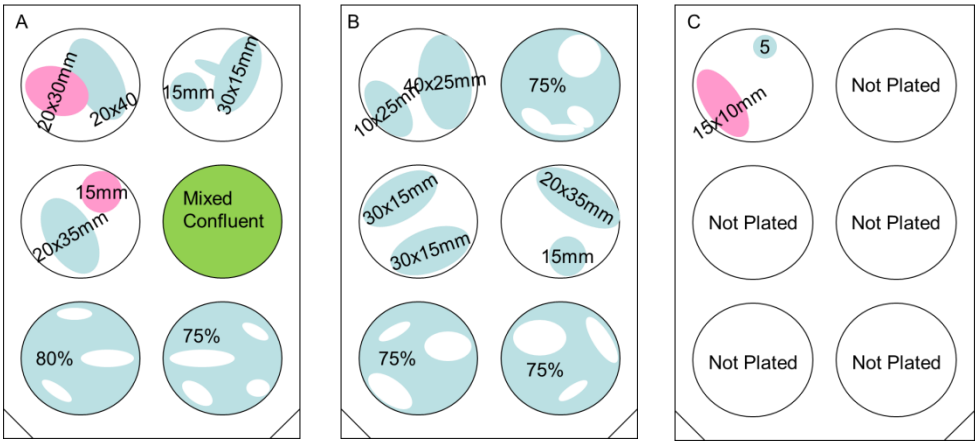

Figure continues on next page.

UCB 12

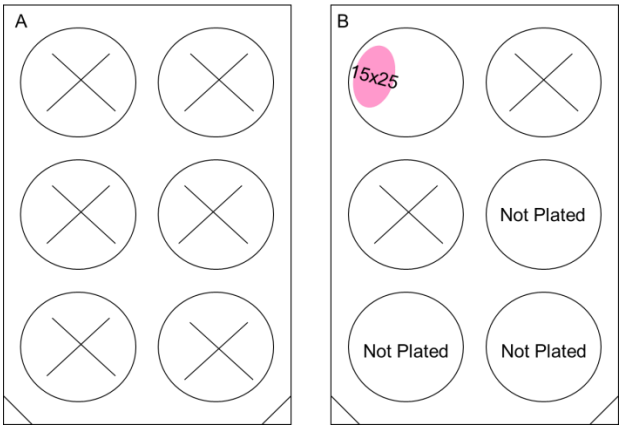

UCB 13

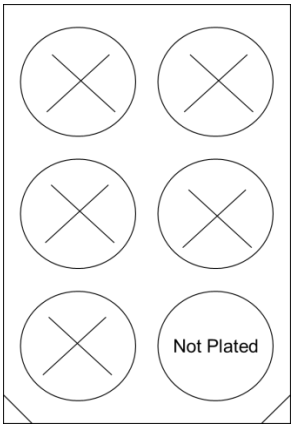

UCB 14

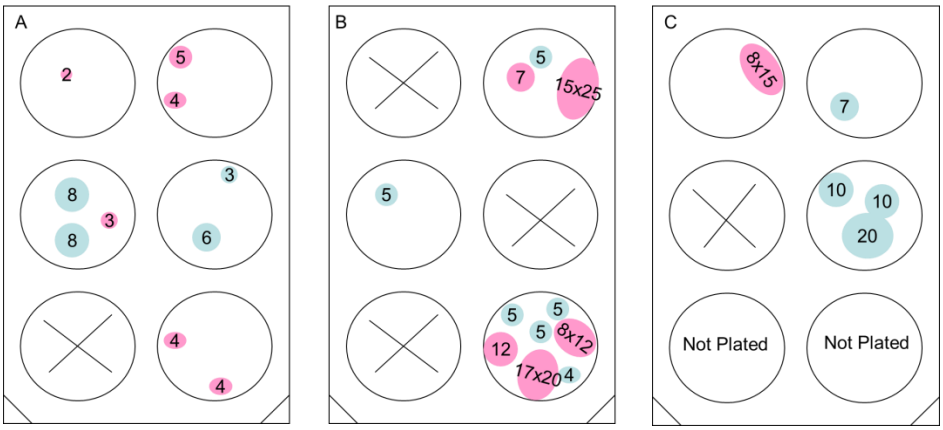

Figure continues on next page.

UCB 15

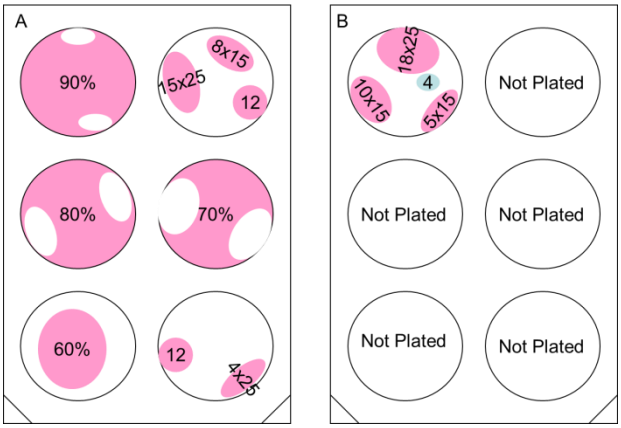

Figure 3.3: Six well plate diagrams of colony formation from the UCB mononuclear cells cultured in EGM-2 media for 2 weeks. A= Key to figure. B= Plates 1 - 15 are diagrammatic representations of colonies formed from individual UCB units after two weeks of culture. Despite cells being plated at a consistent concentration of $1.6x10^7$ mononuclear cells per well, there was great variability in the number, size and morphology of colonies. As indicated in the key (A), cells with morphology reminiscent of mesenchymal stromal cells (MSC, pink), ECFC derived cells (blue) or mixed colonies of MSC and ECFC derived cells (green) were identified by phase contrast microscopy. Using this schematic mapping, ECFC colonies were selected with cloning rings to separate them from cells of differing morphology for further expansion. Colony diameters are indicated in millimetres.

Table 3.1: Summary of ECFC derived colonies formed from 15 UCB units.

UCB number	No. MNCs plated $x10^8$	No. ECFC colonies formed	No. of ECFC colonies/ 10^8 MNCs plated
1	0.9528	0	0
2	2.0880	5	2.39
3	0.8795	0	0
4	3.6792	33	8.97
5	0.6593	1	1.52
6	4.2696	28	6.56
7	3.2844	10	3.04
8	2.2660	8	3.53
9	1.8864	0	0
10	1.9976	18	9.01
11	2.5950	15	5.78
12	1.8432	0	0
13	0.2456	0	0
14	3.1168	14	4.49
15	1.2236	1	0.82
Mean ± SEM	2.0658 ± 0.3016	8.9 ± 2.8	3.07 ± 0.84

3.3.1.2 Cell surface marker analyses of ECFC derived cells from UCB and HUVEC

In order to characterise ECFC derived cells generated for this thesis research, expression of cell surface markers were first validated using flow cytometry on Human Umbilical Vein Endothelial Cells (HUVECs) which were used routinely within our research group. Three batches of HUVECs at passage 3 were used to analyse cell surface markers. The method is described in Chapter 2, section 2.5. Representative histograms of flow cytometric analyses for cell surface markers described in Table 3.2 are shown in Figure 3.4.

After selection of the ECFC colonies derived from UCB, large individual colonies or pooled small colonies from individual cord blood units were cultured and expanded to passage 3 in complete EGM-2 media (Lonza Biologics, Slough, UK). They were analysed for cell surface markers using flow cytometry as above. Figure 3.5 shows representative flow cytometry histograms of UCB ECFC derived cells at passage 3. The histograms are representative figures from my own phenotyping and median fluorescence intensity and standard error of the mean are the mean figures from combined data with other researchers within our group, for the collaborative paper "Effects of obstetric factors and storage temperatures on the yield of endothelial colony forming cells from umbilical cord blood" (204).

Table 3.2 summarises the main antigen expression profiles of UCB ECFC derived cells and HUVECs, confirming the endothelial phenotype of the cells cultured. The positive CD31, CD34, CD73, CD105, CD146, VEGFR2, TIE2 profile and the lack of CD45 and CD14 staining are consistent with that of endothelial cells examined by other researchers (71-73, 77, 78, 205-215).

CD31, also known as PECAM-1 (Platelet/Endothelial Cell Adhesion Molecule 1), mediates endothelial cell to cell adhesion, although it is not specific for these cells and is also expressed by various leucocytes, platelets and haematopoietic stem cells (71, 72). CD34 is another transmembrane protein involved in cell adhesion. It is found on most endothelial cells, but also

haematopoietic stem cells in the early progenitor stages (73). It has been found to have variable expression at different passages (73). Another endothelial cell adhesion molecule, CD146, is found at the endothelial junction and has a role in control of cell to cell cohesion (77). It may also contribute to vascular permeability (77) and is present on activated T cells, allowing them to cross endothelium (78). Permeability of endothelium is also mediated by CD73, but this is also found in lymphatic vessels (206), and so again is non-specific.

CD105, also known as Endoglin, is a transmembrane glycoprotein which binds members of the Transforming Growth Factor Beta (TGFβ) family of peptides (208, 209). These peptides have multiple roles which include vasculogenesis and angiogenesis, hence their presence on endothelial cells. Other roles of the TGFβ peptides include manipulation of bone and cartilage development, haematopoiesis and immune function and so the CD105 protein is also found on various stromal and mesenchymal cells (209) as well as leukaemic and sarcoma cell lines (208).

Vascular Endothelial Growth Factor Receptor 2 (VEGFR2) is a mediator of angiogenesis found on endothelial cells (210, 211) and proangiogenic stem cell subsets such as haematopoietic stem cells (212). The main effects of VEGF on endothelial cells are promotion of migration and differentiation during angiogenesis. The tyrosine kinase receptor TIE2 is also present on both endothelial cells and haematopoietic stem cells (213, 214). This receptor mediates endothelial barrier function (213).

Since none of these endothelial cell surface markers are specific for endothelial cells, it was also necessary to exclude certain cell types by the lack of expression of a series of leucocyte or stromal markers. Both HUVECS and UCB ECFC derived cells were negative for CD14, CD45, CD90 and CD131. CD14 is the primary endotoxin binding molecule found on human monocytes (216). It is a specific marker for this cell type, and its absence confirms the absence of monocytes.

The CD45 antigen used was pan-specific and therefore capable of identifying all isoforms of the CD45 cell surface marker, Protein Tyrosine Phosphatase Receptor type C (PTPRC). This marker is present in different isoforms on all subtypes of leucocytes (74, 75).

CD90 (Thy-1) , was originally identified in thymocytes (T cell precursors) but is a key cell surface marker on fibroblasts, mesenchymal stem cells and haematopoietic stem cells (217). It may play a role in cell contraction, and has variable expression on different subtypes of fibroblastic cells with different contractile properties (217). Differentiated endothelial cells are consistently CD90 negative, as were the HUVECS and UCB ECFCs used in this research.

CD133 is present on a variety of stem and progenitor cells such as haematopoietic, retinal and neural stem cells (218-221). It is also known as Prominin-1 and is found on cell plasma membrane protrusions (219). Its role is mediation of epithelial cell differentiation and it presence may help cells maintain plasticity (218). It is therefore not seen in differentiated endothelial cells.

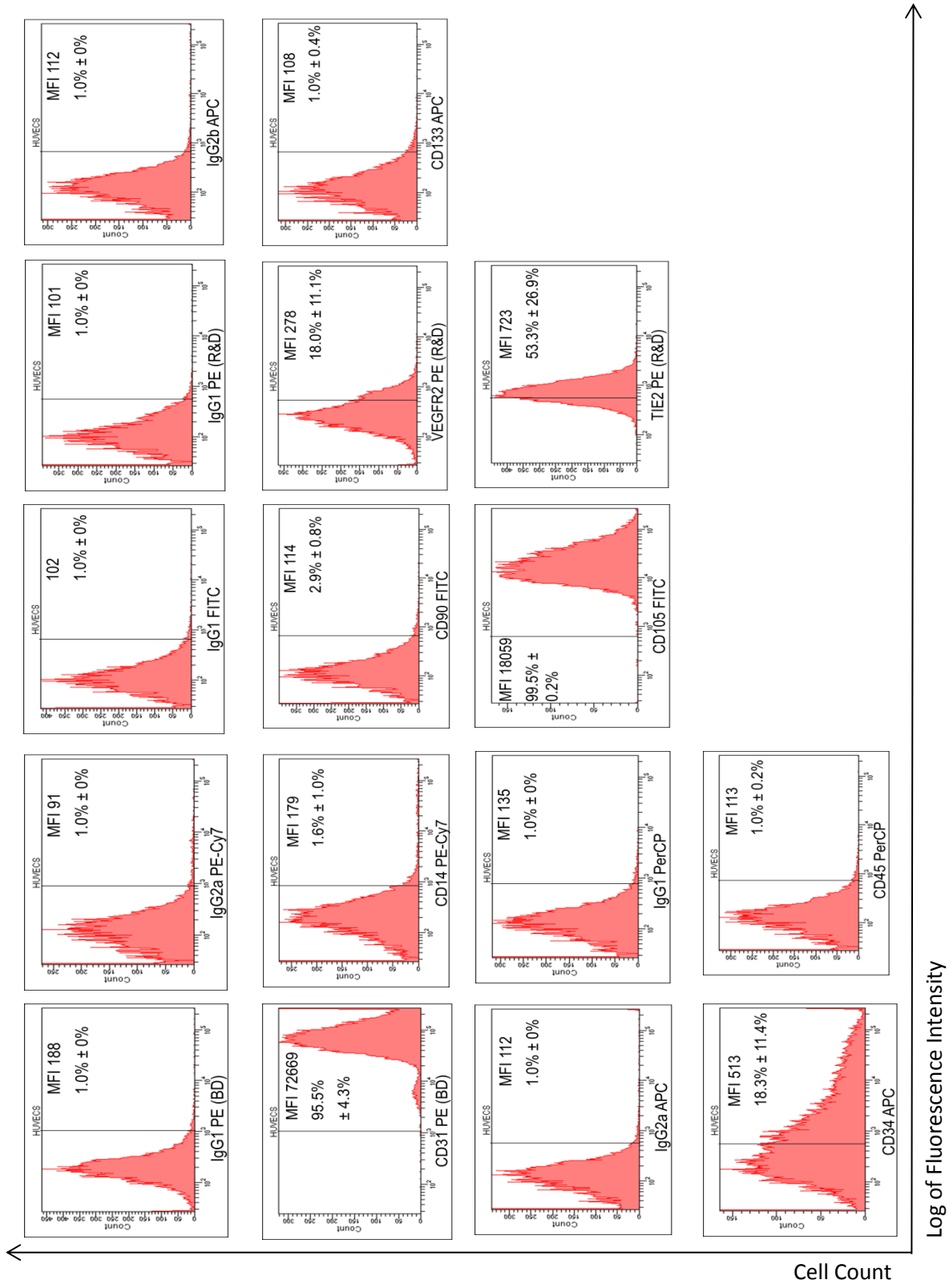

Figure 3.4: Flow cytometry phenotyping of Human Umbilical Vein Endothelial Cells (HUVECs). Representative FACS histograms of HUVEC stained with the antibodies indicated on each histogram. Values on histograms are Median Fluorescence Intensity (MFI) of the peak for the batch of cells shown. Isotype controls had a gate set at 1% positive cells (vertical black line) and the corresponding markers show the mean percentage of cells falling in that gate from three different samples ± SEM. HUVECs were CD31⁺ and CD 105⁺ with variable expression of CD34.

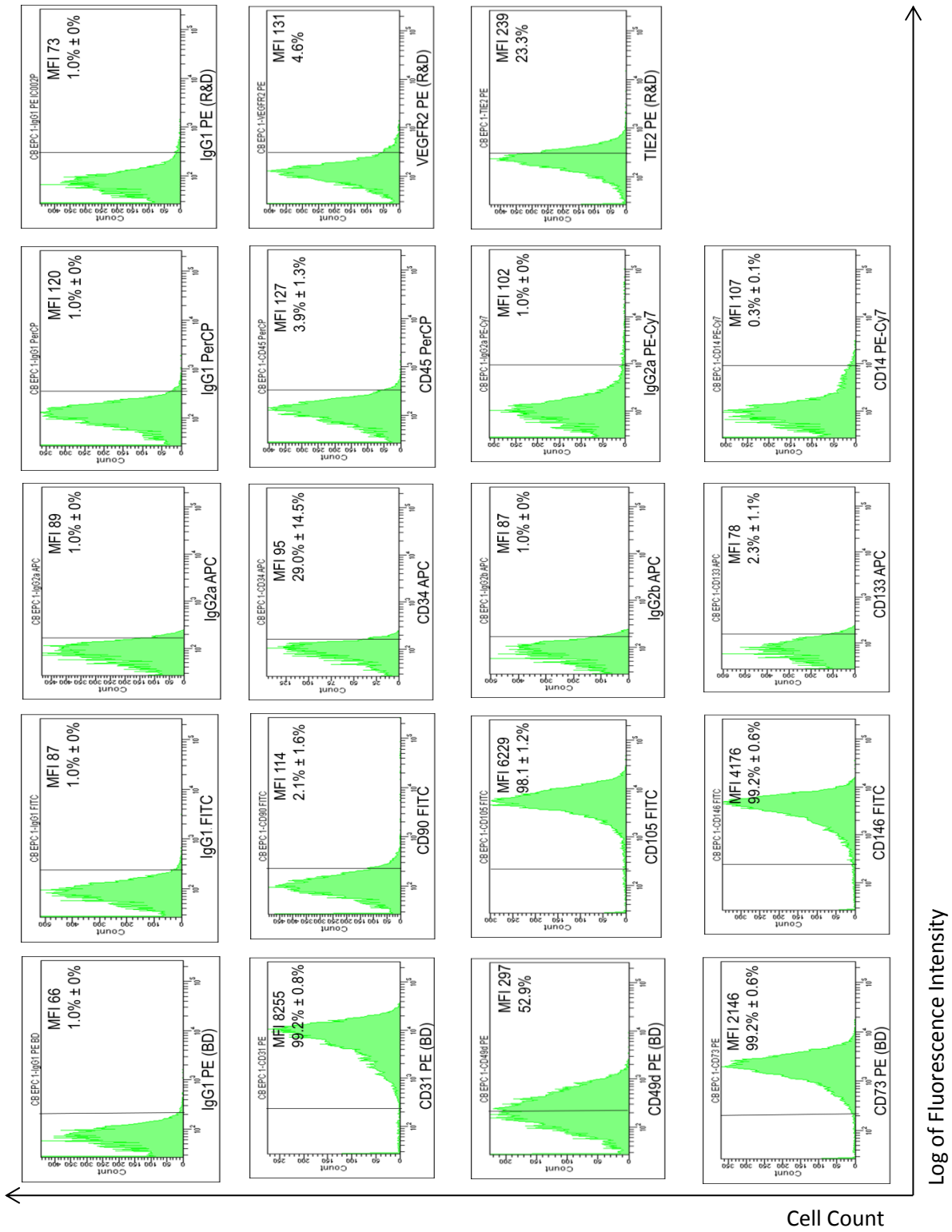

Figure 3.5: Flow cytometry phenotyping of Human Umbilical Cord Blood Endothelial Colony Forming Cell (UCB ECFC) derived cells. Representative FACS histograms of UCB ECFC derived cells stained with antibodies shown on each histogram. Values on histograms are Median Fluorescence Intensity (MFI) for the batch of cells tested. Isotype controls had a gate set at 1% positive cells (vertical black line) and the corresponding markers show the mean percentage of cells falling in that gate from three different samples where data was available ± SEM. UCB ECFCs are CD31$^+$, CD 73$^+$, CD105$^+$ and CD 146$^+$ with low expression of TIE2 and VEGFR2 and variable expression of CD34.

Table 3.2: Cell surface antigen expression of Umbilical Cord Blood Endothelial Colony Forming Cell (UCB ECFC) derived cells and Human Umbilical Vein Endothelial Cells (HUVEC), and the usual antigen associations.

Marker	Main Antigen Expression	UCB ECFC % positive ± SEM	HUVEC % positive ± SEM
CD14	Monocytes.	0.3 ± 0.1% (-)	1.6 ± 1.0% (-)
CD31	Endothelial cells, Platelets, Monocytes, Granulocytes, B cells, Haematopoietic stem cells, Proangiogenic haematopoietic cells	99.2 ± 0.8% (+++)	95.5 ± 4.3% (+++)
CD34	Haematopoietic stem and progenitor cells, Endothelial cells, Subsets of Mesenchymal Stem Cells	29.0 ± 14.5% (+)	18.3 ± 11.4% (+)
CD45 (Pan specific)	Leucocytes	3.9 ± 1.3% (-)	1.0 ± 0.2% (-)
CD49d	Lymphocytes, Monocytes, Eosinophils, Haematopoietic stem and progenitor cells, Mesenchymal Stem Cells	52.9% (++)	Not tested
CD73	B & T Cell Subsets, Endothelial cells, Mesenchymal Stem Cells	99.2 ± 0.6% (+++)	Not tested
CD90	Stromal cells, Mesenchymal Stem Cells , Haematopoietic stem cells	2.1 ± 1.6% (-)	2.9 ± 0.8% (-)
CD105	Endothelial cells, Stromal cells, Mesenchymal Stem Cells	98.1 ± 1.2% (+++)	99.5 ± 0.2% (+++)
CD133	Haematopoietic stem and progenitor cells, Other stem cells eg. Neural, Retinal cells	2.3 ± 1.1% (-)	1.0 ± 0.4% (-)
CD146	Endothelial cells, Activated T cells, Subsets of Mesenchymal Stem Cells , Proangiogenic haematopoietic cells	99.2 ± 0.6% (+++)	Not tested
VEGFR2	Endothelial cells, Stem cell subsets, Proangiogenic haematopoietic cells	4.6% (+)	18.0 ± 11.1% (+)
TIE2	Endothelial cells, Stem cells, Some monocytes, Proangiogenic haematopoietic cells	23.3% (++)	53.3 ± 26.9% (++)

The percentages of positive cells are those falling within a 1% gate set on isotype control histograms. Where SEM is given this is from sets of three different batches of cells.

3.3.1.3 Obstetric factors affecting UCB ECFC recovery

Multiple obstetric, maternal and perinatal factors may have an effect on the yield of ECFC recovery from UCB (204). As part of a larger study, data regarding UCB units which yielded ECFC from my work were pooled with data from others within the National Health Service Blood and Transplant (NHSBT) Stem Cell Research Laboratory (SCRL) group (15 of 52 units). This collaboration allowed us to analyse a number of obstetric and perinatal factors and helped to increase the statistical significance of calculated correlations. Table 3.3 shows the range of various maternal, obstetric and neonatal factors which may potentially affect the number of ECFC colonies formed from each unit. The most significant correlation from our data was with the placental weight – the greater the placental weight the lower the yield of ECFCs ($p<0.05$). The linear model regression is shown in Figure 3.6, and this produced the following formula to predict ECFC yield (E_{pred}) from placental weight:

$$E_{pred} = \left(\frac{1.2421 + 3.226 \times 10^{3}}{P^{2/3}} \right)^{10}$$

This may help predict the best UCB units to select for processing in order to maximise ECFC yield, and to my knowledge is the first time that this has been demonstrated to be a significant correlation.

Table 3.3: Demographics of perinatal maternal, obstetric and neonatal variables.

Factor (n)	**Mean ± SD**		**Range**
Gestational age (weeks) (49)	39 ± 1		37 - 41
Neonatal weight (grams) (49)	3427 ± 472		2620 - 4442
Placental weight (grams) (49)	704 ± 144		450 - 1100
Duration stage 1 labour (hours) (13)	4.4 ± 0.7		1.3 – 9.2
Duration stage 2 labour (hours) (13)	0.8 ± 0.3		0.1 – 3.1
Duration stage 3 labour (hours) (13)	0.2 ± 0.1		0.0 – 1.0
Factor (n)	**Range**	**Number**	**Per cent**
Maternal age (years) (52)	18 - 25	8	15.4
	26 - 35	30	57.7
	>35	14	26.9
Parity (49)	0	13	26.5
	1	18	36.7
	2	15	30.6
	≥3	3	6.1
Gravidity (49)	0	30	61.2
	1	11	22.4
	2	6	12.2
	≥3	2	4.1
Mode of delivery (48)	Vaginal	13	27.1
	Caesarean	35	72.9

Selected data redrawn from Coldwell *et al.* 2011 (204).

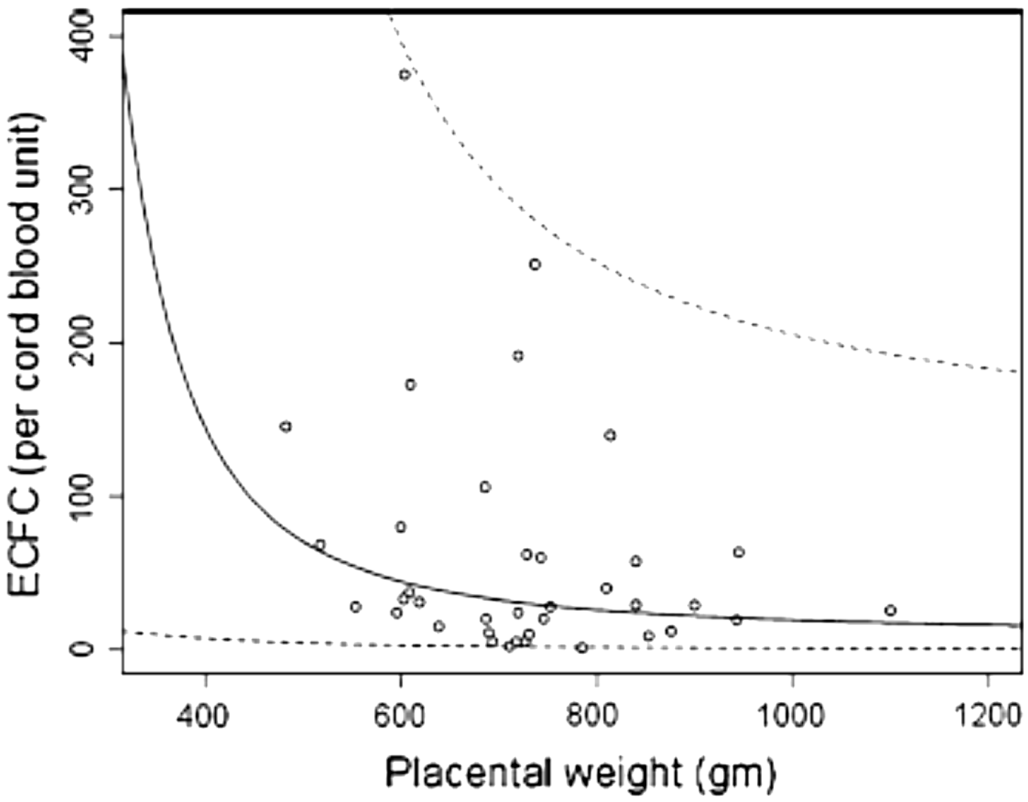

Figure 3.6: Correlation between placental weight and ECFC yield. Model fit of the correlation is shown by the solid line ($p<0.05$) and 95% confidence intervals are shown by the dashed lines. To analyse the correlation all units with a zero yield of ECFCs were excluded. The remaining ECFC colonies per unit were transformed by Box-Cox transformation to achieve a normal distribution and to stabilise the variance before applying a linear model regression. Reproduced from Coldwell *et al.* 2011 (204), published under the CC-BY-NC license.

3.3.2 Adult peripheral blood (PB) endothelial cells

3.3.2.1 Culturing ECFC from PB

Adult PB was also assessed as a source of ECFC derived cells. Fifty millilitres of peripheral blood were obtained with informed consent from adult plastic surgery patients under general anaesthesia prior to breast reconstruction surgery. The mononuclear cell fraction was isolated on Accuspin tubes (Sigma Aldrich Ltd., Gillingham, UK), plated at a concentration of $1.6x10^7$ mononuclear cells per well of a six well plate and cultured in complete EGM-2 medium (Lonza Biologics, Slough, UK) for 4 weeks. In total, only 2 of the 15 processed PB units grew endothelial colonies. Figure 3.7 shows the typical endothelial morphology of ECFCs cultured from adult PB. These were initially frozen at passage 2 in the hope that future samples would yield similar cells for comparison and analysis.

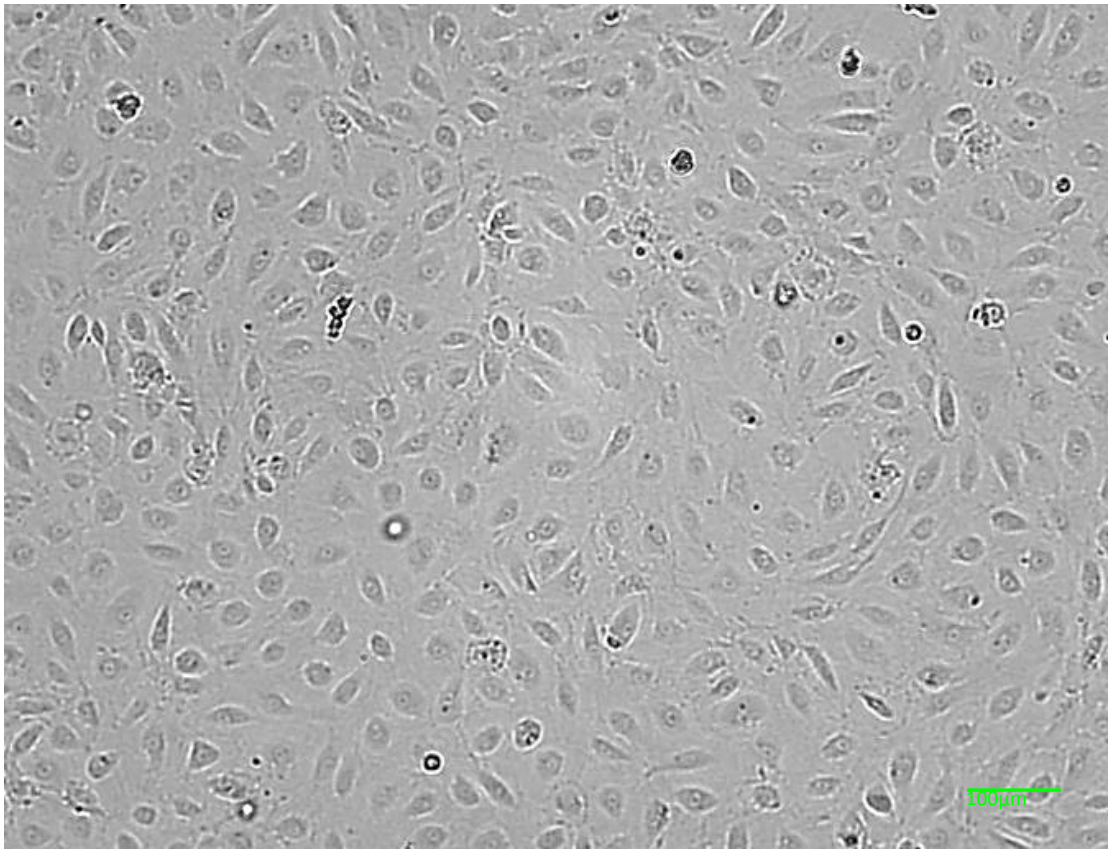

Figure 3.7: Peripheral Blood Endothelial Colony Forming Cell (PB ECFC) derived cells, typical morphology of cells at passage 2 (Phase contrast microscopy, 100µm scale bar).

When these cells were brought back into culture after storage at passage 2 in liquid nitrogen, only one of the samples retained an endothelial morphology. The other sample appeared to be overgrown with fibroblast or mesenchymal-like stromal cells. The mesenchymal-like cells grew quickly and were fully confluent by day 7, at which point they were discarded. The endothelial cells were much slower to grow and did not reach full confluence until day 48 in culture. These samples are shown in Figure 3.8. The cells with endothelial morphology at day 48 were harvested for FACS analysis, using a multicolour assay designed for low cell number samples. This assay is normally used within our laboratory for a clinical research trial involving small blood samples from patients with cancer to assess to effect of an anti-angiogenic drug.

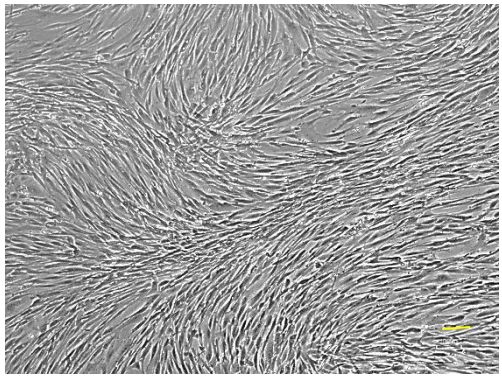

A Peripheral blood sample 7, passage 2 day 7

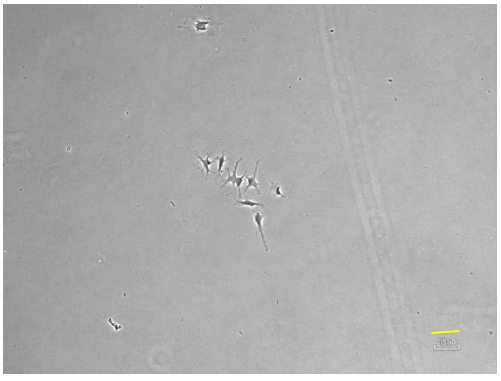

B Peripheral blood sample 12, passage 2 day 7

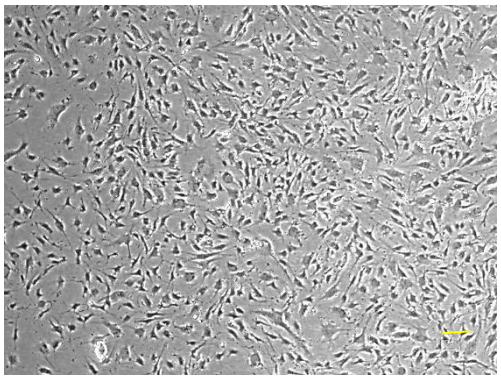

C Peripheral blood sample 12, passage 2 day 35

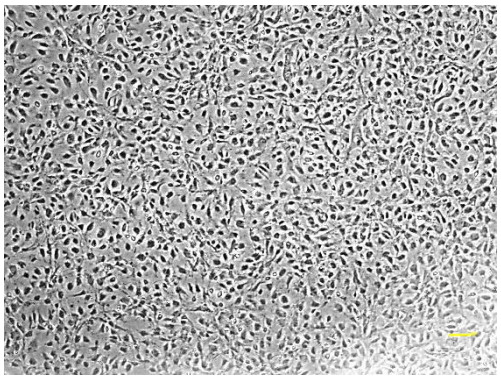

D Peripheral blood sample 12, passage 2 day 48

Figure 3.8: Frozen 'endothelial cell' samples from peripheral blood brought back into culture at passage 2. A= Sample 2 at day 7 showing a fibroblast-like morphology. These cells were discarded. B= Sample 12 at day 7 showing poor growth of sparse endothelial-like cells. C= Sample 12 at day 35 in culture showing 90% confluent cells with mainly endothelial-like morphology. D= Sample 12 at day 48, now showing 100% confluence and a clear endothelial-like morphology. (Phase contrast microscopy, 100µm scale bars)

3.3.2.2 Cell surface marker analyses of ECFC derived cells from peripheral blood

Only one PB ECFC culture survived sufficiently for flow cytometric analysis. Multicolour FACS analysis of the adult PB endothelial cells shows that they were all CD90 negative (Figure 3.9) and mostly CD34, CD144 and TIE2 positive (Figure 3.10). The expression of CD34 can decrease over endothelial passages (222), but CD144 and TIE2 are more consistent endothelial markers. This combination of markers suggests that the cells are endothelial in nature, and not fibroblastic or mesenchymal.

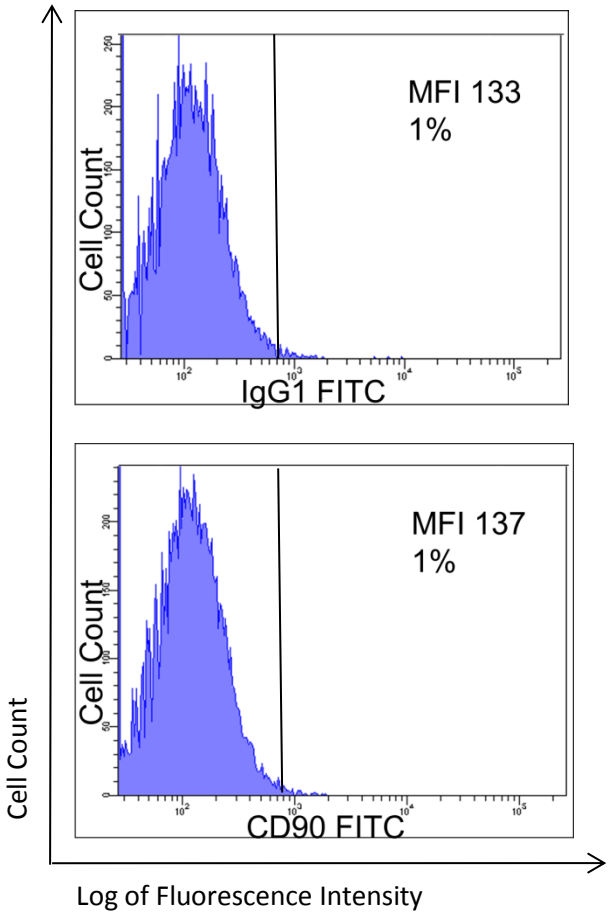

Figure 3.9: Histogram representation of CD90 expression in passage 3 adult peripheral blood endothelial colony forming cell derived cells. The median fluorescent intensity was similar for the isotype and test and there were 1% test cells in the 1% gate set on the isotype control (vertical black line).

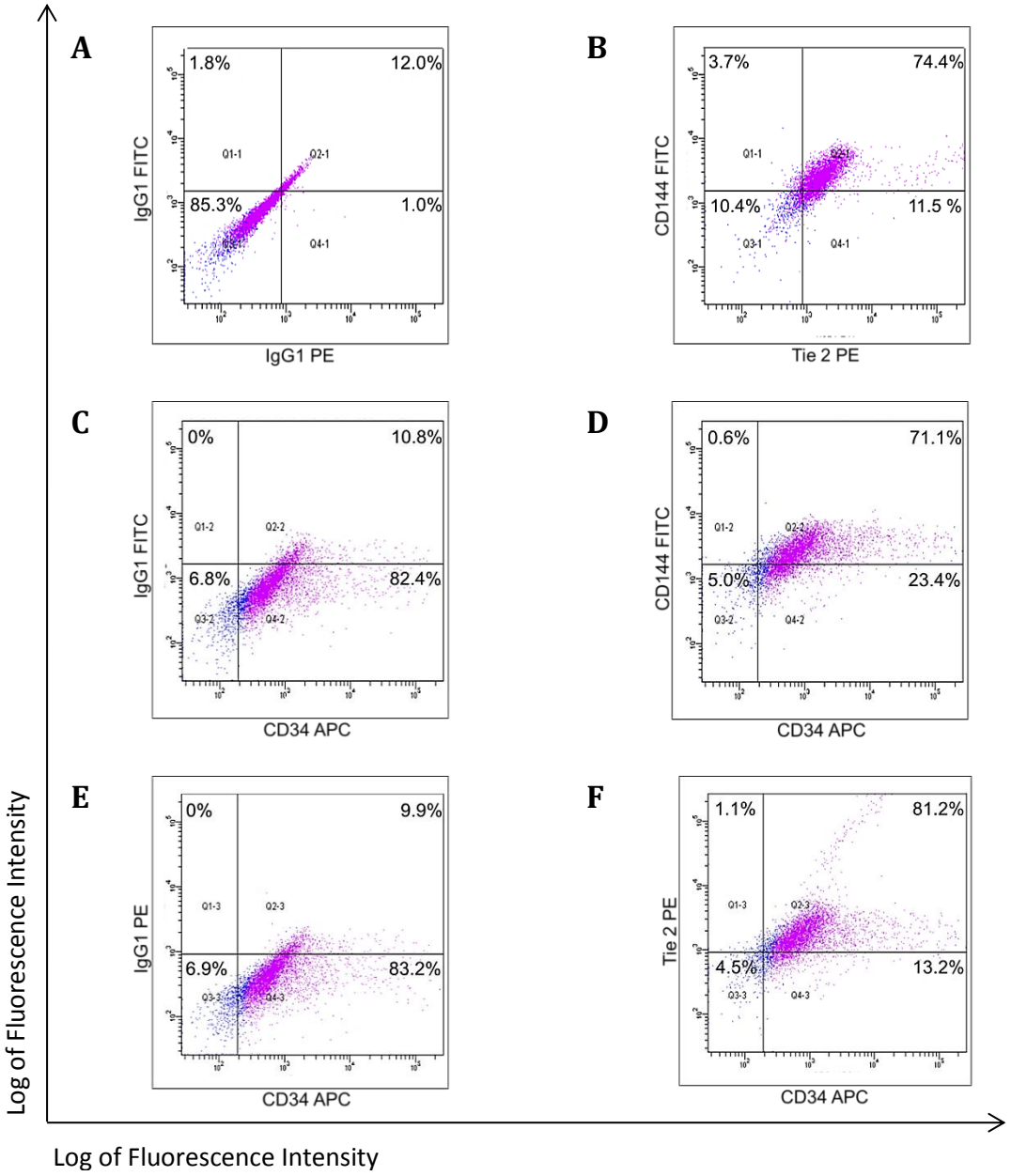

Figure 3.10: Multi-colour FACS analysis of adult peripheral blood 'endothelial cells' at passage 3. Dot plots for each double stained condition show the percentage of live cells in each quadrant with isotype controls in the left hand column and test markers in the right hand column. The population are mostly CD34+, CD144+, TIE2+.

3.3.3 Adipose tissue endothelial cells

We hypothesised that human adipose tissue (AT) might provide the best source of both endothelial and mesenchymal stromal cells for autologous treatments. AT had never previously been analysed within our research group and hence studies were carried out to determine if ECFCs could be recovered from this tissue. Histological staining of adult AT demonstrated microvasculature within the tissue (Figure 3.11), which is a potential niche for ECFCs.

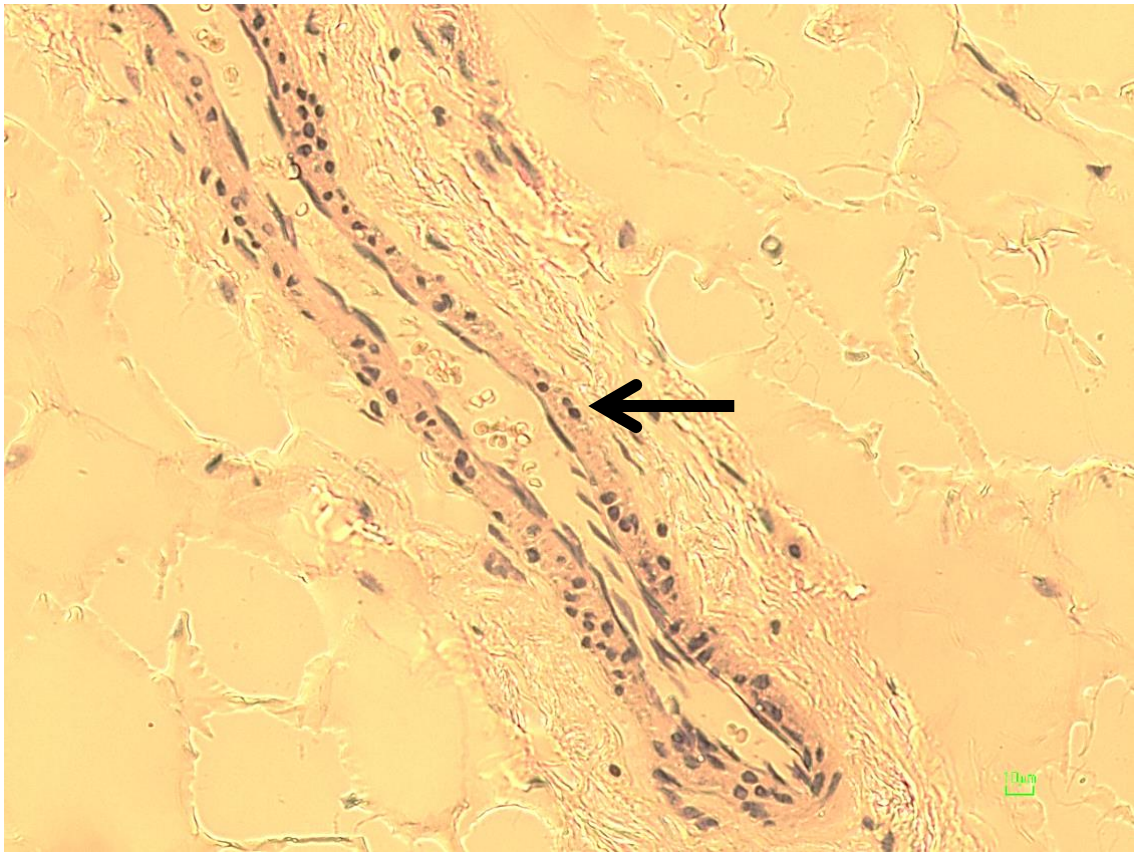

Figure 3.11: Adipose tissue histology. Histological sections of fresh adult AT were paraffin embedded, sectioned and stained with haematoxylin and eosin. There is a clearly delineated vessel seen within the adipocytes (arrow). (Phase contrast microscopy, 10µm scale bar)

AT was processed to isolate viable cells, as described in Chapter 2, section 2.4.3. A basic protocol was established in this thesis to mechanically and chemically dissociate the tissue to a single cell suspension. Optimisation of this protocol is discussed in Chapter 4. Flow

cytometric analysis of freshly processed adult AT showed that it contained heterogeneous cell populations, as might be expected of a primary tissue source. Cell surface marker analysis revealed that the AT suspension contained $CD45^+$ leucocytes (19.7% ± 11.4%) and few $CD133^+$ haematopoietic progenitor cells (4.8% ± 2.0%) (Figure 3.12). However a significant proportion of cells were $CD34^+$ (14.3% ± 3.6%) (Figure 3.12). The data suggest that the cell suspensions contained a significant number of endothelial cells which could be identified as $CD34^+$, $CD45^-$ and $CD133^-$.

In order to enrich the adipose cell isolate for ECFCs, fresh adult AT and dissected microvasculature were cultured under endothelial culture conditions as described in Chapter 2, section 2.4.3. However, after 14 to 21 days in culture, most of the samples produced adherent Mesenchymal Stem/Stromal Cells (MSC), which were $CD\ 90^+$, $CD\ 105^+$ (Figure 3.13). This figure shows one set of selected representative histograms of flow cytometry analysis at P1. Full phenotyping of AT MSC is presented in Chapter 4.

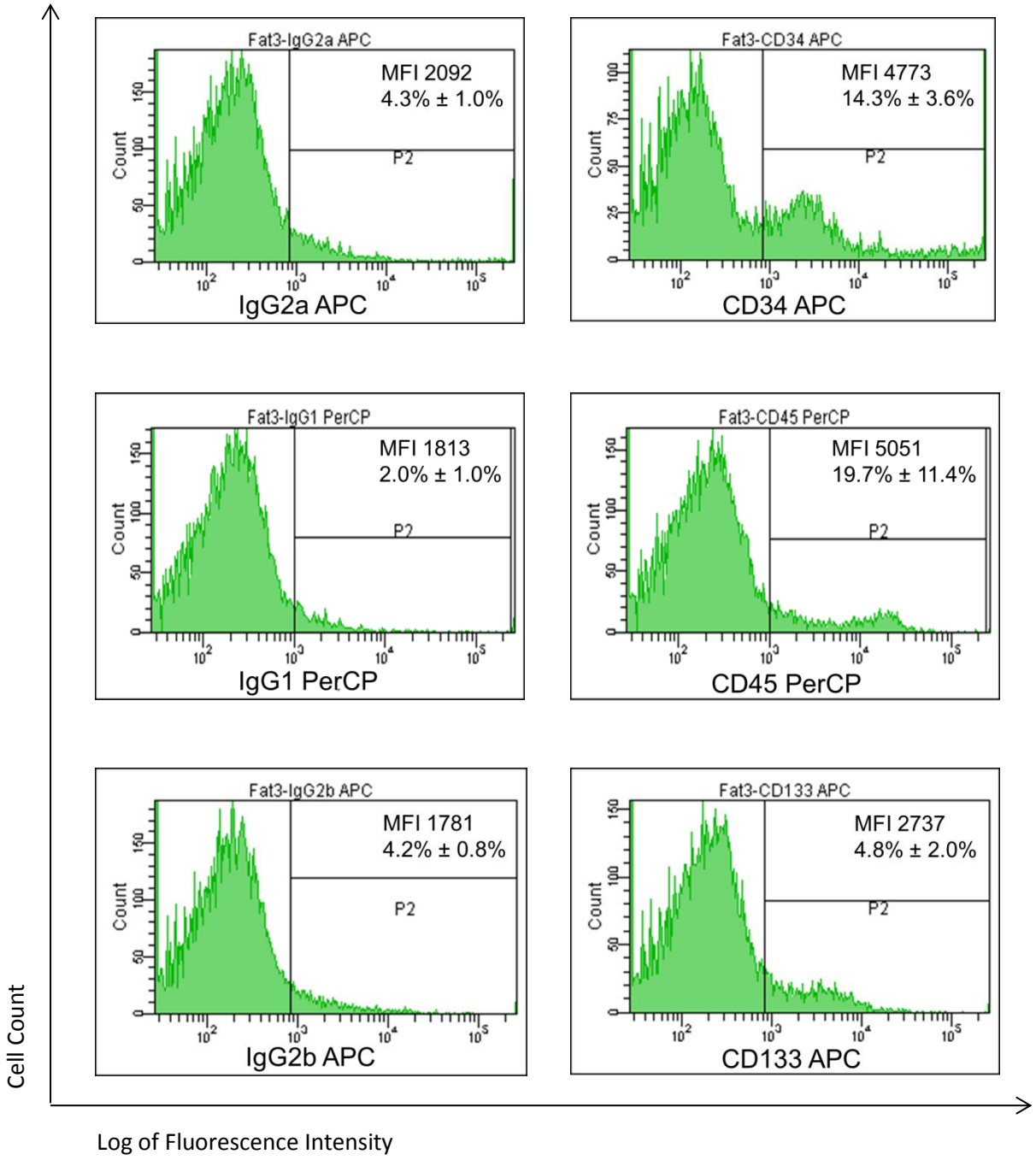

Figure 3.12: Flow cytometry phenotyping of fresh human Adipose Tissue. MFI= Median Fluorescence Intensity of the peak for the representative histogram shown. Isotype controls were used to set an arbitrary gate and the corresponding markers show the mean percentage of cells in that gate from three different samples ± SEM. Adipose tissue shows populations of $CD34^+$, $CD\ 45^+$ and $CD\ 133^+$ cells.

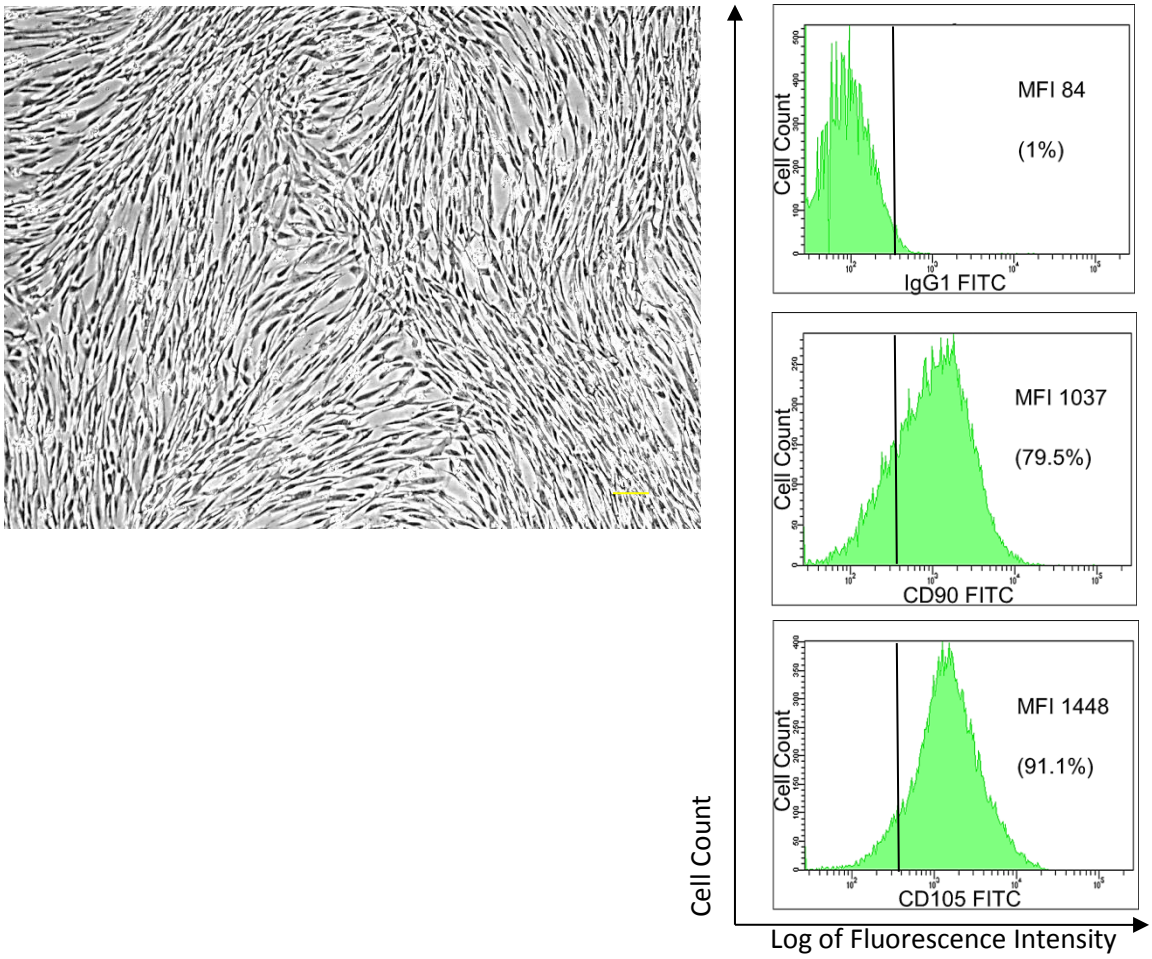

Figure 3.13: Example of morphology of Passage 0 MSC-like cells from human adipose tissue cultured in EGM-2 media for 14 days together with representative flow cytometry analysis of these cells harvested at passage 1. Left: The image demonstrates MSC-like cells with a fibroblastoid morphology (Phase contrast microscopy, 100µm scale bar). RIGHT: Flow cytometry histograms demonstrated that the cells were CD90⁺, CD105⁺. These are representative of P1 AT MSC-like cells. MFI= Median Fluorescent Intensity of all cells. An arbitrary 1% positive gate (vertical black line) was set on the isotype control and the percentage of cells falling within this gate for the CD90 and CD105 markers is shown in brackets.

Three of the thirteen samples produced cells which were morphologically ECFC derived cells (Figure 3.14). Due to the scarce nature of these ECFCs, they were initially frozen at passage 5 and later brought back into culture for FACS analysis. Taken together, our data suggest that MSC-like cells are abundant in adult AT in contrast to ECFCs.

A

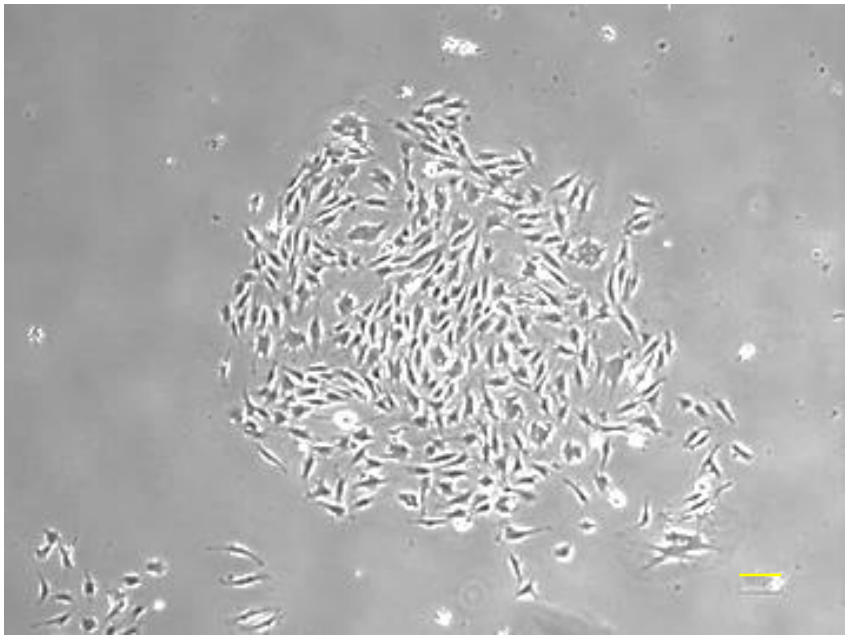

B

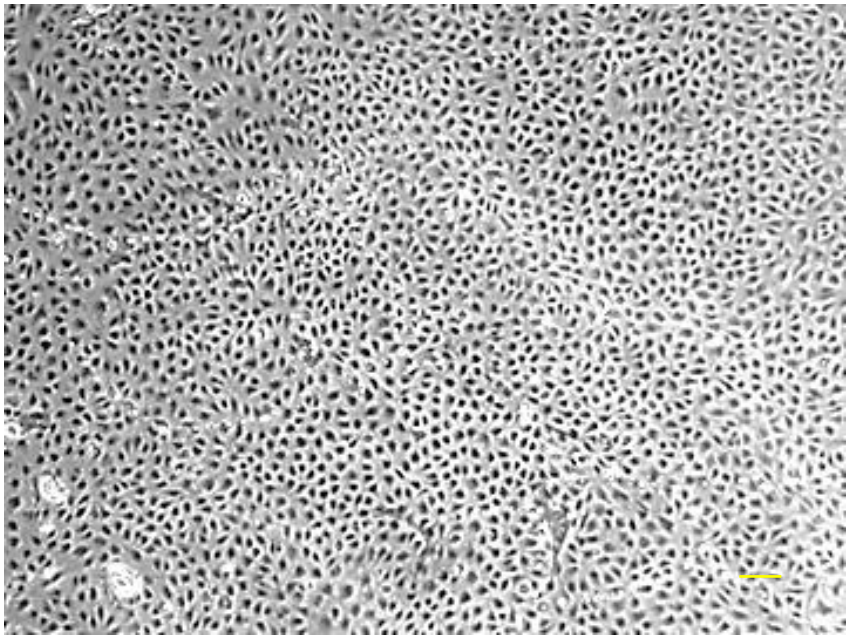

Figure 3.14: Adipose Tissue derived endothelial-like cells. Morphology of: A=Passage 0 ECFC derived cells from processed whole adipose tissue cultured in EGM-2 medium for 14 days. B=Passage 0 ECFC derived cells from processed dissected adipose microvasculature cultured in EGM-2 medium for 14 days. (Phase contrast microscopy, 100µm scale bars).

Of the 3 adipose tissue and adipose microvasculature derived endothelial-like cell samples brought back into culture after cryostorage at passage 5 in liquid nitrogen, only one retained an endothelial morphology. The other samples became overgrown with

mesenchymal stromal cells and were discarded. As with the peripheral blood cells brought back into culture from liquid nitrogen, the mesenchymal-like cells grew quickly and the endothelial cells were much slower to grow. The endothelial-like cells looked senescent and friable from an early stage, however persistent culture and regular media changes allowed continued, gradual expansion until confluence and harvest at day 48 for FACS analysis, using the multi-colour assay for low cell number samples. These samples are shown in Figure 3.15.

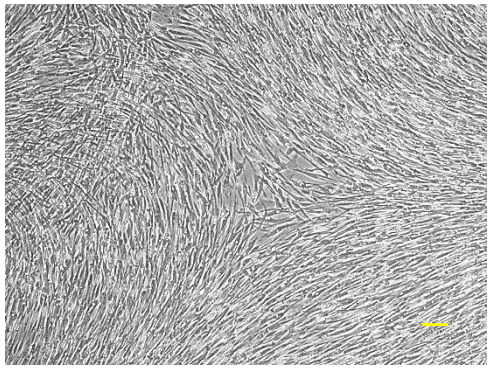

A Adipose microvasculature sample 6, day 6

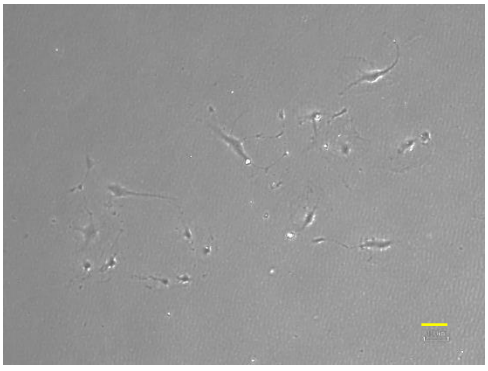

B Adipose tissue sample 8, day 6

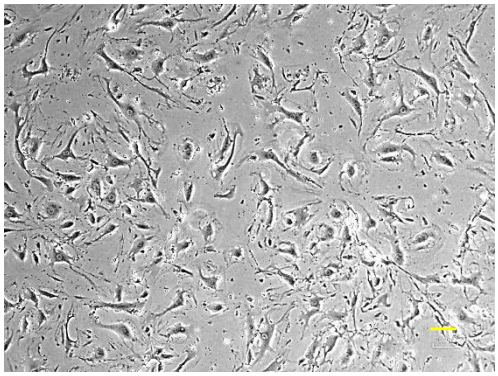

C Adipose tissue sample 8, day 26

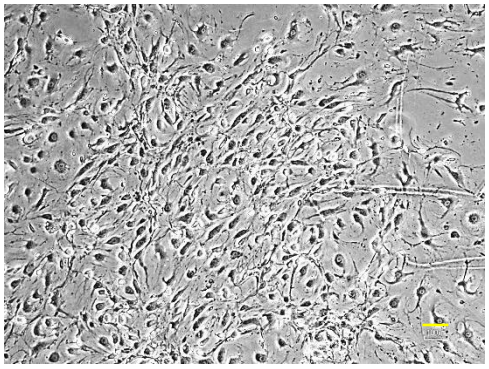

D Adipose tissue sample 8, day 48

Figure 3.15: Frozen 'endothelial cell' samples from adipose tissue and adipose microvasculature brought back into culture at passage 5. Cells were cultured in EGM-2 medium and examined using phase contrast microscopy. A= Sample 6 at day 6 showing a fibroblast-like morphology. These cells were discarded. B= Sample 8 at day 6 showing poor growth of sparse endothelial-like cells. C= Sample 8 at day 26 in culture showing 70% confluent cells with mainly endothelial-like morphology. The cells looked friable and appeared to be senescencing. D= Sample 8 at day 48, now showing 95% confluence and mostly clear endothelial-like morphology with some friable cells. (Phase contrast microscopy, 100µm scale bars)

FACS analysis confirmed that the population of endothelial-like cells from adipose tissue was CD90 negative (Figure 3.16), and therefore neither fibroblastic nor mesenchymal, unlike cultured cells shown in Figure 3.13.

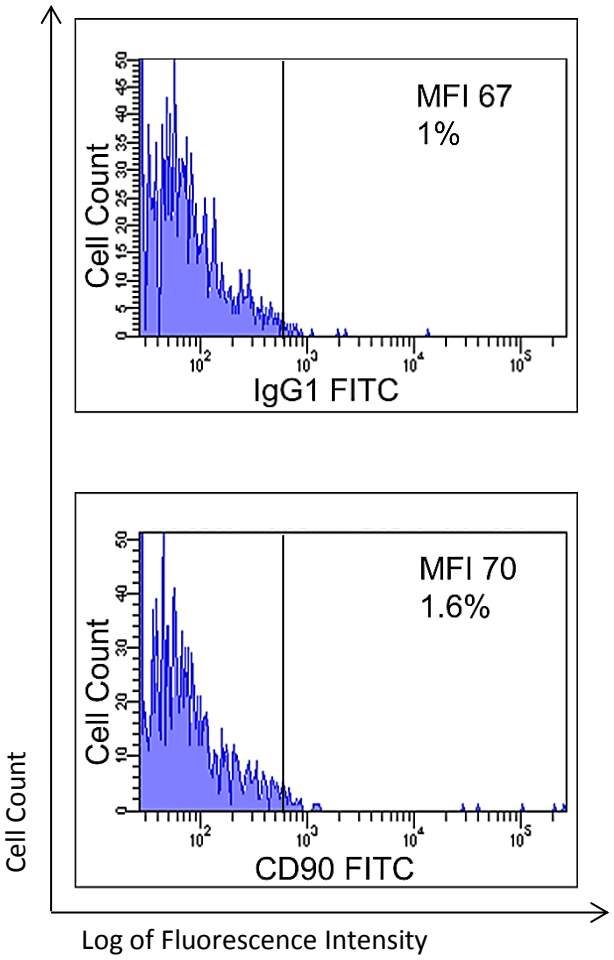

Figure 3.16: Histogram representation of CD90 expression on passage 6 adult adipose tissue ECFC derived cells. The median fluorescent intensity (MFI) of the whole population was similar for the isotype and CD90 antibody stained cells. There were 1.6% CD90 antibody stained cells in the 1% positive gate (vertical black line) set on the isotype control. This indicates that the population is negative for CD90.

Multi-colour FACS analysis demonstrated that the endothelial-like cells from adipose tissue were mostly $CD34^+$, $TIE2^+$ and weakly $CD144^+$ (Figure 3.17). CD144 positivity appeared to correlate with TIE2 positivity. This combination of markers supports the likely endothelial nature of this cell population.

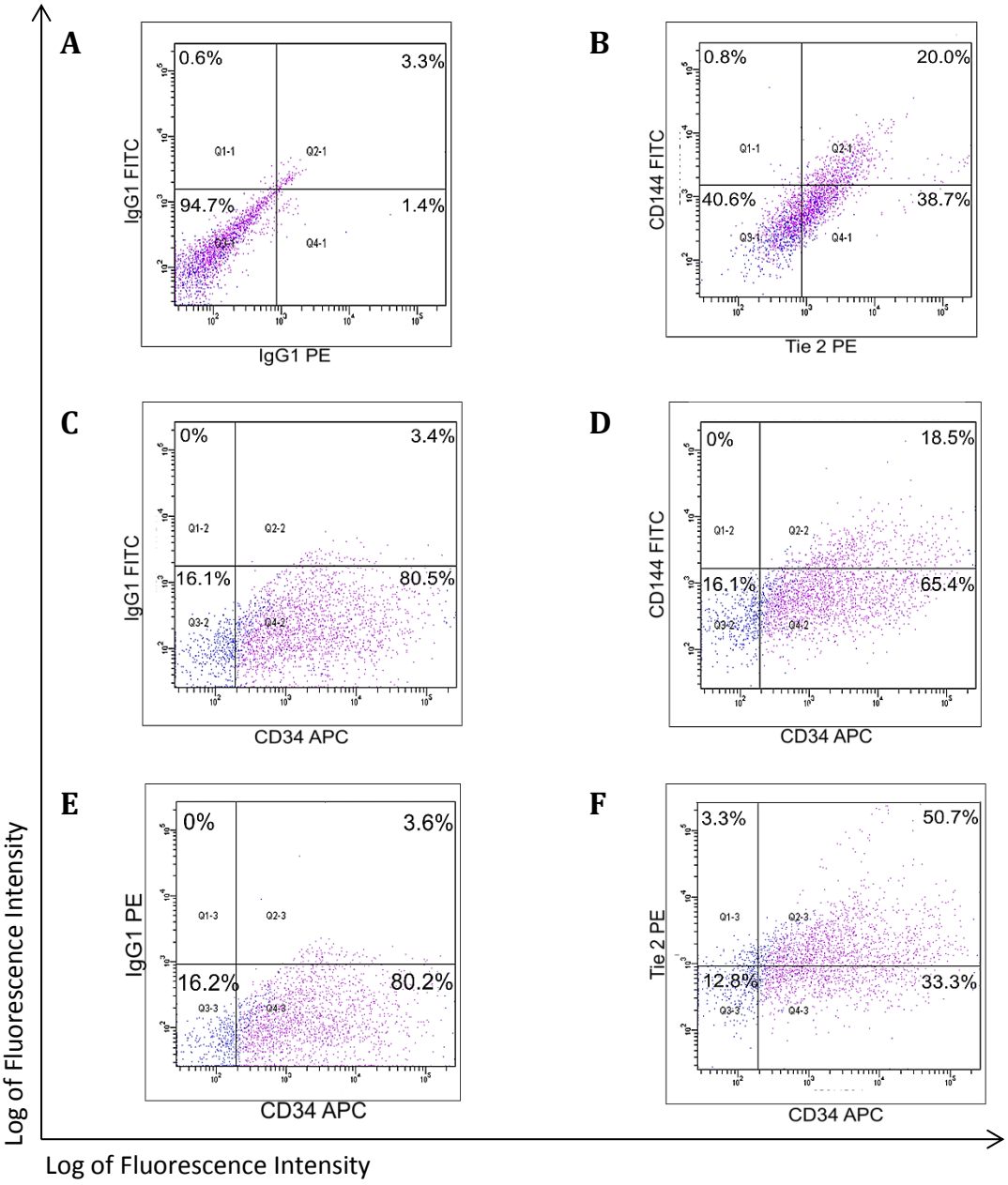

Figure 3.17: Multi-colour FACS analysis of adipose tissue 'endothelial cells' at passage 6. Dot plots for each double stained condition show the percentage of live cells in each quadrant with isotype controls in the left hand column and test markers in the right hand column. The population are mostly CD34⁺, TIE2⁺, with cells expressing CD144 weakly.

3.3.4 Comparison of sources of endothelial colony forming cells

Umbilical cord blood, adult peripheral blood and adult adipose tissue are all capable of producing endothelial colony forming cells. In this chapter, umbilical cord blood (UCB) was found to be the most reliable source of ECFCs, although ECFCs were also obtained from donor adult peripheral blood (PB) and adult AT (Table 3.4). Table 3.5 and Table 3.6 show the number of mononuclear cells (MNCs) plated from UCB and donor adult PB. There was a significant correlation between the number of MNCs plated from umbilical cord blood and the resulting number of ECFCs in UCB (Figure 3.18) but there is no correlation in adult PB (Figure 3.19). On average there were 3.04 ± 0.84 ECFC per 10^8 MNCs in UCB as compared to 0.59 ± 0.37 ECFC per 10^8 MNCs in PB. These results suggest that neonatal tissue might contain more, or may be a better source of ECFCs than adult tissues.

Table 3.4: Comparative yield of endothelial cells from different sources.

Sample Type	**Sample volume (ml)** **Mean [range]**	**Number of samples processed and cultured**	**Number of samples to yield ECFC (%)**	**Number of ECFC colonies in positive cultures** **Mean [range]**
Adult Adipose Tissue (AT)	25	13	3 (23%)	19.7 [2-41]
Umbilical Cord Blood (UCB)	86 [58-118]	15	10 (67%)	13.3 [1-33]
Adult Peripheral Blood (PB)	50	13	2 (15%)	1.7 [1-3]

UCB was the most reliable source of ECFC, although it was also possible to culture ECFC from AT and PB. When ECFC were cultured successfully from AT there was a greater yield of colonies than from UCB cultures, but the number of ECFC positive AT cultures was too small for statistical analysis.

Table 3.5: ECFCs from Umbilical Cord Blood.

Cord Blood Number	Total number of MNCs x10^8	Number of ECFCs	Number of ECFCs / 10^8 MNCs plated
1	0.95	0	0
3	0.88	0	0
9	1.89	0	0
12	1.84	0	0
13	0.25	0	0
5	0.66	1	1.52
15	1.22	1	0.82
2	2.09	5	2.39
8	2.27	8	3.53
7	3.28	10	3.04
14	3.12	14	4.49
11	2.60	15	5.78
10	2.00	18	9.01
6	4.27	28	6.56
4	3.68	33	8.97
Mean ± SEM	2.07 ± 0.30	8.87 ± 2.79	3.07 ± 0.84

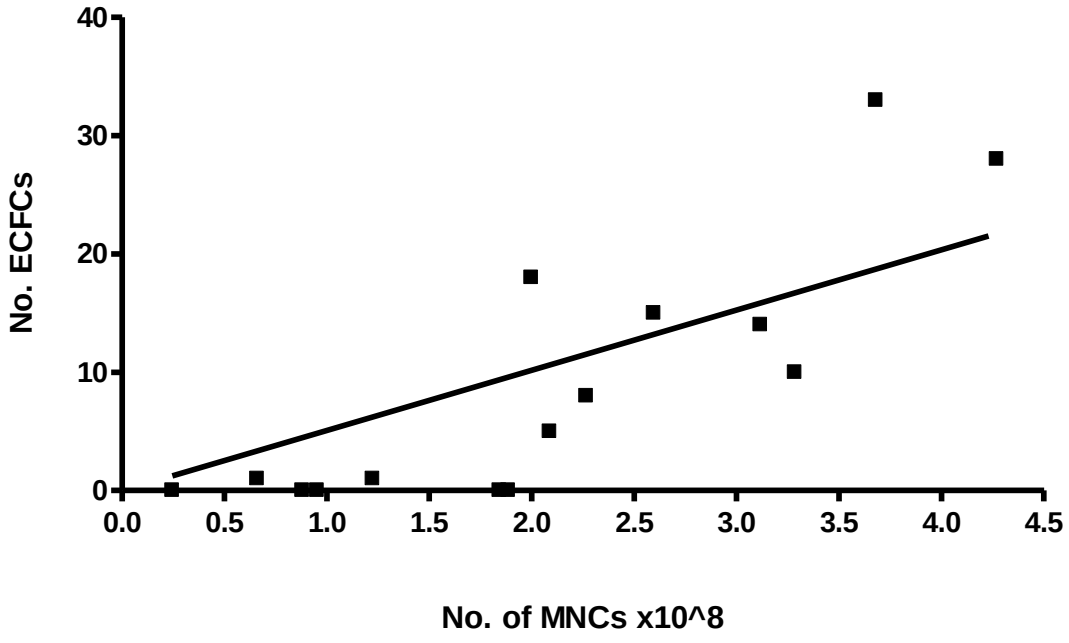

Figure 3.18: Linear correlation between the number of UCB MNCs plated and the number of resulting ECFCs identified. Spearman rank correlation coefficient =0.8318, 95% confidence interval=0.5451 to 0.9443, two-tailed p value=0.0001.

Table 3.6: ECFCs from donor adult Peripheral Blood.

Adult Peripheral Blood Number	Total number of MNCs x10^8	Number of ECFC colonies	Number of ECFCs / 10^8 MNCs plated
2	0.50	0	0
3	0.36	0	0
4	0.46	0	0
5	0.40	0	0
6	0.66	0	0
7	0.96	0	0
8	0.65	0	0
9	0.60	0	0
10	0.40	0	0
13	0.74	0	0
11	0.58	1	1.74
12	0.72	1	1.39
1	0.65	3	4.6
Mean ± SEM	0.59 ± 0.05	0.38 ± 0.24	0.59 ± 0.37

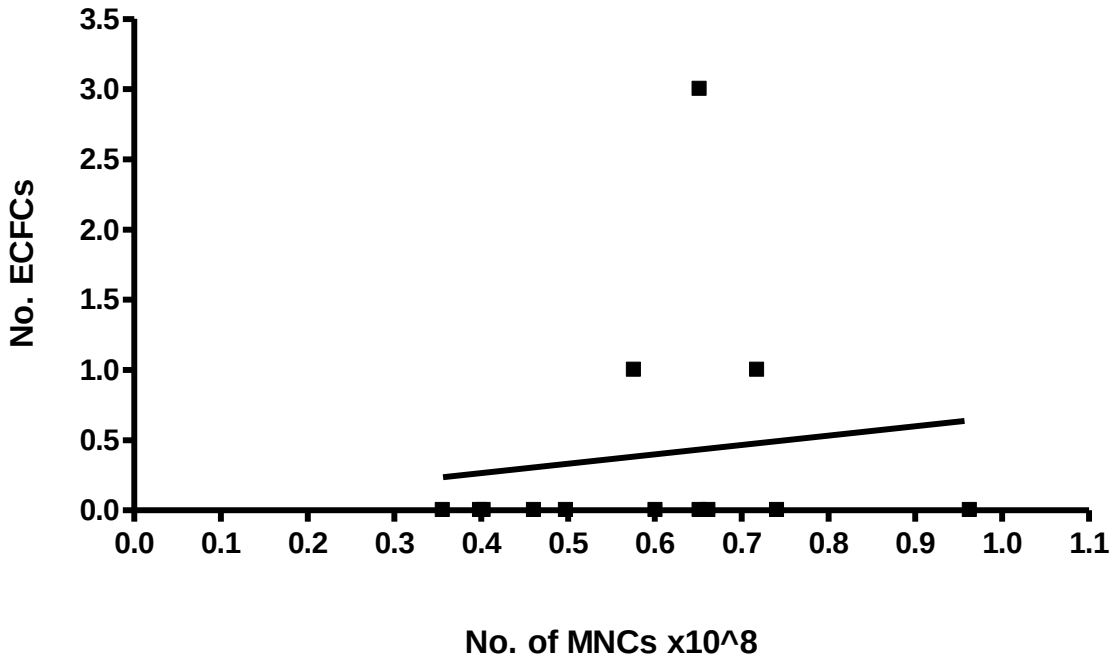

Figure 3.19: Lack of a significant linear correlation between the number of adult PB MNCs plated and the number of resulting ECFCs identified. Spearman rank correlation coefficient = 0.2182, 95% confidence interval= -0.3940 to 0.6963, two-tailed p value= 0.4739.

3.4 Discussion

In this chapter, the isolation, culture, yield and characterisation of endothelial cells from human umbilical cord blood (UCB), adult peripheral blood (PB) and adipose tissue (AT) have been described. The most reliable of these sources is UCB, and in collaboration with other researchers within the group, we have shown that ECFC yield from UCB units can be predicted from placental weight. This inverse correlation is a novel finding, and this work has been published in a peer reviewed journal (204). Ballen *et al*. have previously shown a 28% increase in yield of $CD34^+$ cells for every 500g increase in neonatal birth weight (223), which tend to be haematopoietic progenitor cells rather than ECFC. A similar direct correlation was more recently reported by Chandra *et al.* (224). Placental weight and birth weight have been shown to have a positive correlation by several authors (225-228), and other work has shown that final placental weight can be predicted from first trimester placental volume on three-dimensional ultrasound (226), or second trimester placental thickness on two-dimensional ultrasound (225). This means it may be possible to identify potentially high ECFC yield UCB donors from early pre-natal screening tests.

The findings in this Thesis regarding comparative yield of UCB and PB ECFCs are consistent with those of Ingram *et al*., who found that UCB produced 15 times more colonies than PB (229). In this Thesis, samples which produced ECFC had a mean yield of 13.3 colonies from a mean volume of 86ml UCB and a mean yield of 1.7 colonies from a mean volume of 50ml adult PB. This can be compared with Ingram *et al*. who reported a mean of approximately 8 colonies per 20ml UCB and less than 1 colony per 20ml adult PB (229). From the same work, Ingram *et al.* also postulated a hierarchy of Endothelial Progenitor Cells (EPC) with differences in telomerase activity which may account for the greater yield of ECFCs with younger blood samples (229). Estes *et al*. later developed a Polychromatic Flow Cytometry protocol which confirmed the presence of different subsets of circulating proangiogenic cells in adult PB (70), and very low numbers of ECFC. This

may be a possible explanation for the unreliable ECFC yield from the adult PB samples in this Thesis.

There is potential for further work to improve the yield of ECFC from adult sources, and a recent paper published after completion of this work reports a protocol for reliable culture of ECFCs from adipose tissue (111). Szöke *et al*. used lipoaspirate from liposuction rather than whole excised adipose tissue as per our protocol, and then utilised a similar process of collagenase digestion and centrifugation to obtain the stromal vascular fraction. Prior to plating cells from the stromal vascular fraction in a supplemented endothelial growth medium (MCDB 131, Gibco), Szöke *et al*. used Dynabeads (Invitrogen Dynal AS, Oslo, Norway) to isolate $CD44^{+}$ cells from the heterogenous cell population (111). There was consistent yield of endothelial cells from the lipoaspirate using this technique and cell selection may be the step required to prevent the frequent MSC proliferation found in our protocol. This work will be further explored within the research group, although a recent paper by Nuzzolo *et al.* suggests that there are differences in the gene expression profile of adult PB and UCB endothelial progenitor cells which result in the adult EPC being more pro-inflammatory and pro-thrombotic than UCB cells, thus making adult tissues a less attractive source of endothelial cells for vascular applications (230).

Adipose tissue remains the most clinically feasible autologous source from which to harvest cells in our target patient group as they may have large body surface area burns which precludes harvest of undamaged skin , and they may be too systemically unwell to spare peripheral blood or bone marrow (1). As a result of attempts to yield endothelial cells from the adipose tissue samples collected in this Thesis there was consistent culture of autologous MSCs from both adipose tissue and adipose microvasculature. Both of these cell types were selected for use in future experiments. This will be explored in Chapter 4.

It was decided to continue experimental work using endothelial cells from UCB due to the reliable yield from donor UCB units. Although autologous cells would be preferred for

clinical applications in order to eliminate the risk of rejection (130-132, 202) and to reduce the risk of infection (133, 134, 203), therapeutic use of donor UCB is well established for haematological disorders (231-235). Within Europe in 2011 there were 781 unrelated UCB transplants for indications such as haematological malignancies, solid tumours and primary immune deficiencies (234), and other clinical indications such as treatment of myocardial ischaemia (236) are becoming more common. There is already infrastructure in place in Europe for the collection, processing, storage, matching and allocation of UCB units, both in the public and private sectors (234, 235, 237-240), and this makes UCB a financially and technically feasible source of ECFC for our proposed clinical applications. Whereas existing clinical applications of UCB utilise whole units, *in vitro* vasculogenesis requires *ex vivo* expansion of ECFC derived from UCB units, so further Good Manufacturing Practice (GMP) grade techniques may still require development (222, 241). Further work should include development of a serum free media for ECFC culture such as those developed for culture of MSC using platelet lysate (81, 242, 243), and use of a closed bioreactor system to reduce the risk of contamination during *ex vivo* culture and expansion of cells (83, 244-246).

Chapter 4 Stromal Cell Sources for Clinical Applications

4.1 Background

Within our research laboratory, human dermal fibroblasts have been used as the main supporting stromal cells for *in vitro* microvascular tubule formation (135). Some work has also been undertaken using human bone marrow derived mesenchymal stromal cells (MSC). Patients with severe burns mount a systemic response to their injuries by mobilising cells from bone marrow (32), and as discussed, peripheral blood may not be a feasible source of and may not be available in sufficient volume to generate autologous stromal cells and endothelial cells for treating significant burns. Additionally, undamaged skin may be in short supply, thus obtaining skin biopsies to culture dermal fibroblasts as an autologous stromal cell source is also unlikely to be feasible, although in mixed thickness burns there may be areas of healthy dermis which could be harvested.

Adipose tissue is a mesenchymal derivative and is a potential clinical source of autologous supportive stromal cells for microvasculature formation. Recently, Natesan *et al.* demonstrated that subcutaneous tissue debrided along with burned skin was capable of yielding up to $2.5x10^5$ cells per millilitre of tissue in culture, including a population of viable stem cells (112). Adipose tissue (AT) derived stem cells have been described by several authors and many potential clinical uses are currently being investigated, including enhancing tendon and nerve repair and improving perfusion in ischaemic limbs and traumatic brain injury (97, 113-118). Within current plastic and reconstructive surgical practice, fat transfer is an established technique whereby adipose tissue aspirated from a suitable donor site using liposuction is then re-injected at other anatomical sites (119-122). The technique was standardised by Coleman who showed optimal yield of viable adipocytes by manual liposuction with a large bore cannula and syringe, followed by a short period of centrifugation

(120). Pu *et al.* demonstrated a statistically significant difference in viable adipocyte yield when using the Coleman technique compared with traditional mechanically assisted liposuction to harvest lipoaspirate (123). Recently the fat transfer procedure has been improved by introducing a closed system of adipose digestion and separation for use intra-operatively in order to boost the ratio of adipose derived MSCs within the re-injected solution (125). Results have shown better survival of free fat transfers which are boosted with additional cells from the stromal vascular fraction, and so there is already a clinical precedence for autologous use of these cells *in vivo* (118, 124-129).

This chapter compares the morphology, phenotype and differentiation potential of MSCs from whole AT and MSCs from adipose microvasculature dissected free from whole AT. To my knowledge the comparison of such paired samples has not been previously reported. Recently authors have suggested that adipose tissue MSCs are components of a perivascular niche (113) and so we hypothesised that cells cultured from dissected microvasculature may have different characteristics to those from whole AT.

4.2 Aim and objectives of this chapter

The aim of this chapter is to identify feasible source tissues for stromal cell isolation and culture, for use in clinical applications.

Objectives:

- To establish the phenotype of human dermal fibroblasts commonly used within this research laboratory to form *in vitro* microvascular tubule networks as a control for AT derived stromal cell isolation
- To investigate adipose tissue as a potential autologous source of stromal cells collected from plastic surgery patients
    - Whole adipose tissue from breast reconstruction patient donors
    - Microvasculature dissected free from the whole adipose tissue
- To characterise and compare the phenotype of paired stromal cells from adipose tissue and adipose microvasculature
- To determine and compare the ability of paired stromal cells from adipose tissue and adipose microvasculature to differentiate into three mesenchymal cell lineages

4.3 Results

4.3.1 Human Dermal Fibroblasts

Human Dermal Fibroblasts (HDFs) have been used consistently within our research laboratory as a supportive cell type in co-culture with endothelial cells to form microvascular tubules. HDF were obtained from stock stores of cells within our research group, initially purchased from Lonza Biologics (Slough, UK) and derived from human neonatal foreskin. Typical spindle shaped cell morphology of HDFs is shown in Figure 4.1. In this Thesis, these stromal cells were used as a control for the basic vascular tubule co-culture technique, and later as control cells when comparing new stromal cell types. Hence flow cytometry cell surface marker analysis was

carried out on three separate batches of HDFs at passage 5. The method is described in Chapter 2 Section 2.5, representative histograms of flow cytometric analyses for cell surface markers are shown in Figure 4.2 and a summary of the markers tested is shown in Table 4.1.

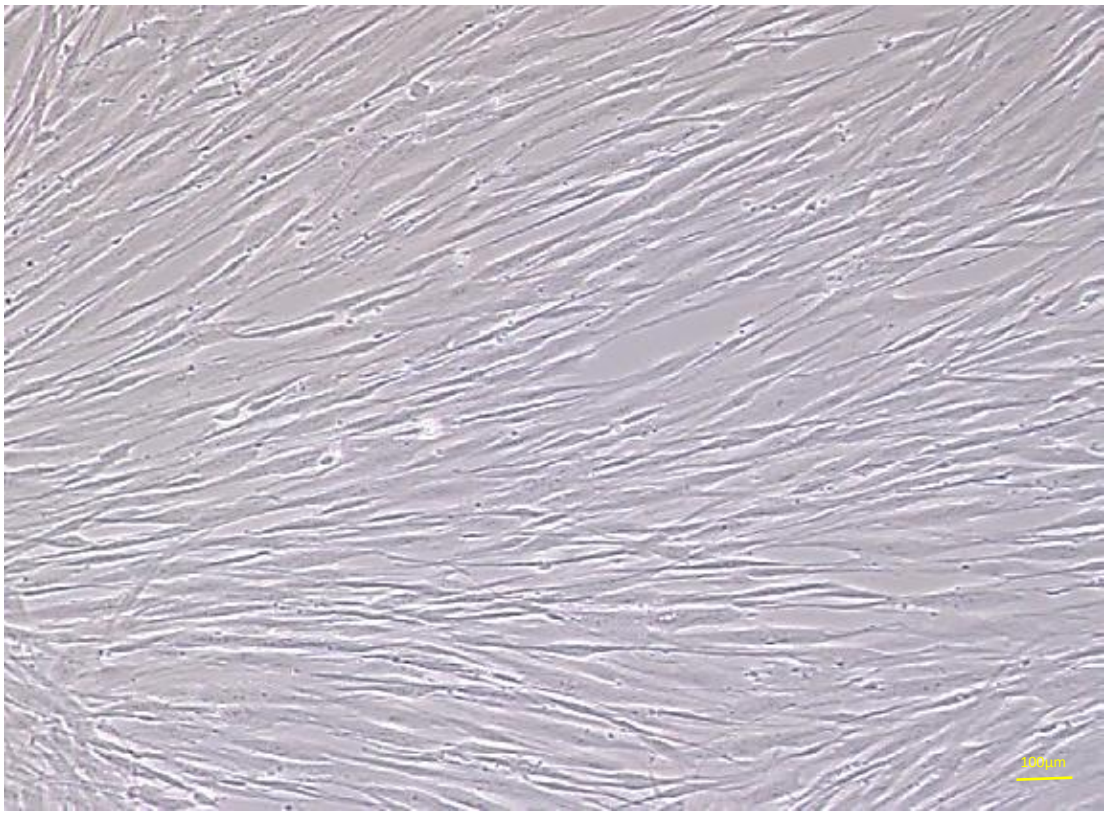

Figure 4.1: Morphology of Human Dermal Fibroblasts (HDF). These cells were cultured in Endothelial Growth Medium 2 (EGM-2). HDF were obtained from stock stores of cells within our research group, initially purchased from Lonza Biologics (Slough, UK) and derived from human neonatal foreskin. (Phase contrast microscopy, 100µm scale bar).

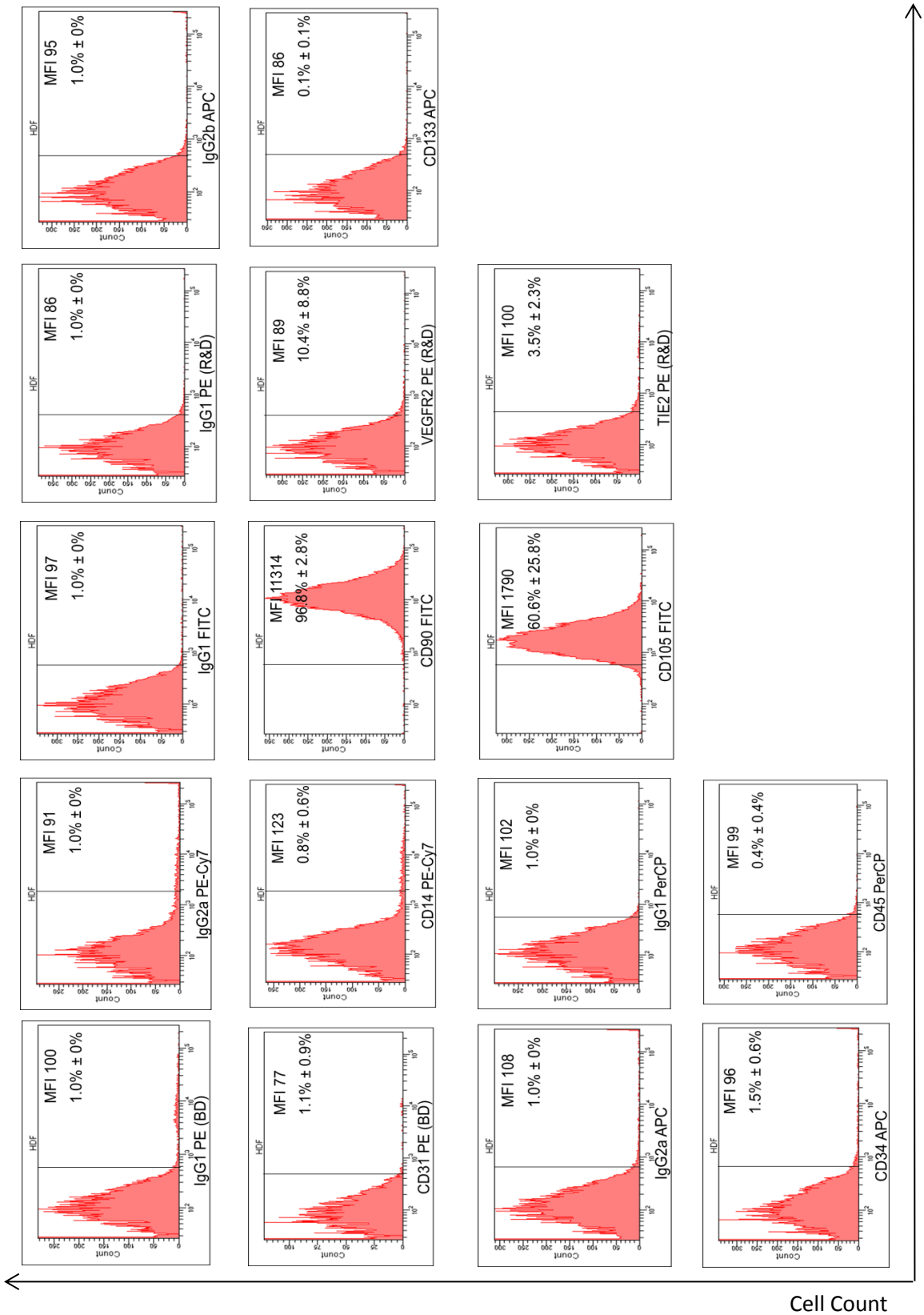

Figure 4.2: Flow cytometry phenotyping of Human Dermal Fibroblasts (HDFs) harvested at passage 5. Representative FACS histograms of HDFs stained with the antibodies indicated on each histogram. Values on histograms are Median Fluorescence Intensity (MFI) from the batch of cells shown. Isotype controls had a gate set at 1% positive cells (vertical black line) and the corresponding markers show the mean percentage of cells falling in that gate from three different samples ± SEM. HDFs are CD90^{+} and CD 105^{+} with no expression of endothelial markers.

The HDFs were consistently $CD90^+$, $CD105^+$ and negative for all haematopoietic and endothelial markers tested. CD90 (Thy-1) is a key cell surface marker on fibroblasts, mesenchymal stem/stromal cells and haematopoietic stem cells (217), and has variable expression on different subtypes of fibroblastic cells with different contractile properties (217). CD105 (Endoglin) is found on various stromal and mesenchymal cells (209) and is a transmembrane glycoprotein which binds members of the Transforming Growth Factor Beta (TGFβ) family of peptides (208, 209). These peptides are involved in vasculogenesis and angiogenesis, and are also produced by endothelial cells. These two cell surface markers are considered as standard markers of mesenchymal stromal cells.

Table 4.1: Cell surface marker expression on cultured human dermal fibroblasts.

Marker	**Main Antigen Expression**	**HDF** **% positive ± SEM**
CD14	Monocytes.	0.8% ± 0.6% (-)
CD31	Endothelial cells, Platelets, Monocytes, Granulocytes, B cells, Haematopoietic stem cells, Proangiogenic haematopoietic cells	1.1% ± 0.9% (-)
CD34	Haematopoietic stem and progenitor cells, Endothelial cells, Subsets of Mesenchymal Stem Cells	1.5% ± 0.6% (-)
CD45 (Pan specific)	Leucocytes	0.4% ± 0.4% (-)
CD90	Stromal cells, Mesenchymal Stem Cells , Haematopoietic stem cells	96.8% ± 2.8% (+++)
CD105	Endothelial cells, Stromal cells, Mesenchymal Stem Cells	60.6% ± 25.8% (+++)
CD133	Haematopoietic stem and progenitor cells, Other stem cells eg. Neural, Retinal cells	0.1% ± 0.1% (-)
VEGFR2	Endothelial cells, Stem cell subsets, Proangiogenic haematopoietic cells	10.4% ± 8.8% (+)
TIE2	Endothelial cells, Stem cells, Some monocytes, Proangiogenic haematopoietic cells	3.5% ± 2.3% (-)

% positive values are the mean results from three different batches of HDF ± Standard Error of the Mean

4.3.2 Adipose tissue and adipose microvasculature derived MSCs

Human adipose tissue was collected with written patient consent and ethical approval from the Southampton and South West Hampshire Research Ethics Committee (A) (REC Reference Number 09/H0502/120). The adipose tissue source was zone 4 of the Deep Inferior Epigastric Perforator (DIEP) flap raised for breast reconstruction surgeries; a procedure described by Blondeel in 1994 (247). This zone of the flap is often discarded in unilateral breast reconstruction where the abdominal tissue is raised on a single vascular pedicle, because flap perfusion at the recipient site is impaired by crossing additional sets of choke vessels across the flap (247-249). This is demonstrated schematically in Figure 4.3.

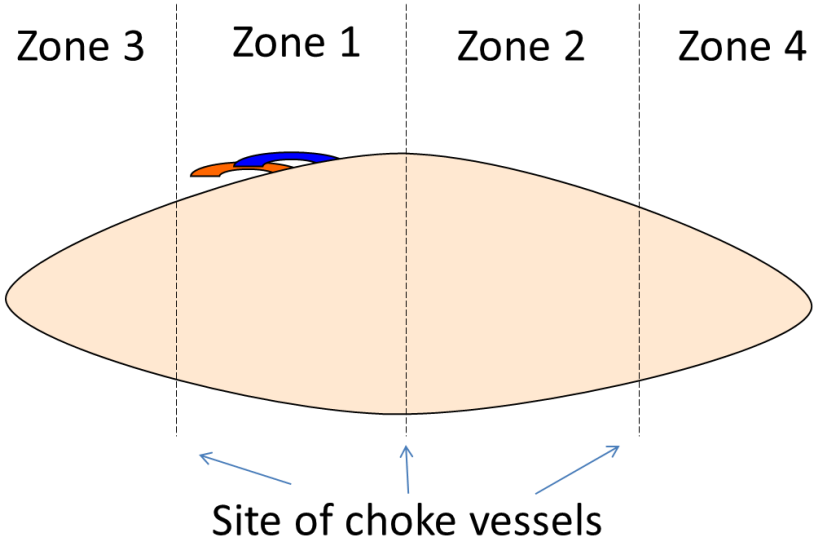

Figure 4.3: Schematic representation of the vascular anatomy of a Deep Inferior Epigastric artery Perforator (DIEP) flap. The vascular pedicle resides in zone 1 and the quality of perfusion diminishes across the zones as blood must cross more 'choke vessels', limiting lateral blood flow. The whole flap is raised to allow for symmetry and ease of closure of the donor site, but zone 4 tissue is often discarded before the flap is inset due to poor reliability of perfusion post anastomosis of the pedicle with recipient vessels. This was the source of human adipose tissue used in the protocol in this Thesis.

Human adult adipose tissue (AT) samples were divided and either had microvasculature (MV) dissected from the tissue or remained as whole AT (Figure 4.4). These samples were finely cut

and dissociated in either 0.5mg/ml Trypsin EDTA (PAA Laboratories Ltd., Yeovil, UK) or 1.0mg/ml Collagenase A (Roche Diagnostics, Basel, Switzerland) as described in Chapter 2 Section 2.4.3. Following centrifugation, the stromal vascular fraction cell pellets were collected, plated on rat tail collagen I coated 6 well plates (BD Biosciences, Franklin Lakes, NJ, U.S.A.) and cultured in complete EGM-2 (Lonza Biologics, Slough, UK) for up to 3 weeks, with media changes every 2-3 days. MSCs were cultured from 100% of AT samples. In samples where MV was dissected free from the AT for separate culture there was also 100% yield of MSCs.

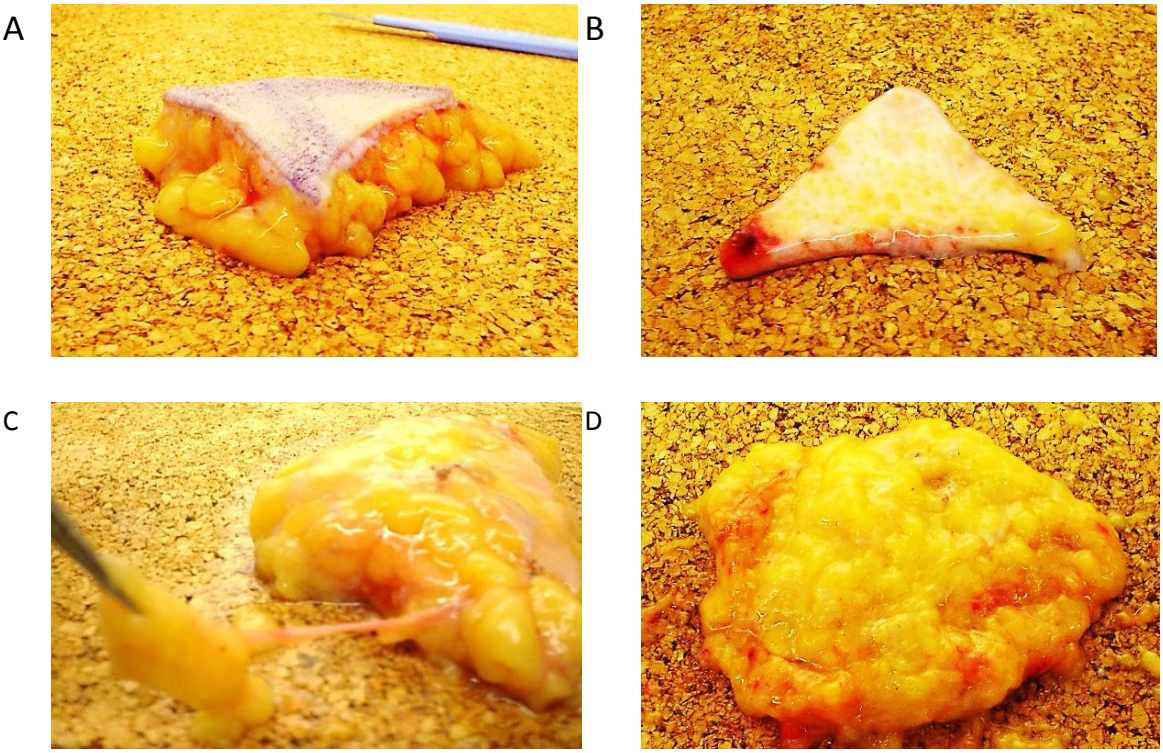

Figure 4.4: Preparation of donor tissue for adipose and microvasculature processing. A- Whole AT from zone 4 of a DIEP flap, with attached skin as collected from the operating theatre. B- Skin was excised and discarded. C- Dissection of microvasculature from within the tissue was performed using 3.5x operating loupe magnification. D- Whole adipose tissue was manually diced into approximately 2x2x2mm cubes prior to collagenase digestion.

The protocol for AT processing within our research group was developed by adapting methods from papers by Xue *et al.* (250) and Mosna *et al.* (138). At the time of developing the method, Xue *et al.* were the most prominent researchers describing isolation of endothelial cells from AT, which was the initial aim of this Thesis. Endothelial cells were separated using plastic cloning rings (Sigma Aldrich Ltd., Gillingham, UK) to isolate colonies, and culture of remaining MSCs continued to build working stock.

Representative morphology of MSCs isolated from adipose tissue and adipose microvasculature is shown in Figure 4.5. Both cell types have a spindle shaped morphology and proliferated very quickly in culture, forming dense monolayers on plastic culture plates.

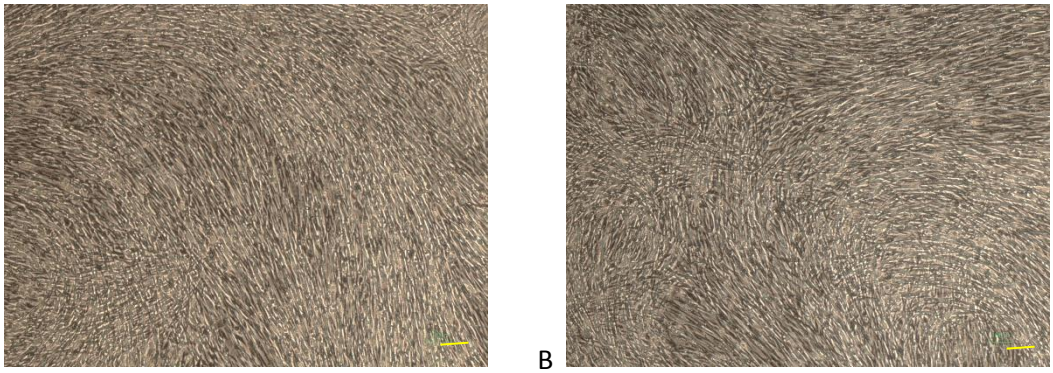

A Adipose MSC at passage 2

B Microvasculature MSC at passage 2

Figure 4.5: Morphology of MSCs cultured from adipose tissue (AT) and adipose microvasculature (MV). These cells were cultured in complete Endothelial Growth Medium 2 (EGM-2). AT MSCs (A) were cultured to passage 2 in complete EGM-2 from the vascular stromal fraction of processed whole human adipose tissue. MV MSCs (B) were cultured to passage 2 in EGM-2 from the vascular stromal fraction of processed microvasculature dissected free from whole human adipose tissue. (Phase contrast microscopy, 100µm scale bars)

Table 4.2 summarises the main stages of the protocol developed in this Thesis to culture AT MSC and MV MSC, compared with the methods by Xue *et al.* (250) and Mosna *et al.* (138). Table 4.3 shows a summary of the cells cultured from all adipose tissue and microvasculature samples.

Table 4.2: Development of a protocol for adipose tissue processing.

	Adipose MSC Protocol developed in this Thesis	**Xue *et al.* (250)**	**Mosna *et al.* (138)**
Source	Human abdominal adipose tissue from DIEP flap harvest.	Lumbar subcutaneous adipose tissue from adult male Wistar rats.	Human subcutaneous fat.
Transport	Tissue block in 200ml HBSS without Ca^{2+} & Mg^{2+}.	-	-
Gross processing	Dissection of microvasculature free from adipose tissue. Separate MV and whole AT finely cut.	Minced with sterile scissors.	-
Digestion	5ml 1.0mg/ml Collagenase A per 25ml processed tissue. 5% CO_2 incubator 37°C, 40 mins.	0.15% (w/v) collagenase type I. 5% CO_2 incubator 37°C, 60 mins.	Type II collagenase, 30 min at 37°C, shaken at 150 rpm. OR Type I collagenase, 60 min at 37°C, in continuous agitation.
Post digestion	Topped up to 40ml with complete EGM-2 with 10% (v/v) Hyclone FCS. Centrifuged 1000g, 10 mins at 22°C.	Neutralised with DMEM/F12 with 10% (v/v) Hyclone FCS. Centrifuged 1500rpm, 10 mins.	Centrifuge 200g, 10 mins, room temp.
Cell collection	Stromal vascular fraction cell pellet aspirated with pipette passed beyond lipid layers.	Stromal cell pellet collected.	Cell pellet washed 3-4x in PBS. Erythrocytes lysed with NH_4Cl. 100µm filter.
Cell solution	Cells resuspended in complete EGM-2 with 10% (v/v) Hyclone FCS.	Cells resuspended in DMEM/F12 with 10% (v/v) Hyclone FCS.	Final pellet resuspended in GM growth media.
Cell culture	Rat tail collagen I coated 6 well plates at $2x10^6$ cells/well. 5% CO_2 incubator, 37°C. Media change day 1, then every 2-3 days for 3 weeks.	5% CO_2 incubator 37°C.	Plated at $1x10^6/cm^2$. Plates washed with PBS at 72 hours & GM changed. 40-50% media change 2x/week.
Cell passage and further processing	Confluent MSCs harvested with 0.5mg/ml Trypsin EDTA. Cultures expanded in complete EGM-2 with 10% (v/v) Hyclone FCS to storage or use at passage 2.	Passage with 0.25% trypsin/EDTA at 80% confluence. Endothelial cells induced by culture in differentiation medium (DMEM low glucose with dexamethasone, 5% (v/v) FCS, VEGF, FGF basic and ILGF).	Detached and replated at lower density (1.8-3.1 x 10^3 cells/cm^2). after 6 days in culture Homogenous MSC cell population after 3-5 weeks.

Table 4.3: Yield of MSC from adipose tissue and adipose microvasculature.

AT number	AT MSC	AT ECFC	MV MSC	MV ECFC
1	6 confluent wells	0	(none plated)	0
2	6 confluent wells	0	(none plated)	0
3	6 confluent wells	0	(none plated)	0
4	6 confluent wells	0	(none plated)	0
5	6 confluent wells	0	6 confluent wells	0
6	2 confluent wells	31 colonies	5 confluent wells	10 colonies
7	1 confluent well	16 colonies	6 confluent wells	0
8	1 confluent well	1 colony	1 confluent well	1 colony
9	6 confluent wells	0	6 confluent wells	0
10	6 confluent wells	0	6 confluent wells	0
11	6 confluent wells	0	6 confluent wells	0
12	6 confluent wells	0	6 confluent wells	0
13	6 confluent wells	0	6 confluent wells	0

The stromal vascular fractions from 13 processed adipose tissue and 9 paired microvasculature samples were suspended in EGM-2 and plated in 6 wells of a rat tail collagen I coated 6 well plate. All samples were a source of MSC and 3 of the samples also yielded ECFC. MSC were expanded until storage or experimental use at passage 2. Both AT and MV MSC wells were fully confluent after 1 week in culture.

Flow cytometry cell surface marker analysis was performed on four paired batches of AT and MV MSCs at passage 3. The method is described in Chapter 2 Section 2.5 and representative histograms of flow cytometric analyses for cell surface markers are shown in Figure 4.6 (AT MSCs) and Figure 4.7 (MV MSCs). Both AT and MV MSCs were consistently $CD73^+$, $CD90^+$, $CD105^+$, $CD140b^+$ and $CD14^-$, $CD34^-$, $CD45^-$ and HLA-DR^-. The stromal markers CD90 and CD105 have previously been described in this chapter. CD105 was low on most cells. CD73 mediates permeability of endothelium and lymphatic vessels (206), and is non-specific for a particular cell type. CD140b (Platelet Derived Growth Factor Receptor β) is a pericytic marker previously noted on adipose derived stem cells and thought to indicate that adipose stem cells arise from a perivascular niche (205).

CD14 is the primary endotoxin binding molecule found on human monocytes (216) and its lack of positivity indicates that the cell lines are not derived from monocytes. CD34 is another transmembrane protein involved in cell adhesion. It is found on most endothelial cells, but also haematopoietic stem cells in the early progenitor stages and on some MSCs (73). The absence

of CD34 makes it unlikely that the cell lines are endothelial or haematopoietic in origin. The CD45 antigen used was pan-specific and therefore capable of identifying all isoforms of the CD45 cell surface marker, Protein Tyrosine Phosphatase Receptor type C (PTPRC). This marker is present in different isoforms on all subtypes of leucocytes (74, 75), so we can conclude that the cells are not cultured from leucocytes. HLA-DR is a cell surface receptor which interacts with antigens to present them to the immune system via T helper cells (251). As such HLA-DR is found on cell types involved in antigen presentation such as B cells, macrophages and dendritic cells and is negative in adipose MSCs.

The combination of positive and negative cell surface markers identified on the adipose and microvasculature MSCs are consistent with the adipose derived stem cell phenotype described by other authors (97, 98, 113). Notably, the cell surface markers did not discriminate between the two subsets of MSCs.

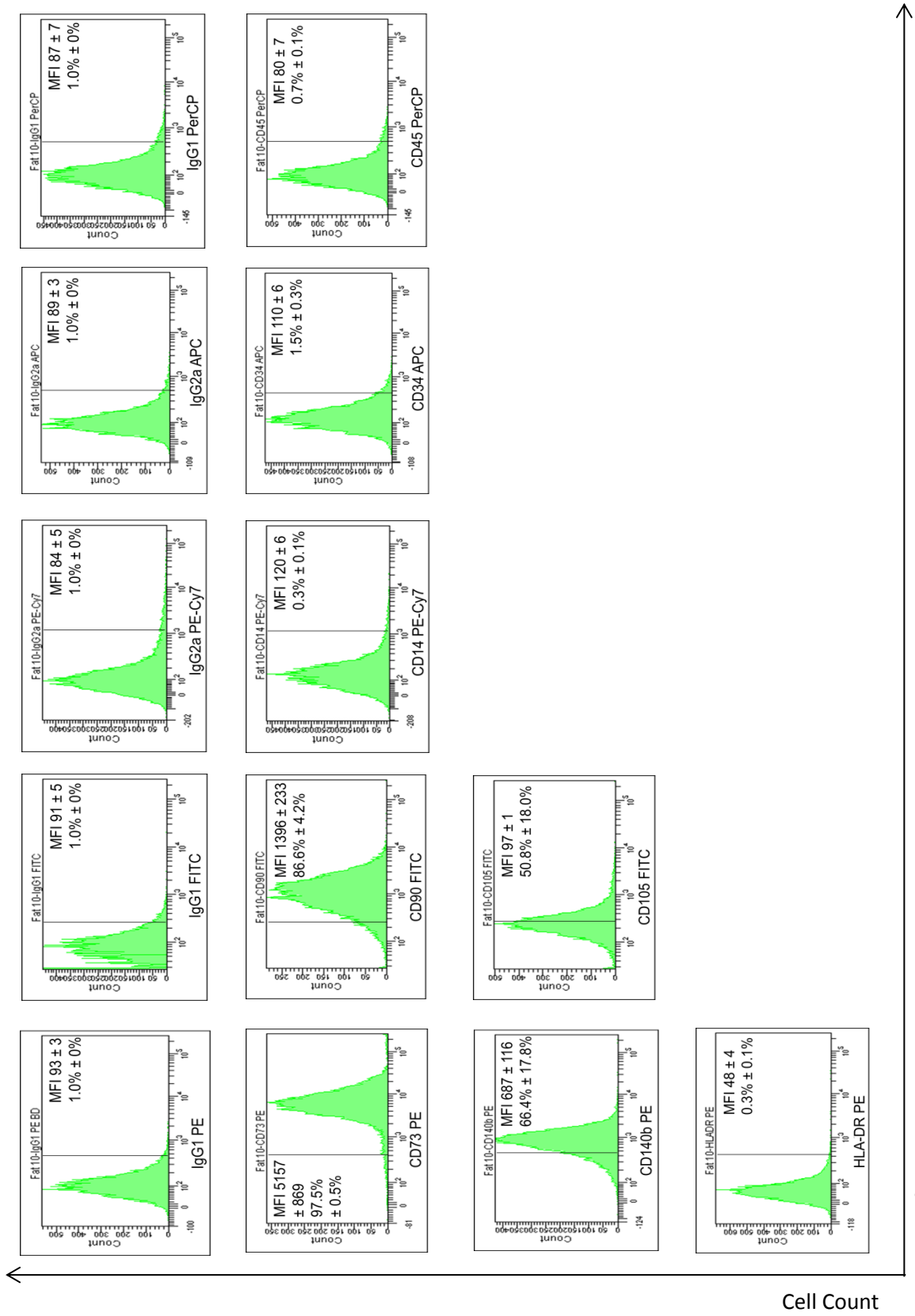

Figure 4.6: Flow cytometry phenotyping of Human Adipose Tissue derived Mesenchymal Stromal Cells (AT MSC) harvested at passage 3. Representative FACS histograms of AT MSCs stained with the antibodies indicated on each histogram. Values on histograms are Median Fluorescence Intensity (MFI) from four different samples ± Standard Error of the Mean (SEM). Isotype controls had a gate set at 1% positive cells (vertical black line) and the corresponding markers show the mean percentage of cells falling in that gate from four different samples ± SEM. Human AT MSCs are $CD73^{+}$, $CD\ 90^{+}$, $CD105^{+}$, $CD\ 140b^{+}$ and $CD14^{-}$, $CD34^{-}$, $CD45^{-}$ and $HLA\text{-}DR^{-}$.

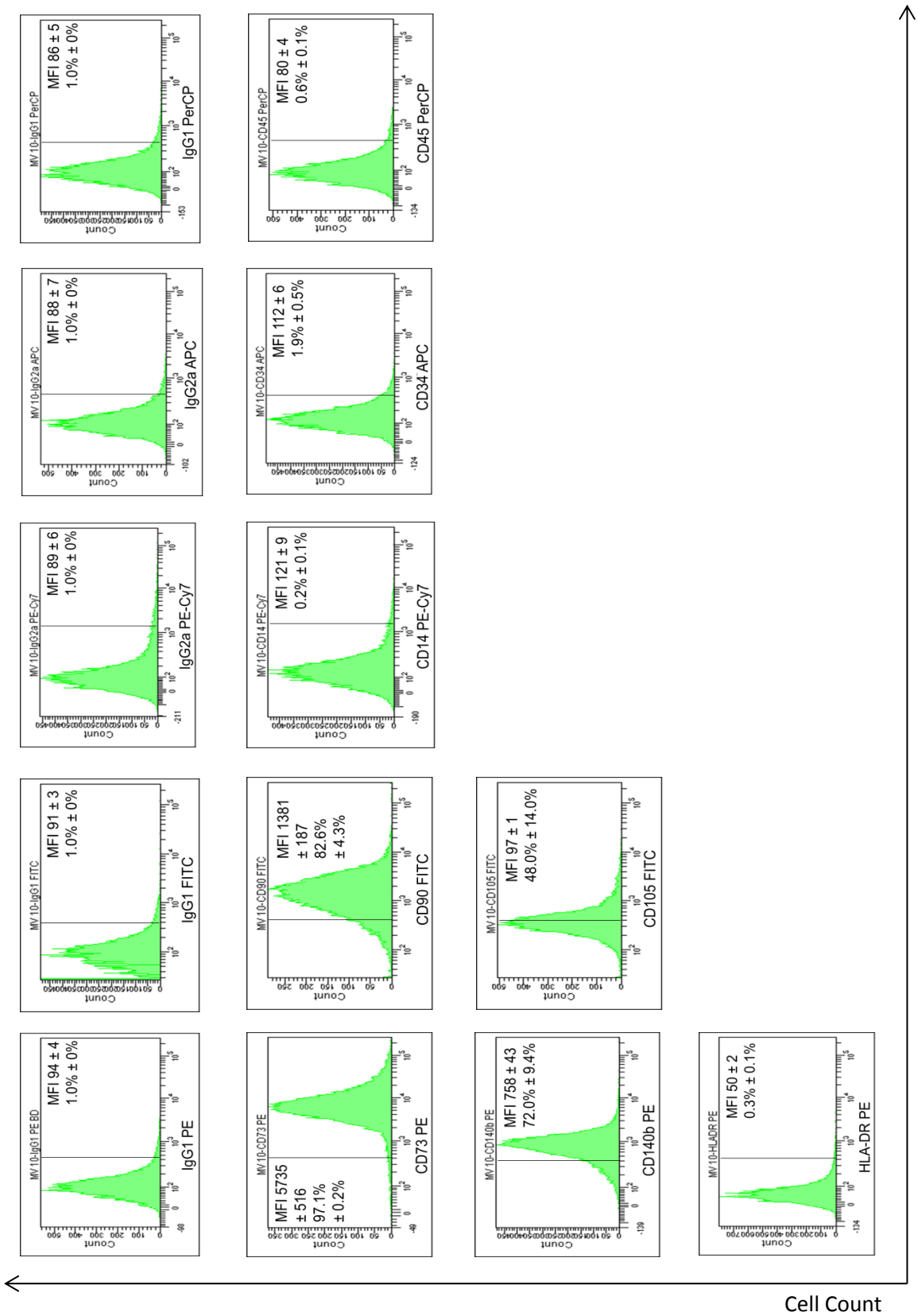

Figure 4.7: Flow cytometry phenotyping of Human Adipose Microvasculature derived Mesenchymal Stromal Cells (MV MSC) harvested at passage 3. Representative FACS histograms of MV MSCs stained with the antibodies indicated on each histogram. Values on histograms are Median Fluorescence Intensity (MFI) from four different samples ± Standard Error of the Mean (SEM). Isotype controls had a gate set at 1% positive cells (vertical black line) and the corresponding markers show the mean percentage of cells falling in that gate from four different samples ± SEM. Human MV MSCs are CD73^{+}, CD 90^{+}, CD105^{+}, CD 140b^{+} and CD14^{-}, CD34^{-}, CD45^{-} and HLA-DR^{-}.

4.3.3 Mesenchymal differentiation of adipose and microvasculature MSCs

In order to describe a cell type as being an MSC it is necessary to demonstrate the potential for the cells to differentiate into three different mesenchymal lineages; adipose, cartilage and bone (95, 98, 101). Mesenchymal differentiation assays were completed on three batches of paired adipose and microvasculature MSCs, with bone marrow MSC controls. There were three repeats of each condition for each cell type. Both AT and MV MSCs within the isolated fractions were capable of differentiation into three mesenchymal stem/stromal lineages, as detailed below.

4.3.3.1 Adipogenesis

Representative images of adipogenic differentiation (n=3) are shown in Figure 4.8. Following a period of culture in adipogenic induction media, as described in Chapter 2 Section 2.7.1, induced cells and non-induced control cells cultured in regular mesenchymal media were stained with Oil Red. The red stain was taken up by adipocytes and coloured the lipid droplets within the cells, whilst control cells did not pick up any stain. All 3 AT MSC and MV MSC paired samples were capable of adipogenic differentiation, as were BM MSC controls. Figure 4.9 shows a higher magnification image of adipogenic differentiated AT MSCs, allowing clear visualisation of the adipocytes with Oil Red stained lipid droplets within the cells.

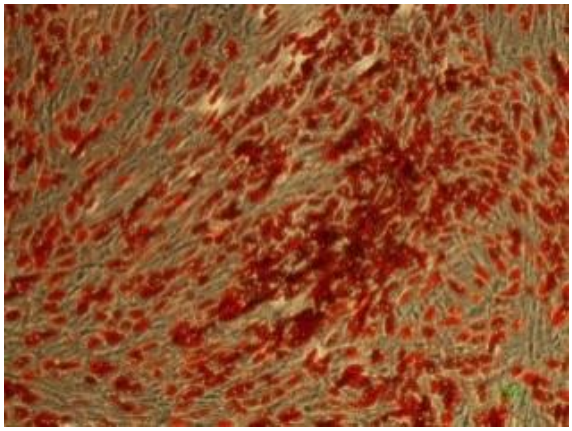

A Adipogenesis differentiated AT MSCs

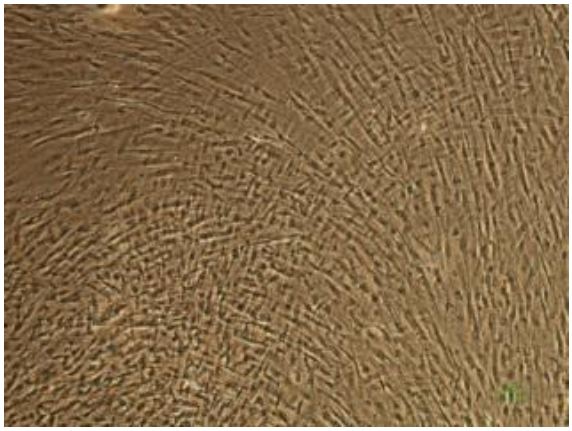

B Non-inducing control AT MSCs

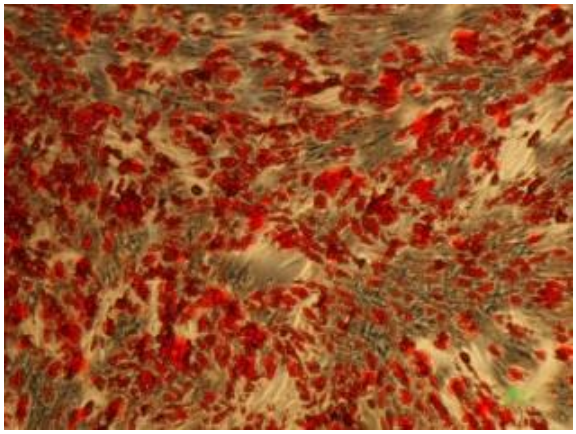

C Adipogenesis differentiated MV MSCs

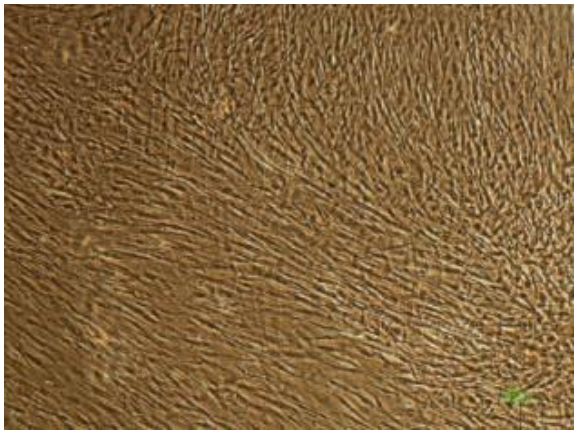

D Non-inducing control MV MSCs

Figure 4.8: Adipogenic differentiation of AT and MV MSCs. MSCs were cultured in adipogenic induction media or non-inducing control media for 3 weeks. Plates were then stained with Oil Red, which coloured the lipid droplets within adipocytes. Control cells did not pick up any staining. A- Adipogenesis differentiated AT MSCs B- Non-inducing control AT MSCs C- Adipogenesis differentiated MV MSCs D- Non-inducing control MV MSCs. (Phase contrast microscopy, 100µm scale bars)

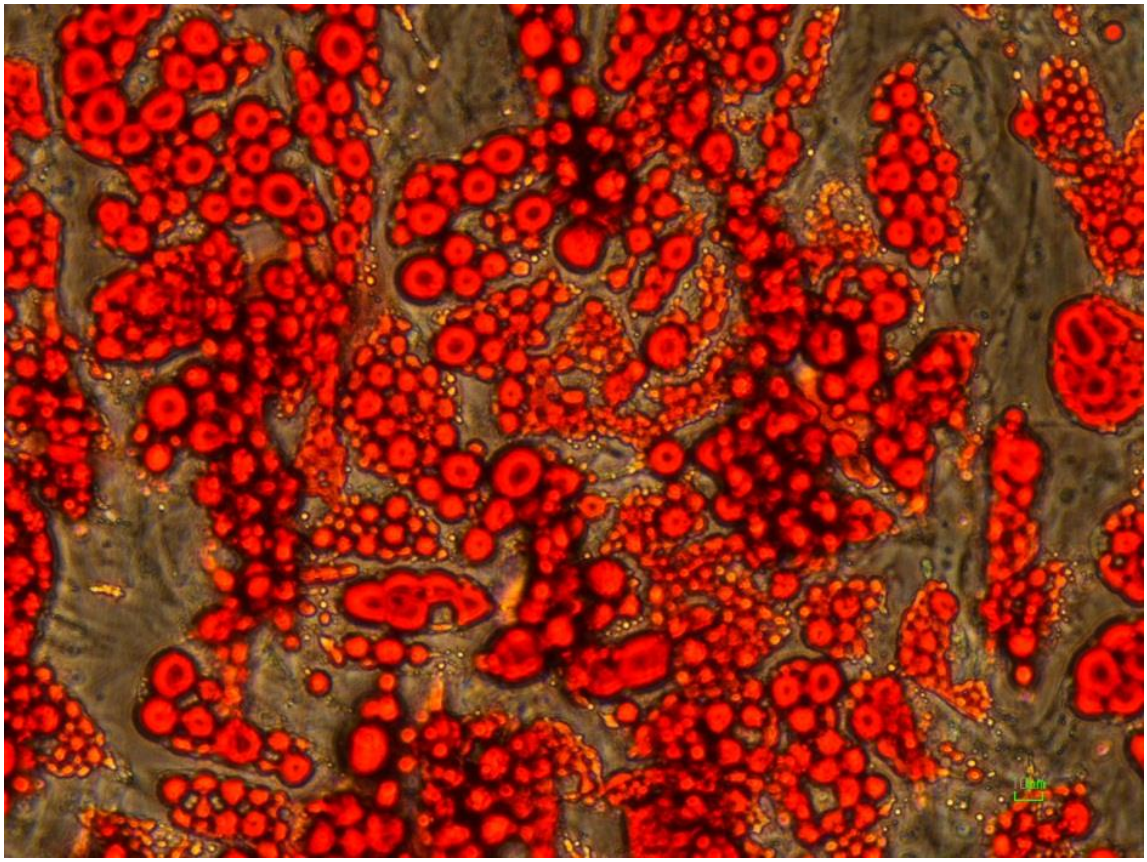

Figure 4.9: Higher magnification microscopy (x10) of adipogenesis differentiated AT MSCs showing Oil Red staining of the lipid droplets within the adipocytes. (Phase contrast microscopy, 10µm scale bar)

4.3.3.2 Osteogenesis

Representative images of osteogenic differentiation are shown in Figure 4.10. Following a period of culture in osteogenic induction media, as described in Chapter 2 Section 2.7.2, induced cells and non-induced control cells cultured in regular mesenchymal media were stained using the von Kossa method to identify calcium deposits, which appeared as dark brown cuboids. The induced cells formed over-confluent monolayers and began to delaminate from the edges of the plastic culture plates. The fast red stain used in combination with the von Kossa method aids visualisation of the calcium deposits associated with osteogenic differentiation. All 3 AT MSC and MV MSC paired samples were capable of osteogenic differentiation, as were BM MSC controls.

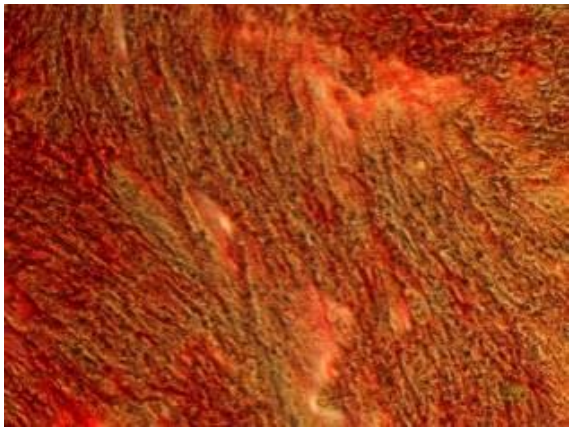

A Osteogenesis differentiated AT MSCs

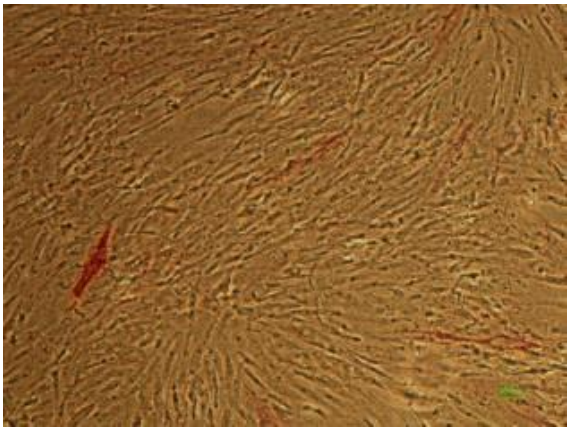

B Non-inducing control AT MSCs

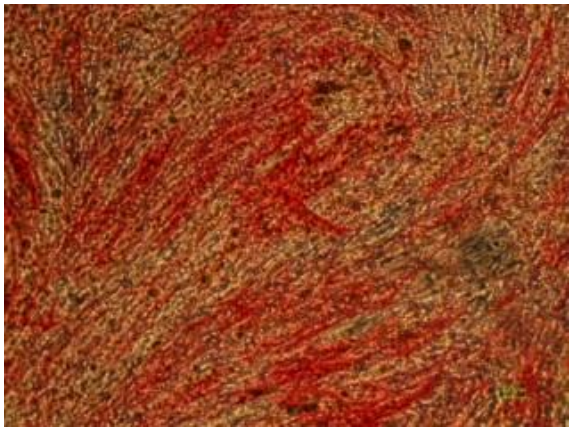

C Osteogenesis differentiated MV MSCs

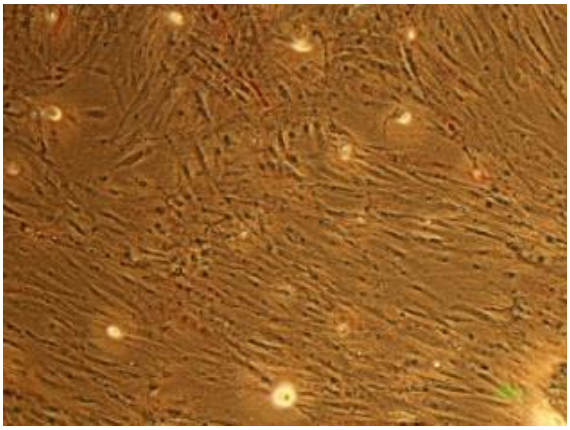

D Non-inducing control MV MSCs

Figure 4.10: Osteogenesis differentiation of AT and MV MSCs. MSCs were cultured in osteogenic induction media or non-inducing control media for 3 weeks. Plates were then stained with von Kossa stain and fast red, which coloured the calcium deposits of the osteocytes. Control cells did not pick up any staining. A- Osteogenesis differentiated AT MSCs B- Non-inducing control AT MSCs C- Osteogenesis differentiated MV MSCs D- Non-inducing control MV MSCs. (Phase contrast microscopy, 100µm scale bars)

4.3.3.3 Chondrogenesis

Representative images of chondrogenic differentiation are shown in Figure 4.11 (AT MSCs) and Figure 4.13 (MV MSCs). Following a period of culture in chondrogenic induction media, induced cell pellets and non-induced control cell pellets cultured in regular mesenchymal media were snap frozen in liquid nitrogen, sectioned and immunostained for the presence of type 2 collagen. Representative images of non-induced control cell pellets are shown in Figure 4.12 (AT MSCs) and Figure 4.14 (MV MSCs). All 3 AT MSC and MV MSC paired samples were capable of chondrogenic differentiation, as were BM MSC controls.

Chondrogenesis differentiated AT MSCs

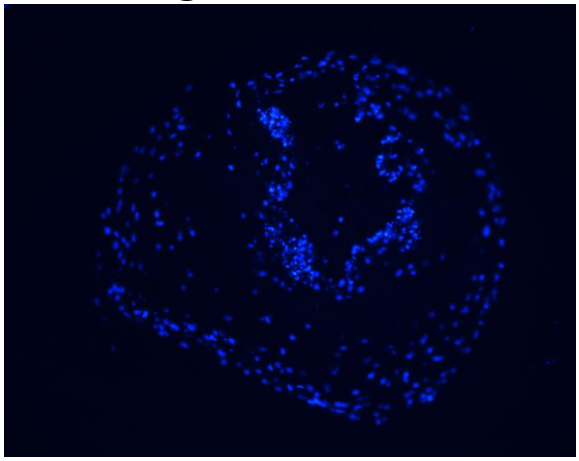

A DAPI stained nuclei
10x magnification

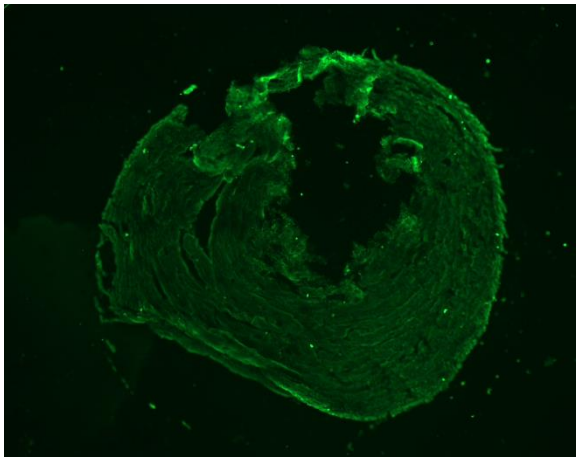

B Alexofluor 488 labelled collagen II staining
10x magnification

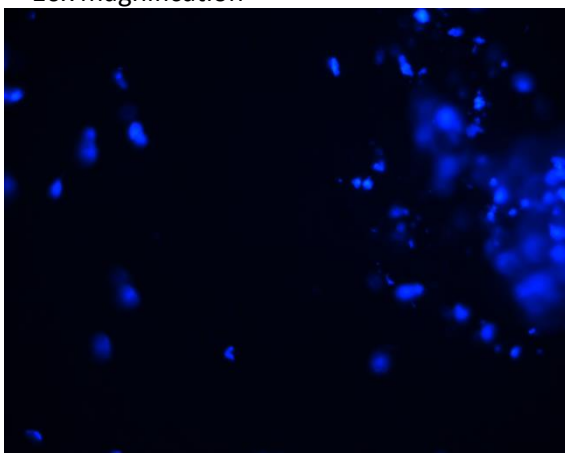

C DAPI stained nuclei
40x magnification

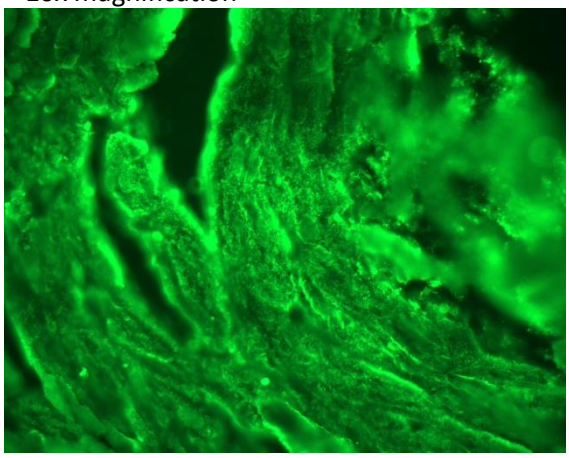

D Alexofluor 488 labelled collagen II staining
40x magnification

Figure 4.11: Chondrogenesis differentiated AT MSCs. MSCs were cultured in chondrogenic induction media for 4 weeks. Cell pellets were then snap frozen in liquid nitrogen, cryosectioned and immunostained for the presence of type 2 collagen. DAPI stain was used to show the nuclei of viable cells within the pellets and Alexofluor 488 labelled immunostain showed the presence of type 2 collagen. A- Chrondrogenesis differentiated AT MSCs DAPI nucleic stain at 10x magnification B- Chrondrogenesis differentiated AT MSCs Alexofluor 488 labelled collagen 2 stain at 10x magnification C- Chrondrogenesis differentiated AT MSCs DAPI nucleic stain at 40x magnification D- Chrondrogenesis differentiated AT MSCs Alexofluor 488 labelled collagen 2 stain at 40x magnification. (Fluorescence microscopy)

Non inducing control AT MSCs

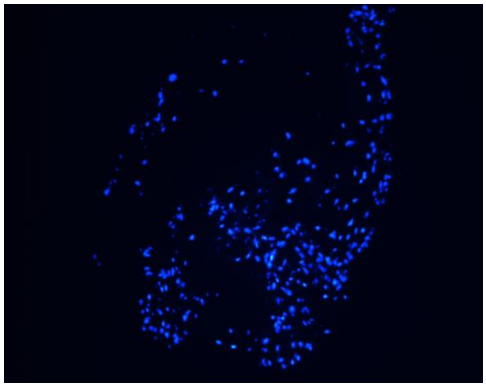

A DAPI stained nuclei
10x magnification

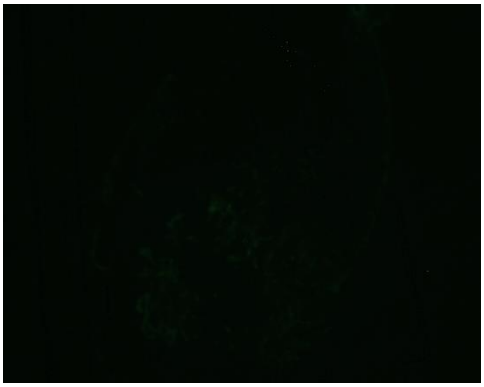

B Alexofluor 488 labelled collagen II staining
10x magnification

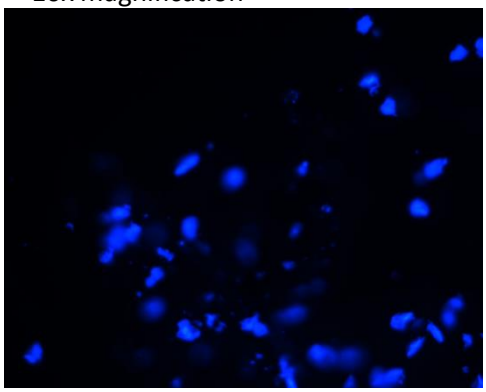

C DAPI stained nuclei
40x magnification

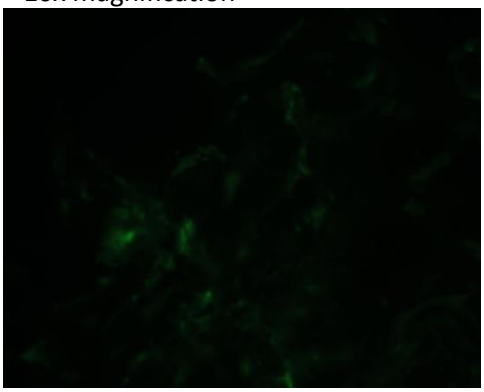

D Alexofluor 488 labelled collagen II staining
40x magnification

Unstained non inducing control AT MSCs

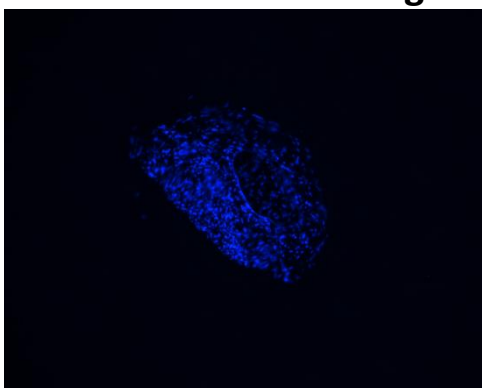

E DAPI stained nuclei of unstained control
10x magnification

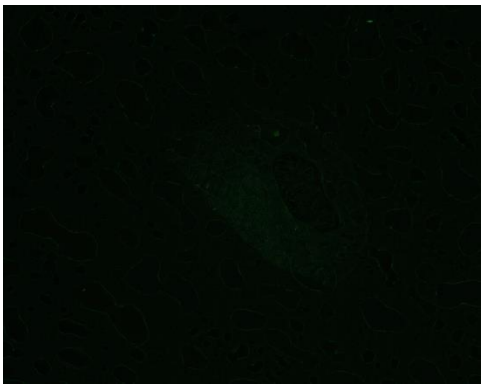

F Unstained control
10x magnification

Figure 4.12: Chondrogenesis non-induced control AT MSCs. MSCs were cultured in non-inducing control media for 4 weeks. Cell pellets were then snap frozen in liquid nitrogen, cryosectioned and immunostained for the presence of type 2 collagen. DAPI stain was used to show the nuclei of viable cells within the control pellets and Alexofluor 488 labelled immunostain showed the absence of type 2 collagen. A- Chrondrogenesis non-induced control AT MSCs DAPI nucleic stain at 10x magnification B- Chrondrogenesis non-induced control AT MSCs Alexofluor 488 labelled collagen 2 stain at 10x magnification C- Chrondrogenesis non-induced control AT MSCs DAPI nucleic stain at 40x magnification D- Chrondrogenesis non-induced control AT MSCs Alexofluor 488 labelled collagen 2 stain at 40x magnification E- Chrondrogenesis non-induced control AT MSCs DAPI nucleic stain of pellets not co-stained with Alexofluor 488 labelled collagen 2 stain at 10x magnification F- Background fluorescence of Chrondrogenesis non-induced control AT MSCs without Alexofluor 488 labelled collagen 2 stain at 10x magnification. (Fluorescence microscopy)

Chondrogenesis differentiated MV MSCs

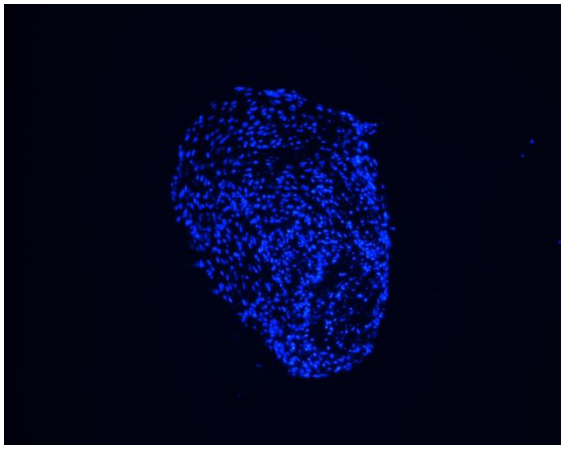

A DAPI stained nuclei
10x magnification

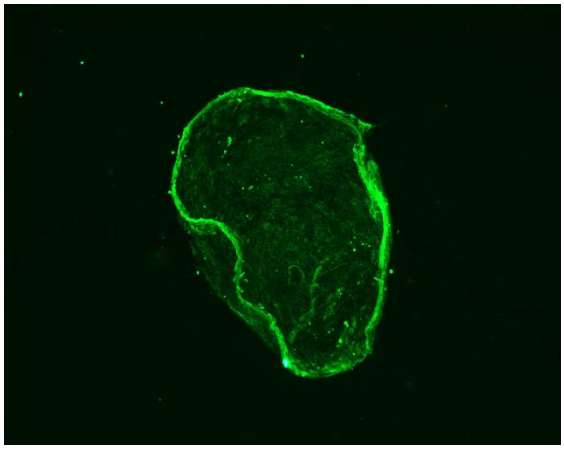

B Alexofluor 488 labelled collagen II staining
10x magnification

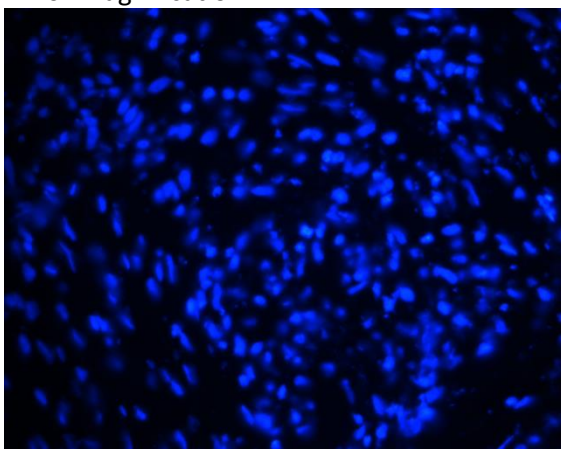

C DAPI stained nuclei
40x magnification

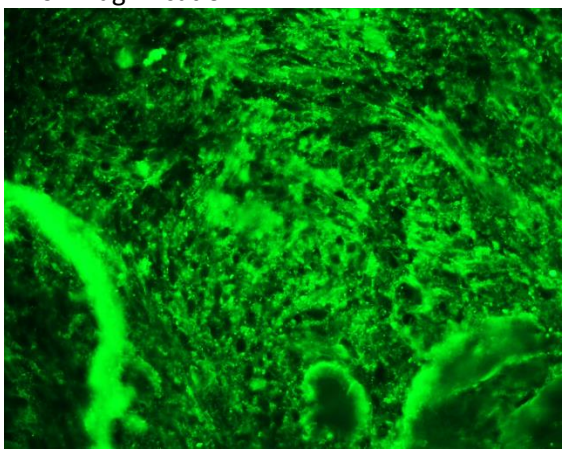

D Alexofluor 488 labelled collagen II staining
40x magnification

Figure 4.13: Chondrogenesis differentiated MV MSCs. MSCs were cultured in chondrogenic induction media for 4 weeks. Cell pellets were then snap frozen in liquid nitrogen, cryosectioned and immunostained for the presence of type 2 collagen. DAPI stain was used to show the nuclei of viable cells within the pellets and Alexofluor 488 labelled immunostain showed the presence of type 2 collagen. A- Chondrogenesis differentiated MV MSCs DAPI nucleic stain at 10x magnification B- Chondrogenesis differentiated MV MSCs Alexofluor 488 labelled collagen 2 stain at 10x magnification C- Chondrogenesis differentiated MV MSCs DAPI nucleic stain at 40x magnification D- Chondrogenesis differentiated MV MSCs Alexofluor 488 labelled collagen 2 stain at 40x magnification. (Fluorescence microscopy)

Non inducing control MV MSCs

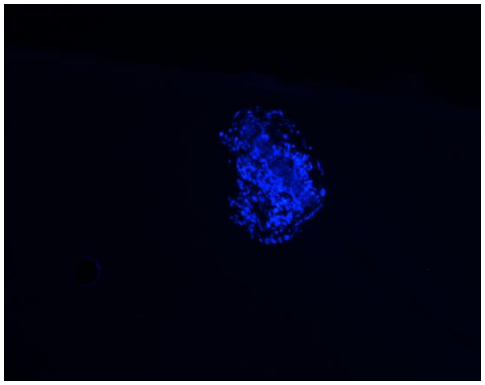

A DAPI stained nuclei
10x magnification

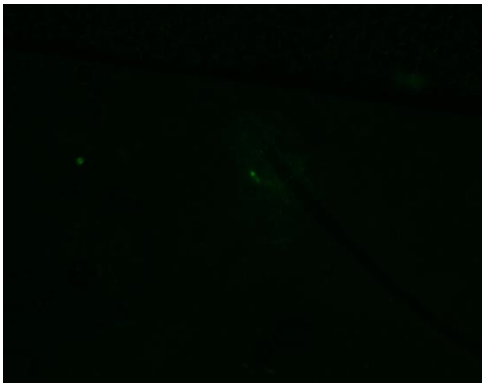

B Alexofluor 488 labelled collagen II staining
10x magnification

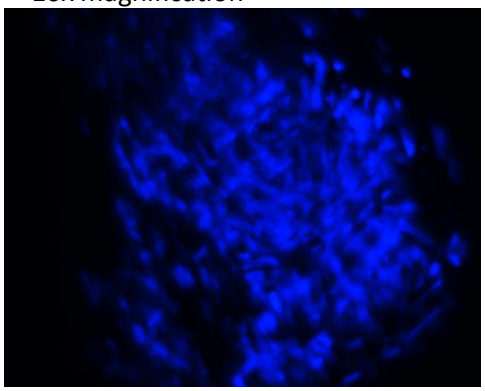

C DAPI stained nuclei
40x magnification

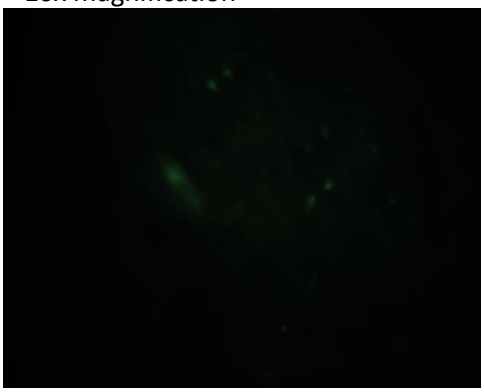

D Alexofluor 488 labelled collagen II staining
40x magnification

Unstained non inducing control MV MSCs

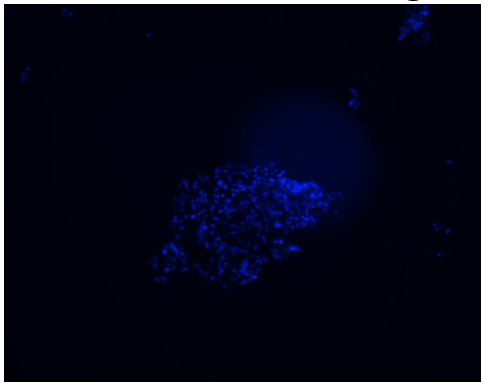

E DAPI stained nuclei
10x magnification

F Unstained control
10x magnification

Figure 4.14: Chondrogenesis non-induced control AT MSCs. MSCs were cultured in non-inducing control media for 4 weeks. Cell pellets were then snap frozen in liquid nitrogen, cryosectioned and immunostained for the presence of type 2 collagen. DAPI stain was used to show the nuclei of viable cells within the control pellets and Alexofluor 488 labelled immunostain showed the absence of type 2 collagen. A- Chrondrogenesis non-induced control MV MSCs DAPI nucleic stain at 10x magnification B- Chrondrogenesis non-induced control MV MSCs Alexofluor 488 labelled collagen 2 stain at 10x magnification C- Chrondrogenesis non-induced control MV MSCs DAPI nucleic stain at 40x magnification D- Chrondrogenesis non-induced control MV MSCs Alexofluor 488 labelled collagen 2 stain at 40x magnification E- Chrondrogenesis non-induced control MV MSCs DAPI nucleic stain of pellets not co-stained with Alexofluor 488 labelled collagen 2 stain at 10x magnification F- Background fluorescence of Chrondrogenesis non-induced control MV MSCs without Alexofluor 488 labelled collagen 2 stain at 10x magnification. (Fluorescence microscopy)

4.4 Discussion

In this chapter, characterisation of human dermal fibroblasts, adipose Mesenchymal Stromal Cells (AT MSC) and microvasculature MSCs (MV MSC) has been described. A protocol for processing of fresh adipose tissue was developed and this enabled the consistent culture of paired stocks of MSCs from whole adipose tissue and from microvasculature dissected free from the whole adipose tissue. These AT MSC and MV MSC have been shown to display similar morphology when cultured on plastic culture plates and both have a $CD73^+$, $CD90^+$, $CD105^+$, $CD140b^+$ and $CD14^-$, $CD34^-$, $CD45^-$ and HLA-DR^- phenotype, consistent with adipose stem cells characterised by other authors (97, 98, 113). Both AT MSC and MV MSC have the potential to differentiate into three mesenchymal cell lineages, confirming their multipotency. Adherence to plastic, consistent phenotyping and ability to differentiate into adipocytes, osteoblasts and chondrocytes are the basic requirements for characterising MSC as determined by the International Society for Cellular Therapy (ISCT) (99, 102). A recent perspective review by Keating suggests that in the absence of a single, unique MSC defining characteristic or cell surface marker, future characterisation methods for commercial and clinical cell lines may require more complex molecular assessments such as proteomic analysis (252). Keating also suggests that adipogenesis, osteogenesis and chondrogenesis may not all be necessary requirements for clinically useful MSCs from different source tissues (252) since not all sources of MSCs need be used for all potential applications. So although the AT and MV MSC in this Thesis meet the basic requirements of ISCT standards for defining MSCs (99, 102), it is more important that they are able to support microvasculature formation for our proposed clinical application. The functional characteristics of AT MSC and MV MSC in this Thesis, with regard to their ability to support *in vitro* microvascular network formation, are explored in Chapter 5.

Blasi *et al.* carried out a comparative study between adipose MSC and HDF (95). Both cell types in their study displayed a comparative phenotype and had the ability to differentiate into adipocytes, osteoblasts and cardiomyocytes, but only the adipose MSC were found to have

strong angiogenic activity (95). This supports Keating's proposal that function may be more important than phenotype and multipotency in determining the usefulness of MSC for clinical applications (252).

Other authors have supported the greater proangiogenic potential of adipose derived MSC (115, 205, 253-257) and several have proposed a similarity to the vascular pericyte phenotype (113, 205, 253, 258, 259). In recent years, collaborative researchers at the University of Edinburgh and the University of California led by Professor Péault have investigated a perivascular origin of MSC (258, 260-270). They built on an initial foundation of identifying pericytes with a $CD44^+$, $CD73^+$, $CD90^+$, $CD105^+$ phenotype in the capillary walls of multiple organs (265) by then prospectively purifying pericytes from adipose tissue and comparing them to cells from the stromal vascular fraction of whole adipose tissue (267). They found that purified pericytes had a greater ability to differentiate into osteoblasts, which was their primary aim for bone tissue engineering (267). Purified pericytes were selected as being $CD34^-$, although the group have shown that populations of both $CD34^+$ and $CD34^-$ cells are multipotent MSC (263, 264, 271). In this Thesis, both cultured AT and MV MSC were $CD34^-$ (1.5% ± 0.3% and 1.9% ± 0.5% $CD34^+$ respectively) although fresh adipose tissue had a heterogenous population of both $CD34^+$ and $CD34^-$ cells (14.3% ± 3.6% $CD34^+$). CD34 expression in haematopoietic cells from UCB is known to decrease in culture with passage (222), and this may also be the case with AT MSC. $CD34^-$ pericytes have the ability to support haematopoietic stem cells (263) and to differentiate into multiple mesenchymal lineages (260, 261, 269, 270).

Cai *et al*. used the pericyte marker alpha Smooth Muscle Actin (α-SMA) to support their hypothesis that all adipose MSC originate from perivascular cells (113). They used α-SMA-GFP transgenic mice, harvested adipose tissue, and sorted cells into GFP positive and negative groups. Only the GFP positive group displayed multipotency, and the GFP negative cells which

were not from a perivascular location could only differentiate into adipocytes (113). This murine model may be comparable with human adipose MSC origins.

AT and MV MSCs are a potentially feasible source of autologous stromal cells for use in clinical applications. Fresh lipoaspirate for fat transfer boosted with cells derived from the stromal vascular fraction of digested and centrifuged adipose tissue is already in clinical use (118, 124-129), and initial results from a trial of this technique in breast reconstruction has not yet reported any adverse outcomes (125). In this fat transfer application cells are not expanded *ex vivo*, and so phenotyping and GMP grade manufacture have not been established. As discussed for ECFC derived cells in Chapter 3, further Good Manufacturing Practice (GMP) grade techniques may still require development (222, 241). Serum free media for MSC culture has been developed using platelet lysate (81, 242, 243), and further work is required to ensure that the AT and MV MSC developed in this Thesis can be cultured and expanded in similar GMP grade media.

Chapter 5 Microvascular Tubule Formation using Adipose Tissue Derived Mesenchymal Stromal Cells and Umbilical Cord Blood Endothelial Cells

5.1 Background

In vitro angiogenesis has been studied using several different assays to look at separate components of the complex process, such as endothelial cell proliferation or cell migration (272). Although this may be useful in the initial assessment of primary endothelial cells, this research required an *in vitro* model more representative of the *in vivo* environment. The ability of endothelial cells to form tubules in culture can be tested using a Matrigel™ basement membrane substitute as a culture surface (273-275). Matrigel ™ is derived from a murine sarcoma cell line but contains all of the components of human basement membrane (275). This is a useful assay to detect changes in tubule forming ability of endothelial cells under different conditions (274), but does not account for the influence of stromal cells nor the microenvironmental niche.

Co-culture of endothelial and stromal cells at an appropriate ratio results in microvascular tubule formation *in vitro* (135). This is more representative of *in vitro* vasculogenesis, which recruits new endothelial and stromal cells from the vascular or bone marrow niche for neovascularisation (61, 136). New microvasculature cultured in this manner has been shown to have a functional lumen (137) which is important for future clinical applications of this research.

Proangiogenic factors are not only supplied to the co-cultures via growth media, but are also expressed by the endothelial and stromal cells (59, 141, 142). In this chapter, a proangiogenic array was used to examine differences in factors produced by different cell lines in co-culture.

Initial findings from the array prompted further experimental work using human recombinant leptin.

5.2 Aim and objectives

The aim in this chapter was to establish the best conditions for forming microvascular networks *in vitro* using primary human endothelial and adipose tissue derived mesenchymal stromal cells.

The specific objectives were:

- To test the ability of paired samples of adipose and adipose microvasculature derived MSCs to support microvascular tubule formation in vitro.
- To investigate the differences in tubule formation observed comparing paired adipose and microvasculature derived MSCs by studying
    - proliferation
    - angiogenic factors in co-culture supernatant
    - the effect of adding exogenous pro-angiogenic factors to co-culture

5.3 Results

5.3.1 Initial assessment of tubule forming potential in Matrigel™

Initially AT MSCs were compared with UCB ECFC derived cells for their ability to form tubules on Matrigel™ basement membrane. The Matrigel™ assay has been used extensively as a measure of *in vitro* angiogenesis and it is well established that endothelial cells will line up to form tubules on the surface of the reconstituted basement membrane (273). This feature has previously been found to be unique to endothelial cells (273) but it was decided to use this

assay to examine the angiogenic potential of the AT MSCs which had been initially cultured in endothelial media.

The full method is described in Chapter 2 Section 2.8.1, from a protocol which was standardised in our laboratory (274). In brief, Matrigel™ solution (BD Biosciences, Franklin Lakes, NJ, U.S.A.) was placed into rat tail collagen I coated 96-well plates (BD Biosciences, Franklin Lakes, NJ, U.S.A.) and kept cool on ice until cells were added on top at 1.5 $x10^4$ cells per well in 100µl complete EGM-2 (Lonza Biologics, Slough, UK). Plates were incubated at 37°C for 24 hours, then wells were fixed with methanol (Sigma Aldrich Ltd., Gillingham, UK) and stained with 50% (v/v) haematoxylin (VWR International Ltd., Leicestershire, UK). Approximately 200µl DPBS without Calcium and Magnesium (PAA Laboratories Ltd., Yeovil, UK) was added to each well prior to examining the cells by bright field microscopy.

Figure 5.1 demonstrates that, unlike the UCB ECFC derived control cells, AT MSCs do not form a distinct network of vascular structures on Matrigel™ solution at 24 hours. Figure 5.1 shows representative microscopy from an experiment with one passage 5 UCB ECFC derived control sample and from one of three different passage 3 AT MSC samples. Each condition was repeated in triplicate. Analysis using the AngioSys Image Analysis Software (Cellworks, Buckingham, UK) confirmed that ECFC formed longer tubules with less junctions than AT MSC. AT MSC formed shorter tubules and clumps with undeveloped sprouts which could not be accurately measured using the automated software (Figure 5.2).

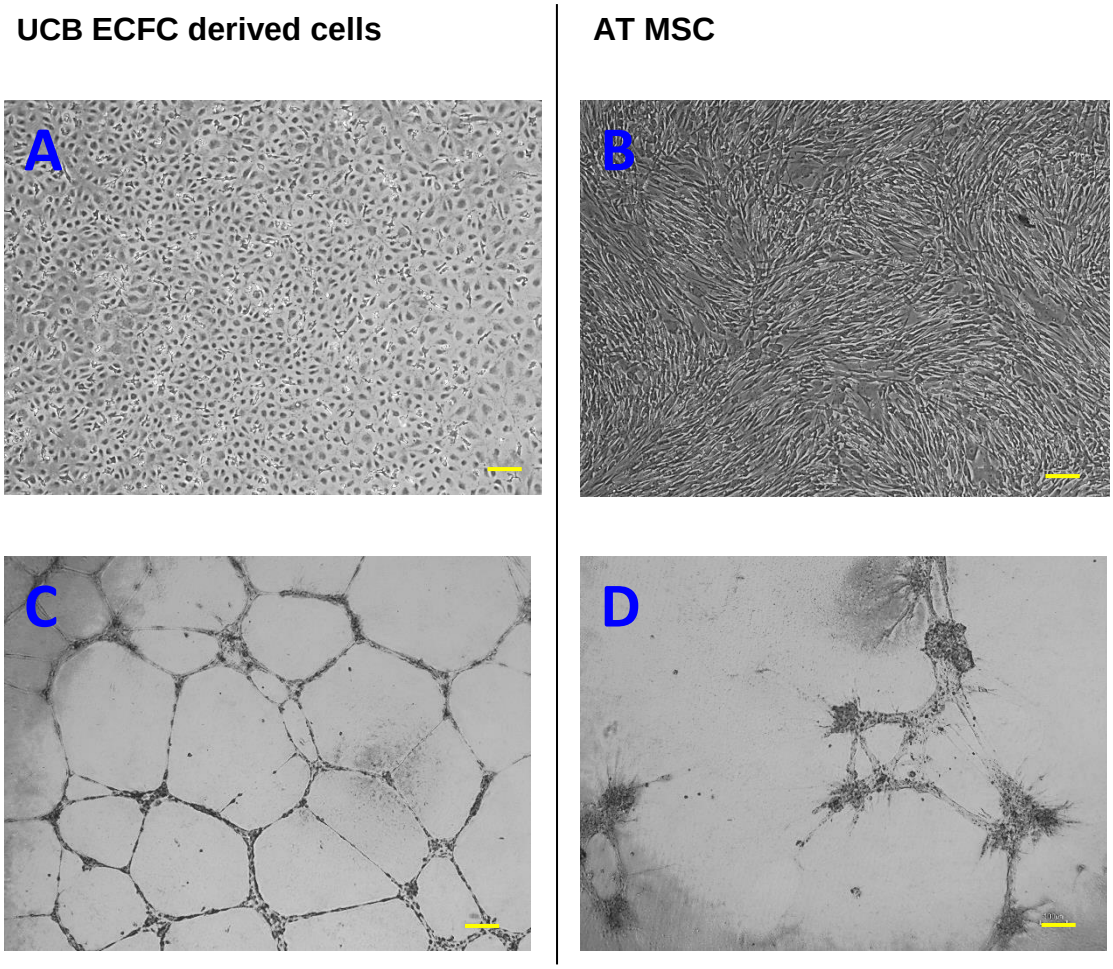

Figure 5.1: Matrigel™ assay comparing tubule forming potential of UCB ECFC derived cells and AT MSCs. A= UCB ECFC derived cells morphology; B= AT MSC morphology; C= Representative image of UCB ECFC derived cell tubule formation on Matrigel™ from batch of passage 5 cells repeated in triplicate; D= Representative image of lack of tubule formation on Matrigel™ with AT MSCs from one of three batches of cells, each repeated in triplicate. (Phase contrast image, 100µm scale bars).

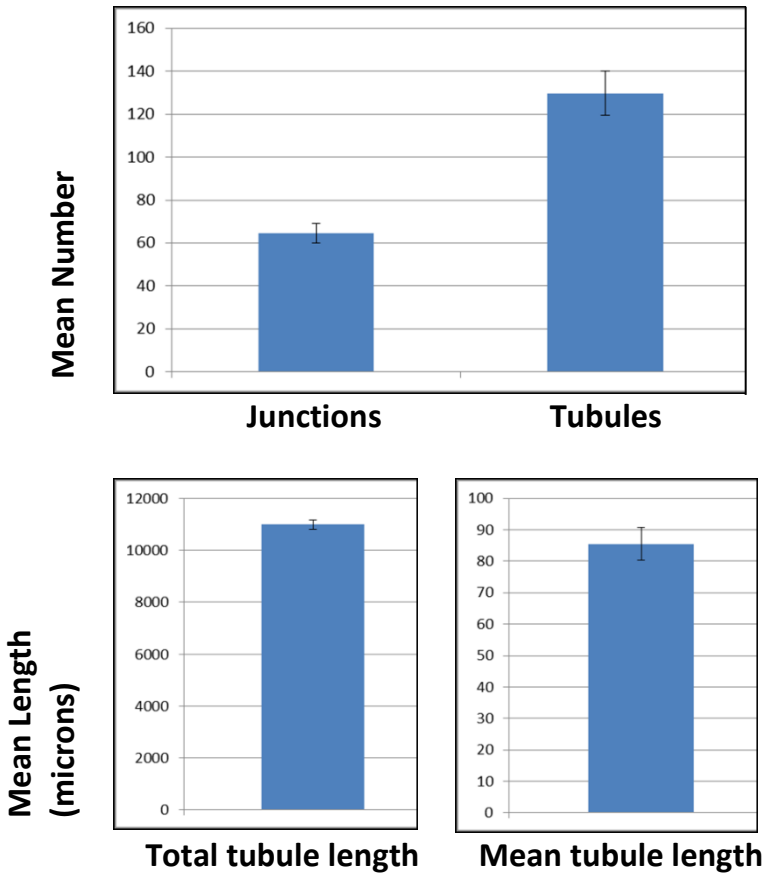

Figure 5.2: Tubule formation of ECFC on Matrigel™. ECFC (n=3) formed longer tubules in an identifiable network than AT MSC (n=9) which therefore could not be analysed accurately using Angiosys Image Analysis Software (Cellworks, Buckingham, UK). Error bars show SEM.

5.3.2 Two-dimensional sandwich co-culture tubule formation

The ability of AT MSCs to support vascular tubule formation in co-culture with UCB ECFC derived cells was determined in an *in vitro* two-dimensional sandwich co-culture tubule assay established within our laboratory and initially standardised using HDF and BM MSC (135).

The method is described in Chapter 2 Section 2.8.2. In brief, HDF, AT MSC and MV MSC were seeded at various concentrations into rat tail collagen I coated 48-well plates (BD Biosciences, Franklin Lakes, NJ, U.S.A.) and incubated in complete EGM-2 (Lonza Biologics, Slough, UK) for two hours at 37°C. UCB ECFC derived cells were then added at different concentrations in the same media. Each condition was repeated in triplicate. Plates were incubated at 37°C for 2 weeks with complete change of media every 2-3 days. After 2 weeks, wells were fixed with

70% (v/v) ethanol (VWR International Ltd., Leicestershire, UK) then stained with primary mouse anti-human CD31 (Clone WM59) (AbD Serotec, Kidlington, UK), secondary goat anti-mouse IgG (H+L) biotinylated (Vector Laboratories Inc., Burlingame, CA, U.S.A.) antibodies, Vectastain® Universal Elite® ABC Kit (Vector Labs, Burlingame, CA U.S.A.) and DAB substrate kit (Vector Laboratories Inc., Burlingame, CA, U.S.A.). Tubules were examined by bright field microscopy.

Figure 5.3 shows representative images of the 2D-tubule formation achieved with $1x10^3$ or $2x10^3$ UCB ECFC derived cells co-cultured with $5x10^3$ HDF, AT MSC and MV MSC following 2 weeks in culture. Each condition was repeated in triplicate. The figure includes representative microscopy from an experiment with one batch of passage 5 UCB ECFC derived cells, one batch of passage 3 HDF and four different paired samples of passage 3 AT MSC and MV MSC. Both ratios of UCB ECFC derived cells with HDF, AT MSC and MV MSC resulted in tubule formation. Later assays therefore selected ratios with lower concentrations of UCB ECFC derived cells, since clinical availability of endothelial cells may be a limiting factor in translational work. Microvascular tubules are quantified in section 5.3.3.

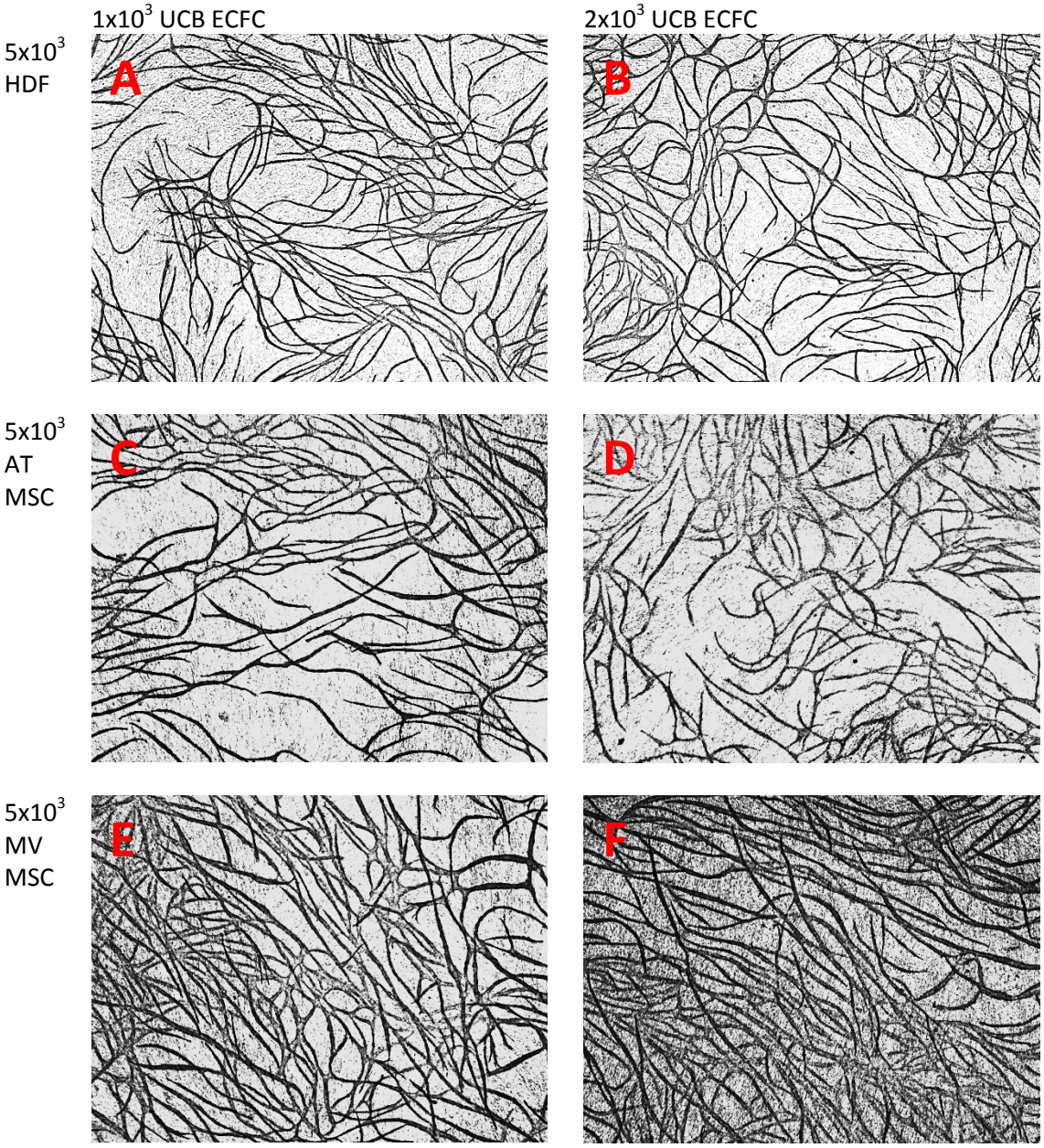

Figure 5.3: 2D tubule formation using UCB ECFC derived cells and HDF, AT MSC and MV MSC in co-culture. Representative figures from an experiment with one batch of P5 UCB ECFC derived cells, one batch of P3 HDF and four different paired samples of P3 AT MSC and MV MSC. Each co-culture ratio was repeated in triplicate. Tubular structures formed by UCB ECFC derived cells were detected by immunostaining. Co-cultures were fixed with 70% (v/v) ethanol and stained with primary mouse anti-human CD31 and secondary goat anti-mouse IgG (H+L) biotinylated antibodies. Tubules were visualised using the Vectastain® Universal Elite® ABC Kit and DAB substrate kit. (Phase contrast microscopy, 100µm scale bars). Mean total tubule length (microns) ± SEM A= 87185 ± 2149 B= 84228 ± 1911 C= 62666 ± 3232 D= 60045 ± 2936 E=85002 ± 3842 F= 69709 ± 3830.

5.3.3 Microvasculature MSCs support more tubule formation than adipose MSCs

Relative microvasculature formation was compared using three different stromal cell sources, to determine if the supportive cell type had any influence on tubule formation *in vitro*. From visual comparison of the representative images in Figure 5.3 it appeared that there was more tubule formation in the MV MSC co-culture wells. Tubule formation was therefore quantitated using the AngioSys Image Analysis Software (Cellworks, Buckingham, UK). Figure 5.4 shows the comparative number of tubule junctions, number of tubules, total tubule length and mean tubule length for tubule formation with $1x10^3$ or $2x10^3$ UCB ECFC derived cells co-cultured with $5x10^3$ control HDF (n=3) and paired samples of AT MSC (n=12) and MV MSC (n=12). The graphs show mean values with standard error of the mean (SEM) error bars.

There was consistently more tubule formation in co-cultures with MV MSC compared with AT MSC, with greater number of tubules, number of junctions and total tubule length at both concentrations of UCB ECFC. In the co-cultures with $1x10^3$ UCB ECFC the differences were statistically significant using a paired Student's T test analysis. There was a 57.5% increase in the number of junctions ($p<0.001$), a 35.5% increase in the number of tubules ($p=0.001$) and a 35.6% increase in total tubule length ($p<0.001$). Data from the analysis are summarised in Table 5.1.

1x10^3 UCB ECFC

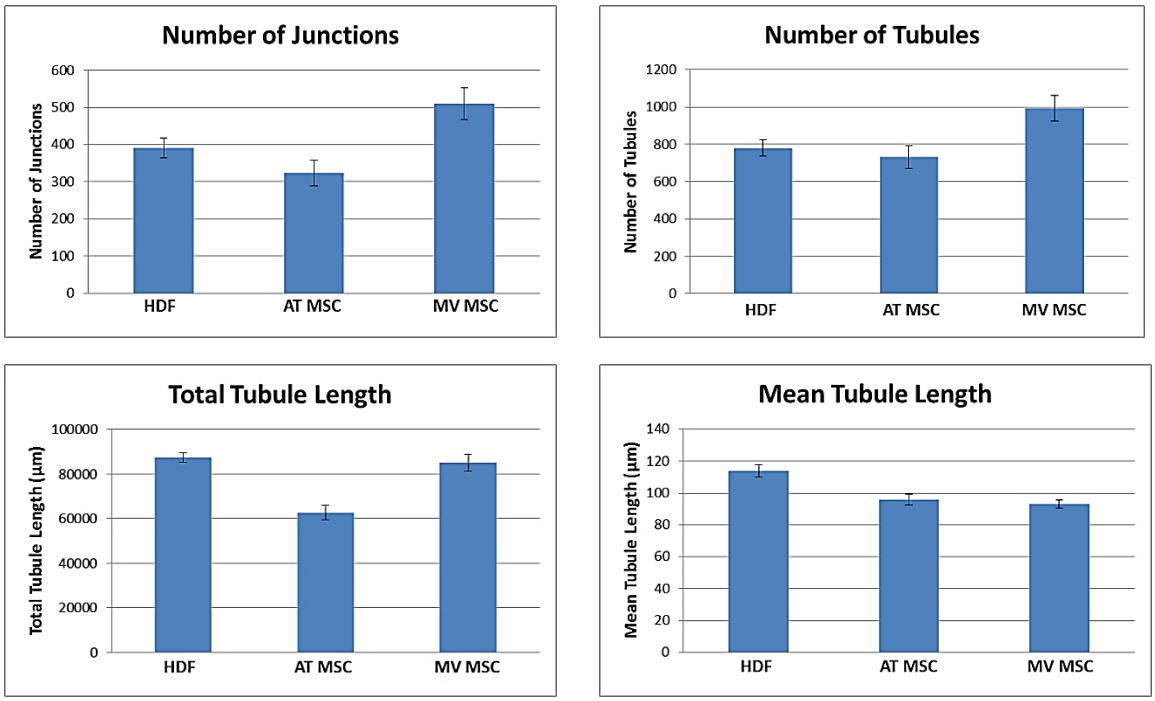

2x10^3 UCB ECFC

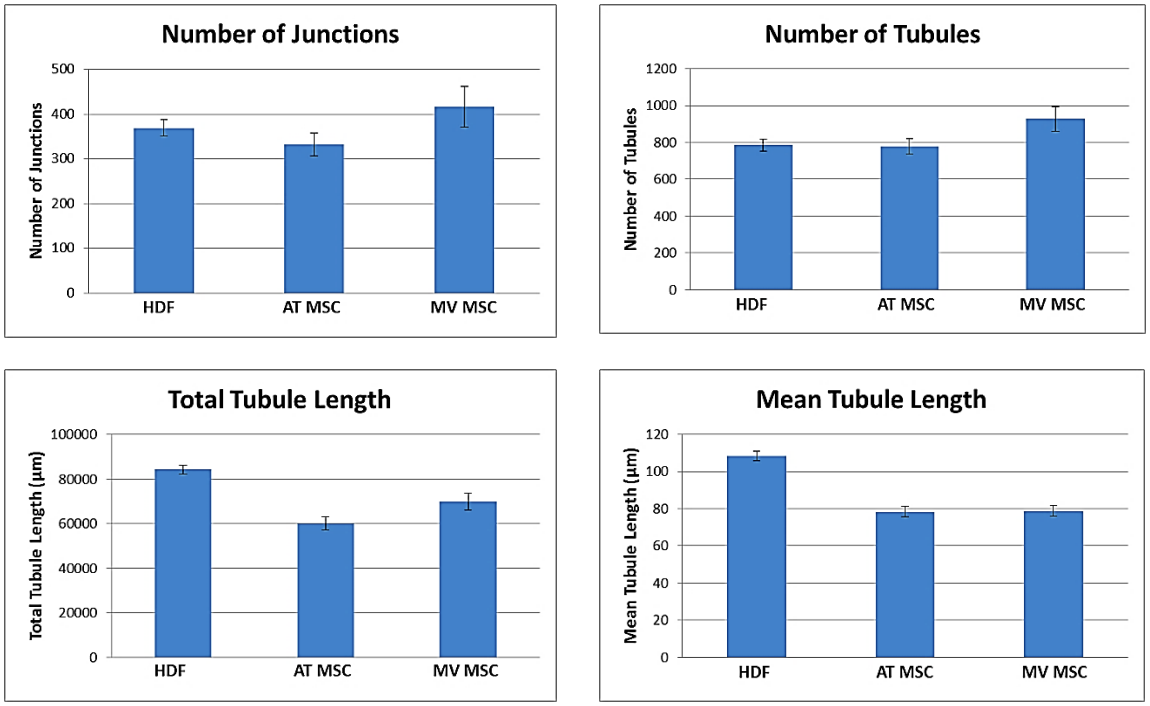

Figure 5.4: Comparison of 2D tubule formation with co-culture of either 1x10^3 or 2x10^3 UCB ECFC derived cells and 5x10^3 HDF (n=3), AT MSC (n=12) or MV MSC (n=12). Data are shown with Standard Error of the Mean (SEM) error bars.

Table 5.1: Statistical analysis of 2D tubule formation with co-culture of either $1x10^3$ or $2x10^3$ UCB ECFC derived cells and $5x10^3$ HDF (n=3), AT MSC (n=12) or MV MSC (n=12).

		HDF and AT MSC (Unpaired Student's T Test)	HDF and MV MSC (Unpaired Student's T Test)	AT MSC and MV MSC (Paired Student's T Test)
Number of Junctions	**$1x10^3$ UCB ECFC**	17.2% decrease p=0.328	30.4% increase p=0.177	57.5% increase p<0.001
	$2x10^3$ UCB ECFC	10.1% decrease p=0.456	12.9% increase p=0.597	25.6% increase p=0.259
Number of Tubules	**$1x10^3$ UCB ECFC**	6.1% decrease p=0.694	27.3% increase p=0.125	35.5% increase p=0.001
	$2x10^3$ UCB ECFC	0.9% decrease p=0.929	18.1% increase p=0.284	19.2% increase p=0.101
Total Tubule Length	**$1x10^3$ UCB ECFC**	28.1% decrease p<0.001	2.5% decrease p=0.781	35.6% increase p<0.001
	$2x10^3$ UCB ECFC	28.7% decrease p<0.001	17.2% decrease p=0.061	16.1% increase p=0.130
Mean Tubule Length	**$1x10^3$ UCB ECFC**	15.8% decrease p=0.016	18.3% decrease p<0.001	2.9% decrease p=0.742
	$2x10^3$ UCB ECFC	27.7% decrease p<0.001	27.3% decrease p<0.001	0.6% increase p=0.811

Values presented are the relative increase or decrease in tubule junctions, number, total length and mean length of the tubule formation on the second named stromal cell source compared with the first. Significance was calculated using the Student's T Test for unpaired samples when the comparison was against control HDF and the Student's T Test for paired samples when the comparison was between paired AT and MV MSC. Statistically significant results are displayed in red.

5.3.4 Comparison of adipose and microvasculature MSC Proliferation

Having discovered a difference in tubule formation with different MSC sources, it was decided to examine the proliferation of the AT and MV MSCs as a difference in proliferation may be responsible for the difference in tubule formation. The MTT absorbance assay is representative of the metabolic rate of the cells at day 4 in culture, as only viable cells will take up the dye and form formazan crystals which are then dissolved and measured by light absorbance (276). The metabolic rate of the cells is normally correlated with proliferation.

Four paired samples of AT and MV MSCs were seeded at densities of 500, 1000, and 2000 cells per well of a 96 well plate. At day 4, viable cell numbers were determined using the MTT assay described in Chapter 2 Section 2.10. Each sample was repeated in triplicate.

Figure 5.5 shows the relative absorbance of MTT comparing paired AT and MV MSC samples at three different seeding densities. Each bar on the graph represents the mean value for each sample group, with error bars showing standard error of the mean. The results showed no significant differences in cell numbers ($p>0.05$) between adipose and microvasculature MSCs when compared using the Student's T test for paired samples.

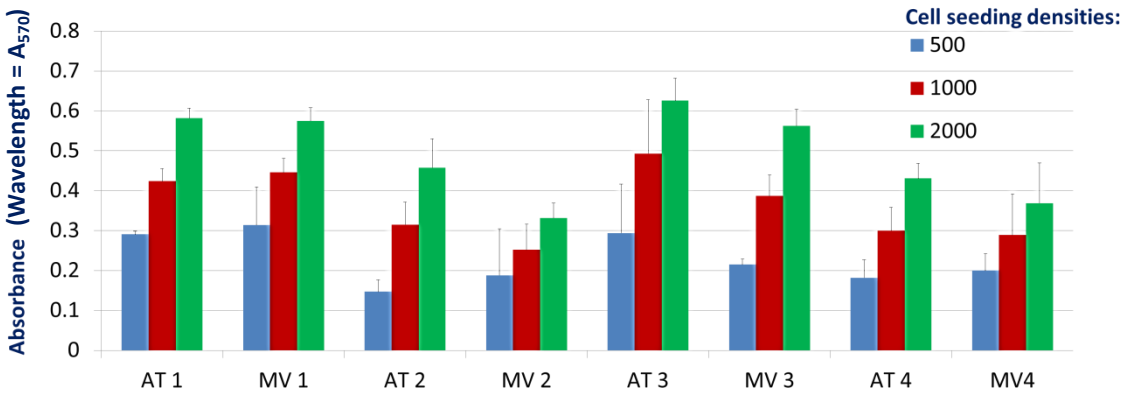

Figure 5.5: MTT absorbance analysis of AT and MV MSCs at three different seeding densities. There was no significant difference between paired samples at any of the seeding densities using the Student's T Test for paired samples. Data are shown with Standard Error of the Mean (SEM) error bars.

5.3.5 Angiogenic factor profiling

Co-culture tubule assays with either AT or MV MSCs at $1x10^4$ per well and UCB ECFC derived cells at $1x10^3$ per well were set as per the standard assay protocol, with three paired MSC samples and each condition repeated in duplicate. The lowest concentration of endothelial cells previously used in the tubule assay was chosen as these cells are likely to be limited in clinical applications. The supernatant was collected at each media change, performed every 2-

3 days, and was stored at -80°C for later analysis. Control media (complete EGM-2 (Lonza Biologics, Slough, UK)) collected from wells without any cells was also stored at each stage. Day 7 supernatants and media controls were then selected for angiogenic factor analysis, since at this stage of the assay there is active tubule formation and maturation. The proangiogenic array (Proteome Profiler™ Antibody Array – Human Angiogenesis Array Kit, R&D Systems, Abingdon, UK) contained capture antibodies for 55 different angiogenesis related proteins on a nitrocellulose membrane. The full method is described in Chapter 2 Section 2.9. In brief, each supernatant or control media sample was incubated with a separate membrane, and binding of sample proteins to the capture antibodies was identified with the use of Streptavidin-HRP (R&D Systems, Abingdon, UK) and chemiluminescent detection reagents (Amersham™ ECL™ Prime Western blotting detection reagent, GE Healthcare Life Sciences, Buckinghamshire, UK) developed in the dark room. Intensity of the developed membrane spots was then compared using the Quantity One® 1-D Analysis Software (Bio-Rad Laboratories Ltd., Hertfordshire, UK).

Pixel density data from the angiogenesis array are shown in Table 5.2, where relative values for each sample have been corrected by subtracting the negative control values for each sample from every other data spot on the same sample. From this data, there was only one of the fifty-five proteins which showed a consistent trend on comparing values between paired AT and MV MSC supernatants. Leptin expression was consistently greater in the MV MSC co-culture supernatant compared with AT MSC co-culture supernatant and was not present in the media control sample, suggesting greater expression of leptin by MV MSC. Mean values for leptin expression from AT and MV MSC co-culture supernatants are shown in Figure 5.6 with standard error of the mean. There was a 112% greater value for mean leptin expression with MV MSC samples compared with AT MSC samples. This was found to be statistically significant using the Student's T test for paired samples ($p=0.025$).

Table 5.2: Angiogenic array data for four paired AT and MV MSC co-culture tubule assay supernatant samples and media control.

Factor	Media	AT 1	MV 1	AT 2	MV 2	AT 3	MV 3	AT 4	MV 4
Positive Control	6425	1124	1574	467	1509	4395	5460	704	1283
Activin A	159	62	34	12	0	577	435	0	79
ADAMTS-1	147	121	45	0	0	451	252	60	74
Angiogenin	407	2388	2759	2776	2579	12608	13720	2667	3026
Angiopoietin-1	94	233	108	166	204	822	874	140	143
Angiopoietin-2	118	360	290	203	253	621	375	126	88
Angiostatin/Plasminogen	0	47	21	0	8	344	252	60	56
Amphiregulin	92	1593	1277	1108	1068	5654	5663	1394	1565
Artemin	0	52	29	0	0	214	219	40	32
Positive Control	5171	1459	1235	1241	1381	5056	5246	1252	1306
Coagulation Factor III	398	211	179	29	76	600	579	131	257
CXCL16	385	456	703	500	905	896	959	140	434
DPPIV	814	196	253	199	270	808	638	110	135
EGF	10463	2448	3018	2535	2769	12163	12312	2374	2550
EG-VEGF	199	94	36	2	35	449	225	49	122
Endoglin	6	137	55	9	168	468	339	56	76
Endostatin/Collagen XVIII	328	525	351	62	117	1111	926	643	431
Endothelin-1	1572	920	767	1007	721	2135	2280	513	344
FGF acidic	109	89	138	0	20	398	160	168	136
FGF basic	1258	221	133	69	132	303	376	168	277
FGF-4	0	21	57	0	44	16	0	45	24
FGF-7	0	750	479	608	1114	2958	4026	280	668
GDNF	531	80	29	0	49	552	471	50	56
GM-CSF	404	77	34	0	0	366	411	18	79
HB-EGF	274	100	67	56	70	740	390	51	122
HGF	457	2055	2680	2454	2786	11048	11168	2101	2394
IGFBP-1	65	225	141	95	139	679	438	86	107
IGFBP-2	380	2386	1926	1916	1750	7964	8605	1672	1375
IGFBP-3	185	1856	1475	1178	1559	6988	5953	843	786
IL-1b	132	73	55	0	33	412	257	91	38
IL-8	2489	3231	3106	2877	2925	14211	12770	2913	2517
LAP (TGF-b1)	0	273	245	223	300	328	563	188	126
Leptin	0	231	305	16	91	33	173	152	347
MCP-1	0	1524	237	480	2543	1247	2091	54	202
MIP-1a	497	62	79	0	25	642	533	50	81
MMP-8	326	91	3	0	3	365	274	0	98
MMP-9	436	628	911	885	1682	3274	3749	273	475
NRG1-b1	208	149	56	112	213	689	470	123	241
Pentraxin 3 (PTX3)	4143	1573	1177	1503	1347	6289	6564	1615	1454
PD-ECGF	0	115	73	0	50	422	506	31	127
PDGF-AA	0	87	57	0	91	497	186	71	105
PDGF-AB/PDGF-BB	210	13	15	0	15	285	157	24	33
Persephin	237	147	170	110	178	488	444	157	276
Platelet Factor 4 (PF4)	0	700	558	211	547	1021	2188	845	760
PlGF	0	745	790	824	1172	852	1329	390	238
Prolactin	0	54	49	5	90	0	0	59	18
Serpin B5	383	65	61	0	0	466	470	59	89
Serpin E1	10262	583	1302	418	893	2204	2165	541	904
Serpin F1	648	185	220	257	218	832	786	286	304
TIMP-1	13199	1907	2219	1938	1903	8674	8878	2099	1885
TIMP-4	269	1950	1893	1747	1671	9636	9766	1465	1390
Thrombospondin-1	0	433	157	258	204	965	618	161	106
Thrombospondin-2	0	36	41	0	0	303	204	37	77
uPA	0	2	42	0	0	196	113	31	36
Vasohibin	156	0	43	21	52	284	199	118	183
VEGF	9800	2733	2894	2835	2699	12811	13744	3260	3078
VEGF-C	0	33	0	0	30	81	87	114	0
Positive Control	5406	1501	1648	515	1368	3094	4117	1304	1734
Negative Control	0	0	0	0	0	0	0	0	0

Leptin was the only protein to show a consistent difference between paired AT and MV samples.

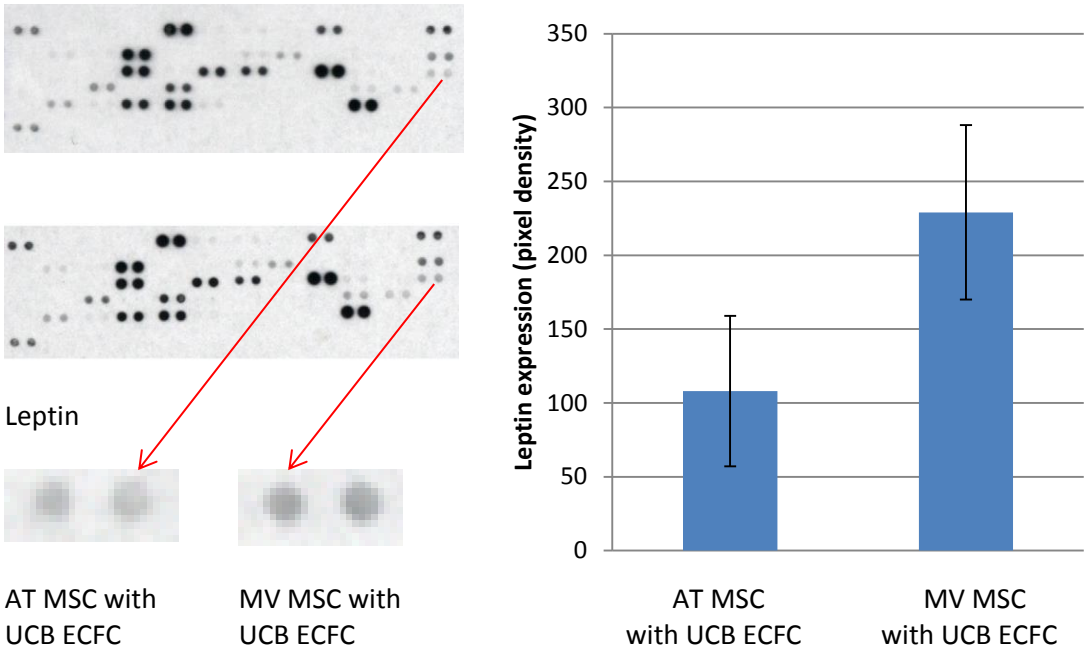

Figure 5.6: Leptin expression. Supernatant from AT MSC and MV MSC co-cultures with UCB ECFC derived cells were analysed using angiogenic arrays. There was consistently greater expression of leptin in MV MSC co-culture supernatant samples (n=4) compared with AT MSC samples (n=4) (112% increase, p=0.025 using Student's T test for paired samples). The image on the left shows magnified views of the leptin protein capture spots on the developed array membranes. The graph shows mean leptin expression values for four samples in each condition with error bars showing standard error of the mean.

In order to further explore the angiogenesis array data directly comparing AT and MV samples, supernatant pixel density values were normalised against the highest value mean positive control in the series of membranes. This was done by finding the multiplication factor required for each membrane mean positive control to equal the highest positive control value in the series, and then using this multiplication factor against all other spots on each membrane. This removed the effect of differences in developing the membranes and allowed more thorough comparisons to be made.

Following this normalisation against positive controls, fourteen of the fifty-five proteins then showed a consistent trend on comparing values between paired AT and MV MSC supernatants (Table 5.3). Leptin remained the only protein to have a higher expression in MV samples compared with AT samples. Normalised values for angiopoietin-1, angiopoietin-2, amphiregulin, endostatin, endothelin-1, Insulin-like Growth Factor Binding Protein (IGFBP) -1,

2 and 3, interleukin-8 (IL-8), pentraxin 3, Tissue Inhibitor of Metalloproteinase-4 (TIMP-4), thrombospondin-1 and Vascular Endothelial Growth Factor (VEGF) were all consistently higher in the AT MSC samples compared with the paired MV MSC samples.

The mean values for AT MSC and MV MSC samples normalised against positive controls were compared using the Student's T Test for paired samples (Table 5.4), with statistically significant results for angiopoietin-2, IGFBP-3 and thrombospondin-1 displayed in red text, highlighted in yellow. Several of the other proteins with consistent trends are approaching statistical significance, such as leptin, IL-8 and angiopoietin-1.

The relative normalised values of expression for all of the proteins tested are shown graphically in Figure 5.7, and there is a more detailed graph of the protein expression from samples with consistent trends and significant values in Figure 5.8.

Table 5.3: Angiogenic array data for four paired AT and MV MSC co-culture tubule assay supernatant samples normalised against the highest positive control value in the series.

Factor	AT 1	AT 2	AT 3	AT 4	MV 1	MV 2	MV 3	MV 4
Activin A	223	80	681	0	113	0	435	271
ADAMTS-1	439	0	532	272	150	0	252	254
Angiogenin	8665	18510	14897	12126	9175	8977	13720	10375
Angiopoietin-1	847	1107	971	636	359	709	874	490
Angiopoietin-2	1305	1354	734	572	964	882	375	302
Angiostatin/Plasminogen	169	0	407	272	70	26	252	192
Amphiregulin	5782	7388	6681	6337	4247	3718	5663	5366
Artemin	190	0	253	180	96	0	219	110
Coagulation Factor III	765	193	709	597	595	263	579	881
CXCL16	1657	3334	1059	638	2338	3151	959	1488
DPPIV	712	1327	955	502	841	939	638	463
EGF	8886	16903	14372	10795	10037	9638	12312	8743
EG-VEGF	341	13	531	221	120	123	225	418
Endoglin	498	60	553	253	183	585	339	261
Endostatin/Collagen XVIII	1904	413	1313	2923	1167	408	926	1478
Endothelin-1	3339	6714	2522	2334	2551	2509	2280	1179
FGF acidic	323	0	470	764	459	69	160	466
FGF basic	803	460	357	764	442	459	376	950
FGF-4	76	0	19	205	190	154	0	82
FGF-7	2721	4054	3495	1271	1593	3877	4026	2290
GDNF	291	0	652	230	96	172	471	192
GM-CSF	280	0	433	84	113	0	411	271
HB-EGF	361	373	875	231	223	245	390	418
HGF	7456	16363	13054	9553	8913	9698	11168	8208
IGFBP-1	816	633	803	390	469	484	438	367
IGFBP-2	8660	12775	9410	7600	6405	6092	8605	4715
IGFBP-3	6737	7855	8257	3832	4905	5427	5953	2695
IL-1b	263	0	487	413	183	114	257	130
IL-8	11727	19183	16792	13244	10329	10183	12770	8630
LAP (TGF-b1)	992	1487	387	857	815	1043	563	432
Leptin	837	107	39	690	1014	316	173	1190
MCP-1	5530	3201	1473	244	788	8852	2091	693
MIP-1a	225	0	758	228	263	88	533	278
MMP-8	331	0	432	0	10	12	274	336
MMP-9	2280	5901	3869	1241	3030	5855	3749	1629
NRG1-b1	540	747	814	560	186	741	470	826
Pentraxin 3 (PTX3)	5708	10022	7432	7341	3914	4689	6564	4985
PD-ECGF	416	0	499	139	243	173	506	435
PDGF-AA	317	0	587	323	190	316	186	360
PDGF-AB/PDGF-BB	47	0	337	107	50	51	157	113
Persephin	533	733	577	716	565	621	444	946
Platelet Factor 4 (PF4)	2541	1407	1207	3840	1856	1904	2188	2606
PlGF	2704	5494	1007	1772	2627	4079	1329	816
Prolactin	197	33	0	266	163	314	0	62
Serpin B5	234	0	550	268	203	0	470	305
Serpin E1	2115	2787	2605	2460	4330	3108	2165	3100
Serpin F1	673	1714	983	1299	732	760	786	1042
TIMP-1	6922	12922	10249	9541	7380	6626	8878	6463
TIMP-4	7076	11649	11386	6661	6295	5816	9766	4766
Thrombospondin-1	1572	1720	1140	734	522	709	618	363
Thrombospondin-2	130	0	358	168	136	0	204	264
uPA	6	0	232	140	140	0	113	123
Vasohibin	0	140	336	535	143	182	199	627
VEGF	9918	18903	15137	14823	9624	9396	13744	10554
VEGF-C	119	0	96	518	0	106	87	0

When values for paired AT and MV samples were normalised against the highest positive control value in the series there were consistent differences in 14 different proteins. Leptin remained the only protein to have a higher expression in MV samples compared with AT samples (highlighted in yellow) but there were 13 other proteins which had a higher expression in AT samples compared with MV samples (highlighted in pink).

Table 5.4: Mean normalised values for AT and MV sample protein expression and significance.

Factor	AT (mean)	SEM	MV (Mean)	SEM	T Test
Activin A	246	152	205	95	0.732
ADAMTS-1	311	117	164	60	0.162
Angiogenin	13550	2088	10562	1097	0.273
Angiopoietin-1	890	100	608	114	0.059
Angiopoietin-2	991	198	631	170	0.003
Angiostatin/Plasminogen	212	86	135	52	0.135
Amphiregulin	6547	336	4748	459	0.066
Artemin	156	54	106	45	0.095
Coagulation Factor III	566	129	580	126	0.902
CXCL16	1672	592	1984	482	0.323
DPPIV	874	177	720	106	0.293
EGF	12739	1794	10183	760	0.239
EG-VEGF	276	108	221	70	0.685
Endoglin	341	114	342	87	0.996
Endostatin/Collagen XVIII	1638	527	995	226	0.126
Endothelin-1	3728	1019	2130	322	0.170
FGF acidic	389	159	289	102	0.456
FGF basic	596	111	557	132	0.755
FGF-4	75	46	107	42	0.653
FGF-7	2885	603	2947	598	0.903
GDNF	293	135	233	82	0.531
GM-CSF	199	98	199	90	0.994
HB-EGF	460	142	319	50	0.379
HGF	11607	1961	9497	635	0.299
IGFBP-1	661	99	439	26	0.074
IGFBP-2	9611	1118	6454	806	0.086
IGFBP-3	6670	999	4745	716	0.007
IL-1b	291	108	171	32	0.271
IL-8	15236	1690	10478	855	0.057
LAP (TGF-b1)	931	226	713	136	0.229
Leptin	418	202	673	252	0.055
MCP-1	2612	1146	3106	1942	0.831
MIP-1a	303	161	290	92	0.873
MMP-8	191	112	158	86	0.831
MMP-9	3323	1015	3566	881	0.316
NRG1-b1	665	68	556	145	0.516
Pentraxin 3 (PTX3)	7625	892	5038	556	0.075
PD-ECGF	263	117	339	79	0.511
PDGF-AA	307	120	263	44	0.789
PDGF-AB/PDGF-BB	123	75	93	26	0.601
Persephin	640	50	644	107	0.960
Platelet Factor 4 (PF4)	2249	606	2139	172	0.844
PlGF	2744	980	2213	730	0.273
Prolactin	124	64	135	68	0.924
Serpin B5	263	113	244	98	0.505
Serpin E1	2492	142	3176	444	0.308
Serpin F1	1167	222	830	72	0.217
TIMP-1	9908	1233	7337	551	0.171
TIMP-4	9193	1346	6661	1083	0.110
Thrombospondin-1	1291	223	553	74	0.023
Thrombospondin-2	164	74	151	57	0.814
uPA	95	56	94	32	0.990
Vasohibin	253	117	288	114	0.603
VEGF	14695	1843	10829	1003	0.157
VEGF-C	183	115	48	28	0.394

Mean values for four paired samples were compared using the Student's T test for paired samples. Significant results are shown in red, highlighted in yellow. SEM= Standard Error of the Mean.

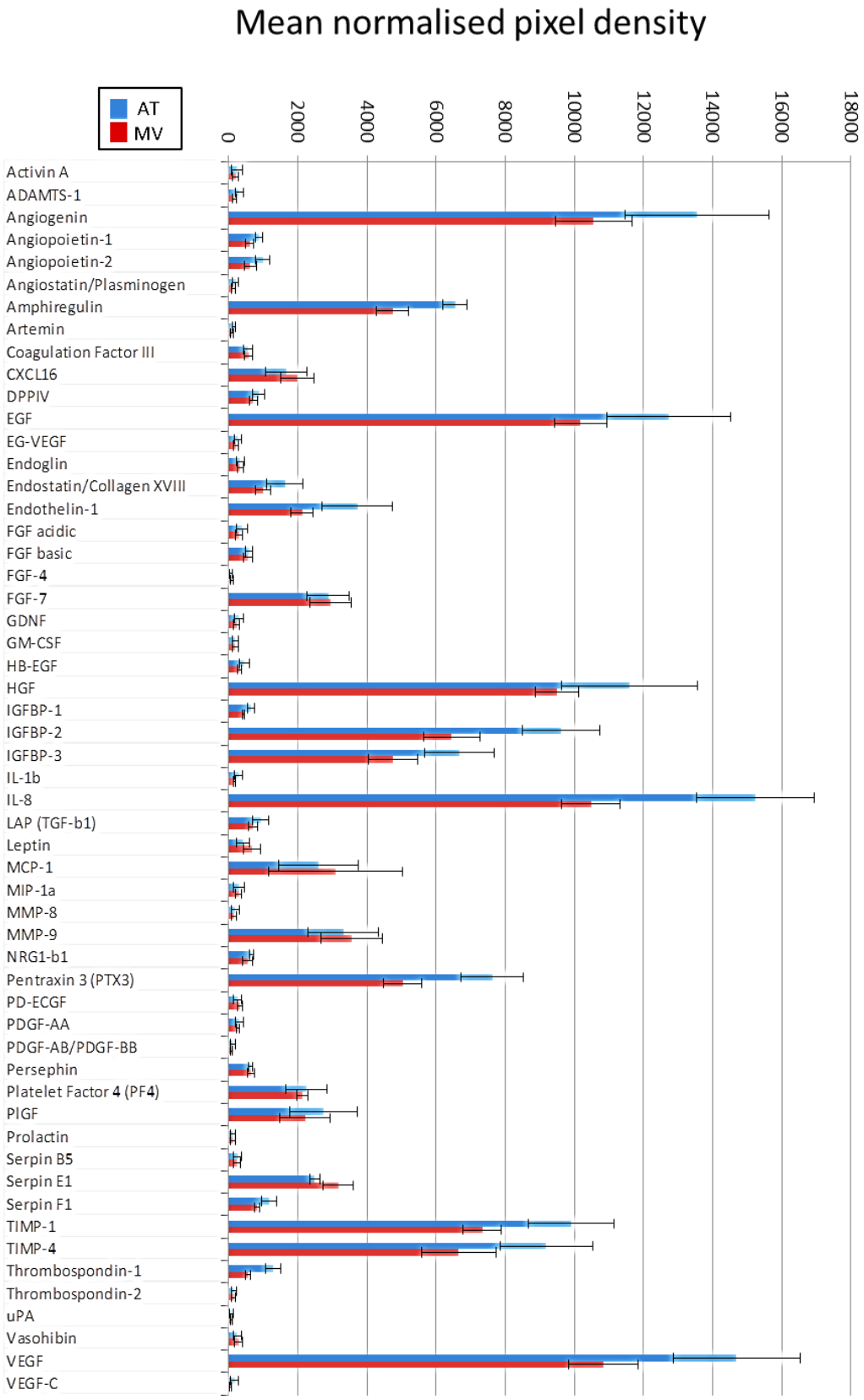

Figure 5.7: Relative values of proangiogenic factors in supernatant from AT and MV MSC co-cultures with UCB ECFC derived cells, corrected to negative controls and normalised against mean positive control values. Normalised values for AT and MV MSC co-cultures were mostly comparable, apart from statistically significant differences in angiopoietin-2, IGFBP-3 and thrombospondin-1 (Student's T test for paired samples). Other proteins such as leptin, IL-8 and angiopoietin-1 are approaching significance in differential expression. Error bars show SEM (n=4 for all samples).

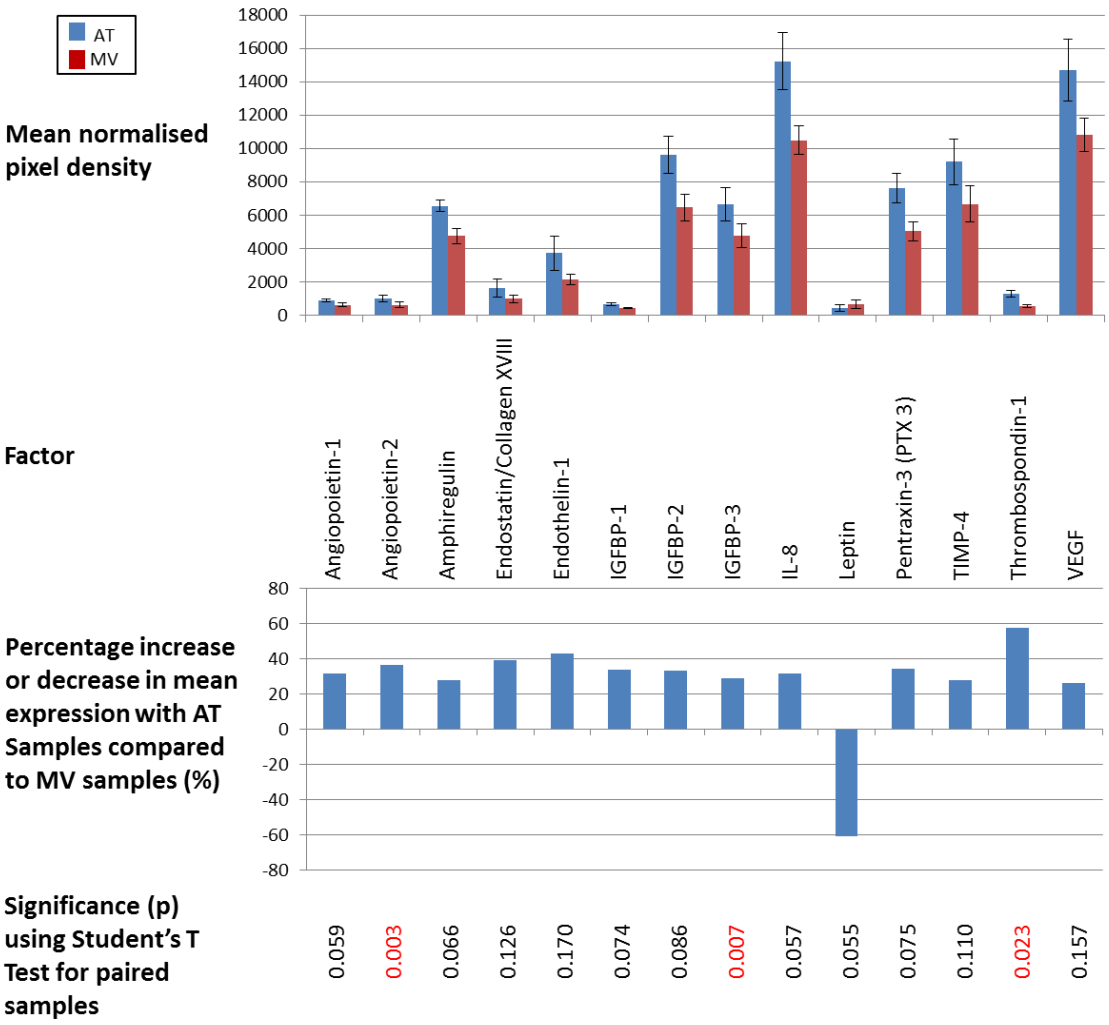

Figure 5.8: Significant variation in values of proangiogenic factors in supernatant from AT and MV MSC co-cultures with UCB ECFC derived cells, corrected to negative controls and normalised against mean positive control values. The largest difference was a 61% lower mean leptin expression in AT samples compared with MV samples. Significantly higher expression of angiopoietin-2 (p=0.003), IGFBP-3 (p=0.007) and thrombospondin-1 (p=0.023) were found in AT samples compared with MV samples using the Student's T test for paired samples. Error bars show SEM (n=4 for all samples).

5.3.6 Effect of exogenous leptin on vascular tubule formation

In order to determine if the difference in leptin expression was related to the previously discovered differences in the numbers of tubules formed in the presence of AT and MV MSCs, the co-culture tubule assay was modified to assess the effect of the addition of exogenous human recombinant leptin (R&D Systems, Abingdon, UK) at 0, 25, 100 and 400ng/ml. Exogenous leptin was added to tubule assays with co-culture of $5x10^3$ AT MSC and $1x10^3$ UCB ECFC derived cells. Initial plates set with different concentrations of leptin were difficult to

analyse due to excess proliferation, early lifting of the cell layers from the plate and clumping of tubules. Where tubules did form, there was a trend towards increased tubule formation with increasing doses of leptin on subjective microscopic examination of viable wells. Representative images of the few viable wells from 25 and 100ng/ml leptin doses are shown in Figure 5.9 with the 0ng/ml control for comparison. The protocol was then optimised as described in Section 5.3.6.1.

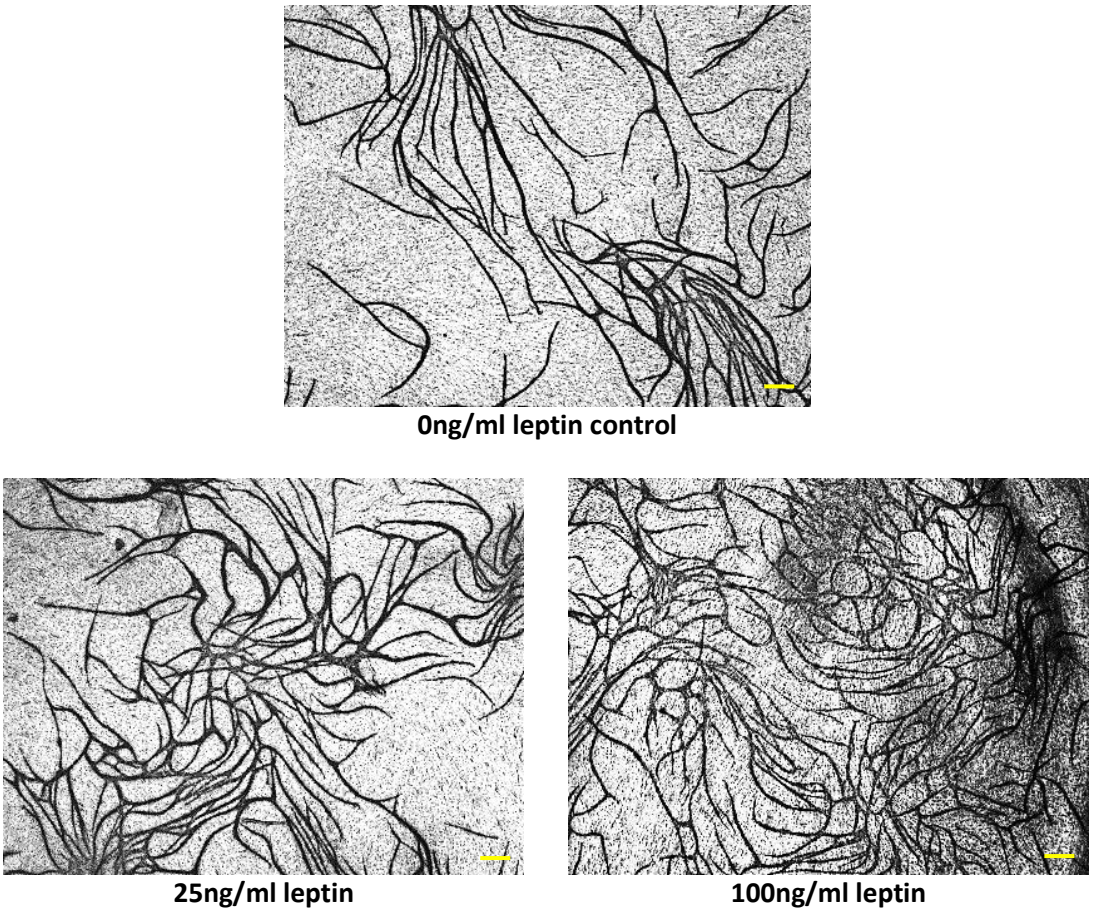

Figure 5.9: Effect of exogenous leptin on vascular tubule formation. Initial trial of leptin doses showed subjective increase in tubule formation with increasing concentrations of leptin, but too few viable wells were available for quantification. (Phase contrast microscopy, 100µm scale bar)

5.3.6.1 Leptin and AT MSC co-culture vascular tubule formation

The protocol was optimised by reducing the time in culture to 10 days instead of the usual 14 day culture and by limiting the dose of leptin to 25ng/ml. Under these conditions, four batches of AT MSC at a concentration of either $5x10^3$ or $1x10^4$ per well were co-cultured with $1x10^3$ UCB ECFC derived cells per well, with or without 25ng/ml leptin. Again the lowest concentration of endothelial cells previously used in the tubule assay was chosen as these cells are likely to be limited in clinical applications. Two different concentrations of MSC were used as these may be a source of autologous leptin. Each condition was repeated in triplicate using four different batches of AT MSCs and mean values of total tubule length per well were calculated with standard error of the mean. Data were compared for leptin and control wells in each batch (n=3) and for the mean of all four batches (n=4) using the two tailed Student's T test for paired samples. Table 5.5 shows a consistently significant increase in tubule formation with the lower concentration of AT MSCs, with a mean increase of 52.8% in total tubule length across all four batches (p=0.019). Figure 5.10 shows a graphical representation of the mean total tubule lengths with leptin versus control wells and shows clear intra-sample consistency.

When the concentration of AT MSCs in co-culture was increased to $1x10^4$ per well the mean increase in total tubule length was greater, as was the statistical significance (p=0.006, Student's T test for paired samples). Table 5.6 shows a consistently significant increase in tubule formation with each batch of AT MSCs, and the mean increase of 59.4% in total tubule length across all four batches. Figure 5.11 highlights the clear intra-sample consistency of the mean total tubule lengths with leptin versus control wells.

Table 5.5: Effect of 25ng/ml leptin on tubule formation with $5x10^3$ AT MSC and $1x10^3$ UCB ECFC derived cells in co-culture.

$5x10^3$ AT MSC with $1x10^3$ UCB ECFC co-culture					
	AT 1 (n=9)	**AT 2 (n=9)**	**AT 3 (n=9)**	**AT 4 (n=9)**	**For all samples (n=4)**
Mean total tubule length of control ± SEM	16866 ± 1653	27507 ± 1850	12079 ± 3070	17132 ± 2005	18396 ± 3251
Mean total tubule length with leptin ± SEM	22434 ± 1497	36112 ±2172	28324 ± 2039	29526 ± 1359	29099 ± 2804
Difference in means (value, percent)	5568 33.0% increase	8605 31.3% increase	16245 134.5% increase	12394 72.3% increase	10703 52.8% increase
Significance (p)	0.0412	0.0027	0.0026	0.0003	0.0191

Values are in microns and significant p values from the two tailed Student's T test for paired samples are shown in red.

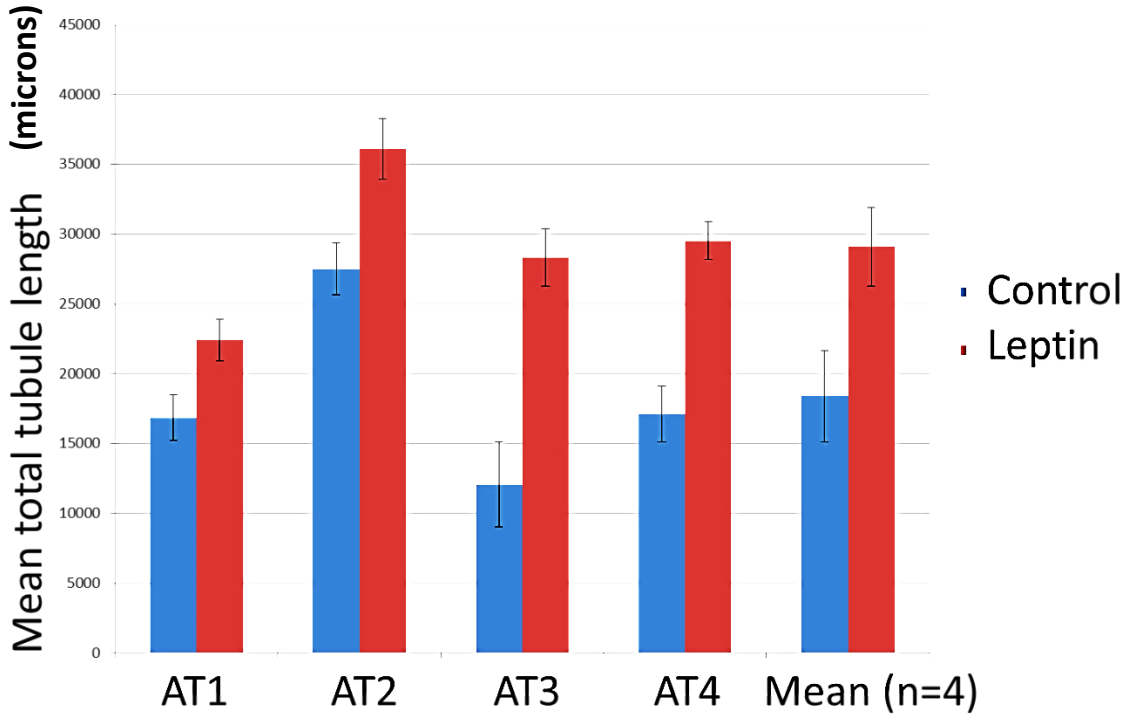

Figure 5.10: Mean total tubule length in $5x10^3$ AT MSC with $1x10^3$ UCB ECFC derived cell co-cultures. There is a consistent significant increase in tubule formation across the samples with addition of 25ng/ml leptin to the co-culture wells. Error bars show Standard Error of the Mean (SEM). Within each individual AT sample n=9, with triplicate imaging of triplicate samples to ensure inter-sample consistency. The final paired columns show the mean values across the four individual samples with n=4 to ensure intra-sample consistency.

Table 5.6: Effect of 25ng/ml leptin on tubule formation with $1x10^4$ AT MSC and $1x10^3$ UCB ECFC derived cells in co-culture.

$1x10^4$ AT MSC with $1x10^3$ UCB ECFC co-culture					
	AT 1 (n=9)	**AT 2 (n=9)**	**AT 3 (n=9)**	**AT 4 (n=9)**	**For all samples (n=4)**
Mean total tubule length of control ± SEM	11086 ± 1440	25178 ± 1210	16081 ± 1009	14255 ± 1314	16650 ± 3024
Mean total tubule length with leptin ± SEM	18121 ± 1597	35623 ± 2236	29768 ± 1763	22637 ± 1330	26537 ± 3863
Difference in means (value, percent)	7035 63.5% increase	10445 41.5% increase	13687 85.1% increase	8382 58.8% increase	9887 59.4% increase
Significance (p)	0.0048	0.0054	<0.0001	0.0045	0.0064

Values are in microns and significant p values from the two tailed Student's T test for paired samples are shown in red.

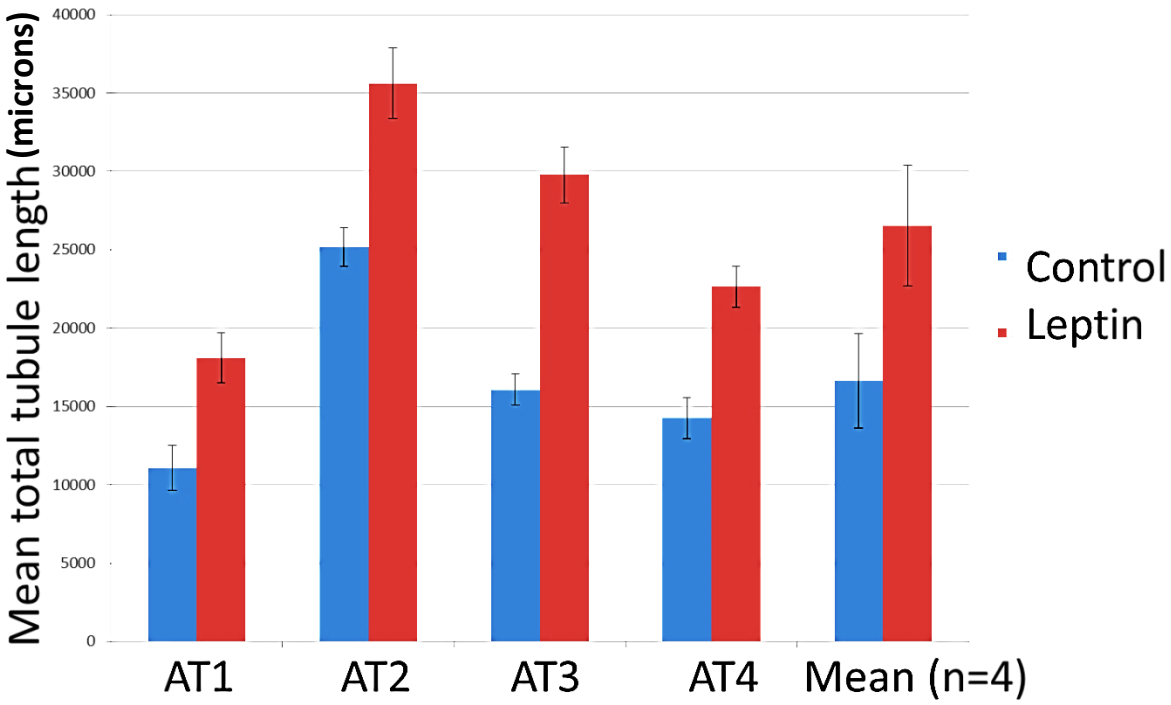

Figure 5.11: Mean total tubule length in $1x10^4$ AT MSC with $1x10^3$ UCB ECFC derived cell co-cultures. There is a consistent significant increase in tubule formation across the individual AT samples with addition of 25ng/ml leptin to the co-culture wells. Error bars show Standard Error of the Mean (SEM). Within each individual AT sample n=9, with triplicate imaging of triplicate samples to ensure inter-sample consistency. The final paired columns show the mean values across the four individual samples with n=4 to ensure intra-sample consistency.

5.3.6.2 Leptin and MV MSC co-culture tubule formation

The effect of leptin on MV MSC co-cultures was also tested. There were no significant increases in total tubule length in these samples with the addition of leptin at either cell concentration ratio (Table 5.7 and Table 5.8). It may be that expressing a greater quantity of endogenous leptin negates the possibility of an additional effect from exogenous leptin. With increased MV MSC cell concentration the difference in total tubule length with the addition of leptin was even smaller and less significant. Graphical representation of the data is shown in Figure 5.12 and Figure 5.13.

Table 5.7: Effect of 25ng/ml leptin on tubule formation with $5x10^3$ MV MSC and $1x10^3$ UCB ECFC derived cells in co-culture.

$5x10^3$ MV MSC with $1x10^3$ UCB ECFC co-culture					
	MV 1 (n=9)	**MV 2 (n=9)**	**MV 3 (n=9)**	**MV 4 (n=9)**	**For all samples (n=4)**
Mean total tubule length of control ± SEM	27322 ± 1489	20595 ± 1945	21465 ± 983	28749 ± 1705	24533 ± 2051
Mean total tubule length with leptin ± SEM	28700 ± 1678	19725 ± 1136	14884 ± 1403	26147 ± 1672	22364 ± 3127
Difference in means (value, percent)	1378 5.0% increase	870 4.2% decrease	6581 30.7% decrease	2602 9.1% decrease	2169 8.8% decrease
Significance (p)	0.4359	0.0156	<0.0001	0.0523	0.2875

Values are in microns and significant p values from the two tailed Student's T test for paired samples are shown in red.

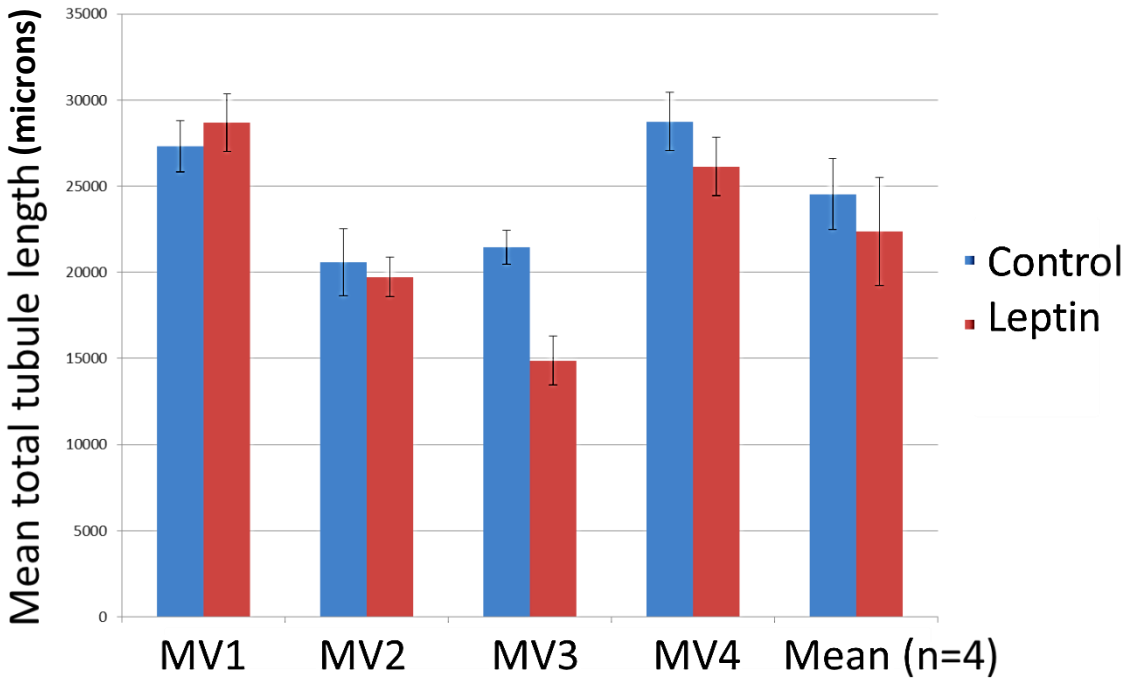

Figure 5.12: Mean total tubule length in $5x10^3$ MV MSC with $1x10^3$ UCB ECFC derived cell co-cultures. There was no significant difference in mean total tubule length with the addition of leptin. Error bars show Standard Error of the Mean (SEM). N=9 for triplicate imaging of triplicate samples for each batch of MV MSCs. N=4 for the final paired columns which show the mean values for the four batches.

Table 5.8: Effect of 25ng/ml leptin on tubule formation with $1x10^4$ MV MSC and $1x10^3$ UCB ECFC derived cells in co-culture.

$1x10^4$ MV MSC with $1x10^3$ UCB ECFC co-culture					
	MV 1 (n=9)	**MV 2 (n=9)**	**MV 3 (n=9)**	**MV 4 (n=9)**	**For all samples (n=4)**
Mean total tubule length of control ± SEM	19559 ± 1373	25096 ± 1742	12843 ± 1130	17951 ± 2586	18862 ± 2523
Mean total tubule length with leptin ± SEM	21308 ± 1986	24094 ± 2288	9460 ± 715	20604 ± 1011	18866 ± 3225
Difference in means (value, percent)	1749 8.9% increase	1002 4.0% decrease	3383 26.3% decrease	2653 14.8% increase	4 0.02% increase
Significance (p)	0.5147	0.5443	0.0274	0.3667	0.9978

Values are in microns and significant p values from the two tailed Student's T test for paired samples are shown in red.

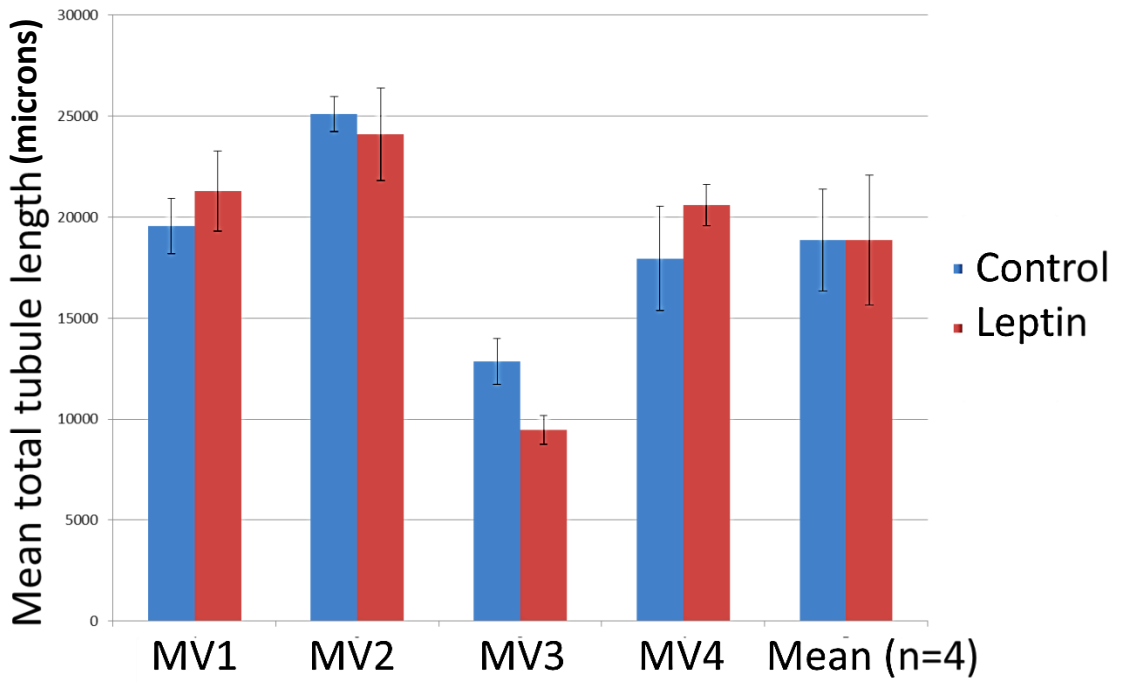

Figure 5.13: Mean total tubule length in $1x10^4$ MV MSC with $1x10^3$ UCB ECFC derived cell co-cultures. There was no significant difference in mean total tubule length with the addition of leptin. Error bars show Standard Error of the Mean (SEM). N=9 for triplicate imaging of triplicate samples for each batch of MV MSCs. N=4 for the final paired columns which show the mean values for the four batches.

5.3.7 Cell proliferation was unaffected by the addition of leptin

It was hypothesised that the effect of increased tubule formation with addition of leptin might be due an increase in the proliferation of either ECFC derived cells or MSCs. It was therefore decided to quantify cell proliferation with and without the addition of leptin using the same MTT assay previously used to examine MSC proliferation. It was decided to run this assay on two different sources of endothelial cells in order to further clarify an effect on this cell type. Figure 5.14 shows no significant difference in proliferation of UCB ECFC derived cells (250 cells p=0.4, 500 cells p=0.7, 1000 cells p=0.8 using the Student's T test for paired samples) or HUVECs (250 cells p=0.2, 500 cells p=0.8, 1000 cells p=0.2 using the Student's T test for paired samples) with the addition of leptin compared with controls at three different cell seeding concentrations, cultured for 4 days in complete EGM-2 (Lonza Biologics, Slough, UK) as described in Chapter 2, Section 2.10.

Proliferation of four different batches of AT and MV MSCs was tested with and without addition of leptin at two different cell seeding concentrations, with each condition repeated in triplicate. AT MSC results are presented in Figure 5.15, which shows no difference in cell proliferation between control cells and cells treated with leptin at either cell seeding density (500 cells p=0.5, 1000 cells p=0.1 using the Student's T test for paired samples). This is clearly seen in each individual batch and in the mean values across the four batches of cells. Similarly, there was no effect on MV MSC cell proliferation with the addition of leptin (500 cells p=0.1, 1000 cells p=0.1 using the Student's T test for paired samples). Figure 5.16 clearly demonstrates no difference in cell proliferation between control cells and cells treated with leptin at either cell seeding density in any batch.

From these MTT assays we can conclude that leptin does not increase tubule formation *in vitro* by up regulation of either ECFC or MSC proliferation.

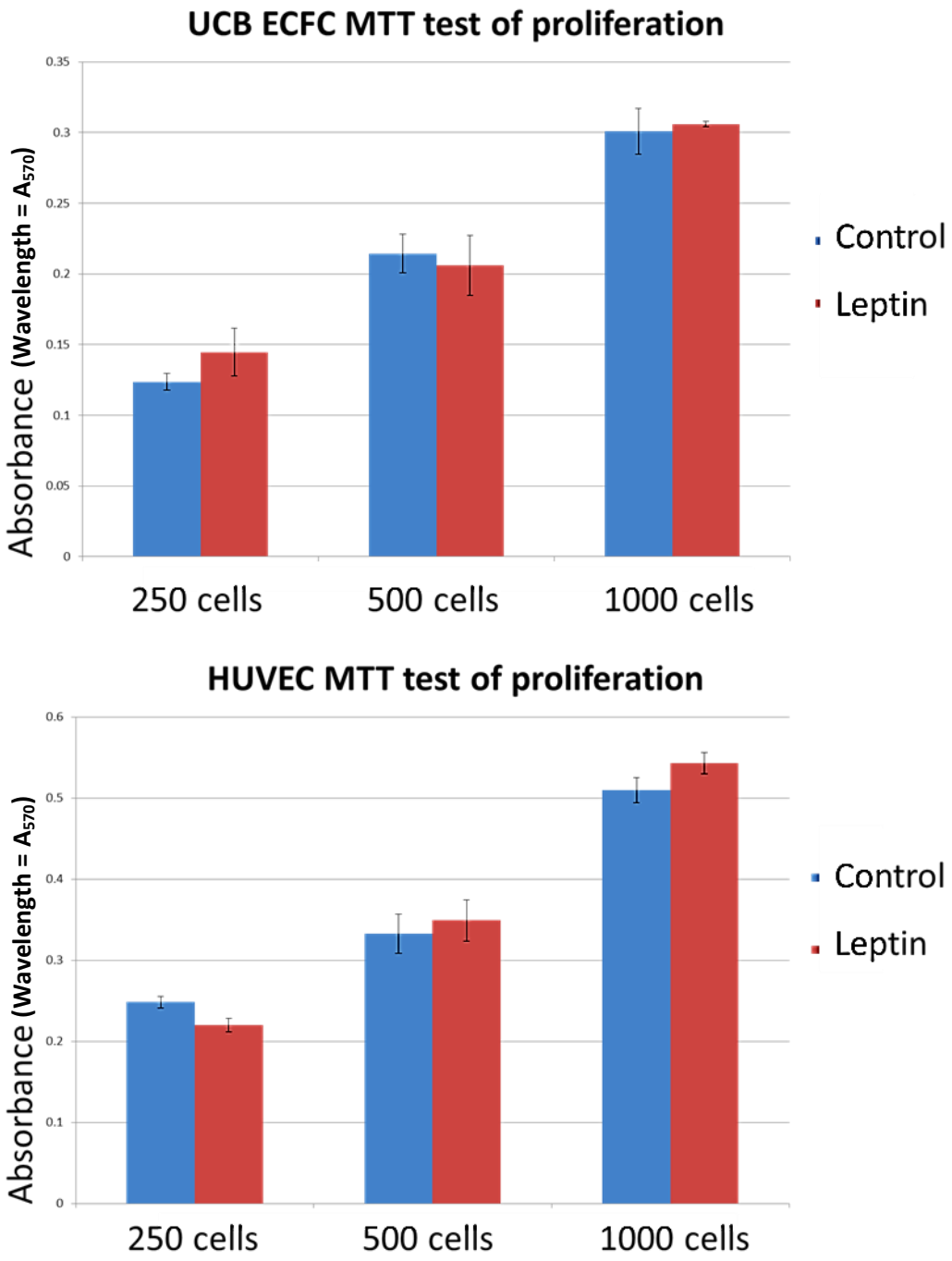

Figure 5.14: Effect of exogenous leptin on endothelial cell proliferation. Umbilical Cord Blood Endothelial Colony Forming Cell derived cells (UCB ECFC) and Human Umbilical Vein Endothelial Cells (HUVEC) were tested for proliferation using an MTT absorbance test to determine relative viable cell counts with and without leptin. Errors bars show Standard Error of the Mean (SEM), samples were repeated in triplicate. There was no significant difference in proliferation following addition of leptin with 250, 500 or 1000 cell per well concentrations (UCB ECFC 250 cells p=0.4, 500 cells p=0.7, 1000 cells p=0.8, HUVEC 250 cells p=0.2, 500 cells p=0.8, 1000 cells p=0.2 using the Student's T test for paired samples).

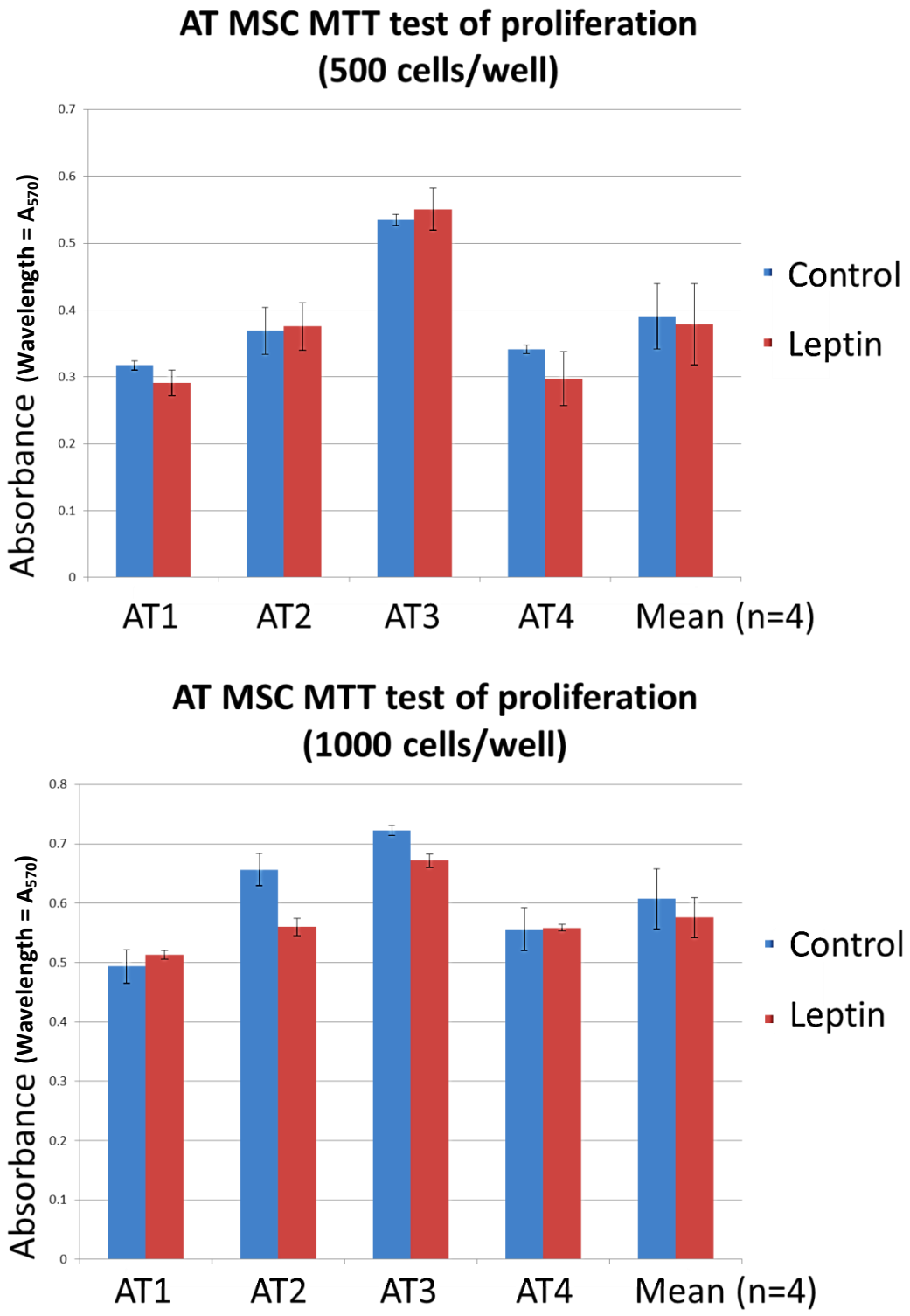

Figure 5.15: Effect of exogenous leptin on AT MSC proliferation. Adipose Tissue Mesenchymal Stromal/Stem Cells (AT MSC) were tested for proliferation using an MTT absorbance test to determine relative viable cell counts with and without leptin. Errors bars show Standard Error of the Mean (SEM), four batches of AT MSCs were repeated in triplicate. The final paired column is the mean of the values for all four batches. There was no significant difference in proliferation following addition of leptin with 500 or 1000 initial cell numbers (500 cells p=0.5, 1000 cells p=0.1 using the Student's T test for paired samples).

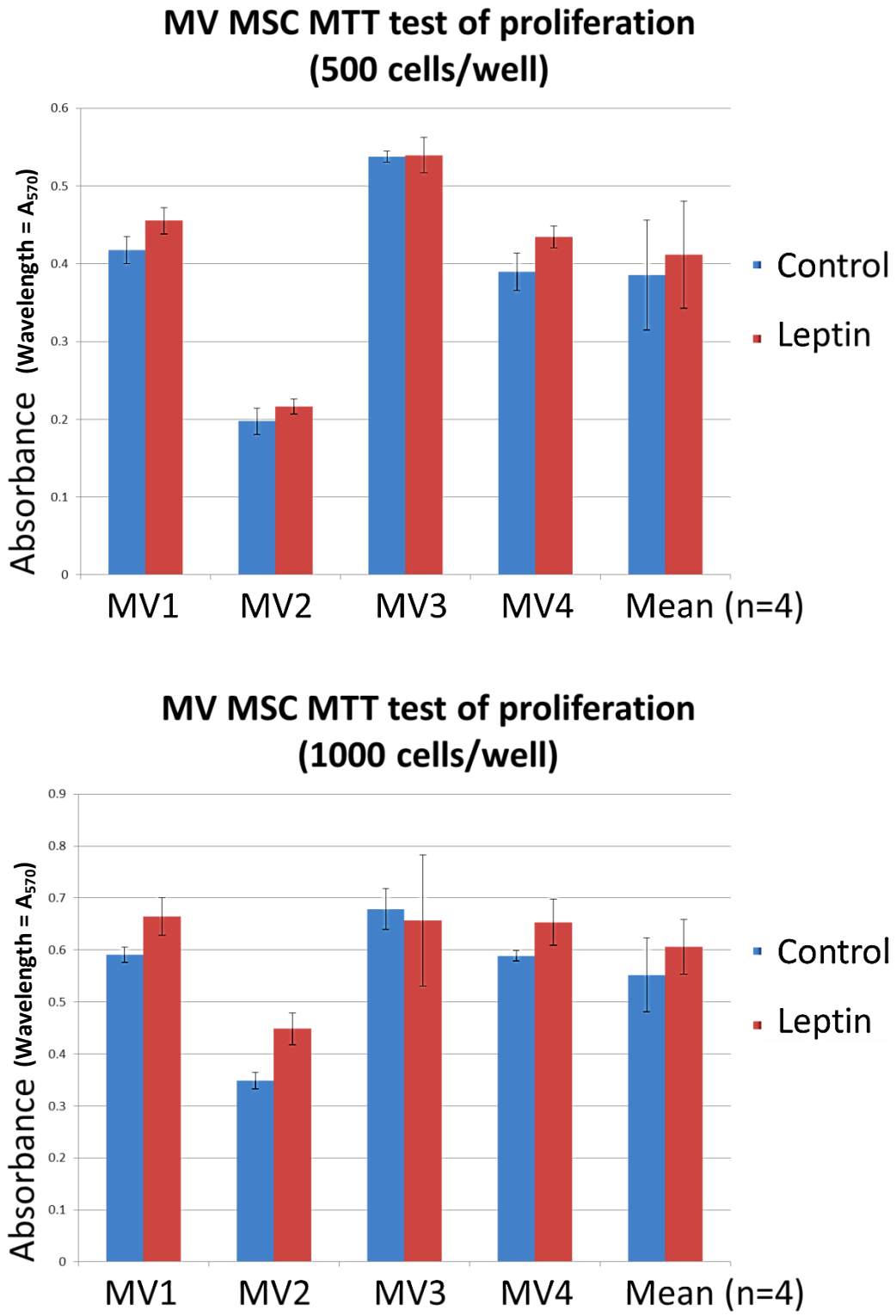

Figure 5.16: Effect of exogenous leptin on MV MSC proliferation. Microvascular Mesenchymal Stromal/Stem Cells (MV MSC) were tested for proliferation using an MTT absorbance test to determine relative viable cell counts with and without leptin. Errors bars show Standard Error of the Mean (SEM), four batches of MV MSCs were repeated in triplicate. The final paired column is the mean of the values for all four batches. There was no significant difference in proliferation following addition of leptin with 500 or 1000 initial cell numbers (500 cells p=0.1, 1000 cells p=0.1 using the Student's T test for paired samples).

5.4 Discussion

In this chapter, MV MSCs were found to support a more robust blood vessel network *in vitro* than AT MSCs. This was demonstrated in four different paired batches of cells. We believe this to be a novel finding, and hence possible underlying mechanisms for this difference in function were investigated.

MV MSCs secreted a significantly higher amount of leptin in co-culture with UCB ECFC derived cells than AT MSCs, as assessed by the antibody array. The differential expression and production of leptin by AT MSC and MV MSC could be assessed using more sensitive methods, such as Enzyme-Linked ImmunoSorbent Assays (ELISA), and this has been proposed for future work.

Leptin is a metabolic hormone expressed by the obese gene which has well-established roles in control of metabolism and satiety (277, 278). In addition to influencing insulin regulation and other mechanisms of fat storage, leptin has also been shown to be involved in the promotion of angiogenesis (146, 279-282) either by its effect on endothelial cells (279, 280, 282) or on *in vivo* angiogenesis in rat models (146, 281), and this is consistent with the increased tubule formation observed in the *in vitro* angiogenesis co-culture assay when MV MSCs were used as the supporting cell source rather than AT MSCs.

Liapakis *et al.* used a murine model of incisional wound angiogenesis to show increased density of neovascularisation with the addition of leptin to the wound bed compared with placebo controls (148). Following this, the group also showed that exogenous leptin increased early wound bed angiogenesis in a rat burn wound model (147) and in a full thickness flap model (149). The flap study found that addition of high dose leptin resulted in a greater increase in neovascularisation than that seen with addition of vascular endothelial growth factor (VEGF) (149), which is a key component of endothelial growth media used in *in vitro*

angiogenesis assays (135) and is one of only a few proangiogenic growth factors to have been tested in human clinical trials for the ability to improve wound healing (283).

Tubule formation in AT MSC co-cultures could be significantly increased with the addition of exogenous leptin, but the effect was not seen with the addition of exogenous leptin to MV MSC co-cultures. It may be that there is an upper limit to the effect of leptin on tubule formation and this was already reached with endogenous leptin from the MV MSCs, thus negating the effect of the exogenous leptin. Higher concentrations of exogenous leptin in the co-culture assay resulted in poor tubule survival due to cell clumping and lifting, so it may be that endogenous leptin expression has a positive feedback mechanism in place to limit tubule formation to a level that can be maintained by the supporting cell source. There is a need to quantitate by ELISA the levels of leptin secreted by each cell type.

In the studies presented in this Thesis, leptin did not modulate UCB ECFC, AT MSC or MV MSC proliferation. Proliferation of AT and MV MSCs was however comparable and there was no difference in UCB ECFC derived cell or MSC proliferation with the addition of leptin to cells in mono-culture. This is in keeping with findings of Wolk *et al.* (2005) and we have therefore excluded up regulation of proliferation as the mechanism of increased tubule formation in leptin treated co-cultures. Wolk *et al.* identified the leptin receptor on the surface of endothelial progenitor cells, but found no change in endothelial progenitor cell proliferation in the presence of leptin (282). Goetze *et al.* (2002) showed that HUVECs migrate towards leptin in *in vitro* culture and postulated that the role of leptin in angiogenesis is to promote cell migration (280). This might result in increased length of individual tubules, as well as an increase in total number of tubules formed.

Differential expression of the thirteen proteins found to be expressed more in the AT samples compared with the MV samples may also benefit from further quantification by ELISA array. This data may not be as useful as data for leptin since expression of these proangiogenic

factors was lower in the MV samples, despite their increased tubule formation compared with AT co-cultures, making a useful clinical application less likely.

There are some concerns over the addition of exogenous proangiogenic factors to *in vitro* microvasculature intended for later clinical use due to the strong association of some factors with aggressive malignancies. For example, the receptor for CXCL16 has been linked to increased cancer invasion and metastases (284, 285) and there is concern regarding potential formation of angiosarcoma or other connective tissue tumours. The specific receptor for HGF, called cMet, is a proto-oncogene and the HGF/cMet pathway has been implicated in formation of several cancers including breast cancer (286), oesophageal carcinoma (287), hepatocellular carcinoma (288), cholangiocarcinoma (289) and multiple intestinal tumours (290). MMP-9 has also been implicated in formation of several cancers including oral squamous cell carcinoma (291), oesophageal carcinoma (292), thyroid carcinoma (293) and prostate carcinoma (294).

MV MSC should be used preferentially as the stromal cell source for *in vitro* microvascular formation for future clinical applications since they support significantly more tubule formation than AT MSC. However, dissection of the microvasculature from adipose tissue samples is both technically challenging and time consuming, so it is useful to know that AT MSC, which are easier and faster to prepare for culture, show significantly increased tubule formation with the addition of exogenous leptin. This may allow optimal tubule formation without the disadvantage of more difficult culture protocols, but appropriate testing in an animal model would be required in order to ensure no problems with tumour formation.

Professor Péault's work with pericytes discussed in Chapter 4, used adipose lipoaspirate purified using fluorescence-activated cell sorting (FACS) to isolate $CD146^{+}$, $CD34^{-}$, $CD45^{-}$, $CD56^{-}$ cells which they identified as MSC progenitors (264, 267). Since the AT and MV MSC in this Thesis displayed no significant differences in their phenotype for the markers tested, it may be that the 'mechanical purification' of the MV MSC was responsible for the greater

proangiogenic activity. If so, FACS purification of the whole adipose tissue to isolate the MSC progenitors prior to culture and expansion may result in a population of cultured MSC with greater proangiogenic activity. Overall, a larger proteomic experiment looking at all of the protein in the AT and MV cells or a whole genome analysis approach may be beneficial in understanding what factors are differentially expressed when comparing these cell types.

Having established that AT and MV MSCs support microvascular tubule formation in co-culture with UCB ECFC derived cells in two dimensional culture, these techniques were applied to three dimensional assays which may enable clinical application of tubule networks in the future. These are discussed in Chapter 6.

Chapter 6 Dermal Scaffolds and Three-Dimensional Vascularisation

6.1 Background

The working hypothesis underlying this research is that clinical application of a skin substitute with a pre-formed vascular network plus split thickness skin grafting may result in improved scarring compared with split thickness skin grafting alone or on top of non-vascularised dermal substitute. Skin grafts heal by a process of fibrin adhesion to the wound bed, plasmatic imbibition of nutrients from the wound bed, inosculation of vessels in the wound bed and the graft, and neovascularisation across the wound bed into the graft (34). As the graft matures, the vessels re-organise into a functional network, but areas of unfavourable hypertrophic or keloid scarring have been shown to contain a disorganised vascular network entangled around dense bundles of fibroblasts (19, 28). Full thickness skin grafts contain the full extent of the dermis, including the existing dermal vasculature, and have consistently better quality scarring than split thickness skin grafting (34, 35). Whereas split thickness grafts scar throughout the entire surface of the graft, full thickness grafts tend to have a linear scar around the periphery of the graft, whilst the central graft remains soft and pliable as it was at the donor site (35). Dermal substitutes have been shown to improve scar quality in two staged procedures which allow initial vascularisation of the dermal substitute prior to application of split thickness skin grafts (50-52). By providing a pre-vascularised dermal scaffold to the wound bed, an improvement in scar quality similar to full thickness skin graft results which can be achieved in a single operative procedure would be predicted, without the donor site limitations experienced with full thickness skin grafting (35, 53).

In order to produce a pre-vascularised dermal substitute with properties similar to a full thickness skin graft, it would be necessary for the vasculature to grow in three dimensions to

populate the depth of the scaffold. Vessels should cross from one side of the scaffold to the other in order to provide vessel ends for inosculation with both the wound bed inferiorly and the split thickness skin graft superiorly.

Attempts to improve three-dimensional *in vitro* cultures have involved scaffolds with different physical properties (295, 296). Scaffolds include acellular Good Manufacturing Practice (GMP) grade constructs already in clinical use, decellularised human dermis, and imprinted gels composed of various molecules including fibrin, collagen, hyaluronic acid, elastin or PolyLactic co-Glycolic Acid (PLGA) (297-299).

As it was found that vasculature networks did not penetrate completely through GMP grade scaffolds in clinical use such as Integra® Dermal Regeneration Template (Integra LifeSciences Corporation, Plainsboro, NJ, U.S.A.) and Matriderm® (Eurosurgical Ltd., Guildford, UK), but were restricted to a depth of 100µm, in this Chapter two new scaffolds were tested for their ability to support the formation of a developing vascular network. These were a thin (200µm) collagen scaffold called Neuskin-F® (Medira Ltd., Sandy, UK), and Decellularised Human Cadaveric Dermis (DHCD) (NHS Blood and Transplant, Liverpool, UK) which retains human matrix components and has spaces where vasculature might reform upon seeding vasculogenic cells (169). Additionally, following the successful increase in two-dimensional microvascular formation with the addition of exogenous leptin to co-cultures described in Chapter 5, leptin was added to the three-dimensional model to determine if this could improve vessel growth.

Three-dimensional vessel growth is a limiting factor in many tissue engineering applications and is thought to be restricted due to poor oxygen diffusion into the tissue (63, 184-186). Since this was found with the scaffolds used here, it was decided to add an artificial oxygen carrier perfluorocarbon compound to the culture media in order to increase the oxygen content of

the media in which the scaffolds were suspended (197, 198), prior to supplying this to the 3D scaffold.

6.2 Aim and objectives

The aim of this chapter was to apply microvasculature formation techniques with our chosen primary cells to three dimensional dermal substitute scaffolds which are currently used as acellular matrices for wound repair.

The specific objectives were:

- To assess pre-vascularisation of the dermal substitute scaffolds Integra® Dermal Regeneration Template (Integra LifeSciences Corporation, Plainsboro, NJ, U.S.A.) and Matriderm® (Eurosurgical Ltd., Guildford, UK) in current clinical use, using GFP labelled UCB ECFC derived cells.
- To investigate methods of improving three dimensional penetration of microvasculature into dermal substitute scaffolds using
    - scaffolds with different physical properties *viz.* Neuskin-F® (Medira Ltd., Sandy, UK) and DHCD (NHS Blood and Transplant, Liverpool, UK)
    - the pro-angiogenic factor leptin to increase tubule numbers
    - perfluorocarbon additives to improve oxygenation

6.3 Results

6.3.1 3D tubule growth in Integra® and Matriderm®

In order to prepare cells for better visualisation in three-dimensional cultures, Green Fluorescent Protein (GFP) lentiviral particles were created for transduction of UCB ECFC derived cells. The sourcing of these cells is described in Chapter 3 and the method of lentiviral particle preparation and transduction is described in Chapter 2 section 2.11.

For UCB ECFCs, GFP transduction at different MOIs and the effect on viability is shown in Figure 6.1. MOIs of 3 were subsequently used in this Thesis to generate GFP expressing UCB ECFC derived cells.

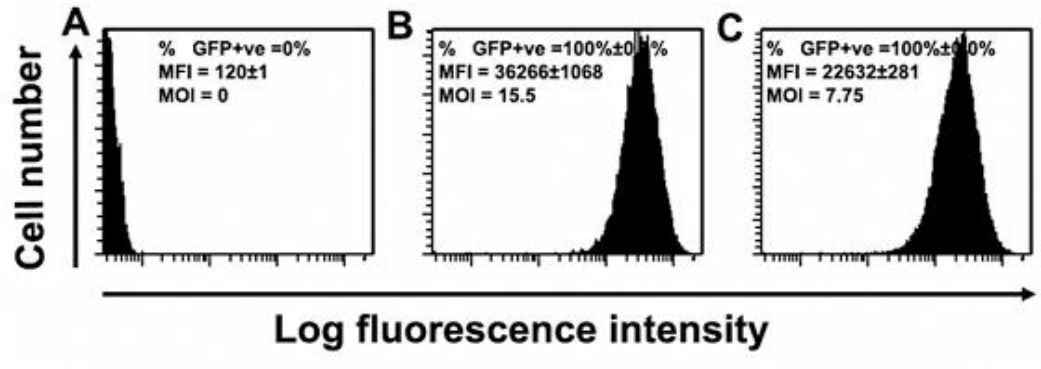

D The Efficiency of and Cell Viability after GFP-lentiviral Transduction at Different Multiplicities of Infection (MOI)

MOI	% Viability (normalized to non-transduced cells)*	% GFP positive cells	MFI± SEM
124.0	59±1.9 (73)*	98.4±0.8	19422±646
62.0	65±0.9 (81)	100±0.0	36302±257
31.0	73±0.7 (91)	100±0.0	46239±5474
15.5	79±1.6 (98)	100±0.0	36266±1068
7.75	81±0.7 (100)	100±0.0	22632±281
3.88	80±0.4 (100)	99.8±0.0	10773±390
1.94	80±0.5 (100)	97.7±0.1	5799±88
0.97	79±0.7 (98)	90.7±0.3	3578±53

Figure 6.1: Transduction efficiency and viability after GFP lentiviral transduction of UCB ECFC derived cells at different Multiplicities of Infection (MOI). A- GFP expression of non-transduced UCB ECFC derived cells. B- GFP expression of UCB ECFC derived cells transduced at MOI 15.5. C- GFP expression of UCB ECFC derived cells transduced at MOI 7.75. D- Comparative viability, normalised against non-transduced control cells, percent GFP positive cells and MFI are presented as mean ± SEM for three batches of UCB ECFC derived cells at various MOI. This figure was prepared using collaborative work as supplemental data for the paper Athanassopoulos A, Tsaknakis G, Newey SE, Harris AL, Kean J, Tyler MP, Watt SM. Microvessel networks [corrected] pre-formed in artificial clinical grade dermal substitutes in vitro using cells from haematopoietic tissues. Burns. 2012;38(5):691-701. Reproduced with permission from Elsevier via Rightslink®, License number 3365570624952.

Initial assays using GFP-labelled UCB ECFC derived cells examined if three-dimensional microvascular networks could be cultured within Integra® and Matriderm®, which are dermal substitutes in current clinical use (158, 163). These assays were performed prior to establishing a bank of our autologous MSCs and instead used unlabelled HDF and Bone Marrow derived MSCs (BM MSC) both purchased from Lonza Biologics (Lonza Biologics, Basel, Switzerland) in order to establish the technique. The HDF phenotyping is shown in Chapter 4, section 4.4 and the BM MSC phenotyping was performed by other scientists within our laboratory and found to be consistent with published data on MSCs (300).

Co-culture of $2x10^4$ GFP labelled UCB ECFCs and $1x10^5$ unlabelled HDF or BM MSC in complete EGM-2 (Lonza Biologics, Slough, UK) formed tubule networks in both 0.8mm Integra® and in 2mm Matriderm® scaffolds. Figure 6.2 shows representative high resolution confocal image stacks of GFP-labelled UCB ECFCs with differing unlabelled supportive cell types and scaffolds, reconstituted using Imaris software (Bitplane AG, version 6.4.0). Quantification of 3D microvasculature using AngioSys Image Analysis Software (Cellworks, Buckingham, UK) is shown in Figure 6.3, with mean values from three independent batches in triplicate presented with standard error of the mean. Analysis demonstrated no significant difference ($p>0.05$, Student's T test for unpaired samples) in the depth of penetration of the networks into the scaffold, the number of tubules, tubule junctions or total tubule length with the differing supportive cell types and scaffolds.

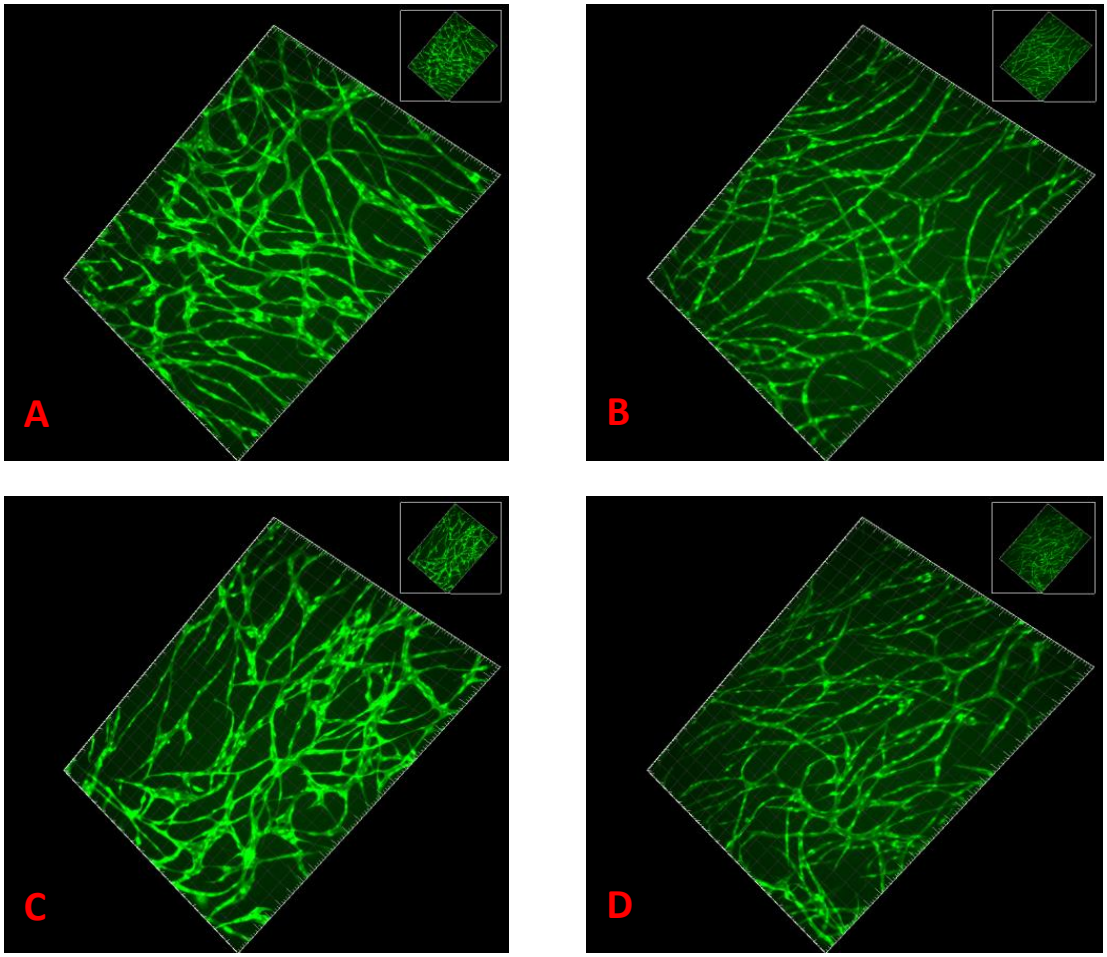

Figure 6.2: Pre-vascularisation of Integra® and Matriderm® dermal scaffolds. 3D-Microvascular network formation using GFP-labelled UCB ECFCs and unlabelled: A- Human Dermal Fibroblasts (HDFs) in Integra®, B- HDFs in Matriderm®, C- Bone Marrow derived human Mesenchymal Stem Cells (BM MSCs) in Integra®, D- BM MSCs in Matriderm®. Scaffolds were examined at day 14 following fixation of scaffolds in 4% PFA and mounting on glass slides, using the Zeiss LSM-510 inverted confocal microscope (Carl Zeiss Ltd., Cambridge, UK). High resolution 3D images were reconstructed using Imaris Version 6.4 software (Bitplane AG, Zurich, Switzerland). This figure was prepared using collaborative work with Mr A. Athanassopoulos and Dr. G. Tsaknakis for the paper Athanassopoulos A, Tsaknakis G, Newey SE, Harris AL, Kean J, Tyler MP, Watt SM. Microvessel networks [corrected] pre-formed in artificial clinical grade dermal substitutes in vitro using cells from haematopoietic tissues. Burns. 2012;38(5):691-701. Reproduced with permission from Elsevier via Rightslink®, License number 3365570624952.

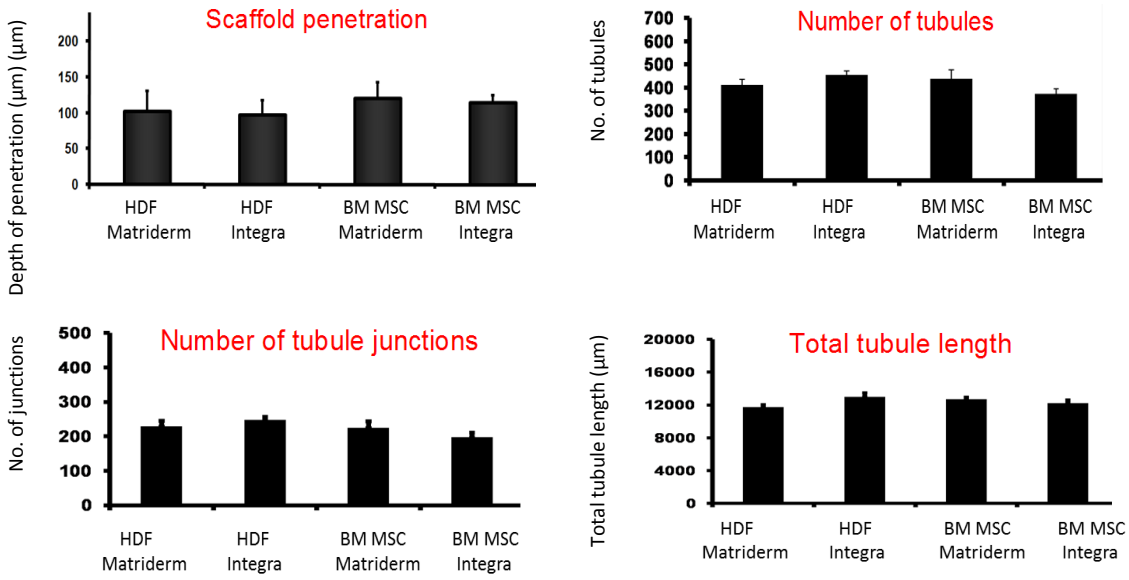

Figure 6.3: Comparative characteristics of 3D-microvascular tubule formation on Integra® and Matriderm® using co-cultures of $2x10^4$ GFP labelled UCB ECFCs and $1x10^5$ unlabelled HDF or BM MSC. Quantification of tubule formation was performed using AngioSys Image Analysis Software (Cellworks, Buckingham, UK). Mean values from three independent batches in triplicate are presented with SEM error bars. Analysis demonstrated no significant difference ($p>0.05$, Student's T test for unpaired samples) in the depth of penetration of the networks into the scaffold, the number of tubules, tubule junctions or total tubule length with the differing supportive cell types and scaffolds. This figure was prepared using collaborative work with Mr A. Athanassopoulos and Dr. G. Tsaknakis for the paper Athanassopoulos A, Tsaknakis G, Newey SE, Harris AL, Kean J, Tyler MP, Watt SM. Microvessel networks [corrected] pre-formed in artificial clinical grade dermal substitutes in vitro using cells from haematopoietic tissues. Burns. 2012;38(5):691-701. Reproduced with permission from Elsevier via Rightslink®, License number 3365570624952.

Cell penetration of 100µm from the surface of the scaffold equates to approximately 12.5% of the total depth of the Integra® scaffold (0.8mm) or 5% of the Matriderm® scaffold (2mm). Since 100µm was the depth of detected vascular penetration into both of the collagen based scaffolds, there may be a common limiting factor either in the structure of the scaffold, the ability of oxygen or nutrients to penetrate the scaffold, or in the ability of the confocal microscope to detect tubules. In other studies, sectioning of these scaffolds by other researchers in this laboratory did not demonstrate tubules beyond 100µm.

Based on these observations, and to take these studies forward with AT MSCs and novel scaffolds, two alternative scaffolds were tested. One of these was a thinner 200µm collagen scaffold (Neuskin-F®), the other was Decellularised Human Cadaveric Dermis (DHCD). Pre-formed channels exist in the DHCD that might allow vascular network penetration (169, 301).

These scaffolds are described in subsequent sections using AT and MV MSCs to support GFP labelled UCB ECFC derived cell network formation.

DSRed transduction of MSCs was performed to try and improve three-dimensional visualisation of co-cultures, but this required the addition of polybrene, and had an adverse effect on MSC proliferation. DSRed transduction data is presented in Appendix 3, and further work continued with unlabelled AT and MV MSC.

6.3.2 Neuskin-F® Scaffold

Neuskin-F® is a brittle scaffold of type I piscine collagen, approximately 0.2mm thick, and which currently has limited clinical use. The main reported uses of this scaffold so far are superficial traumatic or surgical wounds such as split thickness skin graft donor sites, but no peer-reviewed literature exists on the clinical use of this scaffold. It was selected for trial of three-dimensional vascularisation as it was hoped that the thin depth of the scaffold might allow improved penetration of the vasculature across the scaffold. Fluorescent microscopy of the microvascular network formation on Neuskin-F® is shown in Figure 6.4. This is a representative image from co-culture of $1x10^3$ GFP labelled UCB ECFC derived cells and $1x10^4$ unlabelled AT MSC in complete EGM-2 for two weeks. The pink arrows to the left of the image in Figure 6.4 are pointing to the peripheral edge of the scaffold which demonstrates the extent of the microvascular tubules.

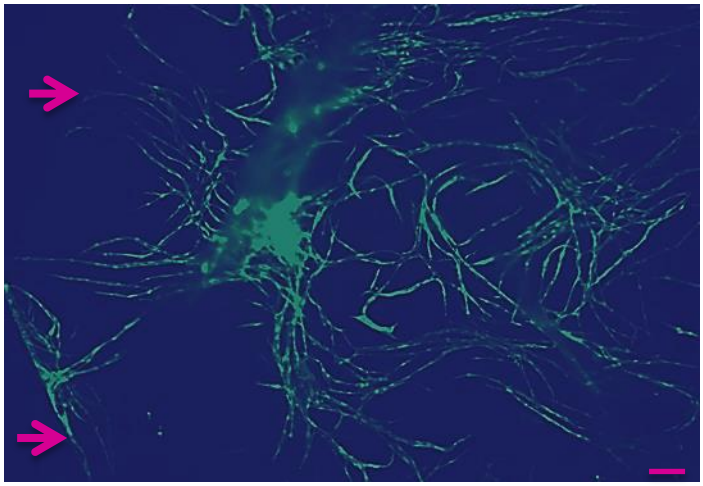

Figure 6.4: Fluorescent microscopy showing representative image of microvascular formation on Neuskin-F®. GFP labelled UCB ECFC derived cells were co-cultured with AT MSC in EGM-2 for two weeks. The pink arrows to the left of the image are pointing to the peripheral edge of the scaffold which demonstrates the extent of the microvascular tubules. (100µm scale bar)

Although there was consistent vessel formation across the Neuskin-F® scaffolds, quantification using the AngioSys Image Analysis Software (Cellworks, Buckingham, UK) was not possible due to areas of endothelial cell clumping (Figure 6.5, image A), a tendency for the vessels to wrap around the periphery of the scaffold (Figure 6.5, image B), and detection of the scaffold background by the software (Figure 6.5, image C).

A

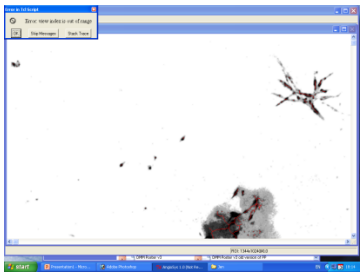

Endothelial clumping

B

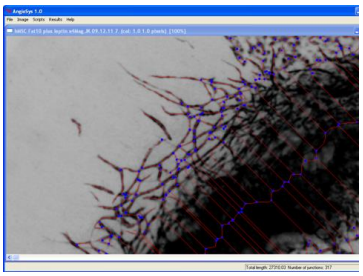

Cluster of vasculature at scaffold periphery

C

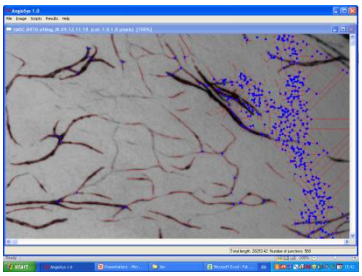

Scaffold background tagging

Figure 6.5: Difficulties in tubule quantification with the angiogenesis co-culture sandwich assay on Neuskin-F® scaffold. Image A shows an example of endothelial clumping, Image B is an example of microvasculature formation clustered at the periphery of the scaffold and growing around the edge and Image C shows how the quantification software erroneously tagged areas of the scaffold background as tubules.

Due to these difficulties, a qualitative grading scale was developed in order to aid evaluation of the effect of different cell concentrations or the addition of exogenous leptin on the formation of tubules on Neuskin-F®. The qualitative scale is shown in Figure 6.6. Grade 0 was awarded for images with sparse or absent tubule formation, Grade 1 for images where the predominant feature was clumps of endothelial cells with or without minimal tubule formation, Grade 2 for images with mainly short individual tubules or limited patchy networks, and Grade 3 for images with longer tubules forming identifiable networks. Each Neuskin-F® angiogenesis co-culture assay was repeated with two different paired batches of AT and MV MSCs. Two different MSC concentrations, $5x10^3$ or $1x10^4$, were cultured with $1x10^3$ UCB ECFC derived cells, with or without 25ng leptin. Each condition was repeated in triplicate. Three images per well were graded for quality of tubule formation and the modal grade (n=9) presented. Each condition supported tubule formation on the scaffold, with an apparent improvement in tubule quality in the presence of leptin (5/8 grade 3 conditions in the leptin groups compared with 2/8 grade 3 conditions in controls). These results are summarised in Table 6.1.

Grade 0 - Sparse or absent tubules.

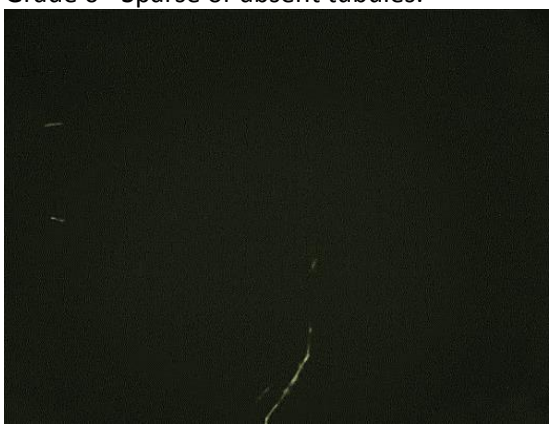

Grade 1 - Endothelial clumping.

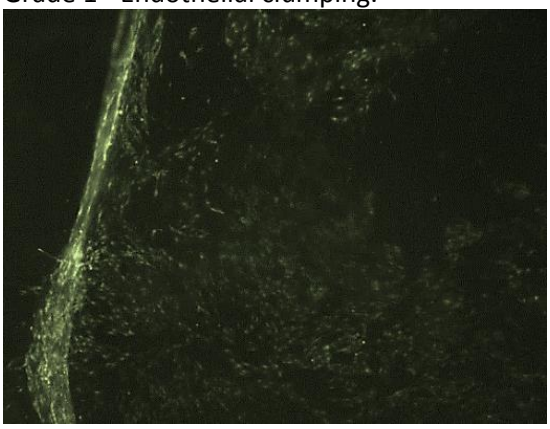

Grade 2 - Shorter tubules, limited network.

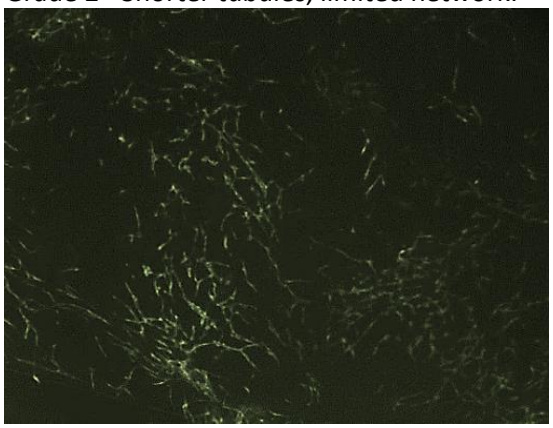

Grade 3 - Longer tubules, identified network.

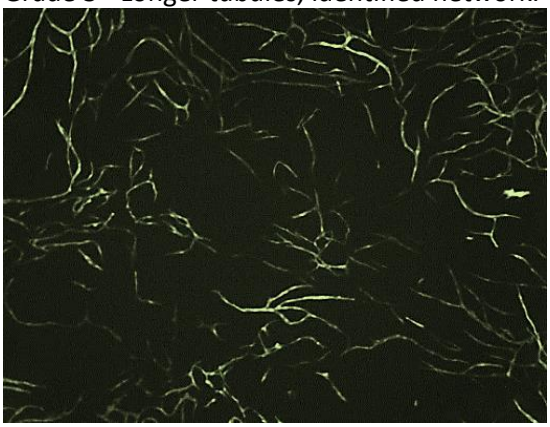

Figure 6.6: Qualitative grading system for tubule formation on Neuskin-F® scaffold. Grade 0 was awarded for images with sparse or absent tubule formation, Grade 1 for images where the predominant feature was clumps of endothelial cells with or without minimal tubule formation, Grade 2 for images with mainly short individual tubules or limited patchy networks, and Grade 3 for images with longer tubules forming identifiable networks.

Table 6.1: Qualitative grading of tubule formation on the Neuskin-F® scaffold using UCB ECFC derived cells and either AT or MV MSC, with and without the addition of leptin.

Batch 1				Batch 2			
ECFC	**MSC**	**Leptin**	**Modal Grade (n=9)**	**ECFC**	**MSC**	**Leptin**	**Modal Grade (n=9)**
$1x10^3$	AT $5x10^3$	0	3	$1x10^3$	AT $5x10^3$	0	2
$1x10^3$	MV $5x10^3$	0	2	$1x10^3$	MV $5x10^3$	0	3
$1x10^3$	AT $1x10^4$	0	2	$1x10^3$	AT $1x10^4$	0	2
$1x10^3$	MV $1x10^4$	0	2	$1x10^3$	MV $1x10^4$	0	2
$1x10^3$	AT $5x10^3$	25ng	3	$1x10^3$	AT $5x10^3$	25ng	3
$1x10^3$	MV $5x10^3$	25ng	2	$1x10^3$	MV $5x10^3$	25ng	3
$1x10^3$	AT $1x10^4$	25ng	2	$1x10^3$	AT $1x10^4$	25ng	2
$1x10^3$	MV $1x10^4$	25ng	3	$1x10^3$	MV $1x10^4$	25ng	3

The assay was repeated with two different paired batches of AT and MV MSCs and each condition was repeated in triplicate. Three images per well were graded for quality of tubule formation and the modal grade (n=9) presented. Each condition supported tubule formation on the scaffold, with an apparent improvement in tubule quality in the presence of leptin (5/8 grade 3 conditions in the leptin groups compared with 2/8 grade 3 conditions in controls).

Six Neuskin-F® scaffolds with Grade 3 vasculature formation were selected for further confocal imaging in order to determine the presence or absence of three-dimensional tubule penetration. Figure 6.7 shows representative two-dimensional and three-dimensional stacked confocal images of the tubule networks formed on the surface of the Neuskin-F® scaffolds using $1x10^4$ unlabelled AT MSC and $1x10^3$ GFP labelled UCB ECFC derived cells, taken at day 14. Figure 6.8 shows similar images for co-cultures of $1x10^4$ unlabelled MV MSC and $1x10^3$ GFP labelled UCB ECFC derived cells formed on the surface of the Neuskin-F® scaffolds. The three-dimensional views show the depth of the vessels in both sets of co-cultures sitting on top of the Neuskin-F® rather than penetrating through. Manual manipulation of the three-dimensional stacked images made it possible to visualise the lack of penetration into the scaffolds. The Neuskin-F® was non-porous and it seems that vasculature was unable to break through the structure of the scaffold and instead treated it as a two-dimensional surface. Due

to this observation, high resolution three-dimensional reconstitution of the networks was not performed.

The Neuskin-F® retained its rigidity throughout the two week culture period and it was possible to physically transport the scaffold out of culture plate wells for analysis without interrupting the vascular networks on the surface. This scaffold may therefore prove suitable for transfer of *in vitro* vasculature into *in vivo* models as it is initially rigid and then resorbs in the wound bed.

Given the failure of Neuskin-F® to allow penetration of the vasculature into the scaffolds, a further approch was to use decellularised human cadaveric dermis. Its advantages are that it is a human scaffold, there are channels within the scaffold which previously contained vasculature which may allow neovasculature penetration, it is a pre-existing full thickness dermis, and it is currently being used in clinical trials of chronic wound repair (169, 301, 302). Recellularisation of this dermis would be expected to improve wound healing.

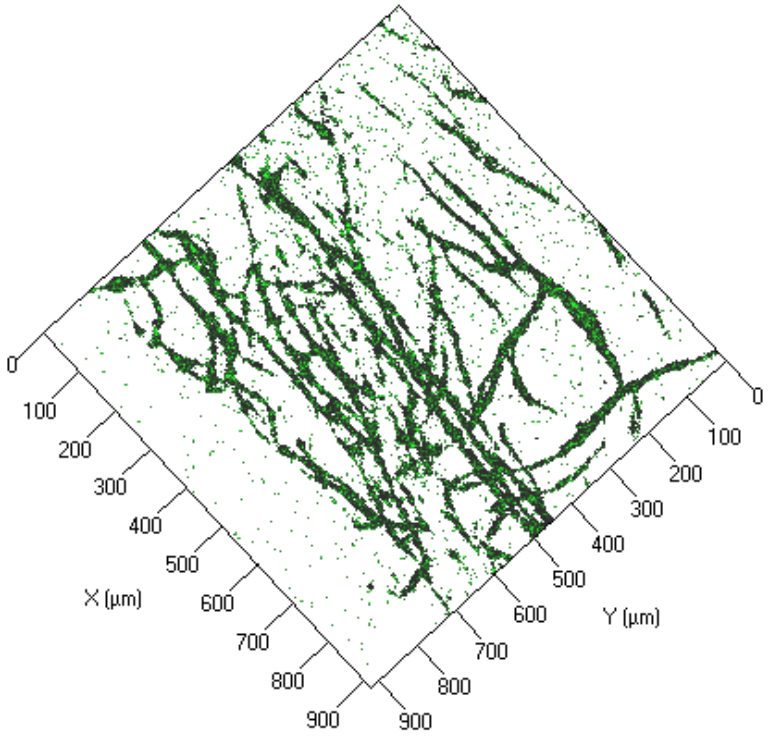

2D view of AT MSC and UCB ECFC co-culture tubule formation on Neuskin-F®

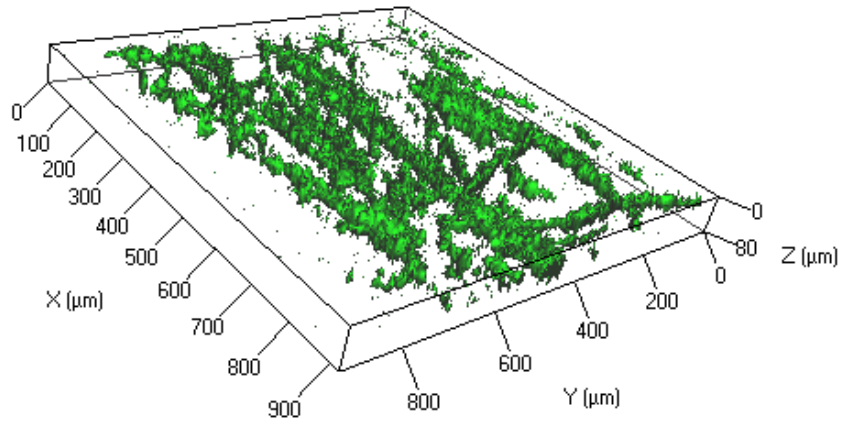

3D view of AT MSC and UCB ECFC co-culture tubule formation on Neuskin-F®

Figure 6.7: Three dimensional confocal imaging of microvascular network formation on Neuskin-F® (AT). Three batches of AT MSC were all capable of supporting microvascular formation in co-culture with GFP labelled UCB ECFCs on this scaffold. These representative images show $1x10^4$ unlabelled AT MSC and $1x10^3$ GFP labelled UCB ECFC derived cells co-cultured for 14 days on Neuskin-F® in EGM-2. The top image is a two-dimensional view and the bottom image shows a three-dimensional view of the confocal stack. Manual manipulation of the three-dimensional stacked images made it possible to visualise the lack of penetration into the scaffold.

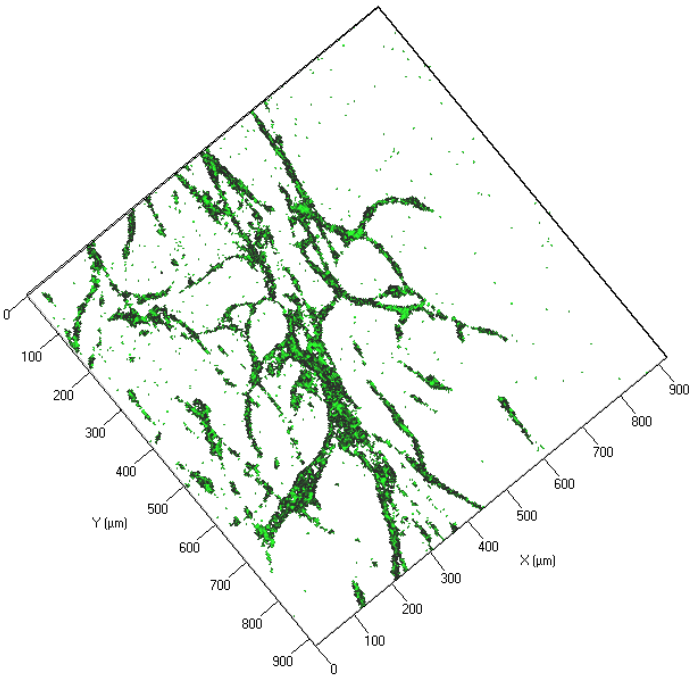

2D view of MV MSC and UCB ECFC co-culture tubule formation on Neuskin-F®

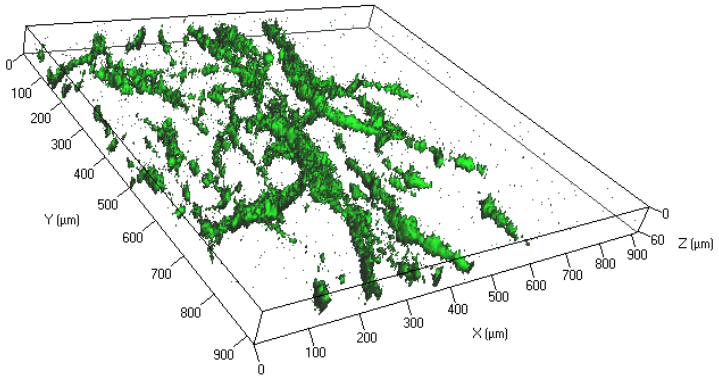

3D view of MV MSC and UCB ECFC co-culture tubule formation on Neuskin-F®

Figure 6.8: Three dimensional confocal imaging of microvascular network formation on Neuskin-F® (MV). Three batches of MV MSC were all capable of supporting microvascular formation in co-culture with GFP labelled UCB ECFCs on this scaffold. These representative images show $1x10^4$ unlabelled MV MSC and $1x10^3$ GFP labelled UCB ECFC derived cells co-cultured for 14 days on Neuskin-F® in EGM-2. The top image is a two-dimensional view and the bottom image shows a three-dimensional view of the confocal stack. Manual manipulation of the three-dimensional stacked images made it possible to visualise the lack of penetration into the scaffold.

6.3.3 De-cellularised Human Cadaveric Dermis (DHCD)

Three groups of culture conditions were set up using the DHCD scaffold; stromal cells only, control co-cultures of AT or MV MSC with UCB ECFC derived cells and co-cultures with 25ng leptin per well. Within each group of conditions there were different subgroups of MSC concentrations, and each individual condition was repeated in triplicate. The range of culture conditions are outlined in Table 6.2.

Multiple conditions were set simultaneously in order to fully utilise the donor DHCD samples, which were prepared by an external laboratory as relatively large strips of dermis that required defrosting and washing prior to plating. Once defrosted and washed, it was not possible to store the DHCD for later use. Additionally, time constraints towards the end of the laboratory phase of the project resulted in all conditions being cultured and fixed before confocal microscope examination of any of the samples had been performed. Poor visualisation of cells due to DHCD autofluorescence was not anticipated, and this unexpected difficulty made quantitative interpretation of microvasculature network formation impossible.

Fluorescent microscopy allowed visualisation of the superficial surface of the formed microvascular networks and confocal microscopy allowed limited assessment of three-dimensional network growth in only a few select samples.

Table 6.2: DHCD culture conditions.

DHCD culture condition	MSC/HDF	UCB ECFC	Media Additives
Stromal cells only	$5x10^3$ GFP AT MSC	None	None
	$1x10^4$ GFP AT MSC	None	None
	$5x10^3$ GFP MV MSC	None	None
	$1x10^4$ GFP MV MSC	None	None
	$5x10^3$ GFP HDF	None	None
	$1x10^4$ GFP HDF	None	None
Control co-cultures	$5x10^3$ AT MSC	$1x10^3$ GFP UCB ECFC	None
	$1x10^4$ AT MSC	$1x10^3$ GFP UCB ECFC	None
	$5x10^3$ MV MSC	$1x10^3$ GFP UCB ECFC	None
	$1x10^4$ MV MSC	$1x10^3$ GFP UCB ECFC	None
Leptin co-cultures	$5x10^3$ AT MSC	$1x10^3$ GFP UCB ECFC	25ng Leptin
	$1x10^4$ AT MSC	$1x10^3$ GFP UCB ECFC	25ng Leptin
	$5x10^3$ MV MSC	$1x10^3$ GFP UCB ECFC	25ng Leptin
	$1x10^4$ MV MSC	$1x10^3$ GFP UCB ECFC	25ng Leptin

Three groups of culture conditions were set using the DHCD scaffold; stromal cells only, control co-cultures of AT or MV MSC with UCB ECFC derived cells, and co-cultures with 25ng leptin per well. Within each group of conditions there were different subgroups of stromal cell concentrations, and each individual condition was repeated in triplicate.

Figure 6.9 and Figure 6.10 show the two best confocal images obtained from the DHCD co-culture assay with AT or MV MSCs and UCB ECFC derived cells. The three-dimensional reconstitution of the image stack in the confocal microscope software identifies the most superficial and deep images with evidence of GFP labelled endothelial cells. Due to interference from DHCD auto-fluorescence the reconstituted images were not suitable for quantification, but general depth of penetration could be determined. Maximal depth of penetration of microvasculature into the DHCD was 120µm, similar to that achieved in Integra® and Matriderm®.

It is possible that these selected samples were not as significantly affected by background autofluorescence as the others because the DHCD in these wells was much thinner than most. The DHCD is initially harvested manually from the skin on the back of cadaveric donors using an electric dermatome, and the thickness of the dermis is therefore not uniform throughout the sample. Towards the edge of the sample in particular, the dermis is oblique in sagittal cross-section.

A - Fluorescent microscopy (100µm scale bar)

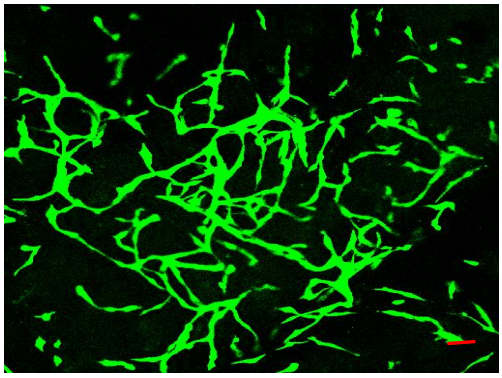

B - 2D view of 3D stack

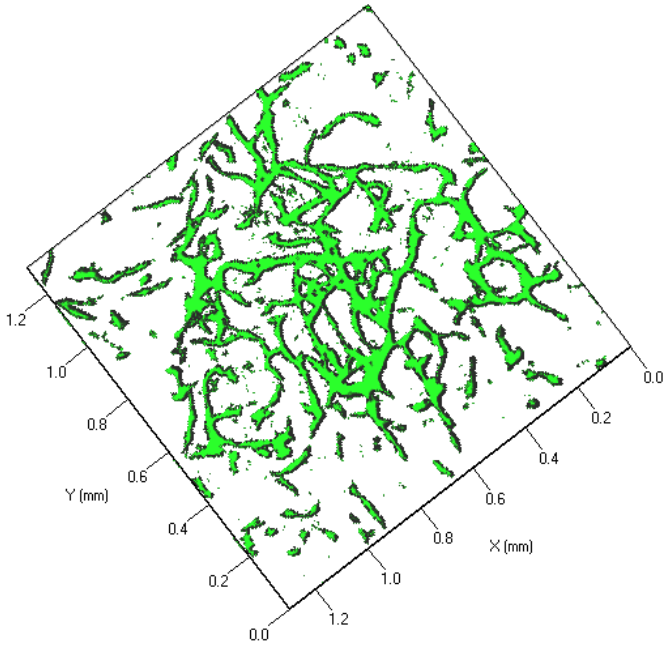

C - 3D view of stack images showing maximum depth of 60µm

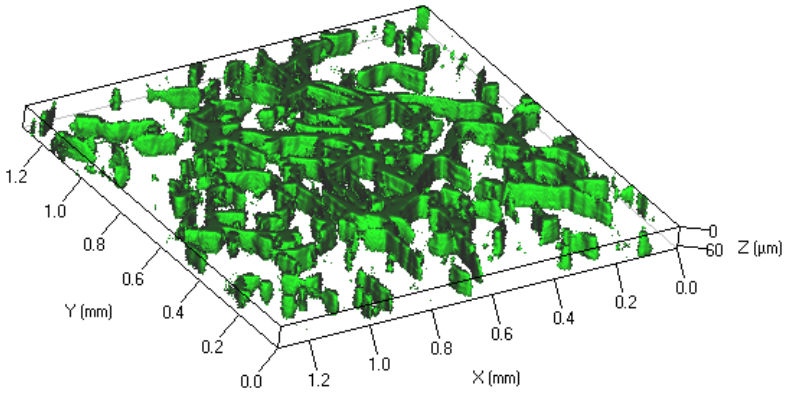

Figure 6.9: Imaging of 3D microvascular networks grown on De-cellularised Human Cadaveric Dermis (DHCD) (AT). A- Fluorescent microscopy of DHCD with AT MSC and GFP UCB ECFC derived cells co-culture B- Two-dimensional confocal microscopy image of the same sample C- Three-dimensional stack of confocal images showing maximum vessel penetration of 60µm.

A - Fluorescent microscopy (100µm scale bar)

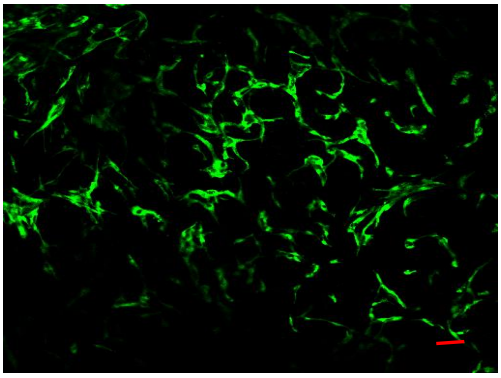

B - 2D view of 3D stack

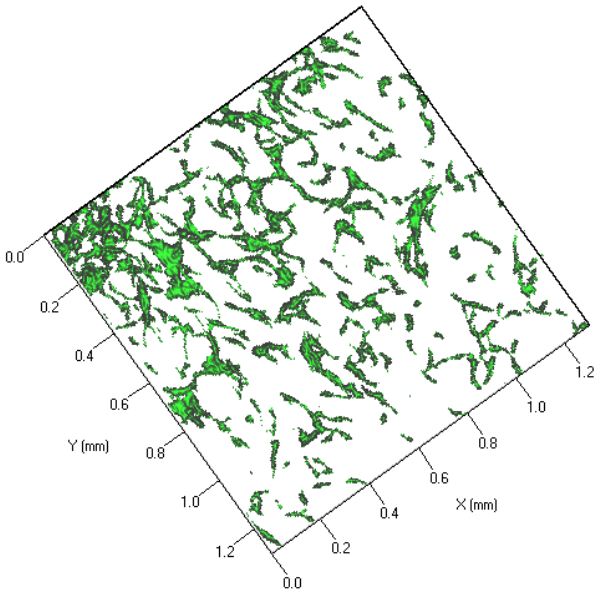

C - 3D view of stack images showing maximum depth of 60µm

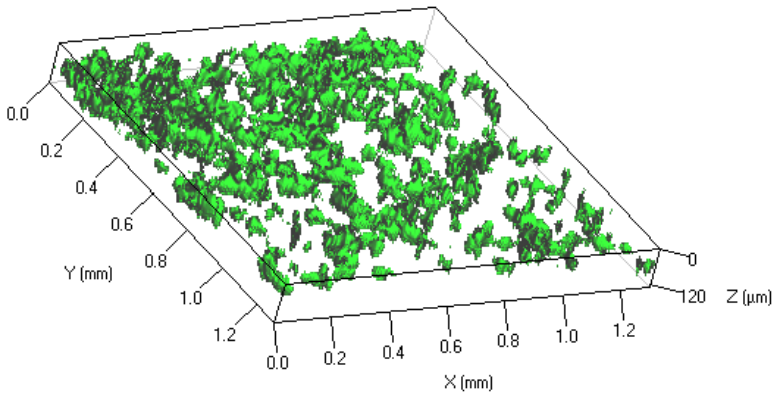

Figure 6.10: Imaging of 3D microvascular networks grown on De-cellularised Human Cadaveric Dermis (DHCD) (MV). A- Fluorescent microscopy of DHCD with MV MSC and GFP UCB ECFC derived cells co-culture B- Two-dimensional confocal microscopy image of the same sample C- Three-dimensional stack of confocal images showing maximum vessel penetration of 120µm.

Due to difficulties regarding quantification of three-dimensional confocal imaging, fluorescent microscopy of cryosectioned DHCD was performed. Up to ten 10µm sections were taken of each DHCD three-dimensional co-culture fixed with 4% (w/v) paraformaldehyde and snap frozen in liquid nitrogen (Figure 6.11). Images A and B are representative of most slices in which it is difficult to visualise the GFP ECFCs due to the DHCD auto-fluorescence. Images C and D are unique, but appear to show clearly delineated microvasculature running though the DHCD. No similar images were found in sections from the DHCD scaffold samples from any of the culture conditions outlined in Table 6.2. Unfortunately, time constraints did not allow these and other sections to be stained histochemically with anti-GFP antibodies. This may have overcome the difficulties with autofluorescence observed here.

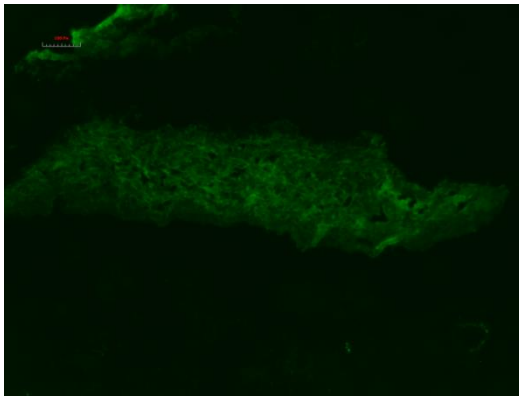

A Representative image (x4 magnification)

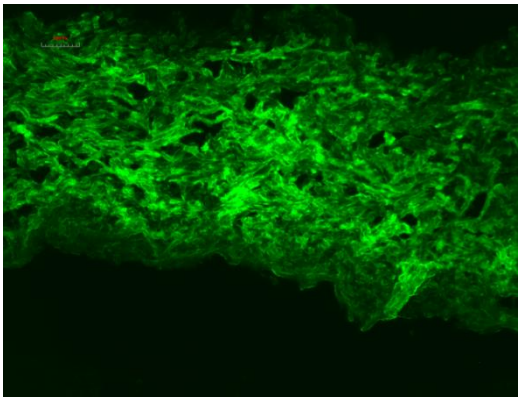

B Representative image (x10 magnification)

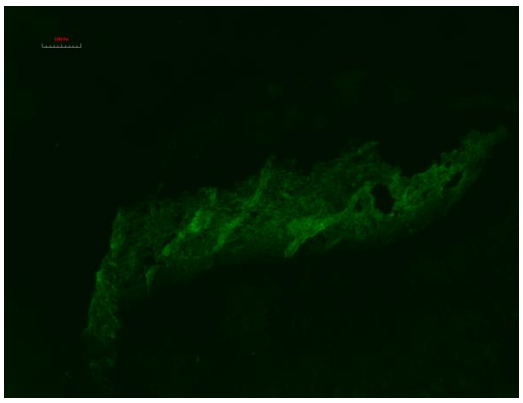

C Unique image (x4 magnification)

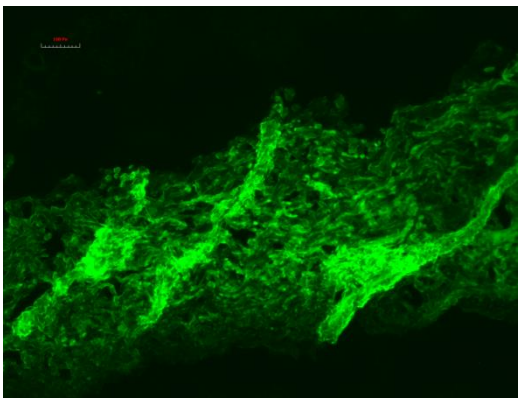

D Unique image (x10 magnification)

Figure 6.11: Microscopy of 10µm sections through De-cellularised Human Cadaveric Dermis (DHCD) co-cultured with AT MSC and GFP labelled UCB ECFC derived cells. Vascularised scaffolds were fixed with 4% (w/v) paraformaldehyde and snap frozen in liquid nitrogen. Images A and B are representative of slices in which it is difficult to visualise the GFP UCB ECFC derived cells due to DHCD auto-fluorescence. Images C and D are unique, but appear to show clearly delineated microvasculature running though the DHCD. (100µm scale bars)

6.3.4 Perfluorocarbon artificial oxygen carrier

The most promising 3D vessel formation results were obtained with 0.8mm Integra® and 2mm Matriderm® scaffolds. However the vessels did not penetrate across the scaffolds. Since the critical limiting depth of vessel penetration into the scaffolds appears to be around 100µm, it was hypothesised that this may be the limit of oxygen diffusion as proposed by previous authors (63, 184-186). It was decided to try addition of an artificial oxygen carrier perfluorocarbon compound to the culture media in order to increase the oxygen content of the media in which the scaffolds were suspended (197, 198). Before trying this in the three-dimensional cultures, two-dimensional tubule assays were set to examine the effect of different perfluorocarbon concentrations on the established vessel formation assay.

Four batches of AT MSC at a concentration of either $5x10^3$ or $1x10^4$ per well were co-cultured with $1x10^3$ UCB ECFC derived cells per well, with either low concentration perfluorocarbon supplemented EGM-2 (0.05%, 0.5mg/l (w/v)), high concentration perfluorocarbon supplemented EGM-2 (0.5%, 5mg/l (w/v)) or EGM-2 alone. Each condition was repeated in triplicate and mean values of total tubule length per well were calculated with standard error of the mean. Data were compared for perfluorocarbon and control wells in each batch (n=3) and for the mean of all four batches (n=4) using the two tailed Student's T test for paired samples. Table 6.3 shows a consistently significant increase in tubule formation with the lower concentration of AT MSCs, with a mean increase of 70.9% in total tubule length with low concentration perfluorocarbon compared with control across all four batches (p=0.0364). There was also a mean increase of 49.8% in total tubule length with high concentration perfluorocarbon compared with control across all four batches but this did not reach statistical significance (p=0.1831). Figure 6.12 shows a graphical representation of the mean total tubule lengths with low and high concentration perfluorocarbon versus control wells for all four batches.

Since data from the AT1 batch showed a lesser effect than batches 2-4, additional analysis was performed with batch AT1 excluded. This resulted in an overall increase in total tubule length of 80.9% with the addition of low concentration PFC ($p<0.0001$), and an increase of 70.4% with high concentration PFC ($p<0.0001$), both of which were statistically significant.

Table 6.3: Effect of perfluorocarbon on mean total tubule length in $5x10^3$ AT MSC with $1x10^3$ UCB ECFC co-culture.

$5x10^3$ AT MSC with $1x10^3$ UCB ECFC co-culture					
	AT 1 (n=9)	**AT 2 (n=9)**	**AT 3 (n=9)**	**AT 4 (n=9)**	**For all samples (n=4)**
Mean total tubule length of control ± SEM	16866 ± 1653	27507 ± 1850	12079 ± 3070	17132 ± 2005	18396 ± 3251
Mean total tubule length with low concentration (0.05%) perfluorocarbon ± SEM	23120 ± 4039	37599 ± 1688	35186 ± 1827	29824 ± 2488	31433 ± 3212
Difference in means of control vs. low concentration (0.05%) perfluorocarbon (Value, per cent)	6254 37.1% increase	10092 36.7% increase	23107 191.3% increase	12692 42.6% increase	13037 70.9% increase
Significance (Two tailed Student's T Test for paired samples)	0.3083	0.0012	0.0001	0.0061	0.0364
Mean total tubule length with high concentration (0.5%) perfluorocarbon ± SEM	13534 ± 2724	35394 ±1845	34671 ± 1722	26606 ± 1983	27551 ± 5079
Difference in means of control vs. high concentration (0.5%) perfluorocarbon (Value, per cent)	3332 19.8% decrease	7887 28.7% increase	22592 187.0% increase	9474 55.3% increase	9155 49.8% increase
Significance (Two tailed Student's T Test for paired samples)	0.3332	0.0068	0.0001	0.0026	0.1831

Effect of low (0.05%) and high (0.5%) concentration perfluorocarbon added to two-dimensional tubule assay media with co-culture of $5x10^3$ AT MSC and $1x10^3$ UCB ECFC . Values are mean total tubule length in microns +/- SEM and significant p values from the two tailed Student's T test for paired samples are shown in red.

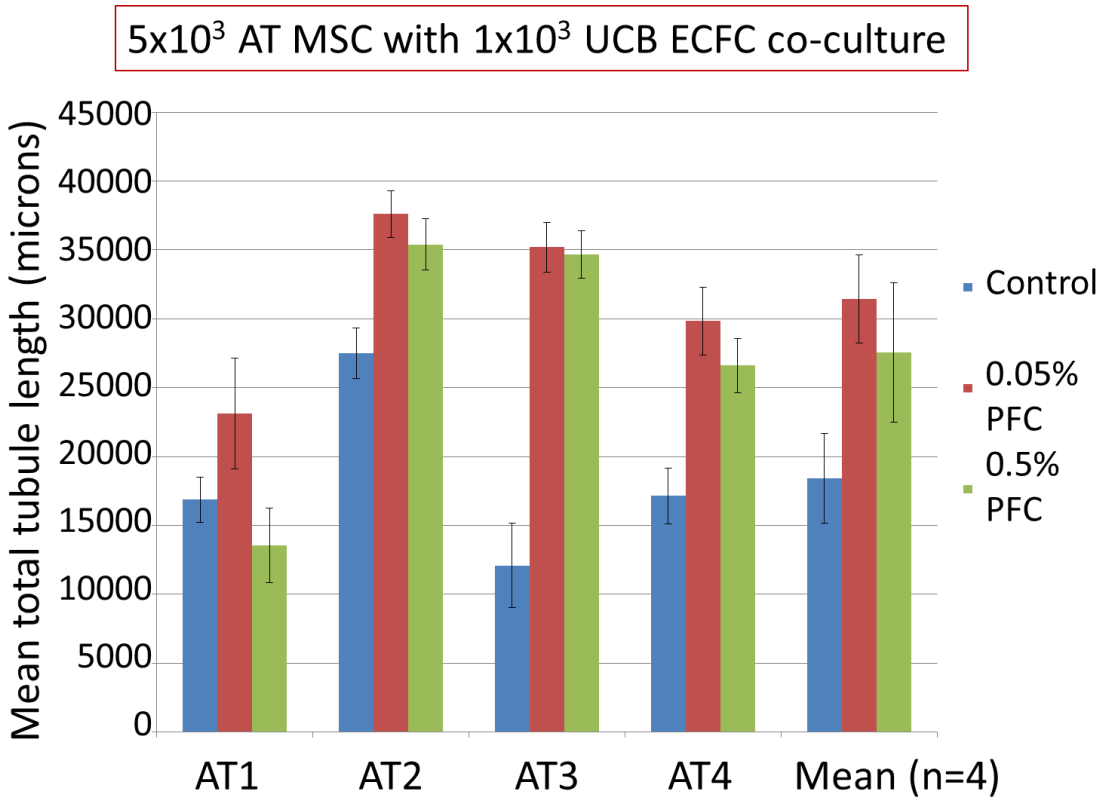

Figure 6.12: Effect of low and high concentration perfluorocarbon added to two-dimensional tubule assay media with co-culture of $5x10^3$ AT MSC and $1x10^3$ UCB ECFC derived cells. Values are mean total tubule length in microns. Error bars show Standard Error of the Mean (SEM). Within each individual AT sample n=9, with triplicate imaging of triplicate samples to ensure inter-sample consistency. The final paired columns show the mean values across the four individual samples with n=4 to ensure intra-sample consistency.

When the concentration of AT MSCs in co-culture was increased to $1x10^4$ per well, there was a lesser mean increase in total tubule length which again only reached statistical significance with the lower concentration perfluorocarbon (Table 6.4). There was a mean increase of 52.0% in total tubule length across all four batches with low concentration perfluorocarbon ($p=0.0405$), and a 25.5% mean increase across all four batches with high concentration perfluorocarbon ($p=0.0638$). Figure 6.13 highlights the clear influence of the AT1 batch wells on the mean total tubule length significance. Additional analysis was again performed with batch AT1 excluded. This resulted in an overall increase in total tubule length of 58.0% with the addition of low concentration PFC ($p<0.0001$), and an increase of 30.1% with high concentration PFC ($p=0.0004$), both of which were statistically significant.

Table 6.4: Effect of perfluorocarbon on mean total tubule length in $1x10^4$ AT MSC with $1x10^3$ UCB ECFC co-culture.

$1x10^4$ AT MSC with $1x10^3$ UCB ECFC co-culture					
	AT 1 (n=9)	**AT 2 (n=9)**	**AT 3 (n=9)**	**AT 4 (n=9)**	**For all samples (n=4)**
Mean total tubule length of control ± SEM	11086 ± 1440	25178 ± 1210	16081 ± 1009	14255 ± 1314	16650 ± 3024
Mean total tubule length with low concentration (0.05%) perfluorocarbon ± SEM	13534 ± 1573	31976 ± 1898	29138 ± 2348	26606 ± 1983	25313 ± 4077
Difference in means of control vs. low concentration (0.05%) perfluorocarbon (Value, per cent)	2448 22.1% increase	6798 27.0% increase	13057 81.2% increase	12351 86.6% increase	8663 52.0% increase
Significance (Two tailed Student's T Test for paired samples)	0.1863	0.0082	0.0006	0.0005	0.0405
Mean total tubule length with high concentration (0.5%) perfluorocarbon ± SEM	13429 ± 2156	27637 ± 1631	24669 ± 1803	17825 ± 1449	20890 ± 3226
Difference in means of control vs. high concentration (0.5%) perfluorocarbon (Value, per cent)	3332 19.8% decrease	7887 28.7% increase	22592 187.0% increase	9474 55.3% increase	4240 25.5% increase
Significance (Two tailed Student's T Test for paired samples)	0.5948	0.3391	0.0024	0.0191	0.0638

Effect of low (0.05%) and high (0.5%) concentration perfluorocarbon added to two-dimensional tubule assay media with co-culture of $1x10^4$ AT MSC and $1x10^3$ UCB ECFC . Values are mean total tubule length in microns +/- SEM and significant p values from the two tailed Student's T test for paired samples are shown in red.

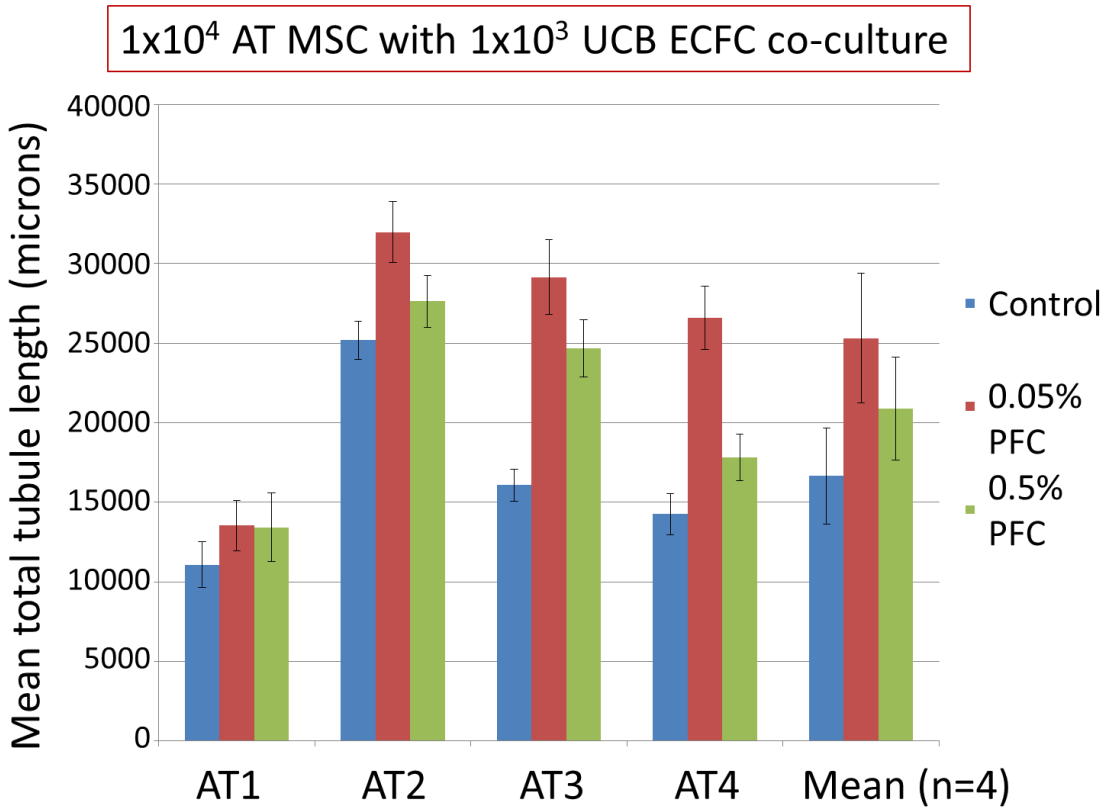

Figure 6.13: Effect of low and high concentration perfluorocarbon added to two-dimensional tubule assay media with co-culture of $1x10^4$ AT MSC and $1x10^3$ UCB ECFC. Values are mean total tubule length in microns. Error bars show Standard Error of the Mean (SEM). Within each individual AT sample n=9, with triplicate imaging of triplicate samples to ensure inter-sample consistency. The final paired columns show the mean values across the four individual samples with n=4 to ensure intra-sample consistency.

The effect of perfluorocarbon on MV MSC two-dimensional co-cultures was also tested. Four batches of MV MSC at a concentration of either $5x10^3$ or $1x10^4$ per well were co-cultured with $1x10^3$ UCB ECFC derived cells per well, with either low concentration perfluorocarbon supplemented EGM-2, high concentration perfluorocarbon supplemented EGM-2 or EGM-2 alone. Each condition was repeated in triplicate and mean values of total tubule length per well were calculated with standard error of the mean. Data were compared for perfluorocarbon and control wells in each batch (n=3) and for the mean of all four batches (n=4) using the two tailed Student's T test for paired samples. Perfluorocarbon addition increased mean total tubule length in all conditions, but less markedly than AT MSC co-cultures. Table 6.5 shows an overall increase in tubule formation with the lower concentration

of MV MSCs, with statistically significant mean increases of 35.0% in total tubule length with low concentration perfluorocarbon compared with control across all four batches ($p<0.0001$) and 12.3% in total tubule length with high concentration perfluorocarbon compared with control across all four batches ($p=0.0060$). Figure 6.14 shows a graphical representation of the mean total tubule lengths with low and high concentration perfluorocarbon versus control wells and shows the intra-sample inconsistency responsible for the lack of statistical significance.

Table 6.5: Effect of perfluorocarbon on mean total tubule length in $5x10^3$ MV MSC with $1x10^3$ UCB ECFC co-culture.

$5x10^3$ MV MSC with $1x10^3$ UCB ECFC co-culture					
	MV 1 (n=9)	**MV 2 (n=9)**	**MV 3 (n=9)**	**MV 4 (n=9)**	**For all samples (n=4)**
Mean total tubule length of control ± SEM	27322 ± 1489	20595 ± 1945	21465 ± 983	28749 ± 1705	24533 ± 2051
Mean total tubule length with low concentration (0.05%) perfluorocarbon ± SEM	35255 ± 2593	36684 ± 1879	20672 ± 976	39888 ± 1824	33125 ± 4262
Difference in means of control vs. low concentration (0.05%) perfluorocarbon (Value, per cent)	7933 29.0% increase	16089 78.1% increase	793 3.7% decrease	11139 38.7% increase	8592 35.0% increase
Significance (Two tailed Student's T Test for paired samples)	0.0480	0.0036	0.5678	0.0002	<0.0001
Mean total tubule length with high concentration (0.5%) perfluorocarbon ± SEM	24546 ± 1566	31398 ± 3421	14236 ± 1149	40012 ± 1634	27548 ± 5450
Difference in means of control vs. high concentration (0.5%) perfluorocarbon (Value, per cent)	2776 10.2% decrease	10803 52.5% increase	7229 33.7% decrease	11263 39.2% increase	3015 12.3% increase
Significance (Two tailed Student's T Test for paired samples)	0.0010	0.0765	0.0010	0.0039	0.0060

Effect of low (0.05%) and high (0.5%) concentration perfluorocarbon added to two-dimensional tubule assay media with co-culture of $5x10^3$ MV MSC and $1x10^3$ UCB ECFC. Values are mean total tubule length in microns +/- SEM and significant p values from the two tailed Student's T test for paired samples are shown in red.

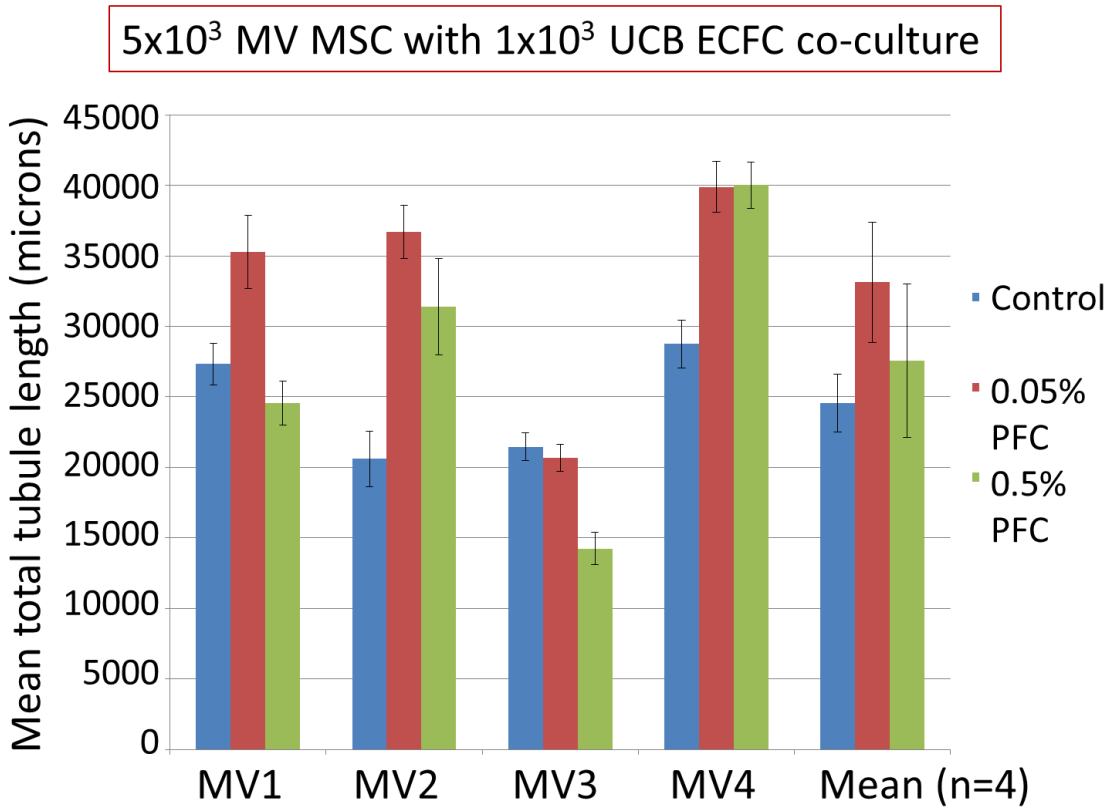

Figure 6.14: Effect of low and high concentration perfluorocarbon added to two-dimensional tubule assay media with co-culture of $5x10^3$ MV MSC and $1x10^3$ UCB ECFC. Values are mean total tubule length in microns. Error bars show Standard Error of the Mean (SEM). Within each individual MV sample n=9, with triplicate imaging of triplicate samples to ensure inter-sample consistency. The final paired columns show the mean values across the four individual samples with n=4 to ensure intra-sample consistency.

When the concentration of MV MSCs in co-culture was increased to $1x10^4$ per well there was a lesser mean increase in total tubule length, as seen with the AT MSC samples (Table 6.6). A mean increase of 32.2% in total tubule length across all four batches with low concentration perfluorocarbon reached statistical significance (p=0.0015), but the 15.1% mean increase across all four batches with high concentration perfluorocarbon (p=0.0556) did not. Figure 6.15 highlights the variability between batches.

Table 6.6: Effect of perfluorocarbon on mean total tubule length in $1x10^4$ MV MSC with $1x10^3$ UCB ECFC co-culture.

$1x10^4$ MV MSC with $1x10^3$ UCB ECFC co-culture					
	MV 10 (n=9)	**MV 11 (n=9)**	**MV 12 (n=9)**	**MV 13 (n=9)**	**For all samples (n=4)**
Mean total tubule length of control ± SEM	19559 ± 1373	25096 ± 1742	12843 ± 1130	17951 ± 2586	18862 ± 2523
Mean total tubule length with low concentration (0.05%) perfluorocarbon ± SEM	24546 ± 1918	31976 ± 1898	13442 ± 590	29744 ± 1866	24927 ± 4133
Difference in means of control vs. low concentration (0.05%) perfluorocarbon (Value, per cent)	7933 29.0% increase	6880 27.4% increase	599 4.7% increase	12093 67.4% increase	6065 32.2% increase
Significance (Two tailed T Test for unpaired samples)	0.0890	0.5724	0.5133	0.0107	0.0015
Mean total tubule length with high concentration (0.5%) perfluorocarbon ± SEM	22996 ± 1413	31725 ± 1540	12265 ± 1635	19888 ± 2322	21719 ± 4026
Difference in means of control vs. high concentration (0.5%) perfluorocarbon (Value, per cent)	3437 17.6% increase	6629 26.4% increase	578 4.5% decrease	1937 10.8% increase	2857 15.1% increase
Significance (Two tailed T Test for unpaired samples)	0.1235	0.1305	0.6983	0.3065	0.0556

Effect of low (0.05%) and high (0.5%) concentration perfluorocarbon added to two-dimensional tubule assay media with co-culture of $1x10^4$ MV MSC and $1x10^3$ UCB ECFC. Values are mean total tubule length in microns +/- SEM and significant p values from the two tailed T test for unpaired samples are shown in red.

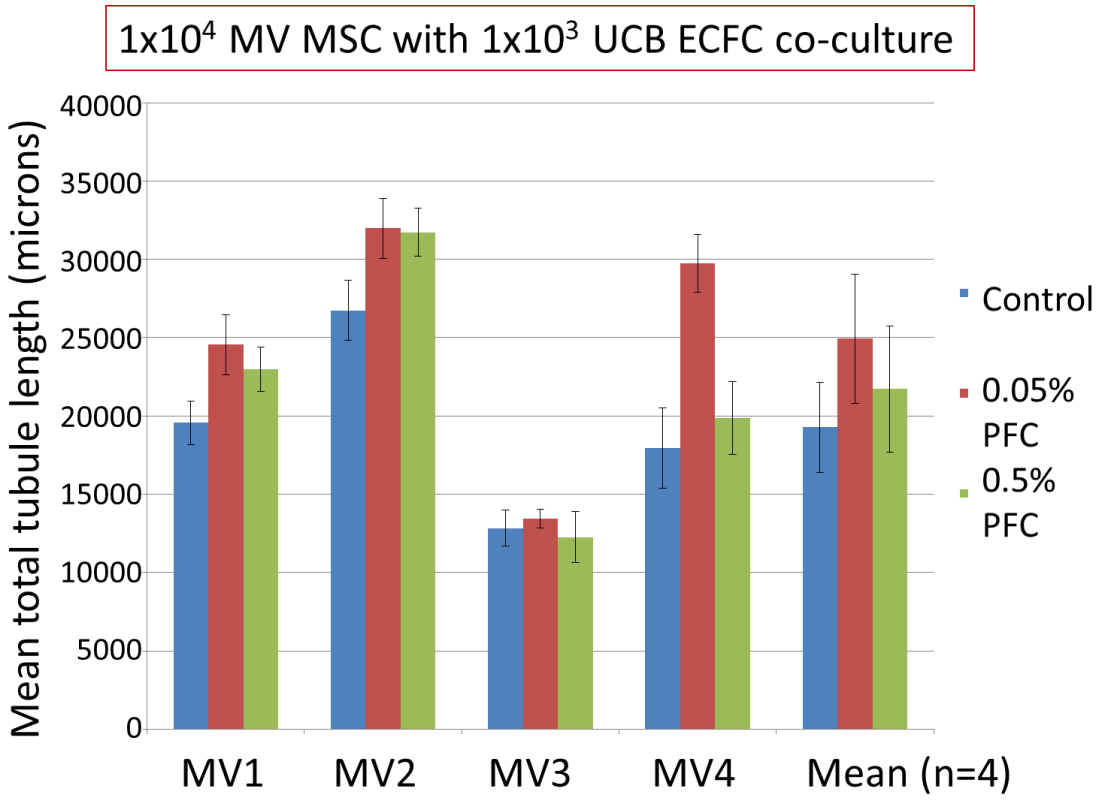

Figure 6.15: Effect of low and high concentration perfluorocarbon added to two-dimensional tubule assay media with co-culture of $1x10^4$ MV MSC and $1x10^3$ UCB ECFC. Values are mean total tubule length in microns. Error bars show Standard Error of the Mean (SEM). Within each individual MV sample n=9, with triplicate imaging of triplicate samples to ensure inter-sample consistency. The final paired columns show the mean values across the four individual samples with n=4 to ensure intra-sample consistency.

When the mean total tubule length for all four batches of AT and MV MSC in the perfluorocarbon assay was normalised against the values for the relative control cultures transformed to equal zero, there was a clear trend in the effect of the perfluorocarbon concentration on the extent of increased tubule formation (Figure 6.16). In both AT and MV assays, there was a significantly greater increase in tubule formation in the $1x10^4$ MSC cultures with 0.05% perfluorocarbon compared with 0.5% perfluorocarbon (Two-tailed Student's T Test for paired samples, AT p=0.003, MV p=0.029). This comparison was not significant at the $5x10^3$ MSC concentrations with either AT or MV MSCs, but the graph supports the trend and so 0.05% would be the preferred concentration of perfluorocarbon utilised in future co-culture applications. It also seems that perfluorocarbon has a greater effect with lower cell densities.

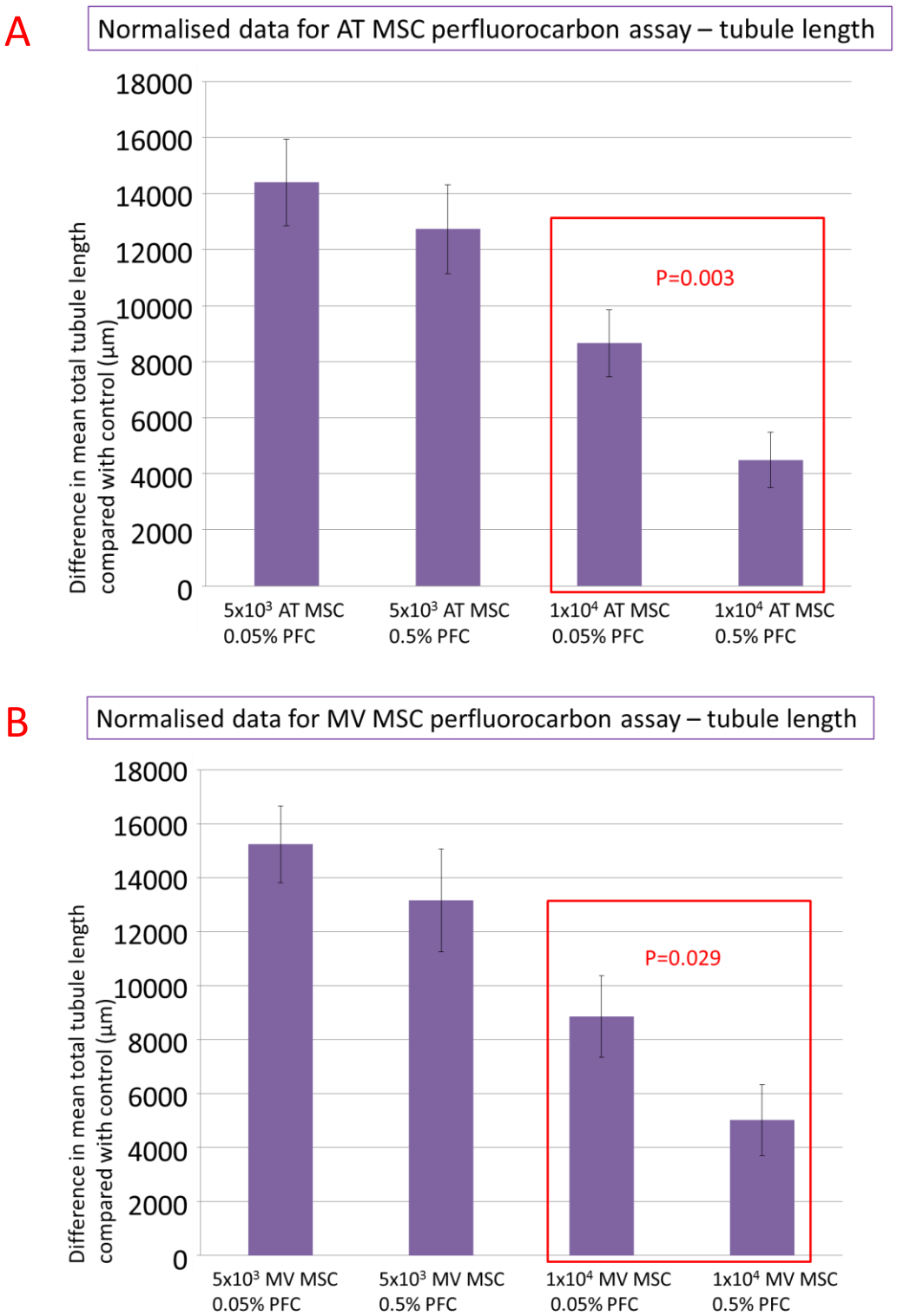

Figure 6.16: Normalised data for total tubule length in AT and MV MSC and UCB ECFC derived cell perfluorocarbon assays. Mean total tubule length is consistently increased with the addition of perfluorocarbon to co-cultures compared with equivalent controls. Charts A and B show the difference in mean total tubule length in co-cultures with UCB ECFC derived cells and either AT or MV MSCs, with $5x10^3$ and $1x10^4$ MSC concentrations and either 0.05% or 0.5% perfluorocarbon, normalised against control values for corresponding cell concentrations without the addition of perfluorocarbon. The data show that there is a variable increase in tubule length with the addition of perfluorocarbon at low or high concentration with both MSC concentrations, and that this is consistent with both AT and MV derived MSCs. In both AT and MV assays there was a significantly greater increase in tubule formation in the $1x10^4$ MSC cultures with 0.05% perfluorocarbon compared with 0.5% perfluorocarbon (Two-tailed Student's T Test for paired samples, AT p=0.003, MV p=0.029). This comparison was not significant at the $5x10^3$ MSC concentrations, but the graph supports the trend. Error bars show SEM.

Statistical analysis was also performed on the number of tubule junctions in the assay under the same conditions. Tubule junction data were again compared for perfluorocarbon and control wells in each batch (n=3) and for the mean of all four batches (n=4) using the two tailed Student's T test for paired samples. Table 6.7 shows a consistently significant increase in the number of tubule junctions with the lower concentration of AT MSCs, with a mean increase of 196.9% in the number of junctions with low concentration perfluorocarbon compared with control across all four batches ($p<0.0001$) and a mean increase of 183.6% in the number of junctions with high concentration perfluorocarbon compared with control across all four batches ($p<0.0001$). Figure 6.17 shows a graphical representation of the mean number of tubule junctions with low and high concentration perfluorocarbon versus control wells and shows clear intra-sample consistency.

Table 6.7: Effect of perfluorocarbon on mean number of tubule junctions in $5x10^3$ AT MSC with $1x10^3$ UCB ECFC co-culture.

$5x10^3$ AT MSC with $1x10^3$ UCB ECFC co-culture					
	AT 1 (n=9)	**AT 2 (n=9)**	**AT 3 (n=9)**	**AT 4 (n=9)**	**For all samples (n=4)**
Mean number of tubule junctions of control ± SEM	118.2 ± 22.2	248.3 ± 26.1	85.3 ± 28.5	115.3 ± 28.3	141.8 ± 16.5
Mean number of tubule junctions with low concentration (0.05%) perfluorocarbon ± SEM	269.7 ± 63.1	578.2 ± 51.6	412.4 ± 38.2	322. 7 ± 48.4	421.0 ± 31.6
Difference in means of control vs. low concentration (0.05%) perfluorocarbon (Value, per cent)	151.5 128.2% increase	329.9 132.9% increase	327.1 383.5% increase	207.4 179.9% increase	279.2 196.9% increase
Significance (Two tailed Student's T Test for paired samples)	0.1269	0.0003	<0.0001	0.0071	<0.0001
Mean number of tubule junctions with high concentration (0.5%) perfluorocarbon ± SEM	295 ± 68.5	527.2 ± 56.5	421. 7 ± 44.1	293.3 ± 32.9	402.2 ± 29.6
Difference in means of control vs. high concentration (0.5%) perfluorocarbon (Value, per cent)	176.8 149.6% increase	278.9 112.3% increase	336.4 394.4% increase	178 154.4% increase	260.4 183.6% increase
Significance (Two tailed Student's T Test for paired samples)	0.1101	0.0008	0.0004	0.0008	<0.0001

Effect of low (0.05%) and high (0.5%) concentration perfluorocarbon added to two-dimensional tubule assay media with co-culture of $5x10^3$ AT MSC and $1x10^3$ UCB ECFC . Values are mean number of tubule junctions +/- SEM and significant p values from the two tailed Student's T test for paired samples are shown in red.

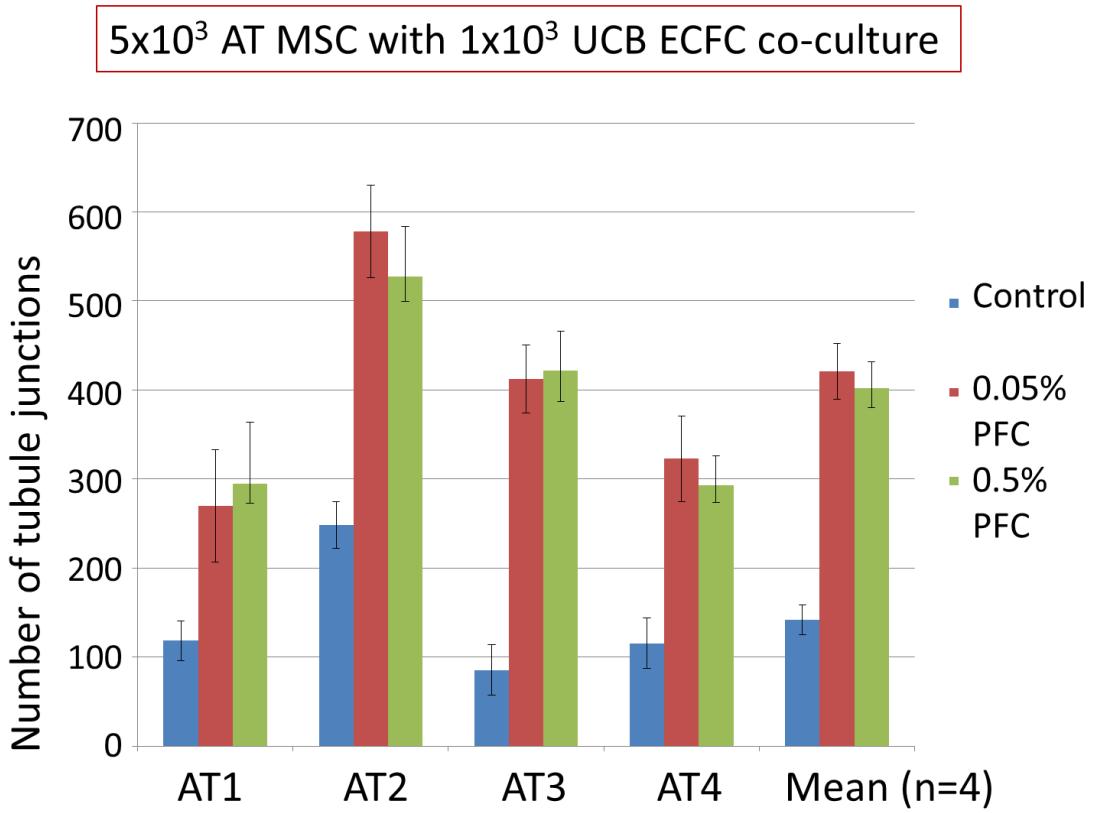

Figure 6.17: Effect of low and high concentration perfluorocarbon added to two-dimensional tubule assay media with co-culture of $5x10^3$ AT MSC and $1x10^3$ UCB ECFC derived cells. Values are mean number of tubule junctions. Error bars show Standard Error of the Mean (SEM). Within each individual AT sample n=9, with triplicate imaging of triplicate samples to ensure inter-sample consistency. The final paired columns show the mean values across the four individual samples with n=4 to ensure intra-sample consistency.

When the concentration of AT MSCs in co-culture was increased to $1x10^4$ per well there was a lesser mean increase in number of tubule junctions, but this was still statistically significant (Table 6.8). There was a mean increase of 101.8% in the number of tubule junctions across all four batches with low concentration perfluorocarbon ($p<0.0001$), and a mean increase of 76.6% across all four batches with high concentration perfluorocarbon ($p<0.0001$). Figure 6.18 highlights the greater variability between batches; however, statistical significance has been maintained. The effect of inter-sample variability on mean number of tubule junctions is less marked than the effect on mean total tubule length (Table 6.4).

Table 6.8: Effect of perfluorocarbon on mean number of tubule junctions in $1x10^4$ AT MSC with $1x10^3$ UCB ECFC co-culture.

$1x10^4$ AT MSC with $1x10^3$ UCB ECFC co-culture					
	AT 1 (n=9)	**AT 2 (n=9)**	**AT 3 (n=9)**	**AT 4 (n=9)**	**For all samples (n=4)**
Mean number of tubule junctions of control ± SEM	59.4 ± 14.2	235.9 ± 19.8	103.6 ± 7.3	95.6 ± 14.1	123.6 ± 13.3
Mean number of tubule junctions with low concentration (0.05%) perfluorocarbon ± SEM	121.8 ± 19.2	379.9 ± 40.1	290.8 ± 36.5	205.3 ± 32.3	249.4 ± 22.6
Difference in means of control vs. low concentration (0.05%) perfluorocarbon (Value, per cent)	62.4 105.1% increase	144 61.0% increase	187.2 180.7% increase	109.7 114.7% increase	125.8 101.8% increase
Significance (Two tailed Student's T Test for paired samples)	0.0257	0.0111	0.0007	0.0091	<0.0001
Mean number of tubule junctions with high concentration (0.5%) perfluorocarbon ± SEM	106 ± 21.9	338.4 ± 27.3	224.7 ± 34.7	140.8 ± 19.3	218.3 ± 21.6
Difference in means of control vs. high concentration (0.5%) perfluorocarbon (Value, per cent)	46.6 78.5% increase	102.5 43.5% increase	121.1 116.9% increase	45.2 47.3% increase	94.7 76.6% increase
Significance (Two tailed Student's T Test for paired samples)	0.3271	0.0231	0.0058	0.0152	<0.0001

Effect of low (0.05%) and high (0.5%) concentration perfluorocarbon added to two-dimensional tubule assay media with co-culture of $1x10^4$ AT MSC and $1x10^3$ UCB ECFC . Values are mean number of tubule junctions +/- SEM and significant p values from the two tailed Student's T test for paired samples are shown in red.

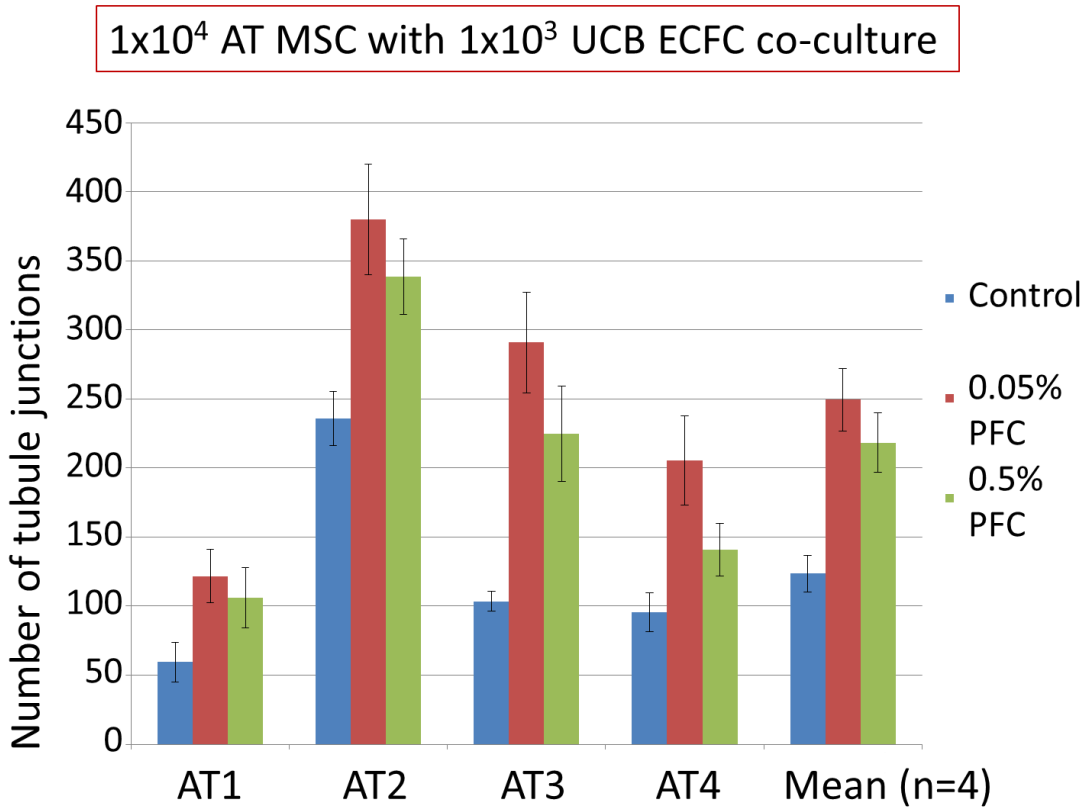

Figure 6.18: Effect of low and high concentration perfluorocarbon added to two-dimensional tubule assay media with co-culture of $1x10^4$ AT MSC and $1x10^3$ UCB ECFC. Values are mean number of tubule junctions. Error bars show Standard Error of the Mean (SEM). Within each individual AT sample n=9, with triplicate imaging of triplicate samples to ensure inter-sample consistency. The final paired columns show the mean values across the four individual samples with n=4 to ensure intra-sample consistency.

The effect of perfluorocarbon on number of tubule junctions in the MV MSC two-dimensional co-cultures was also analysed from the previously described assay. Data were compared for perfluorocarbon and control wells in each batch (n=3) and for the mean of all four batches (n=4) using the two tailed Student's T test for paired samples. Perfluorocarbon addition increased mean number of tubule junctions in all conditions, but less markedly than AT MSC co-cultures. Table 6.9 shows an overall increase in tubule junctions with the lower concentration of MV MSCs, with a mean increase of 105.0% in number of tubule junctions with low concentration perfluorocarbon compared with control across all four batches ($p<0.0001$) and a mean increase of 85.4% in total tubule length with high concentration perfluorocarbon compared with control across all four batches ($p<0.0001$). These results are statistically

significant, unlike the results for increased mean total tubule length for these conditions. Figure 6.19 shows a graphical representation of the mean number of tubule junctions with low and high concentration perfluorocarbon versus control wells and highlights the single batch which did not achieve a significant increase in number of tubule junctions. This had little effect on the overall data as the other samples had large, consistent increases in tubule junctions.

Table 6.9: Effect of perfluorocarbon on mean number of tubule junctions in $5x10^3$ MV MSC with $1x10^3$ UCB ECFC co-culture.

$5x10^3$ MV MSC with $1x10^3$ UCB ECFC co-culture					
	MV 1 (n=9)	**MV 2 (n=9)**	**MV 3 (n=9)**	**MV 4 (n=9)**	**For all samples (n=4)**
Mean number of tubule junctions of control ± SEM	300.8 ± 26.9	385.6 ± 63.5	187.4 ± 18.6	293.0 ± 24.4	291.7 ± 21.6
Mean number of tubule junctions with low concentration (0.05%) perfluorocarbon ± SEM	522.6 ± 72.1	1053.2 ± 68.5	317.1 ± 47.9	651.2 ± 38.5	598.1 ± 51.7
Difference in means of control vs. low concentration (0.05%) perfluorocarbon (Value, per cent)	221.8 73.7% increase	667.6 173.1% increase	129.7 69.2% increase	358.2 122.3% increase	306.4 105.0% increase
Significance (Two tailed Student's T Test for paired samples)	0.0320	0.0022	0.0282	<0.0001	<0.0001
Mean number of tubule junctions with high concentration (0.5%) perfluorocarbon ± SEM	600.8 ± 45.2	870.5 ± 145.3	180.3 ± 17.6	621.9 ± 45.2	540.9 ± 52.1
Difference in means of control vs. high concentration (0.5%) perfluorocarbon (Value, per cent)	300 99.7% increase	484.9 125.8% increase	7.1 3.8% decrease	328.9 112.3% increase	249.2 85.4% increase
Significance (Two tailed Student's T Test for paired samples)	0.0003	0.0678	0.7573	0.0006	<0.0001

Effect of low (0.05%) and high (0.5%) concentration perfluorocarbon added to two-dimensional tubule assay media with co-culture of $5x10^3$ MV MSC and $1x10^3$ UCB ECFC. Values are mean number of tubule junctions +/- SEM and significant p values from the two tailed Student's T test for paired samples are shown in red.

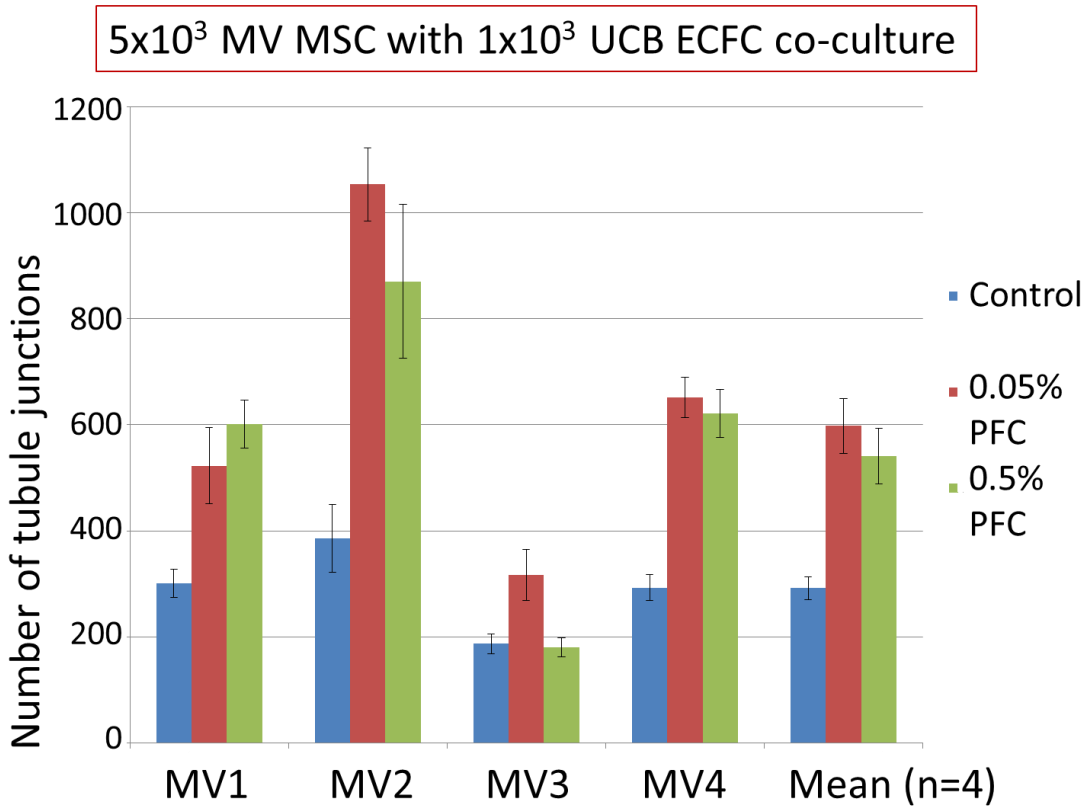

Figure 6.19: Effect of low and high concentration perfluorocarbon added to two-dimensional tubule assay media with co-culture of $5x10^3$ MV MSC and $1x10^3$ UCB ECFC. Values are mean number of tubule junctions. Error bars show Standard Error of the Mean (SEM). Within each individual MV sample n=9, with triplicate imaging of triplicate samples to ensure inter-sample consistency. The final paired columns show the mean values across the four individual samples with n=4 to ensure intra-sample consistency.

When the concentration of MV MSCs in co-culture was increased to $1x10^4$ per well there was a greater mean increase in number of tubule junctions with the addition of perfluorocarbon, which was statistically significant (Table 6.10). There was a mean increase of 110.8% in number of tubule junctions across all four batches with low concentration perfluorocarbon (p=0.0010), and a mean increase of 124.6% across all four batches with high concentration perfluorocarbon (p=0.0001). Figure 6.20 highlights the variability of the effect of perfluorocarbon between batches which still led to significant overall increased mean number of tubule junctions due to size of the effect.

Table 6.10: Effect of perfluorocarbon on mean number of tubule junctions in $1x10^4$ MV MSC with $1x10^3$ UCB ECFC co-culture.

$1x10^4$ MV MSC with $1x10^3$ UCB ECFC co-culture					
	MV 1 (n=9)	**MV 2 (n=9)**	**MV 3 (n=9)**	**MV 4 (n=9)**	**For all samples (n=4)**
Mean number of tubule junctions of control ± SEM	178.6 ± 25.3	356.7 ± 38.5	71.0 ± 9.6	140.0 ± 33.5	152.5 ± 19.6
Mean number of tubule junctions with low concentration (0.05%) perfluorocarbon ± SEM	281.8 ± 31.3	386.7 ± 45.7	149.8 ± 21.0	397.1 ± 46.2	321.5 ± 26.8
Difference in means of control vs. low concentration (0.05%) perfluorocarbon (Value, per cent)	103.2 57.8% increase	30.0 8.4% increase	78.8 111.0% increase	257.1 183.6% increase	169 110.8% increase
Significance (Two tailed Student's T Test for paired samples)	0.0432	0.2747	0.0102	0.0034	0.0010
Mean number of tubule junctions with high concentration (0.5%) perfluorocarbon ± SEM	295.3 ± 36.4	663.6 ± 51.5	156.7 ± 49.8	210.7 ± 31.6	342.5 ± 41.9
Difference in means of control vs. high concentration (0.5%) perfluorocarbon (Value, per cent)	116.7 65.3% increase	306.9 86.0% increase	85.7 120.7% increase	70.7 50.5% increase	190 124.6% increase
Significance (Two tailed Student's T Test for paired samples)	0.0259	0.0340	0.1119	0.1306	0.0001

Effect of low (0.05%) and high (0.5%) concentration perfluorocarbon added to two-dimensional tubule assay media with co-culture of $1x10^4$ MV MSC and $1x10^3$ UCB ECFC. Values are mean number of tubule junctions +/- SEM and significant p values from the two tailed Student's T test for paired samples are shown in red.

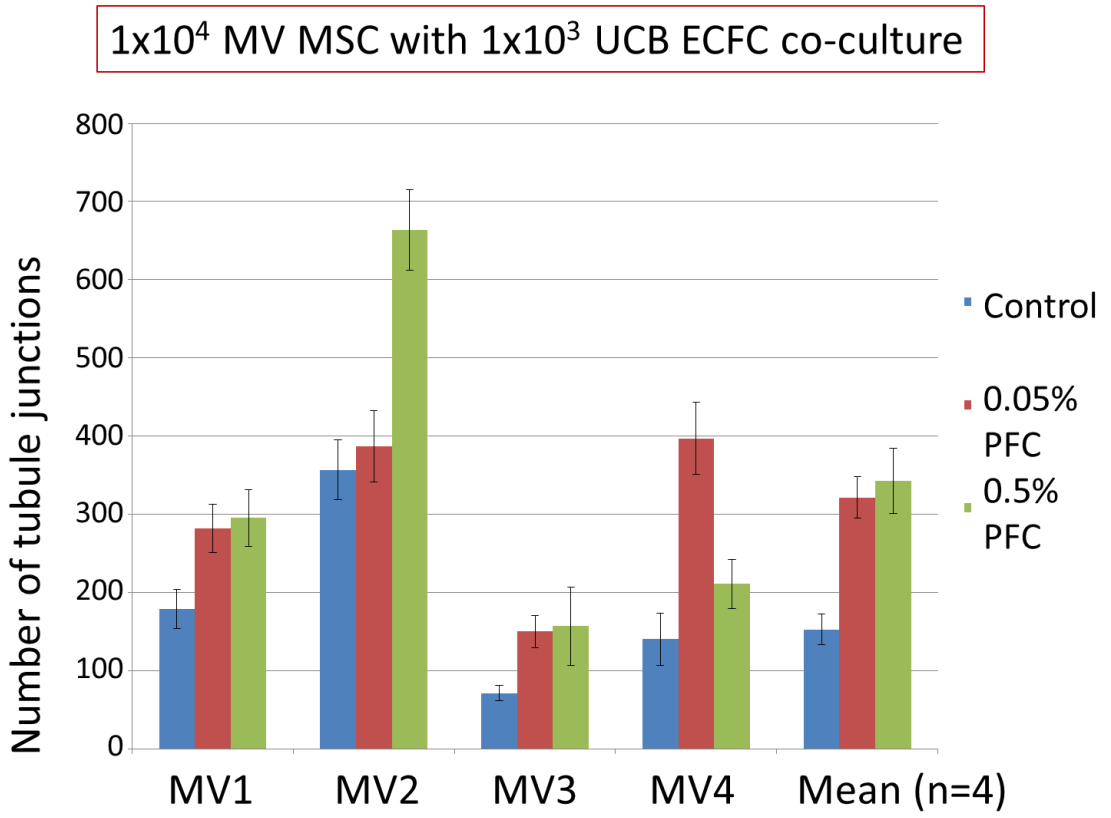

Figure 6.20: Effect of low and high concentration perfluorocarbon added to two-dimensional tubule assay media with co-culture of $1x10^4$ MV MSC and $1x10^3$ UCB ECFC. Values are mean number of tubule junctions. Error bars show Standard Error of the Mean (SEM). Within each individual MV sample n=9, with triplicate imaging of triplicate samples to ensure inter-sample consistency. The final paired columns show the mean values across the four individual samples with n=4 to ensure intra-sample consistency.

When the mean number of tubule junctions for all four batches of AT and MV MSC in the perfluorocarbon assay was normalised against the values for the relative control cultures transformed to equal zero, there was a clear trend in the effect of the perfluorocarbon concentration on the extent of increased tubule formation in the $5x10^3$ MSC concentrations with either AT or MV MSCs (Figure 6.21). This comparison was not significant with either AT or MV MSCs, but the graph supports the trend previously seen with the relative increase in total tubule length (Figure 6.16) and so 0.05% remains the preferred concentration of perfluorocarbon for utilisation in future co-culture applications.

A

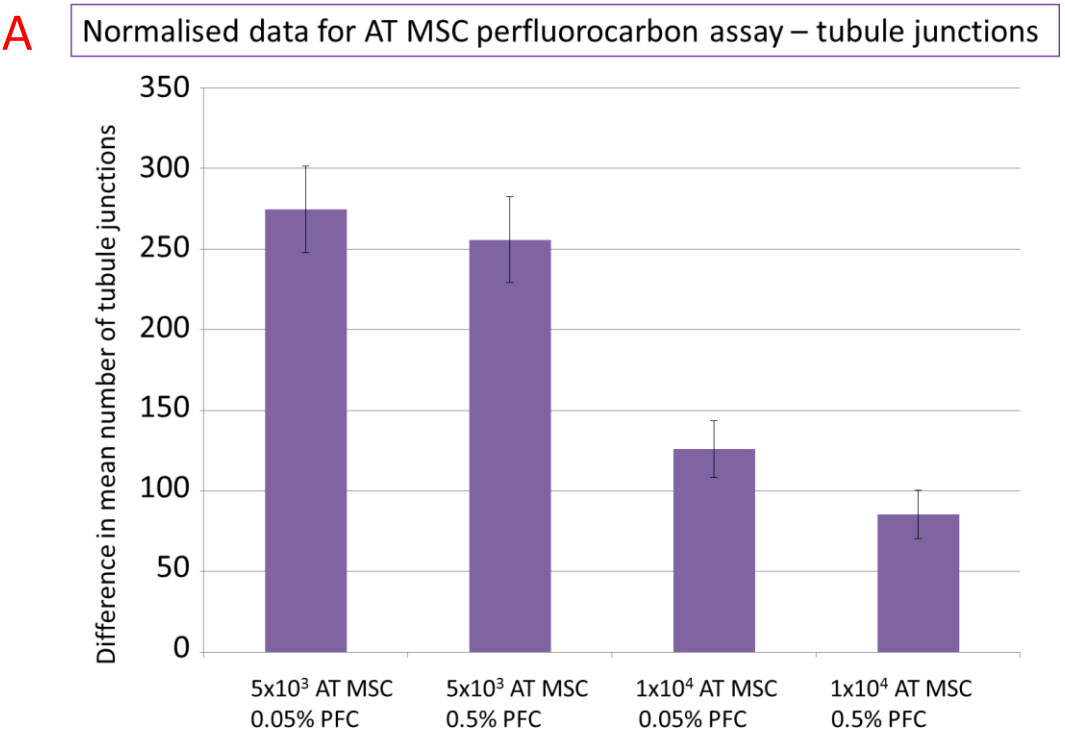

B

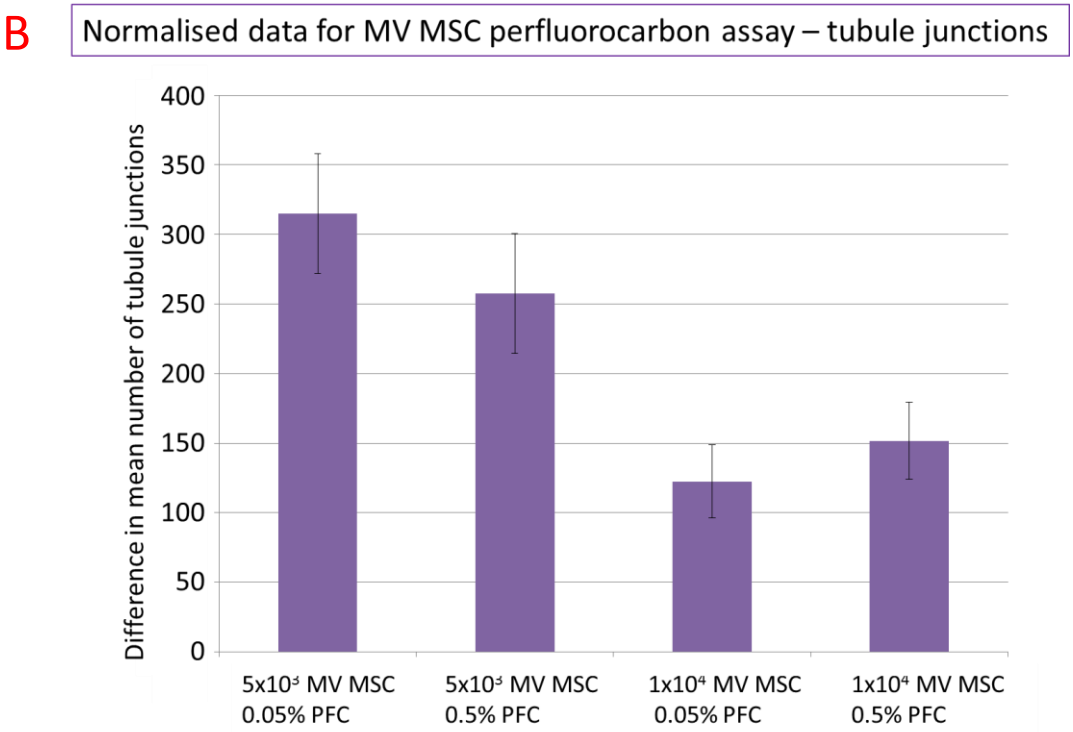

Figure 6.21: Normalised data for number of tubule junctions in AT and MV MSC and UCB ECFC derived cell perfluorocarbon assays. Mean number of tubule junctions is consistently increased with the addition of perfluorocarbon to co-cultures compared with equivalent controls. Charts A and B show the difference in mean number of tubule junctions in co-cultures with UCB ECFC derived cells and either AT or MV MSCs, with $5x10^3$ and $1x10^4$ MSC concentrations and either 0.05% or 0.5% perfluorocarbon, normalised against control values for corresponding cell concentrations without the addition of perfluorocarbon. The data show that there is a variable increase in tubule length with the addition of perfluorocarbon at low or high concentration with both MSC concentrations. In both AT and MV assays there was a greater increase in tubule formation in the $5x10^3$ MSC cultures with 0.05% perfluorocarbon compared with 0.5% perfluorocarbon but this was not statistically significant. This trend was not seen with the $1x10^4$ MSC concentrations. Error bars show SEM.

6.4 Discussion

In this chapter, GFP lentiviral transduction of endothelial cells for immunofluorescent imaging in three dimensions was described. DSRed transduction of MSCs required the addition of polybrene, but this had an adverse effect on MSC proliferation as previously described by Lin *et al.* (201) and so experiments were continued with GFP labelled UCB ECFC derived cells only.

The widely used clinical scaffolds Integra® and Matriderm® were pre-vascularised with co-cultured endothelial and mesenchymal cells, but depth of penetration was limited to 100 microns (300). Integra® is a biological construct of bovine cross-linked collagen and shark glycosaminoglycans (GAG) (151) and Matriderm® is a biological construct of bovine collagen types I, III and V, and bovine elastin fibres (156). Neither of these constructs have a structure comparable with the complexity of human dermis (42, 152), but cross-links and GAGs provide mechanical structure to the scaffolds without antigens (42), and pores of 70-200µm have been designed to allow migration of cells from the wound bed *in vivo*.

Several small clinical trials have shown an improvement in scar quality with two stage use of Integra® and split thickness skin grafts (SSG) compared with SSG alone (50-52, 154, 155). Case series of single stage Matriderm® and SSG reconstructive procedures have also shown good results with regard to scar stability, pliability and function, despite prolonged graft take (159-162), but no control trials exist to compare results with SSG alone. SSG take is clinical evidence that these scaffolds fully vascularise *in vivo,* but the clinical application proposed in this Thesis requires full thickness vascularisation *in vitro*.

Neuskin-F®, a biological construct of intact type I piscine collagen (164), was investigated as a potential alternative scaffold for pre-vascularisation because it is thinner than the Integra® and Matriderm® scaffolds, but still maintains stability in culture. No peer-reviewed literature exists on this scaffold as it is not yet in clinical use; however, Lin *et al*. have reported successful *in vitro* corneal regeneration on a similar, thin fish scale collagen scaffold (165) and Neuskin-F®

has been shown to be fully biodegradeable and biocompatible (164). Shiratsuchi *et al.* have shown that piscine elastin peptides enhance human fibroblast migration and proliferation (166), but such effects with piscine collagen have not been documented.

Neuskin-F® was capable of supporting two-dimensional vessel formation *in vitro* and may be a useful transport medium for pre-formed vasculature due to retained rigidity in culture and ease of handling. It did not allow three-dimensional penetration of vasculature *in vitro*, but the manufacturer's data sheet claims that the collagen scaffold is absorbable *in vivo*, so it may allow for both inferior and superior inosculation in a clinical model. This is most likely to be useful in chronic wound applications where there may be a lack of neovascularisation in the wound bed (64, 303). Pre-vascularised Neuskin-F® could be used as a sandwich layer between the wound bed and a split thickness skin graft to provide stimulus for improved graft take which relies upon an adequate vascular supply for inosculation and neovascularisation (37).

DHCD was chosen as a possible alternative scaffold for pre-vascularisation as it is a natural biological scaffold, devoid of cellular content (169), which retains the negative impression of the original donor vasculature (182). This may allow engineered vasculature to follow these impressions through the depth of the dermis. As well as being able to follow pre-existing donor vasculature channels within the scaffold, it was hypothesised that *in vitro* microvascular networks may also receive molecular cues as to where the endothelial and mesenchymal cells should migrate and attach (183). This hypothesis is based on work by Barnes *et al.* who used a rat model to investigate de-cellularised scaffold extra-cellular matrix components and found residual molecular surface markers with the potential to guide seeded or repopulating cells throughout the tissue (183). The de-cellularisation protocol used by NHS Blood and Transplant (Liverpool, UK), who provided the DHCD for use in this Thesis, was adapted from a technique used to de-cellularise heart valves (169). The existing literature on de-cellularised allogeneic and xenogeneic matrices for tissue engineering for heart valve replacement is well established,

and in that context the scaffolds have been shown to be capable of re-cellularisation, integration and long-term growth *in vivo* (178-181).

Despite the potential biological and structural advantages of DHCD, the observation of *in vitro* DHCD vascularisation in this Thesis suggested similar limitation to the depth of vessel penetration found with Integra® and Matriderm®. This is consistent with findings from other tissue engineering applications, which support the hypothesis of limited oxygen diffusion beyond this depth (63, 184-190). Various methods to improve oxygenation of three dimensional *in vitro* cultures have been attempted by other researchers, including fabrication of culture scaffolds with channels or pores to improve oxygen transport (191-193), incorporating proangiogenic growth factors into scaffold material to increase neovascularisation (186, 194), use of bioreactors to improve flow of fresh media (188, 189, 195, 196), and use of perfluorocarbon additives to increase the oxygen carrying capacity of the culture media (197, 198). In this Thesis, there was no scope to develop a bespoke scaffold or perfusion bioreactor and so it was decided to try addition of an artificial oxygen carrier perfluorocarbon compound to the culture media in order to increase the oxygen content of the media in which the available scaffolds were suspended. Perfluorocarbon has been shown to significantly increase the oxygen uptake rate of hepatocytes in three dimensional *in vitro* culture (197) and to improve epithelial metabolism and partial tissue oxygen tension in a tissue engineered tracheal construct (198).

In this Thesis, two-dimensional co-culture assays showed an increase in microvascular tubule formation with the addition of perfluorocarbon, but analysis of three-dimensional network growth in the presence of perfluorocarbon was not taken forward in Integra®, Matriderm® or DHCD because of time constraints. The effect of the pro-angiogenic factors leptin was also unquantified due to three-dimensional imaging difficulties. The addition of perfluorocarbon

and leptin remain promising techniques for potential improvement in three-dimensional vascularisation of dermal scaffolds.

Chapter 7 General Discussion

The main aims of this Thesis were to identify feasible source tissues for endothelial and stromal cell isolation and culture, for use in clinical applications; to establish the best conditions for forming microvascular networks *in vitro* using these cells; and to apply these microvasculature formation techniques to three-dimensional dermal substitute scaffolds. The working hypothesis is that the pre-vascularisation of dermal substitutes may result in improved scar quality and a reduction in the number of surgical procedures required in order to provide good functional and aesthetic outcomes for patients with large burn injuries. Most of the key objectives of this Thesis have been achieved, and there is scope for future work to expand upon the findings presented here.

7.1 Endothelial cells

Human UCB is a reliable source of ECFC derived cells, and has the highest and most reproducible yield of the different source tissues tested in this Thesis. ECFC yield was consistent with that of Ingram *et al*. (229), and from extensive collaborative work within our research laboratory, factors affecting the yield of ECFCs from UCB were identified. The inverse correlation of placental weight and ECFC yield is a novel finding, and this work has been published in a peer reviewed journal (204). Since final placental weight can be predicted from first trimester placental volume on three-dimensional ultrasound (226), or second trimester placental thickness on two-dimensional ultrasound (225) it may be possible to identify potentially high ECFC yield UCB donors from early pre-natal screening tests.

Both adult PB and AT are possible sources of autologous ECFCs, supported by characteristic morphology and limited multicolour FACS analysis for low volume samples

in this Thesis. Isolation and culture was more difficult and less reliable than from UCB, but a possible modification to the protocol as reported by Szöke *et al*. may improve ECFC yield from AT in future work (111). AT remains the most clinically feasible autologous source from which to harvest cells in our target patient group, but therapeutic use of donor UCB is well established for haematological disorders within Europe (231-235) and services in place for collection, processing, storage, matching and allocation of UCB units (234, 235, 237-240) could be utilised for cultured ECFCs from the same source.

7.2 Stromal cells

A protocol for harvest, transport, dissection and processing of fresh human adipose tissue and adipose microvasculature was established, and this protocol resulted in a reliable yield of paired stocks of adipose and microvasculature derived MSC. These spindle-shaped cells, cultured on plastic, were reliably $CD73^+$, $CD90^+$, $CD105^+$, $CD140b^+$ and $CD14^-$, $CD34^-$, $CD45^-$ and $HLA\text{-}DR^-$, which is consistent with adipose stem cells characterised by other authors (97, 98, 113). Adipose and microvasculature MSCs have comparable morphology and phenotype and are both able to differentiate into three different mesenchymal cell lineages.

Adult adipose tissue was therefore found to be a reliable and clinically feasible autologous source of MSCs and met the basic requirements for characterising mesenchymal stromal cells as determined by the ISCT (99, 102). A single, unique MSC defining characteristic or cell surface marker is yet to be discovered, and MSC from different tissues have different functional characteristics (252), yet phenotyping is useful to ensure specific efficacy and safety when MSC are used for clinical applications (304).

7.3 Microvascular Tubule Formation

UCB ECFC derived cells and either AT or MV MSC, were the primary cells selected as feasible sources for proposed clinical use, and were subsequently used in two-dimensional *in vitro* tubule formation assays. Both AT and MV MSCs support microvascular tubule formation in co-culture with UCB ECFC derived cells, although MV MSCs support significantly more tubule formation than paired AT MSCs (35.6% increase in total tubule length, $p<0.001$).

Possible reasons for this difference in tubule formation were investigated. AT and MV MSCs had comparable rates of proliferation, but MV MSC were found to express a significantly higher level of leptin in co-culture with UCB ECFC derived cells than AT MSCs (112% greater expression [p=0.025] with original data, 61% greater expression [p=0.55] with normalised data). Addition of exogenous leptin to AT MSC, but not MV MSC, and UCB ECFC derived cell co-cultures significantly increases microvascular tubule formation *in vitro*, suggesting an upper limit to the effect of leptin on tubule formation, which was already achieved with endogenous leptin from the MV MSCs.

Leptin did not increase proliferation of UCB ECFC derived cells, AT MSCs or MV MSCs in this Thesis, and these findings were consistent with Wolk *et al.* (282). Increased length of individual tubules, as well as an increase in total number of tubules formed, might result from promotion of cell migration as proposed by Goetze *et al.* from their work with leptin and HUVECs (280).

7.4 Three-dimensional vascular formation

Microvasculature formation techniques with our chosen primary cells were applied to three-dimensional dermal substitute scaffolds which are currently used as acellular matrices for wound repair.

UCB ECFC derived cells were transduced to express Green Fluorescent Protein for immunofluorescent imaging in three dimensions, but attempted DSRed transduction of AT and MV MSC had an adverse effect on MSC proliferation and this was not subsequently used.

Initial attempts at three-dimensional vascularisation of existing dermal substitutes Integra® and Matriderm® showed the ability to form robust three-dimensional vascular networks, but the depth of pre-vascularisation was limited to 100 microns (300). As such, two scaffolds in early clinical use were selected for further study. Neuskin-F® is a thin brittle layer of piscine collagen and was selected because it is thinner than Integra® and Matriderm® whilst still maintaining stability in culture. Neuskin-F® was capable of supporting two-dimensional vessel formation *in vitro* and may be a useful transport medium for pre-formed vasculature, but did not allow three-dimensional penetration of vasculature. De-cellularised Human Cadaveric Dermis (DHCD) retains the negative impression of the original donor vasculature (182) and it was hypothesised that engineered vasculature may follow these impressions through the depth of the dermis. DHCD also supported two-dimensional network formation, but analysis of three-dimensional network growth via GFP fluorescence detection was limited due to dermal auto-fluorescence.

Initial two-dimensional co-culture sandwich assays showed significant increases in microvascular tubule formation with the addition of perfluorocarbon (up to 80.9% increase in total tubule length with 0.05% perfluorocarbon, $p<0.0001$), similar to previous results achieved with addition of leptin to such cultures. Perfluorocarbon has been shown to significantly increase the oxygen uptake rate of hepatocytes in three dimensional *in vitro* culture (197) and to improve epithelial metabolism and partial tissue oxygen tension in a tissue engineered tracheal construct (198), and is promising in the potential to improve three-dimensional vascular formation.

7.5 Evaluation of the study design

From the outset, this study utilised human source tissues which are potentially feasible for clinical use. UCB units used in this Thesis were specifically collected for research purposes, however NHS Blood and Transplant has the infrastructure in place to collect, store and issue UCB units for transplantation. A new ethical application obtained by the primary researcher specifically for this project facilitated use of further relevant human adult tissue. Adult tissues were harvested from plastic surgery patients undergoing procedures under general anaesthesia, and this would be a similar method of tissue procurement and laboratory transfer in our proposed future patients requiring autologous therapy.

Ideally, the study would have utilised adipose tissue harvested from burns patients, but samples would have been infrequent and lab work less easy to plan. It was deemed more ethical to carry out initial research on tissue which would normally be discarded from other plastic surgery procedures in order to establish a feasible technique.

7.5.1 Strengths of the study

By collaborating with other researchers in the laboratory, it was possible to determine statistically significant correlations regarding UCB units and ECFC yield. These findings could facilitate potentially useful predictions for targeting of high yield UCB donors for clinical use and provide good evidence of the reliability of UCB as a source of ECFC derived cells for therapeutic use. Development of protocols for culture of ECFC from adult PB and AT within the laboratory also allowed comparisons to be made between different source tissues directly prepared by the same researcher.

The final protocol for adipose tissue processing resulted in multiple paired samples of AT and MV MSC which allowed direct comparisons to be made between these two varieties of

primary cells. To my knowledge, this is a novel approach and potentially adds to the field of research in the perivascular origin of MSCs (258, 260-270).

The two-dimensional tubule formation assays used in this Thesis are not only well established as a method for testing angiogenic effects (135), but have also been shown to form tubules with a functional lumen, important for future clinical applications (137). Investigation of the differences in proangiogenic factors expressed by tubule assay co-cultures with AT and MV MSC facilitated the identification of leptin as a useful exogenous additive to increase tubule formation. Investigation of the perfluorocarbon artificial oxygen carrier also led to identification of this as a potentially useful additive to increase *in vitro* tubule formation.

All of the scaffolds tested are suitable for use in humans *in vivo* (150) and are potentially useful for our proposed clinical usage.

All statistical results presented in this Thesis are derived from rigorous repeat experiments with at least three biological repeats and comparable controls.

7.5.2 Limitations of the study

The main limitations of the study resulted from difficulties in three-dimensional imaging of DHCD. DSRed transduction of MSCs required the addition of polybrene, but this had an adverse effect on MSC proliferation as previously described by Lin *et al.* (201) and so experiments were continued with GFP labelled UCB ECFC derived cells only. The extent of DHCD autofluorescence found was not predicted, and made it difficult to detect GFP labelled ECFC derived cells using either confocal microscopy or cryosectioning and fluorescent microscopy.

Time constraints did not allow further techniques for DHCD imaging to be explored, such as immunohistochemistry of samples after fixing, paraffin embedding and sectioning.

7.5.3 Potential improvements for experimental work

It may be possible to improve the yield of ECFC from adipose tissue by incorporating a cell sorting stage to the existing culture protocol used in this Thesis. Szöke *et al*. used Dynabeads (Invitrogen Dynal AS, Oslo, Norway) to isolate $CD44^{+}$ cells from the heterogenous cell population prior to plating cells from the stromal vascular fraction of lipoaspirate (111). This cell selection may be the step required to prevent the frequent MSC proliferation found in our protocol and may also be useful in PB samples to concentrate cells with potential to form endothelial colonies.

A different approach to imaging DHCD samples may achieve better visualisation of GFP labelled ECFC derived cells *in situ*. At the end of the culture period samples could be fixed, embedded in paraffin, sectioned, de-paraffinised and then stained histochemically with anti-GFP or CD31 antibodies. This may overcome the difficulties with autofluorescence observed with confocal imaging and fluorescent microscopy, and staining of sequential sections may allow a three-dimensional image to be reconstituted.

7.6 Contribution of this work to the field of wound healing research and clinical implications of the results

This study has contributed to the existing body of research in wound healing by identification of feasible source tissues of endothelial and stromal cells which could be used for *in vitro* vascularisation techniques. These cells may also be suitable for other wound healing applications such as direct application to chronic wound beds in order to stimulate neovascularisation *in vivo*. ECFC yield comparisons compared with UCB donor demographics has provided potentially useful predictions for targeting of high ECFC yield UCB donors for clinical use (204).

The direct comparison of paired AT and MV MSC samples is novel and adds to hypotheses regarding the perivascular origin of MSC. These cells, isolated and cultured using a new laboratory protocol, allowed consistent yield of cells which met the ISCT criteria for MSC (99, 102) and which were capable of supporting *in vitro* microvasculature formation. These are therefore a potentially feasible source of MSC for formation of patient specific autologous vascular networks.

Identification of the pro-angiogenic effects of exogenous leptin and perfluorocarbon may be useful in further wound healing research, either as topical treatments to improve neovascularisation in chronic wounds or to improve *in vitro* vascular networks for dermal tissue engineering.

Neuskin-F® has potential to be used as a resorbable carrier for microvasculature formed *in vitro*. Testing in an animal model is required, but it may be useful to transport new vasculature into chronic wounds or to prepare wound beds for revision surgery in burns patients. The partial pre-vascularisation of Integra®, Matriderm® and DHCD may also be useful in chronic wounds or single stage resurfacing of the burn wound bed with SSG, and there is scope for further investigation. Layered vascular network provision along with dermal substitute application may still have a beneficial effect on resulting scar quality of SSG without immediate inosculation of vessels at both surfaces of the scaffold.

7.7 Suggestions for further work

In addition to the specific experimental improvements described in section 7.5.3, there are several other areas which would benefit from further work.

Cell culture protocols for both UCB ECFC and AT and MV MSC require further development to achieve GMP standards (222, 241). Further work should include development of a serum free

media for ECFC and MSC culture such as those developed by other researchers for culture of MSC using platelet lysate (81, 242, 243). Use of a closed bioreactor system to reduce the risk of contamination during *ex vivo* culture and expansion of cells may also be worth investigation (83, 244-246).

Detailed proteomics and ELISA detection and quantification of proteins expressed by AT and MV MSC may be beneficial in more fully characterising and comparing these cell types, and thus accounting for the functional differences seen in support of microvascular formation. Comparison *in vivo* in a relevant animal model should also follow such as the skin humanised mouse model described by Carretero *et al*. (305), especially to ensure no adverse effects such as tumour formation.

The Neuskin-F® scaffold with surface vascular network is also ready for trial in such an animal model. The scaffold retains rigidity *in vitro* and should degrade in the wound bed *in vivo*, thus providing a layer of vasculature to the wound bed. It would be beneficial to determine if this vascular layer has any effect on either wound healing by secondary intention or on the quality of scarring with and without an overlying SSG. If an improvement in scar quality is seen with the presence of additional vasculature then further work to improve three-dimensional vascularisation of the other scaffolds in this Thesis would be worthwhile.

It may also be useful to examine the effect of partially pre-vascularised Integra®, Matriderm® and DHCD scaffolds on either wound healing by secondary intention or on the quality of scarring with and without an overlying SSG in a skin humanised mouse model, as full penetration of *in vitro* vasculature may not actually be required in order to improve healing or scarring.

Due to difficulties in achieving full penetration of vasculature across the four different scaffolds tested in this Thesis, it may be useful to try further scaffolds with further different physical properties. Chen *et al*. have recently shown a macroporous hydrogel scaffold to be

capable of carrying viable cells throughout the structure, on which HUVEC also form a preliminary network on the surface (192). The surface vasculature appears similar to that presented in this Thesis, but the presence of viable cells throughout the construct may be functionally better *in vivo*. Whilst decreasing the density of scaffolds may improve cellular penetration and survival, this is at the expense of rigidity and ease of handling which are important in order to place scaffolds *in vivo*. An ideal compromise would be a gel that could remain fluidity during *in vitro* vascularisation and then attain suitable rigidity for surgical application *in vivo*.

Another scaffold modification may be the use of 3D stereolithography to pattern dermal architecture into a gelatin methacrylate scaffold (306, 307), thus laying down the pathways for seeded cells to revascularise. This technique has been utilised by Grogan *et al*. to design meniscal scaffolds and the authors found improved cellular alignment and tissue formation *in vitro* (307).

Finally, it may be possible to coat specific proangiogenic factors on the internal surface of scaffold pores in order to encourage penetrative cell homing and migration despite less favourable media and oxygen perfusion towards the centre of the scaffold. Sheridan *et al.* have recently shown it is possible for a hydrogel to maintain prolonged release of HGF *in vitro,* and it may be possible to apply this technique to other scaffolds and growth factors (308).

References

1. Brusselaers N, Monstrey S, Vogelaers D, Hoste E, Blot S. Severe Burn Injury In Europe: A Systematic Review Of The Incidence, Etiology, Morbidity, And Mortality. Critical Care. 2010;14(5):R188. Epub 2010/10/21.
2. Olah A, Szollosi AG, Biro T. The Channel Physiology Of The Skin. Reviews Of Physiology, Biochemistry And Pharmacology. 2012;163:65-131. Epub 2012/11/28.
3. Papini R. Management Of Burn Injuries Of Various Depths. British Medical Journal. 2004;329 (7458):158–60.
4. Janzekovic Z. Once Upon A Time…How West Discovered East. Journal Of Plastic, Reconstructive And Aesthetic Surgery. 2008;61:240-4.
5. Brusselaers N, Pirayesh A, Hoeksema H, Richters CD, Verbelen J, Beele H, Et Al. Skin Replacement In Burn Wounds. Journal Of Trauma. 2010;68(2):490-501. Epub 2010/02/16.
6. Łabuś W, Kawecki M, Nowak M. The Role Of Tissue Engineering In The Treatment Of Burn Wounds. Polski Przeglad Chirurgiczny. 2012;84(3):167-71.
7. Van Der Veen VC, Van Der Wal MB, Van Leeuwen MC, Ulrich MM, Middelkoop E. Biological Background Of Dermal Substitutes. Burns. 2010;36(3):305-21. Epub 2009/11/10.
8. Harding K, Queen D. Chronic Wounds And Their Management And Prevention Is A Significiant Public Health Issue. International Wound Journal. 2010;7(3):125-6.
9. Sen CK, Gordillo GM, Roy S, Kirsner R, Lambert L, Hunt TK, Et Al. Human Skin Wounds: A Major And Snowballing Threat To Public Health And The Economy. Wound Repair And Regeneration. 2009;17(6):763-71. Epub 2009/11/12.
10. Posnett J, Franks PJ. The Burden Of Chronic Wounds In The UK. Nursing Times. 2008;104(3):44-5.
11. Reinke JM, Sorg H. Wound Repair And Regeneration. European Surgical Research. 2012;49(1):35-43. Epub 2012/07/17.
12. Bezuhly M, Fish JS. Acute Burn Care. Plastic And Reconstructive Surgery. 2012;130(2):349e-58e. Epub 2012/07/31.
13. Calvin M. Cutaneous Wound Repair. Wounds 1998;10(1):12-32.
14. Murawala P, Tanaka EM, Currie JD. Regeneration: The Ultimate Example Of Wound Healing. Seminars In Cell & Developmental Biology. 2012;23(9):954-62. Epub 2012/10/13.
15. Halloran CM, Slavin JP. Pathophysiology Of Wound Healing. Surgery. 2002;20(5):I-V.
16. Enoch S, Price P. Cellular, Molecular And Biochemical Differences In The Pathophysiology Of Healing Between Acute Wounds, Chronic Wounds And Wounds In The Aged. World Wide Wounds [Online]. 2004.
17. Enoch S, Leaper DJ. Basic Science Of Wound Healing. Surgery. 2005;23(2):37-42.
18. Brown BC, Moss TP, Mcgrouther DA, Bayat A. Skin Scar Pre-Conceptions Must Be Challenged: Importance Of Self-Perception In Skin Scarring. Journal Of Plastic, Reconstructive & Aesthetic Surgery. 2010;63(6):1022-9. Epub 2009 Jun 5.
19. Urioste SS, Arndt KA, Dover JS. Keloids And Hypertrophic Scars: Review And Treatment Strategies. Seminars In Cutaneous Medicine And Surgery. 1999;18(2):159-71.
20. Cerda E. Mechanics Of Scars. Journal Of Biomechanics. 2005;38:1598-603.
21. Wood FM, Currie K, Backman B, Cena B. Current Difficulties And The Possible Future Directions In Scar Assessment. Burns. 1996;22(6):455-8.
22. Durani P, Mcgrouther DA, Ferguson MWJ. Current Scales For Assessing Human Scarring: A Review. Journal Of Plastic, Reconstructive & Aesthetic Surgery 2009;62:713-20.
23. Durani P, Mcgrouther DA, Ferguson MWJ. The Patient Scar Assessment Questionnaire: A Reliable And Valid Patient-Reported Outcomes Measure For Linear Scars. Plastic And Reconstructive Surgery. 2009;123:1481-9.

24. Berchialla P, Gangemi EN, Foltran F, Haxhiaj A, Buja A, Lazzarato F, Et Al. Predicting Severity Of Pathological Scarring Due To Burn Injuries: A Clinical Decision Making Tool Using Bayesian Networks. International Wound Journal. 2012. Epub 2012/09/11.
25. Gangemi EN, Gregori D, Berchialla P, Zingarelli E, Cairo M, Bollero D, Et Al. Epidemiology And Risk Factors For Pathologic Scarring After Burn Wounds. Archives Of Facial Plastic Surgery. 2008;10(2):93-102.
26. Chapman TT. Burn Scar And Contracture Management. Journal Of Trauma. 2007;62(6 Suppl):S8. Epub 2007/07/13.
27. Shimizu R, Kishi K. Skin Graft. Plastic Surgery International. 2012;2012:563493. Epub 2012/05/10.
28. Huang C, Akaishi S, Hyakusoku H, Ogawa R. Are Keloid And Hypertrophic Scar Different Forms Of The Same Disorder? A Fibroproliferative Skin Disorder Hypothesis Based On Keloid Findings. International Wound Journal. 2012. Epub 2012/11/24.
29. Xi-Qiao W, Ying-Kai L, Chun Q, Shu-Liang L. Hyperactivity Of Fibroblasts And Functional Regression Of Endothelial Cells Contribute To Microvessel Occlusion In Hypertrophic Scarring. Microvascular Research. 2009;77:204-11.
30. Evers LH, Bhavsar D, Mailander P. The Biology Of Burn Injury. Experimental Dermatology. 2010;19(9):777-83. Epub 2010/07/16.
31. Jackson DM. The Diagnosis Of The Depth Of Burning. British Journal Of Surgery. 1953;40(164):588-96.
32. Pham TN, Cancio LC, Gibran NS. American Burn Association Practice Guidelines Burn Shock Resuscitation. Journal Of Burn Care & Research. 2008;29(1):257-66. Epub 2008/01/10.
33. Omi T, Kawanami O, Matsuda K, Tsujii A, Kawai M, Henmi H, Et Al. Histological Characteristics Of The Healing Process Of Frozen Skin Allograft Used In The Treatment Of Burns. Burns. 1996;22(3):206-11.
34. Andreassi A, Bilenchi R, Biagioli M, D'Aniello C. Classification And Pathophysiology Of Skin Grafts. Clinics In Dermatology. 2005;23(4):332-7. Epub 2005/07/19.
35. Davis WJ, 3rd, Wu C, Sieber D, Vandevender DK. A Comparison Of Full And Split Thickness Skin Grafts In Radial Forearm Donor Sites. Journal Of Hand & Microsurgery. 2011;3(1):18-24. Epub 2012/06/02.
36. Wang Q, Cai M, Wu YL, Zhang GC. Mathematical Guide To Minimize Donor Size In Full-Thickness Skin Grafting. Dermatologic Surgery. 2009;35(9):1364-7. Epub 2009/06/09.
37. Laschke MW, Vollmar B, Menger MD. Inosculation: Connecting The Life-Sustaining Pipelines. Tissue Engineering: Part B. 2009;15(4):455-65.
38. O'Ceallaigh S, Herrick SE, Bluff JE, Mcgrouther DA, Ferguson MWJ. Quantification Of Total And Perfused Blood Vessels In Murine Skin Autografts Using A Fluorescent Double-Labeling Technique. Plastic And Reconstructive Surgery. 2006;117(1):140-51.
39. O'Ceallaigh S, Herrick SE, Bennett WR, Bluff JE, Ferguson MW, Mcgrouther DA. Perivascular Cells In A Skin Graft Are Rapidly Repopulated By Host Cells. Journal Of Plastic, Reconstructive & Aesthetic Surgery. 2007;60(8):864-75. Epub 2007/07/10.
40. Baldwin C, Potter M, Clayton E, Irvine L, Dye J. Topical Negative Pressure Stimulates Endothelial Migration And Proliferation A Suggested Mechanism For Improved Integration Of Integra. Annals Of Plastic Surgery. 2009;62:92-6.
41. Greenwood J, Amjadi M, Dearman B, Mackie I. Real-Time Demonstration Of Split Skin Graft Inosculation And Integra Dermal Matrix Neovascularization Using Confocal Laser Scanning Microscopy. Eplasty Open Access Journal Of Plastic Surgery. 2009;9:309-18.
42. Van Der Veen VC, Boekema BK, Ulrich MM, Middelkoop E. New Dermal Substitutes. Wound Repair & Regeneration. 2011;19(Suppl 1):S59-65. Epub 2011/08/04.
43. Richters CD, Hoekstra MJ, Van Baare J, Du Pont JS, Kamperdijk EWA. Morphology Of Glycerol-Preserved Human Cadaver Skin. Burns. 1996;22(2):113-6.

44. Burd A. Glycerolised Allogenic Skin: Transplant Or Dressing? A Medico-Legal Question. Burns. 2002;28:S34-S9.
45. Moerman E, Middelkoop E, Mackie D, Groenevelt F. The Temporary Use Of Allograft For Complicated Wounds In Plastic Surgery. Burns. 2002;28:S13-S5.
46. Wood FM, Kolybaba ML, Allen P. The Use Of Cultured Epithelial Autograft In The Treatment Of Major Burn Injuries: A Critical Review Of The Literature. Burns. 2006;32(4):395-401. Epub 2006/04/20.
47. Atiyeh BS, Costagliola M. Cultured Epithelial Autograft (CEA) In Burn Treatment: Three Decades Later. Burns. 2007;33(4):405-13. Epub 2007/04/03.
48. Cirodde A, Leclerc T, Jault P, Duhamel P, Lataillade JJ, Bargues L. Cultured Epithelial Autografts In Massive Burns: A Single-Center Retrospective Study With 63 Patients. Burns. 2011;37(6):964-72. Epub 2011/05/10.
49. Sood R, Roggy D, Zieger M, Balledux J, Chaudhari S, Koumanis DJ, Et Al. Cultured Epithelial Autografts For Coverage Of Large Burn Wounds In Eighty-Eight Patients: The Indiana University Experience. Journal Of Burn Care & Research. 2010;31(4):559-68. Epub 2010/07/10.
50. Nguyen DQ, Potokar TS, Price P. An Objective Long-Term Evaluation Of Integra (A Dermal Skin Substitute) And Split Thickness Skin Grafts, In Acute Burns And Reconstructive Surgery. Burns. 2010;36(1):23-8. Epub 2009/10/30.
51. Dantzer E, Braye FM. Reconstructive Surgery Using An Artificial Dermis (Integra): Results With 39 Grafts. British Journal Of Plastic Surgery. 2001;54(8):659-64. Epub 2001/12/01.
52. Branski LK, Herndon DN, Pereira C, Mlcak RP, Celis MM, Lee JO, Et Al. Longitudinal Assessment Of Integra In Primary Burn Management: A Randomized Pediatric Clinical Trial. Critical Care Medicine. 2007;35(11):2615-23. Epub 2007/09/11.
53. Rigg BM. Importance Of Donor Site Selection In Skin Grafting. Canadian Medical Association Journal. 1977;117:1028-9.
54. Marcelo KL, Goldie LC, Hirschi KK. Regulation Of Endothelial Cell Differentiation And Specification. Circulation Research. 2013;112(9):1272-87. Epub 2013/04/27.
55. Fabbri-Arrigoni FI, Clarke L, Wang G, Charakida M, Ellins E, Halliday N, Et Al. Levels Of Circulating Endothelial Cells And Colony-Forming Units Are Influenced By Age And Dyslipidemia. Pediatric Research. 2012;72(3):299-304. Epub 2012/07/13.
56. Fox A, Smythe J, Fisher N, Tyler MP, Mcgrouther DA, Watt SM, Et Al. Mobilization Of Endothelial Progenitor Cells Into The Circulation In Burned Patients. The British Journal Of Surgery. 2008;95(2):244-51. Epub 2007/08/19.
57. Grenier G, Scime A, Le Grand F, Asakura A, Perez-Iratxeta C, Andrade-Navarro MA, Et Al. Resident Endothelial Precursors In Muscle, Adipose, And Dermis Contribute To Postnatal Vasculogenesis. Stem Cells. 2007;25(12):3101-10. Epub 2007/09/08.
58. Morris LM, Klanke CA, Lang SA, Pokall S, Maldonado AR, Vuletin JF, Et Al. Characterization Of Endothelial Progenitor Cells Mobilization Following Cutaneous Wounding. Wound Repair & Regeneration. 2010;18(4):383-90. Epub 2010/06/16.
59. Watt SM, Athanassopoulos A, Harris AL, Tsaknakis G. Human Endothelial Stem/Progenitor Cells, Angiogenic Factors And Vascular Repair. Journal Of The Royal Society Interface. 2010;7 Suppl 6:S731-51. Epub 2010/09/17.
60. Carmeliet P. Mechanisms Of Angiogenesis And Arteriogenesis. Nature Medicine. 2000;6(3):389-95.
61. Semenza GL. Vasculogenesis, Angiogenesis, And Arteriogenesis: Mechanisms Of Blood Vessel Formation And Remodeling. Journal Of Cellular Biochemistry. 2007;102:840–7.
62. Pandya NM, Dhalla NS, Santani DD. Angiogenesis--A New Target For Future Therapy. Vascular Pharmacology. 2006;44(5):265-74. Epub 2006/03/21.
63. Rabbany SY, James D, Rafii S. New Dimensions In Vascular Engineering: Opportunities For Cancer Biology. Tissue Engineering Part A. 2010;16(7):2157-9. Epub 2010/04/07.

64. Eming SA, Brachvogel B, Odorisio T, Koch M. Regulation Of Angiogenesis: Wound Healing As A Model. Progress In Histochemistry And Cytochemistry. 2007;42(3):115-70. Epub 2007/11/06.
65. Pearson JD. Endothelial Progenitor Cells--An Evolving Story. Microvascular Research. 2010;79(3):162-8. Epub 2010/01/02.
66. Prater DN, Case J, Ingram DA, Yoder MC. Working Hypothesis To Redefine Endothelial Progenitor Cells. Leukemia. 2007;21(6):1141-9. Epub 2007/03/30.
67. Richardson MR, Yoder MC. Endothelial Progenitor Cells: Quo Vadis? Journal Of Molecular And Cellular Cardiology. 2011;50(2):266-72. Epub 2010/08/03.
68. Timmermans F, Plum J, Yoder MC, Ingram DA, Vandekerckhove B, Case J. Endothelial Progenitor Cells: Identity Defined? Journal Of Cellular And Molecular Medicine. 2009;13(1):87-102. Epub 2008/12/11.
69. Yoder MC. Defining Human Endothelial Progenitor Cells. Journal Of Thrombosis And Haemostasis : JTH. 2009;7 Suppl 1:49-52. Epub 2009/07/28.
70. Estes ML, Mund JA, Mead LE, Prater DN, Cai S, Wang H, Et Al. Application Of Polychromatic Flow Cytometry To Identify Novel Subsets Of Circulating Cells With Angiogenic Potential. Cytometry Part A : The Journal Of The International Society For Analytical Cytology. 2010;77(9):831-9. Epub 2010/08/31.
71. Ayalon O, Sabanai H, Lampugnani M-G, Dejana E, Geiger B. Spatial And Temporal Relationships Between Cadherins And PECAM-1 In Cell-Cell Junctions Of Human Endothelial Cells. The Journal Of Cell Biology. 1994;126:247-58.
72. Jackson DE, Ward CM, Wang R, Newman PJ. The Protein-Tyrosine Phosphatase SHP-2 Binds Platelet/Endothelial Cell Adhesion Molecule-1 (PECAM-1) And Forms A Distinct Signaling Complex During Platelet Aggregation. The Journal Of Biological Chemistry. 1997;272(11):6986–93.
73. Felschow DM. The Adapter Protein Crkl Associates With CD34. Blood. 2001;97(12):3768-75.
74. Herold C, Elhabazi A, Bismuth G, Bensussan A, Boumsell L. CD100 Is Associated With CD45 At The Surface Of Human T Lymphocytes. The Journal Of Immunology. 1996;157:5262-8.
75. Mcfarland EDC, Pingel J, Thomas ML. Definition Of Amino Acids Sufficient For Plasma Membrane Association Of CD45 And CD45-Associated Protein. Biochemistry. 1997;36:7169-75.
76. Mund JA, Estes ML, Yoder MC, Ingram DA, Jr., Case J. Flow Cytometric Identification And Functional Characterization Of Immature And Mature Circulating Endothelial Cells. Arteriosclerosis, Thrombosis, And Vascular Biology. 2012;32(4):1045-53. Epub 2012/01/28.
77. Boneberg EM, Illges H, Legler DF, Furstenberger G. Soluble CD146 Is Generated By Ectodomain Shedding Of Membrane CD146 In A Calcium-Induced, Matrix Metalloprotease-Dependent Process. Microvascular Research. 2009;78(3):325-31. Epub 2009/07/21.
78. Pickl WF, Majdic O, Fischer GF, Petzelbauer P, Fae I, Waclavicek M, Et Al. Mucl8/MCAM (CD146), An Activation Antigen Of Human T Lymphocytes. The Journal Of Immunology. 1997;158: 2107-15.
79. Zhang Y, Fisher N, Newey SE, Smythe J, Tatton L, Tsaknakis G, Et Al. The Impact Of Proliferative Potential Of Umbilical Cord-Derived Endothelial Progenitor Cells And Hypoxia On Vascular Tubule Formation In Vitro. Stem Cells Dev. 2009;18(2):359-75. Epub 2008/07/30.
80. Bani D, Nistri S. New Insights Into The Morphogenic Role Of Stromal Cells And Their Relevance For Regenerative Medicine. Lessons From The Heart. Journal Of Cellular And Molecular Medicine. 2014;18(3):363-70. Epub 2014/02/19.
81. Fekete N, Rojewski MT, Furst D, Kreja L, Ignatius A, Dausend J, Et Al. GMP-Compliant Isolation And Large-Scale Expansion Of Bone Marrow-Derived MSC. Plos One. 2012;7(8):E43255. Epub 2012/08/21.

82. Lin RZ, Moreno-Luna R, Zhou B, Pu WT, Melero-Martin JM. Equal Modulation Of Endothelial Cell Function By Four Distinct Tissue-Specific Mesenchymal Stem Cells. Angiogenesis. 2012;15(3):443-55. Epub 2012/04/25.
83. Rojewski MT, Fekete N, Baila S, Nguyen K, Furst D, Antwiler D, Et Al. GMP-Compliant Isolation And Expansion Of Bone Marrow-Derived Mscs In The Closed, Automated Device Quantum Cell Expansion System. Cell Transplantation. 2013;22(11):1981-2000. Epub 2012/10/31.
84. Wang X, Li C, Zheng Y, Xia W, Yu Y, Ma X. Bone Marrow Mesenchymal Stem Cells Increase Skin Regeneration Efficiency In Skin And Soft Tissue Expansion. Expert Opin Biol Ther. 2012;12(9):1129-39.
85. Pittenger MF, Mackay AM, Beck SC, Jaiswal RK, Douglas R, Mosca JD, Et Al. Multilineage Potential Of Adult Human Mesenchymal Stem Cells. Science. 1999;284:143-7.
86. Jiang Y, Jahagirdar BN, Reinhardt RL, Schwartz RE, Keene CD, Ortiz-Gonzalez XR, Et Al. Pluripotency Of Mesenchymal Stem Cells Derived From Adult Marrow. Nature. 2002;418:41-9.
87. Fuchs E. Scratching The Surface Of Skin Development. Nature. 2007;445(7):834-42.
88. Zouboulis CC, Adjaye J, Akamatsu H, Moe-Behrens G, Niemann C. Human Skin Stem Cells And The Ageing Process. Experimental Gerontology. 2008;43:986-97.
89. Buckingham M. Skeletal Muscle Progenitor Cells And The Role Of Pax Genes. C R Biologies. 2007;330:530-3.
90. Relaix F, Rocancourt D, Mansouri A, Buckingham M. A Pax3/Pax7-Dependent Population Of Skeletal Muscle Progenitor Cells. Nature. 2005;435(7044):948-53.
91. Lee JY, Qu-Petersen Z, Cao B, Kimura S, Jankowski R, Cummins J, Et Al. Clonal Isolation Of Muscle-Derived Cells Capable Of Enhancing Muscle Regeneration And Bone Healing. The Journal Of Cell Biology. 2000;150(5):1085-99.
92. Wada MR, Inagawa-Ogashiwa M, Shimizu S, Yasumoto S, Hashimoto N. Generation Of Different Fates From Multipotent Muscle Stem Cells. Development. 2002;129:2987-95.
93. Astori G, Vignati F, Bardelli S, Tubio M, Gola M, Albertini V, Et Al. "In Vitro" And Multicolor Phenotypic Characterization Of Cell Subpopulations Identified In Fresh Human Adipose Tissue Stromal Vascular Fraction And In The Derived Mesenchymal Stem Cells. Journal Of Translational Medicine. 2007;5:55. Epub 2007/11/02.
94. Baer PC, Kuci S, Krause M, Kuci Z, Zielen S, Geiger H, Et Al. Comprehensive Phenotypic Characterization Of Human Adipose-Derived Stromal/Stem Cells And Their Subsets By A High Throughput Technology. Stem Cells Dev. 2013;22(2):330-9. Epub 2012/08/28.
95. Blasi A, Martino C, Balducci L, Saldarelli M, Soleti A, Navone SE, Et Al. Dermal Fibroblasts Display Similar Phenotypic And Differentiation Capacity To Fat-Derived Mesenchymal Stem Cells, But Differ In Anti-Inflammatory And Angiogenic Potential. Vascular Cell. 2011;3(1):5. Epub 2011/02/26.
96. Conde-Green A, De Amorim NF, Pitanguy I. Influence Of Decantation, Washing And Centrifugation On Adipocyte And Mesenchymal Stem Cell Content Of Aspirated Adipose Tissue: A Comparative Study. Journal Of Plastic, Reconstructive & Aesthetic Surgery : JPRAS. 2010;63(8):1375-81. Epub 2009/08/15.
97. Katz AJ, Tholpady A, Tholpady SS, Shang H, Ogle RC. Cell Surface And Transcriptional Characterization Of Human Adipose-Derived Adherent Stromal (Hadas) Cells. Stem Cells. 2005;23(3):412-23. Epub 2005/03/08.
98. Zuk PA, Zhu M, Ashjian P, De Ugarte DA, Huang JI, Mizuno H, Et Al. Human Adipose Tissue Is A Source Of Multipotent Stem Cells. Molecular Biology Of The Cell. 2002;13(12):4279-95. Epub 2002/12/12.
99. Horwitz EM, Le Blanc K, Dominici M, Mueller I, Slaper-Cortenbach I, Marini FC, Et Al. Clarification Of The Nomenclature For MSC: The International Society For Cellular Therapy Position Statement. . Cytotherapy. 2005;7:393-5.

100. Lin C-S, Xin Z-C, Deng C-H, Ning H, Lin G, Lue TF. Defining Adipose Tissue-Derived Stem Cells In Tissue And In Culture. Histology And Histopathology. 2010;25:807-15.
101. Lin G, Garcia M, Ning H, Banie L, Guo YL, Lue TF, Et Al. Defining Stem And Progenitor Cells Within Adipose Tissue. Stem Cells Dev. 2008;17(6):1053-63. Epub 2008/07/04.
102. Dominici M, Le Blanc K, Mueller I, Slaper-Cortenbach I, Marini FC, Krause DS, Et Al. Minimal Criteria For Defining Multipotent Mesenchymal Stromal Cells. The International Society For Cellular Therapy Position Statement. Cytotherapy. 2006;8:315-7.
103. Bonish BK, Foreman KE, Gutierrez-Steil C, Nickoloff BJ. Phenotype And Proliferation Characteristics Of Cultured Spindle-Shaped Cells Obtained From Normal Human Skin And Lesions Of Dermatofibroma, Kaposi's Sarcoma, And Dermatofibrosarcoma Protuberans: A Comparison With Fibroblast And Endothelial Cells Of The Dermis. Journal Of Dermatological Science. 1997;16:52-8.
104. Xu Y, Huang S, Fu X. Autologous Transplantation Of Bone Marrow-Derived Mesenchymal Stem Cells: A Promising Therapeutic Strategy For Prevention Of Skin-Graft Contraction. Clinical And Experimental Dermatology. 2012;37(5):497-500. Epub 2012/02/04.
105. Jiang D, Qi Y, Walker NG, Sindrilaru A, Hainzl A, Wlaschek M, Et Al. The Effect Of Adipose Tissue Derived Mscs Delivered By A Chemically Defined Carrier On Full-Thickness Cutaneous Wound Healing. Biomaterials. 2013;34(10):2501-15. Epub 2013/01/16.
106. Critser PJ, Voytik-Harbin SL, Yoder MC. Isolating And Defining Cells To Engineer Human Blood Vessels. Cell Proliferation. 2011;44 Suppl 1:15-21. Epub 2011/04/22.
107. Fox A, Smythe J, Fisher N, Tyler MPH, Mcgrouther DA, Watt SM, Et Al. Mobilization Of Endothelial Progenitor Cells Into The Circulation In Burned Patients. British Journal Of Surgery. 2008;95:244-51.
108. Sengenes C, Miranville A, Maumus M, De Barros S, Busse R, Bouloumie A. Chemotaxis And Differentiation Of Human Adipose Tissue CD34+/CD31- Progenitor Cells: Role Of Stromal Derived Factor-1 Released By Adipose Tissue Capillary Endothelial Cells. Stem Cells. 2007;25:2269-76.
109. Curinga G, Jain A, Feldman M, Prosciak M, Phillips B, Milner S. Red Blood Cell Transfusion Following Burn. Burns. 2011;37(5):742-52. Epub 2011/03/04.
110. Posluszny JA, Jr., Conrad P, Halerz M, Shankar R, Gamelli RL. Classifying Transfusions Related To The Anemia Of Critical Illness In Burn Patients. The Journal Of Trauma. 2011;71(1):26-31. Epub 2010/12/07.
111. Szoke K, Beckstrom KJ, Brinchmann JE. Human Adipose Tissue As A Source Of Cells With Angiogenic Potential. Cell Transplantation. 2012;21(1):235-50. Epub 2011/06/15.
112. Natesan S, Wrice NL, Baer DG, Christy RJ. Debrided Skin As A Source Of Autologous Stem Cells For Wound Repair. Stem Cells. 2011;29(8):1219-30. Epub 2011/06/16.
113. Cai X, Lin Y, Hauschka PV, Grottkau BE. Adipose Stem Cells Originate From Perivascular Cells. Biology Of The Cell / Under The Auspices Of The European Cell Biology Organization. 2011;103(9):435-47. Epub 2011/06/18.
114. Choi SA, Lee JY, Wang KC, Phi JH, Song SH, Song J, Et Al. Human Adipose Tissue-Derived Mesenchymal Stem Cells: Characteristics And Therapeutic Potential As Cellular Vehicles For Prodrug Gene Therapy Against Brainstem Gliomas. Eur J Cancer. 2012;48(1):129-37. Epub 2011/06/15.
115. Bhang SH, Cho SW, Lim JM, Kang JM, Lee TJ, Yang HS, Et Al. Locally Delivered Growth Factor Enhances The Angiogenic Efficacy Of Adipose-Derived Stromal Cells Transplanted To Ischemic Limbs. Stem Cells. 2009;27(8):1976-86. Epub 2009/06/23.
116. Gir P, Oni G, Brown SA, Mojallal A, Rohrich RJ. Human Adipose Stem Cells: Current Clinical Applications. Plast Reconstr Surg. 2012;129(6):1277-90. Epub 2012/05/29.
117. Uysal CA, Tobita M, Hyakusoku H, Mizuno H. Adipose-Derived Stem Cells Enhance Primary Tendon Repair: Biomechanical And Immunohistochemical Evaluation. Journal Of Plastic, Reconstructive & Aesthetic Surgery : JPRAS. 2012;65(12):1712-9. Epub 2012/07/10.

118. Yoshimura K, Sato K, Aoi N, Kurita M, Hirohi T, Harii K. Cell-Assisted Lipotransfer For Cosmetic Breast Augmentation: Supportive Use Of Adipose-Derived Stem/Stromal Cells. Aesthetic Plastic Surgery. 2008;32(1):48-55; Discussion 6-7. Epub 2007/09/04.
119. Clauser LC, Tieghi R, Galie M, Carinci F. Structural Fat Grafting: Facial Volumetric Restoration In Complex Reconstructive Surgery. The Journal Of Craniofacial Surgery. 2011;22(5):1695-701. Epub 2011/10/01.
120. Coleman S. Structural Fat Grafting. Aesthetic Surgery Journal. 1998;18(5):386-8.
121. Nguyen PS, Desouches C, Gay AM, Hautier A, Magalon G. Development Of Micro-Injection As An Innovative Autologous Fat Graft Technique: The Use Of Adipose Tissue As Dermal Filler. Journal Of Plastic, Reconstructive & Aesthetic Surgery : JPRAS. 2012;65(12):1692-9. Epub 2012/07/04.
122. Sultan SM, Barr JS, Butala P, Davidson EH, Weinstein AL, Knobel D, Et Al. Fat Grafting Accelerates Revascularisation And Decreases Fibrosis Following Thermal Injury. Journal Of Plastic, Reconstructive & Aesthetic Surgery : JPRAS. 2012;65(2):219-27. Epub 2011/10/04.
123. Pu LL, Coleman SR, Cui X, Ferguson RE, Jr., Vasconez HC. Autologous Fat Grafts Harvested And Refined By The Coleman Technique: A Comparative Study. Plast Reconstr Surg. 2008;122(3):932-7. Epub 2008/09/04.
124. Lu F, Li J, Gao J, Ogawa R, Ou C, Yang B, Et Al. Improvement Of The Survival Of Human Autologous Fat Transplantation By Using VEGF-Transfected Adipose-Derived Stem Cells. Plast Reconstr Surg. 2009;124(5):1437-46. Epub 2009/12/17.
125. Perez-Cano R, Vranckx JJ, Lasso JM, Calabrese C, Merck B, Milstein AM, Et Al. Prospective Trial Of Adipose-Derived Regenerative Cell (ADRC)-Enriched Fat Grafting For Partial Mastectomy Defects: The RESTORE-2 Trial. European Journal Of Surgical Oncology : The Journal Of The European Society Of Surgical Oncology And The British Association Of Surgical Oncology. 2012;38(5):382-9. Epub 2012/03/20.
126. Pu LL. Discussion. Improvement Of The Survival Of Human Autologous Fat Transplantation By Using VEGF-Transfected Adipose-Derived Stem Cells. Plast Reconstr Surg. 2009;124(5):1447-9. Epub 2009/12/17.
127. Sterodimas A, De Faria J, Nicaretta B, Boriani F. Autologous Fat Transplantation Versus Adipose-Derived Stem Cell-Enriched Lipografts: A Study. Aesthetic Surgery Journal / The American Society For Aesthetic Plastic Surgery. 2011;31(6):682-93. Epub 2011/08/05.
128. Trojahn Kolle SF, Oliveri RS, Glovinski PV, Elberg JJ, Fischer-Nielsen A, Drzewiecki KT. Importance Of Mesenchymal Stem Cells In Autologous Fat Grafting: A Systematic Review Of Existing Studies. Journal Of Plastic Surgery And Hand Surgery. 2012;46(2):59-68. Epub 2012/04/05.
129. Zhu M, Zhou Z, Chen Y, Schreiber R, Ransom JT, Fraser JK, Et Al. Supplementation Of Fat Grafts With Adipose-Derived Regenerative Cells Improves Long-Term Graft Retention. Annals Of Plastic Surgery. 2010;64(2):222-8. Epub 2010/01/26.
130. Chang J, Davis CL, Mathes DW. The Impact Of Current Immunosuppression Strategies In Renal Transplantation On The Field Of Reconstructive Transplantation. Journal Of Reconstructive Microsurgery. 2012;28(1):7-19. Epub 2011/08/16.
131. Priyadharshini B, Greiner DL, Brehm MA. T-Cell Activation And Transplantation Tolerance. Transplant Rev (Orlando). 2012;26(3):212-22. Epub 2011/11/15.
132. Thaunat O. Humoral Immunity In Chronic Allograft Rejection: Puzzle Pieces Come Together. Transplant Immunology. 2012;26(2-3):101-6. Epub 2011/11/24.
133. Allice T, Busca A, Locatelli F, Falda M, Pittaluga F, Ghisetti V. Valganciclovir As Pre-Emptive Therapy For Cytomegalovirus Infection Post-Allogenic Stem Cell Transplantation: Implications For The Emergence Of Drug-Resistant Cytomegalovirus. The Journal Of Antimicrobial Chemotherapy. 2009;63(3):600-8. Epub 2009/01/17.

134. Ballester JM, Rivero RA, Villaescusa R, Merlin JC, Arce AA, Castillo D, Et Al. Hepatitis C Virus Antibodies And Other Markers Of Blood-Transfusion-Transmitted Infection In Multi-Transfused Cuban Patients. Journal Of Clinical Virology. 2005;34(Suppl 2):S39-S46.
135. Zhang Y, Fisher N, Newey SE, Smythe J, Tatton L, Tsaknakis G, Et Al. The Impact Of Proliferative Potential Of Umbilical Cord-Derived Endothelial Progenitor Cells And Hypoxia On Vascular Tubule Formation In Vitro. Stem Cells And Development. 2009;18(2):359-75.
136. Zengin E, Chalajour F, Gehling UM, Ito WD, Treede H, Lauke H, Et Al. Vascular Wall Resident Progenitor Cells: A Source For Postnatal Vasculogenesis. Development. 2006;133(8):1543-51. Epub 2006/03/10.
137. Athanassopoulos A, Tsaknakis G, Newey SE, Harris AL, Kean J, Tyler MP, Et Al. Microvessel Networks In Pre-Formed In Artificial Clinical Grade Dermal Substitutes In Vitro Using Cells From Haematopoietic Tissues. Burns. 2012. Epub 2012/03/01.
138. Mosna F, Sensebe L, Krampera M. Human Bone Marrow And Adipose Tissue Mesenchymal Stem Cells: A User's Guide. Stem Cells And Development. 2010;19(10):1449-70.
139. Khoo CP, Pozzilli P, Alison MR. Endothelial Progenitor Cells And Their Potential Therapeutic Applications. Regenerative Medicine. 2008;3(6):863-76.
140. Watt SM, Athanassopoulos A, L. HA, Tsaknakis G. Human Endothelial Stem/Progenitor Cells, Angiogenic Factors And Vascular Repair. J R Soc Interface. 2010;7:S731-S51.
141. Neofytou EA, Chang E, Patlola B, Joubert LM, Rajadas J, Gambhir SS, Et Al. Adipose Tissue-Derived Stem Cells Display A Proangiogenic Phenotype On 3D Scaffolds. Journal Of Biomedical Materials Research Part A. 2011;98(3):383-93. Epub 2011/06/02.
142. Thangarajah H, Vial IN, Chang E, El-Ftesi S, Januszyk M, Chang EI, Et Al. IFATS Collection: Adipose Stromal Cells Adopt A Proangiogenic Phenotype Under The Influence Of Hypoxia. Stem Cells. 2009;27(1):266-74. Epub 2008/11/01.
143. Bae H, Puranik AS, Gauvin R, Edalat F, Carrillo-Conde B, Peppas NA, Et Al. Building Vascular Networks. Science Translational Medicine. 2012;4(160):160ps23. Epub 2012/11/16.
144. Ackermann M, Wolloscheck T, Wellmann A, Li VW, Li WW, Konerding MA. Priming With A Combination Of Proangiogenic Growth Factors Enhances Wound Healing In Streptozotocin-Induced Diabetes In Mice. European Surgical Research Europaische Chirurgische Forschung Recherches Chirurgicales Europeennes. 2011;47(2):81-9. Epub 2011/07/02.
145. Cianfarani F, Tommasi R, Failla CM, Viviano MT, Annessi G, Papi M, Et Al. Granulocyte/Macrophage Colony-Stimulating Factor Treatment Of Human Chronic Ulcers Promotes Angiogenesis Associated With De Novo Vascular Endothelial Growth Factor Transcription In The Ulcer Bed. The British Journal Of Dermatology. 2006;154(1):34-41. Epub 2006/01/13.
146. Anagnostoulis S, Karayiannakis AJ, Lambropoulou M, Efthimiadou A, Polychronidis A, Simopoulos C. Human Leptin Induces Angiogenesis In Vivo. Cytokine. 2008;42(3):353-7. Epub 2008/05/02.
147. Liapakis I, Anagnostoulis S, Karayiannakis A, Korkolis D, Lambropoulou M, Matarasso A, Et Al. Burn Wound Angiogenesis Is Increased By Exogenously Administered Recombinant Leptin In Rats. Acta Cirúrgica Brasileira. 2008;23(2):118-24.
148. Liapakis IE, Anagnostoulis S, Karayiannakis AJ, Korkolis DP, Lambropoulou M, Anastakis D, Et Al. Exogenously-Administered Leptin Increases Early Incisional Wound Angiogenesis In An Experimental Animal Model. In Vivo. 2007;21:797-802.
149. Liapakis IE, Anagnostoulis S, Karayiannakis AJ, Korkolis DP, Lambropoulou M, Arnaud E, Et Al. Recombinant Leptin Administration Improves Early Angiogenesis In Full-Thickness Skin Flaps: An Experimental Study. In Vivo. 2008;22:247-52.
150. Shakespeare P, Shakespeare V. Survey: Use Of Skin Substitute Materials In UK Burn Treatment Centres. Burns. 2002;28:295-7.

151. Jones I, Currie L, Martin R. A Guide To Biological Skin Substitutes. British Journal Of Plastic Surgery. 2002;55(3):185-93. Epub 2002/06/04.
152. Moiemen NS, Vlachou E, Staiano JJ, Thawy Y, Frame JD. Reconstructive Surgery With Integra Dermal Regeneration Template: Histologic Study, Clinical Evaluation, And Current Practice. Plast Reconstr Surg. 2006;117(7 Suppl):160S-74S. Epub 2006/06/27.
153. Moiemen NS, Statiano JJ, Ojeh NO, Thway Y, Frame JD. Reconstructive Surgery With A Dermal Regeneration Template: Clinical And Histologic Study. Plastic And Reconstructive Surgery. 2001;108(1):93-103.
154. Frame JD, Still J, Lakhel-Lecoadou A, Carstens MH, Lorenz C, Orlet H, Et Al. Use Of Dermal Regeneration Template In Contracture Release Procedures: A Multicenter Evaluation. Plastic And Reconstructive Surgery. 2004;113(5):1330-8.
155. Stiefel D, Schiestl C, Meuli M. Integra Artificial Skin For Burn Scar Revision In Adolescents And Children. Burns. 2010;36(1):114-20. Epub 2009/05/30.
156. Waaijman T, Breetveld M, Ulrich M, Middelkoop E, Scheper RJ, Gibbs S. Use Of A Collagen-Elastin Matrix As Transport Carrier System To Transfer Proliferating Epidermal Cells To Human Dermis In Vitro. Cell Transplantation. 2010;19(10):1339-48. Epub 2010/06/08.
157. Lamme EN, De Vries HJ, Van Veen H, Gabbiani G, Westerhof W, Middelkoop E. Extracellular Matrix Characterization During Healing Of Full-Thickness Wounds Treated With A Collagen/Elastin Dermal Substitute Shows Improved Skin Regeneration In Pigs. Journal Of Histochemistry & Cytochemistry. 1996;44(11):1311-22.
158. Bottcher-Haberzeth S, Biedermann T, Schiestl C, Hartmann-Fritsch F, Schneider J, Reichmann E, Et Al. Matriderm(R) 1 Mm Versus Integra(R) Single Layer 1.3 Mm For One-Step Closure Of Full Thickness Skin Defects: A Comparative Experimental Study In Rats. Pediatric Surgery International. 2012;28(2):171-7. Epub 2011/11/08.
159. Haslik W, Kamolz LP, Manna F, Hladik M, Rath T, Frey M. Management Of Full-Thickness Skin Defects In The Hand And Wrist Region: First Long-Term Experiences With The Dermal Matrix Matriderm. Journal Of Plastic, Reconstructive & Aesthetic Surgery : JPRAS. 2010;63(2):360-4. Epub 2008/12/02.
160. Haslik W, Kamolz LP, Nathschlager G, Andel H, Meissl G, Frey M. First Experiences With The Collagen-Elastin Matrix Matriderm As A Dermal Substitute In Severe Burn Injuries Of The Hand. Burns. 2007;33(3):364-8. Epub 2007/01/24.
161. Ryssel H, Gazyakan E, Germann G, Ohlbauer M. The Use Of Matriderm In Early Excision And Simultaneous Autologous Skin Grafting In Burns--A Pilot Study. Burns. 2008;34(1):93-7. Epub 2007/07/24.
162. Ryssel H, Radu CA, Germann G, Otte M, Gazyakan E. Single-Stage Matriderm® And Skin Grafting As An Alternative Reconstruction In High-Voltage Injuries. Int Wound J. 2010;7:385-92.
163. Schneider J, Biedermann T, Widmer D, Montano I, Meuli M, Reichmann E, Et Al. Matriderm Versus Integra: A Comparative Experimental Study. Burns. 2009;35(1):51-7. Epub 2008/10/28.
164. MA_Healthcare_Ltd. Wound Care Handbook. London, UK: MA Healthcare Ltd.; 2011 [Cited 2014 06/03/2014]; Available From: Http://Www.Woundcarehandbook.Com/.
165. Lin CC, Ritch R, Lin SM, Ni M, Chang Y, Lu YL, Et Al. A New Fish Scale-Derived Scaffold For Corneal Regeneration. European Cells And Materials. 2010;19:50-7.
166. Shiratsuchi E, Ura M, Nakaba M, Maeda I, Okamoto K. Elastin Peptides Prepared From Piscine And Mammalian Elastic Tissues Inhibit Collagen-Induced Platelet Aggregation And Stimulate Migration And Proliferation Of Human Skin Fibroblasts. Journal Of Peptide Science : An Official Publication Of The European Peptide Society. 2010;16(11):652-8. Epub 2010/09/21.
167. Nagai T, Suzuki N. Isolation Of Collagen From Fish Waste Material - Skin, Bone And Fins. Food Chemistry. 2000;68:277-81.

168. Sankar S, Sekar S, Mohan R, Rani S, Sundaraseelan J, Sastry TP. Preparation And Partial Characterization Of Collagen Sheet From Fish (Lates Calcarifer) Scales. International Journal Of Biological Macromolecules. 2008;42(1):6-9. Epub 2007/10/16.
169. Hogg P, Rooney P, Ingham E, Kearney JN. Development Of A Decellularised Dermis. Cell And Tissue Banking. 2013;14(3):465-74. Epub 2012/08/10.
170. Freedlander E, Boyce S, Ghosh M, Ralston DR, Macneil S. Skin Banking In The UK: The Need For Proper Organization. Burns. 1998;24:19-24.
171. Deshpande P, Ralston DR, Macneil S. The Use Of Allodermis Prepared From Euro Skin Bank To Prepare Autologous Tissue Engineered Skin For Clinical Use. Burns. 2013;39(6):1170-7. Epub 2013/04/20.
172. Horner CW, Crighton E, Dwiewulski P. Challenges In The Provision Of Skin In The UK: The Use Of Human Deceased Donor Skin In Burn Care Relating To Mass Incidents In The UK. Cell And Tissue Banking. 2013;14(4):579-88. Epub 2013/06/26.
173. Leon-Villapalos J, Eldardiri M, Dziewulski P. The Use Of Human Deceased Donor Skin Allograft In Burn Care. Cell And Tissue Banking. 2010;11(1):99-104. Epub 2010/01/16.
174. Sheridan R, Mahe J, Walters P. Autologous Skin Banking. Burns. 1998;24:46-8.
175. Crapo PM, Gilbert TW, Badylak SF. An Overview Of Tissue And Whole Organ Decellularization Processes. Biomaterials. 2011;32(12):3233-43. Epub 2011/02/08.
176. Gilbert TW, Sellaro TL, Badylak SF. Decellularization Of Tissues And Organs. Biomaterials. 2006;27(19):3675-83. Epub 2006/03/08.
177. Hoshiba T, Lu H, Kawazoe N, Chen G. Decellularized Matrices For Tissue Engineering. Expert Opin Biol Ther. 2010;10(12):1717-28.
178. Weber B, Emmert MY, Schoenauer R, Brokopp C, Baumgartner L, Hoerstrup SP. Tissue Engineering On Matrix: Future Of Autologous Tissue Replacement. Seminars In Immunopathology. 2011;33(3):307-15. Epub 2011/02/01.
179. Gerson CJ, Elkins RC, Goldstein S, Heacox AE. Structural Integrity Of Collagen And Elastin In Synergraft(R) Decellularized-Cryopreserved Human Heart Valves. Cryobiology. 2012;64(1):33-42. Epub 2011/11/29.
180. Kneib C, Von Glehn CQ, Costa FD, Costa MT, Susin MF. Evaluation Of Humoral Immune Response To Donor HLA After Implantation Of Cellularized Versus Decellularized Human Heart Valve Allografts. Tissue Antigens. 2012;80(2):165-74. Epub 2012/05/29.
181. Neumann A, Sarikouch S, Breymann T, Cebotari S, Boethig D, Horke A, Et Al. Early Systemic Cellular Immune Response In Children And Young Adults Receiving Decellularized Fresh Allografts For Pulmonary Valve Replacement. Tissue Engineering Part A. 2014;20(5-6):1003-11. Epub 2013/10/22.
182. Sclafani AP, Mccormick SA, Cocker R. Biophysical And Microscopic Analysis Of Homologous Dermal And Fascial Materials For Facial Aesthetic And Reconstructive Uses. Arch Facial Plast Surg. 2002;4:164-71.
183. Barnes CA, Brison J, Michel R, Brown BN, Castner DG, Badylak SF, Et Al. The Surface Molecular Functionality Of Decellularized Extracellular Matrices. Biomaterials. 2011;32(1):137-43. Epub 2010/11/09.
184. Stefanini MO, Qutub AA, Mac Gabhann F, Popel AS. Computational Models Of VEGF-Associated Angiogenic Processes In Cancer. Mathematical Medicine And Biology : A Journal Of The IMA. 2012;29(1):85-94. Epub 2011/01/27.
185. Verbridge SS, Choi NW, Zheng Y, Brooks DJ, Stroock AD, Fischbach C. Oxygen-Controlled Three-Dimensional Cultures To Analyze Tumor Angiogenesis. Tissue Engineering Part A. 2010;16(7):2133-41.
186. Yao C, Prevel P, Koch S, Schenck P, Noah EM, Pallua N, Et Al. Modification Of Collagen Matrices For Enhancing Angiogenesis. Cells, Tissues, Organs. 2004;178(4):189-96. Epub 2005/04/07.

187. Neumann T, Nicholson BS, Sanders JE. Tissue Engineering Of Perfused Microvessels. Microvascular Research. 2003;66:59-67.
188. Volkmer E, Drosse I, Otto S, Stangelmayer A, Stengele M, Kallukalam BC, Et Al. Hypoxia In Static And Dynamic 3D Culture Systems For Tissue Engineering Of Bone. Tissue Engineering Part A. 2008;14(8):1331- 40.
189. Volkmer E, Otto S, Polzer H, Saller M, Trappendreher D, Zagar D, Et Al. Overcoming Hypoxia In 3D Culture Systems For Tissue Engineering Of Bone In Vitro Using An Automated, Oxygen-Triggered Feedback Loop. Journal Of Materials Science Materials In Medicine. 2012;23:2793-801.
190. Provin C, Takano K, Sakai Y, Fujii T, Shirakashi R. A Method For The Design Of 3D Scaffolds For High-Density Cell Attachment And Determination Of Optimum Perfusion Culture Conditions. Journal Of Biomechanics. 2008;41:1436-49.
191. Bettahalli NMS, Vicente J, Moroni L, Higuera GA, Van Blitterswijk CA, Wessling M, Et Al. Integration Of Hollow Fiber Membranes Improves Nutrient Supply In Three-Dimensional Tissue Constructs. Acta Biomaterialia. 2011;7:3312-24.
192. Chen P, Yang K, Wu C, Yu J, Lin F, Sun J. Fabrication Of Large Perfusable Macroporous Cell-Laden Hydrogel Scaffolds Using Microbial Transglutaminase. Acta Biomaterialia. 2014;10:912-20.
193. Yuen PK, Su H, Goral VN, Fink KA. Three-Dimensional Interconnected Microporous Poly(Dimethylsiloxane) Microfluidic Devices. Lab On A Chip. 2011;11:1541-4.
194. Takemoto S, Morimoto N, Kimura Y, Taira T, Kitagawa T, Tomihata K, Et Al. Preparation Of Collagen/Gelatin Sponge Scaffold For Sustained Release Of Bfgf. Tissue Engineering Part A. 2008;14(10):1629-38. Epub 2008/06/27.
195. Kitagawa T, Yamaoka T, Iwase R, Murakami A. Three-Dimensional Cell Seeding And Growth In Radial-Flow Perfusion Bioreactor For In Vitro Tissue Reconstruction. Biotechnology And Bioengineering. 2006;93(5):947-54.
196. Sugiura S, Sakai Y, Nakazawa K, Kanamori T. Superior Oxygen And Glucose Supply In Perfusion Cell Cultures Compared To Static Cell Cultures Demonstrated By Simulations Using The Finite Element Method. Biomicrofluidics. 2011;5:1-11.
197. Chin K, Khattak SF, Bhatia SR, Roberts SC. Hydrogel-Perfluorocarbon Composite Scaffold Promotes Oxygen Transport To Immobilized Cells. Biotechnol Prog. 2008;24:358-66.
198. Tan Q, El-Badry AM, Contaldo C, Steiner R, Hillinger S, Welti M, Et Al. The Effect Of Perfluorocarbon-Based Artificial Oxygen Carriers On Tissue-Engineered Trachea. Tissue Engineering Part A. 2009;15(9):2471-80.
199. Demaison C, Parsley K, Brouns G, Scherr M, Battmer K, Kinnon C, Et Al. High-Level Transduction And Gene Expression In Hematopoietic Repopulating Cells Using A Human Imunodeficiency Virus Type 1-Based Lentiviral Vector Containing An Internal Spleen Focus Forming Virus Promoter. Human Gene Therapy. 2002;13(7):803-13.
200. Vincze T. Nebcutter: A Program To Cleave DNA With Restriction Enzymes. Nucleic Acids Research. 2003;31(13):3688-91.
201. Lin P, Correa D, Lin Y, Caplan AI. Polybrene Inhibits Human Mesenchymal Stem Cell Proliferation During Lentiviral Transduction. Plos One. 2011;6(8):E23891.
202. Van Besien K. Allogeneic Transplantation For AML And MDS: GVL Versus GVHD And Disease Recurrence. Hematology. 2013;2013:56-62.
203. Tong J, Sun Z, Liu H, Geng L, Zheng C, Tang B, Et Al. Risk Factors Of CMV Infection In Patients After Umbilical Cord Blood Transplantation: A Multicenter Study In China. Chinese Journal Of Cancer Research = Chung-Kuo Yen Cheng Yen Chiu. 2013;25(6):695-703. Epub 2014/01/05.
204. Coldwell KE, Lee SJ, Kean J, Khoo CP, Tsaknakis G, Smythe J, Et Al. Effects Of Obstetric Factors And Storage Temperatures On The Yield Of Endothelial Colony Forming Cells From Umbilical Cord Blood. Angiogenesis. 2011;14(3):381-92. Epub 2011/07/02.

205. Traktuev DO, Merfeld-Clauss S, Li J, Kolonin M, Arap W, Pasqualini R, Et Al. A Population Of Multipotent CD34-Positive Adipose Stromal Cells Share Pericyte And Mesenchymal Surface Markers, Reside In A Periendothelial Location, And Stabilize Endothelial Networks. Circulation Research. 2008;102(1):77-85. Epub 2007/10/31.
206. Ålgars A, Karikoski M, Yegutkin GG, Stoitzner P, Niemelä J, Salmi M, Et Al. Different Role Of CD73 In Leukocyte Trafficking Via Blood And Lymph Vessels. Blood. 2011;117:4387-93.
207. Ode A, Kopf J, Kurtz A, Schmidt-Bleek K, Schrade P, Kolar P, Et Al. CD73 And CD29 Concurrently Mediate The Mechanically Induced Decrease Of Migratory Capacity Of Mesenchymal Stromal Cells. European Cells And Materials. 2011;22:26-42.
208. Balza E, Castellani P, Zijlstra A, Neri D, Zardi L, Siri A. LACK OF SPECIFICITY OF ENDOGLIN EXPRESSION FOR TUMOR BLOOD VESSELS. International Journal Of Cancer. 2001;94:579-85.
209. Barbara NP, Wrana JL, Letarte M. Endoglin Is An Accessory Protein That Interacts With The Signaling Receptor Complex Of Multiple Members Of The Transforming Growth Factor-B Superfamily. The Journal Of Biological Chemistry. 1999;274(2):584-94.
210. Garonna E, Botham KM, Birdsey GM, Randi AM, Gonzalez-Perez RR, Wheeler-Jones CP. Vascular Endothelial Growth Factor Receptor-2 Couples Cyclo-Oxygenase-2 With Pro-Angiogenic Actions Of Leptin On Human Endothelial Cells. Plos One. 2011;6(4):E18823. Epub 2011/05/03.
211. Smadja DM, Bieche I, Helley D, Laurendeau I, Simonin G, Muller L, Et Al. Increased VEGFR2 Expression During Human Late Endothelial Progenitor Cells Expansion Enhances In Vitro Angiogenesis With Up-Regulation Of Integrin Alpha(6). Journal Of Cellular And Molecular Medicine. 2007;11(5):1149-61. Epub 2007/11/06.
212. Ziegler BL. KDR Receptor: A Key Marker Defining Hematopoietic Stem Cells. Science. 1999;285(5433):1553-8.
213. Minhas N, Xue M, Fukudome K, Jackson CJ. Activated Protein C Utilizes The Angiopoietin/Tie2 Axis To Promote Endothelial Barrier Function. FASEB Journal : Official Publication Of The Federation Of American Societies For Experimental Biology. 2010;24(3):873-81. Epub 2009/10/28.
214. Yuasa H, Takakura N, Shimomura T, Suenobu S, Yamada T, Nagayama H, Et Al. Analysis Of Human TIE2 Function On Hematopoietic Stem Cells In Umbilical Cord Blood. Biochemical And Biophysical Research Communications. 2002;298:731-7.
215. Walenta K, Friedrich EB, Sehnert F, Werner N, Nickenig G. In Vitro Differentiation Characteristics Of Cultured Human Mononuclear Cells-Implications For Endothelial Progenitor Cell Biology. Biochemical And Biophysical Research Communications. 2005;333(2):476-82. Epub 2005/06/18.
216. Antal-Szalma´S P, Poppelier MJJG, Broekhuizen R, Verhoef J, Van Strijp JAG, Van Kessel KPM. Diverging Pathways For Lipopolysaccharide And CD14 In Human Monocytes. Cytometry. 2000;41:279-88.
217. Koumas L, Smith TJ, Feldon S, Blumberg N, Phipps RP. Thy-1 Expression In Human Fibroblast Subsets Defines Myofibroblastic Or Lipofibroblastic Phenotypes. American Journal Of Pathology. 2003;163(4):1291-300.
218. Bauer N, Wilsch-Brauninger M, Karbanova J, Fonseca AV, Strauss D, Freund D, Et Al. Haematopoietic Stem Cell Differentiation Promotes The Release Of Prominin-1/CD133-Containing Membrane Vesicles--A Role Of The Endocytic-Exocytic Pathway. EMBO Molecular Medicine. 2011;3(7):398-409. Epub 2011/05/19.
219. Corbeil D, Marzesco AM, Wilsch-Brauninger M, Huttner WB. The Intriguing Links Between Prominin-1 (CD133), Cholesterol-Based Membrane Microdomains, Remodeling Of Apical Plasma Membrane Protrusions, Extracellular Membrane Particles, And (Neuro)Epithelial Cell Differentiation. FEBS Letters. 2010;584(9):1659-64. Epub 2010/02/04.

220. Pellacani D, Packer RJ, Frame FM, Oldridge EE, Berry PA, Labarthe MC, Et Al. Regulation Of The Stem Cell Marker CD133 Is Independent Of Promoter Hypermethylation In Human Epithelial Differentiation And Cancer. Molecular Cancer. 2011;10:94. Epub 2011/08/02.
221. Rustemeyer P, Wittkowski W, Greve B, Stehling M. Flow-Cytometric Identification, Enumeration, Purification, And Expansion Of CD133+ And VEGF-R2+ Endothelial Progenitor Cells From Peripheral Blood. Journal Of Immunoassay & Immunochemistry. 2007;28(1):13-23. Epub 2007/01/24.
222. Falkenberg H, Radke TF, Kogler G, Stuhler K. Proteomic Profiling Of Ex Vivo Expanded CD34-Positive Haematopoetic Cells Derived From Umbilical Cord Blood. Stem Cells International. 2013;2013:245695. Epub 2013/04/23.
223. Ballen KK, Wilson M, Wuu J, Ceredona AM, Hsieh C, Stewart FM, Et Al. Bigger Is Better: Maternal And Neonatal Predictors Of Hematopoietic Potential Of Umbilical Cord Blood Units. Bone Marrow Transplantation. 2001;27:7-14.
224. Chandra T, Afreen S, Kumar A, Singh U, Gupta A. Does Umbilical Cord Blood-Derived CD34+ Cell Concentration Depend On The Weight And Sex Of A Full-Term Infant? J Pediatr Haematol Oncol. 2012;34(3):184-7.
225. Afrakhteh M, Moeini A, Taheri MS, Haghghatkhah HR. Correlation Between Placental Thickness In The Second And Third Trimester And Fetal Weight. Rev Bras Ginecol Obstet. 2013;35(7):317-22.
226. Effendi M, Demers S, Giguere Y, Forest JC, Brassard N, Girard M, Et Al. Association Between First-Trimester Placental Volume And Birth Weight. Placenta. 2013. Epub 2013/12/19.
227. Haeussner E, Schmitz C, Von Koch F, Frank HG. Birth Weight Correlates With Size But Not Shape Of The Normal Human Placenta. Placenta. 2013;34(7):574-82. Epub 2013/05/16.
228. Pathak S, Jessop F, Hook L, Sebire NJ, Lees CC. Placental Weight, Digitally Derived Placental Dimensions At Term And Their Relationship To Birth Weight. The Journal Of Maternal-Fetal & Neonatal Medicine : The Official Journal Of The European Association Of Perinatal Medicine, The Federation Of Asia And Oceania Perinatal Societies, The International Society Of Perinatal Obstet. 2010;23(10):1176-82. Epub 2010/03/04.
229. Ingram D, Mead L, Tanaka H, Meade V, Fenoglio A, Mortell K, Et Al. Identification Of A Novel Hierarchy Of Endothelial Progenitor Cells Using Human Peripheral And Umbilical Cord Blood. Blood. 2004;104(9):2752-60.
230. Nuzzolo ER, Capodimonti S, Martini M, Iachininoto MG, Bianchi M, Cocomazzi A, Et Al. Adult And Cord Blood Endothelial Progenitor Cells Have Different Gene Expression Profiles And Immunogenic Potential. Blood Transfusion = Trasfusione Del Sangue. 2013:1-8. Epub 2013/07/23.
231. Cheuk DK. Optimal Stem Cell Source For Allogeneic Stem Cell Transplantation For Hematological Malignancies. World Journal Of Transplantation. 2013;3(4):99-112. Epub 2014/01/07.
232. Metheny L, Caimi P, De Lima M. Cord Blood Transplantation: Can We Make It Better? Frontiers In Oncology. 2013;3:238. Epub 2013/09/26.
233. Oran B, Shpall E. Umbilical Cord Blood Transplantation: A Maturing Technology. Hematology. 2012;2012:215-22.
234. Passweg JR, Baldomero H, Bregni M, Cesaro S, Dreger P, Duarte RF, Et Al. Hematopoietic SCT In Europe: Data And Trends In 2011. Bone Marrow Transplantation. 2013;48(9):1161-7. Epub 2013/04/16.
235. Rao M, Ahrlund-Richter L, Kaufman DS. Concise Review: Cord Blood Banking, Transplantation And Induced Pluripotent Stem Cell: Success And Opportunities. Stem Cells. 2012;30:55-60.

236. Acosta SA, Franzese N, Staples M, Weinbren NL, Babilonia M, Patel J, Et Al. Human Umbilical Cord Blood For Transplantation Therapy In Myocardial Infarction. J Stem Cell Res Ther. 2013;Jul 1((Suppl 4)):S4-005.
237. Butler MG, Menitove JE. Umbilical Cord Blood Banking: An Update. Journal Of Assisted Reproduction And Genetics. 2011;28(8):669-76. Epub 2011/05/28.
238. Donaldson C, Buchanan R, Webster J, Laundy V, Horsley H, Barron C, Et Al. Development Of A District Cord Blood Bank: A Model For Cord Blood Banking In The National Health Service. Bone Marrow Transplantation. 2000;25:899-905.
239. Lubin BH, Shearer WT. Cord Blood Banking For Potential Future Transplantation. Pediatrics. 2007;119(1):165-70. Epub 2007/01/04.
240. Smythe J, Armitage S, Mcdonald D, Pamphilon D, Guttridge M, Brown J, Et Al. Directed Sibling Cord Blood Banking For Transplantation: The 10-Year Experience In The National Blood Service In England. Stem Cells. 2007;25(8):2087-93. Epub 2007/05/19.
241. Moon SH, Kim SM, Park SJ, Kim H, Bae D, Choi YS, Et Al. Development Of A Xeno-Free Autologous Culture System For Endothelial Progenitor Cells Derived From Human Umbilical Cord Blood. Plos One. 2013;8(9):E75224. Epub 2013/10/03.
242. Bieback K. Platelet Lysate As Replacement For Fetal Bovine Serum In Mesenchymal Stromal Cell Cultures. Transfusion Medicine And Hemotherapy : Offizielles Organ Der Deutschen Gesellschaft Fur Transfusionsmedizin Und Immunhamatologie. 2013;40(5):326-35. Epub 2013/11/26.
243. Rauch C, Feifel E, Amann E, Spotl HP, Schennack H, Pfaller W, Et Al. Alternatives To The Use Of Fetal Bovine Serum: Human Platelet Lysates As A Serum Substitute In Cell Culture Media. Altex. 2011;28(4/11):305-16.
244. Dos Santos F, Campbell A, Fernandes-Platzgummer A, Andrade PZ, Gimble JM, Wen Y, Et Al. A Xenogeneic-Free Bioreactor System For The Clinical-Scale Expansion Of Human Mesenchymal Stem/Stromal Cells. Biotechnology And Bioengineering. 2014. Epub 2014/01/15.
245. Dos Santos FF, Andrade PZ, Da Silva CL, Cabral JMS. Bioreactor Design For Clinical-Grade Expansion Of Stem Cells. Biotechnol J. 2013;8:644-54.
246. Nold P, Brendel C, Neubauer A, Bein G, Hackstein H. Good Manufacturing Practice-Compliant Animal-Free Expansion Of Human Bone Marrow Derived Mesenchymal Stroma Cells In A Closed Hollow-Fiber-Based Bioreactor. Biochemical And Biophysical Research Communications. 2013;430(1):325-30. Epub 2012/11/14.
247. Blondeel PN, Boeckx WD. Refinements In Free Flap Breast Reconstruction : The Free Bilateral Deep Inferior Epigastric Perforator Flap Anastomosed To The Internal Mammary Artery. British Journal Of Plastic Surgery. 1994;47:495-501.
248. Blondeel PN. One Hundred Free DIEP Flap Breast Reconstructions: A Personal Experience. British Journal Of Plastic Surgery. 1999;52:104–11.
249. Blondeel PN, Beyens G, Verhaeghe R, Van Landuyt K, Tonnard R, Monstrey SJ, Et Al. Doppler Flowmetry In The Planning Of Perforator Flaps. British Journal Of Plastic Surgery. 1998;51:202-09.
250. Xue S, Zhang H, Zhang P, Luo J, Chen Z, Jang X, Et Al. Functional Endothelial Progenitor Cells Derived From Adipose Tissue Show Beneficial Effect On Cell Therapy Of Traumatic Brain Injury. Neuroscience Letters. 2010;473:186-91.
251. D'ARENA G, MUSTO P, CASCAVILLA N, DI GIORGIO G, FUSILLI S, ZENDOLI F, Et Al. Flow Cytometric Characterization Of Human Umbilical Cord Blood Lymphocytes: Immunophenotypic Features. Haematologica. 1998;83:197-203.
252. Keating A. Mesenchymal Stromal Cells: New Directions. Cell Stem Cell. 2012;10(6):709-16. Epub 2012/06/19.
253. Amos PJ, Shang H, Bailey AM, Taylor A, Katz AJ, Peirce SM. IFATS Collection: The Role Of Human Adipose-Derived Stromal Cells In Inflammatory Microvascular Remodeling And Evidence Of A Perivascular Phenotype. Stem Cells. 2008;26:2682–90.

254. Fischer LJ, Mcilhenny S, Tulenko T, Golesorkhi N, Zhang P, Larson R, Et Al. Endothelial Differentiation Of Adipose-Derived Stem Cells: Effects Of Endothelial Cell Growth Supplement And Shear Force. The Journal Of Surgical Research. 2009;152(1):157-66. Epub 2009/11/04.
255. Lee EY, Xia Y, Kim WS, Kim MH, Kim TH, Kim KJ, Et Al. Hypoxia-Enhanced Wound-Healing Function Of Adipose-Derived Stem Cells: Increase In Stem Cell Proliferation And Up-Regulation Of VEGF And Bfgf. Wound Repair And Regeneration : Official Publication Of The Wound Healing Society [And] The European Tissue Repair Society. 2009;17(4):540-7. Epub 2009/07/21.
256. Meruane MA, Rojas M, Marcelain K. The Use Of Adipose Tissue-Derived Stem Cells Within A Dermal Substitute Improves Skin Regeneration By Increasing Neoangiogenesis And Collagen Synthesis. Plast Reconstr Surg. 2012;130(1):53-63. Epub 2012/03/16.
257. Murohara T. Autologous Adipose Tissue As A New Source Of Progenitor Cells For Therapeutic Angiogenesis. Journal Of Cardiology. 2009;53(2):155-63. Epub 2009/03/24.
258. Crisan M, Yap S, Casteilla L, Chen CW, Corselli M, Park TS, Et Al. A Perivascular Origin For Mesenchymal Stem Cells In Multiple Human Organs. Cell Stem Cell. 2008;3(3):301-13. Epub 2008/09/13.
259. Feng J, Mantesso A, Sharpe PT. Perivascular Cells As Mesenchymal Stem Cells. Expert Opin Biol Ther. 2010;10(10):1441-51.
260. Chen CW, Corselli M, Peault B, Huard J. Human Blood-Vessel-Derived Stem Cells For Tissue Repair And Regeneration. Journal Of Biomedicine & Biotechnology. 2012;2012:597439. Epub 2012/04/14.
261. Chen WC, Park TS, Murray IR, Zimmerlin L, Lazzari L, Huard J, Et Al. Cellular Kinetics Of Perivascular MSC Precursors. Stem Cells International. 2013;2013:983059. Epub 2013/09/12.
262. Corselli M, Chen CW, Crisan M, Lazzari L, Peault B. Perivascular Ancestors Of Adult Multipotent Stem Cells. Arteriosclerosis, Thrombosis, And Vascular Biology. 2010;30(6):1104-9. Epub 2010/05/11.
263. Corselli M, Chin CJ, Parekh C, Sahaghian A, Wang W, Ge S, Et Al. Perivascular Support Of Human Hematopoietic Stem/Progenitor Cells. Blood. 2013;121:2891-901.
264. Corselli M, Crisan M, Murray IR, West CC, Scholes J, Codrea F, Et Al. Identification Of Perivascular Mesenchymal Stromal/Stem Cells By Flow Cytometry. Cytometry Part A. 2013;83A:714-20.
265. Crisan M, Corselli M, Chen CW, Peault B. Multilineage Stem Cells In The Adult: A Perivascular Legacy? Organogenesis. 2011;7(2):101-4. Epub 2011/05/20.
266. Crisan M, Corselli M, Chen WC, Peault B. Perivascular Cells For Regenerative Medicine. Journal Of Cellular And Molecular Medicine. 2012;16(12):2851-60. Epub 2012/08/14.
267. James AW, Zara JN, Zhang X, Askarinam A, Goyal R, Chiang M, Et Al. Perivascular Stem Cells: A Prospectively Purified Mesenchymal Stem Cell Population For Bone Tissue Engineering. Stem Cells Translational Medicine. 2012;1(6):510-9. Epub 2012/12/01.
268. Mravic M, Asatrian G, Soo C, Lugassy C, Barnhill RL, Dry SM, Et Al. From Pericytes To Perivascular Tumours: Correlation Between Pathology, Stem Cell Biology, And Tissue Engineering. International Orthopaedics. 2014. Epub 2014/02/26.
269. Murray IR, Corselli M, Petrigliano FA, Soo C, Peault B. Recent Insights Into The Identity Of Mesenchymal Stem Cells: Implications For Orthopaedic Applications. Bone Joint J. 2014;96(B):291-8.
270. Murray IR, West CC, Hardy WR, James AW, Park TS, Nguyen A, Et Al. Natural History Of Mesenchymal Stem Cells, From Vessel Walls To Culture Vessels. Cellular And Molecular Life Sciences : CMLS. 2014;71(8):1353-74. Epub 2013/10/26.
271. Corselli M, Chen CW, Sun B, Yap S, Rubin JP, Peault B. The Tunica Adventitia Of Human Arteries And Veins As A Source Of Mesenchymal Stem Cells. Stem Cells And Development. 2012;21(8):1299-308. Epub 2011/08/25.

272. Staton CA, Reed MW, Brown NJ. A Critical Analysis Of Current In Vitro And In Vivo Angiogenesis Assays. International Journal Of Experimental Pathology. 2009;90(3):195-221. Epub 2009/07/01.
273. Arnaoutova I, George J, Kleinman HK, Benton G. The Endothelial Cell Tube Formation Assay On Basement Membrane Turns 20: State Of The Science And The Art. Angiogenesis. 2009;12(3):267-74. Epub 2009/04/29.
274. Khoo CP, Micklem K, Watt SM. A Comparison Of Methods For Quantifying Angiogenesis In The Matrigel Assay In Vitro. Tissue Engineering Part C, Methods. 2011;17(9):895-906. Epub 2011/04/27.
275. Kleinman HK, Martin GR. Matrigel: Basement Membrane Matrix With Biological Activity. Seminars In Cancer Biology. 2005;15(5):378-86. Epub 2005/06/25.
276. Twentyman PR, Luscombe M. A Study Of Some Variables In A Tetrazolium Dye (MTT) Based Assay For Cell Growth And Chemosensitivity. Br J Cancer. 1987;56:279-85.
277. Fruhbeck G. Intracellular Signalling Pathways Activated By Leptin. The Biochemical Journal. 2006;393(Pt 1):7-20. Epub 2005/12/13.
278. Lu H, Li C. Leptin: A Multifunctional Hormone. Cell Research. 2000;10:81- 92.
279. Cao R, Brakenhielm E, Wahlestedt C, Thyberg J, Cao Y. Leptin Induces Vascular Permeability And Synergistically Stimulates Angiogenesis With FGF-2 And VEGF. Proceedings Of The National Academy Of Sciences Of The United States Of America. 2001;98(11):6390-5. Epub 2001/05/10.
280. Goetze S. Leptin Induces Endothelial Cell Migration Through Akt, Which Is Inhibited By Ppargamma-Ligands. Hypertension. 2002;40(5):748-54.
281. Jin X. Effects Of Leptin On Endothelial Function With OB-Rb Gene Transfer In Zucker Fatty Rats. Atherosclerosis. 2003;169(2):225-33.
282. Wolk R, Deb A, Caplice NM, Somers VK. Leptin Receptor And Functional Effects Of Leptin In Human Endothelial Progenitor Cells. Atherosclerosis. 2005;183(1):131-9. Epub 2005/06/14.
283. Hanft JR, Pollak RA, Barbul A, Van Gils C, Kwon PS, Gray SM, Et Al. Phase I Trial On The Safety Of Topical Rhvegf On Chronic Neuropathic Diabetic Foot Ulcers. J Wound Care. 2008;17(1):30-2, 4-7.
284. Deng L, Chen N, Li Y, Zheng H, Lei Q. CXCR6/CXCL16 Functions As A Regulator In Metastasis And Progression Of Cancer. Biochimica Et Biophysica Acta. 2010;1806(1):42-9. Epub 2010/02/04.
285. Darash-Yahana M, Gillespie JW, Hewitt SM, Chen YY, Maeda S, Stein I, Et Al. The Chemokine CXCL16 And Its Receptor, CXCR6, As Markers And Promoters Of Inflammation-Associated Cancers. Plos One. 2009;4(8):E6695. Epub 2009/08/20.
286. Eterno V, Zambelli A, Pavesi L, Villani L, Zanini V, Petrolo G, Et Al. Adipose-Derived Mesenchymal Stem Cells (Ascs) May Favour Breast Cancer Recurrence Via HGF/C-Met Signaling. Oncotarget. 2013;5(3):613-33.
287. Xu Z, Wang S, Wu M, Zeng W, Wang X, Dong Z. Tgfbeta1 And HGF Protein Secretion By Esophageal Squamous Epithelial Cells And Stromal Fibroblasts In Oesophageal Carcinogenesis. Oncology Letters. 2013;6(2):401-6. Epub 2013/10/19.
288. Goyal L, Muzumdar MD, Zhu AX. Targeting The HGF/C-MET Pathway In Hepatocellular Carcinoma. Clinical Cancer Research : An Official Journal Of The American Association For Cancer Research. 2013;19(9):2310-8. Epub 2013/02/08.
289. Ge X, Wang Y, Li Q, Yu H, Miao L. NK4 Gene Therapy Inhibits HGF/Met-Induced Growth Of Human Cholangiocarcinoma Cells. Digestive Diseases And Sciences. 2013;58(6):1636-43. Epub 2013/01/15.
290. Hoshiko S, Kawaguchi M, Fukushima T, Haruyama Y, Yorita K, Tanaka H, Et Al. Hepatocyte Growth Factor Activator Inhibitor Type 1 Is A Suppressor Of Intestinal Tumorigenesis. Cancer Research. 2013;73(8):2659-70. Epub 2013/03/01.

291. Vilen ST, Salo T, Sorsa T, Nyberg P. Fluctuating Roles Of Matrix Metalloproteinase-9 In Oral Squamous Cell Carcinoma. Thescientificworldjournal. 2013;2013:920595. Epub 2013/02/01.
292. Xu Y-B, Du Q-H, Zhang M-Y, Yun P, He C-Y. Propofol Suppresses Proliferation, Invasion And Angiogenesis By Down-Regulating ERK-VEGF/MMP-9 Signaling In Eca-109 Esophageal Squamous Cell Carcinoma Cells. Eur Rev Med Pharmacol Sci. 2013;17:2486-94.
293. Jia W, Gao X-J, Zhang Z-D, Yang Z-X, Zhang G. S100A4 Silencing Suppresses Proliferation, Angiogenesis And Invasion Of Thyroid Cancer Cells Through Downregulation Of MMP-9 And VEGF. Eur Rev Med Pharmacol Sci. 2013;17:1495-508.
294. Wang X, Lee SO, Xia S, Jiang Q, Luo J, Li L, Et Al. Endothelial Cells Enhance Prostate Cancer Metastasis Via IL-6-->Androgen Receptor-->TGF-Beta-->MMP-9 Signals. Molecular Cancer Therapeutics. 2013;12(6):1026-37. Epub 2013/03/29.
295. Haycock JW. 3D Cell Culture: A Review Of Current Approaches And Techniques. Methods Mol Biol. 2011;695:1-15. Epub 2010/11/03.
296. Scherberich A, Galli R, Jaquiery C, Farhadi J, Martin I. Three-Dimensional Perfusion Culture Of Human Adipose Tissue-Derived Endothelial And Osteoblastic Progenitors Generates Osteogenic Constructs With Intrinsic Vascularization Capacity. Stem Cells. 2007;25(7):1823-9. Epub 2007/04/21.
297. Chang NJ, Lam CF, Lin CC, Chen WL, Li CF, Lin YT, Et Al. Transplantation Of Autologous Endothelial Progenitor Cells In Porous PLGA Scaffolds Create A Microenvironment For The Regeneration Of Hyaline Cartilage In Rabbits. Osteoarthritis And Cartilage / OARS, Osteoarthritis Research Society. 2013;21(10):1613-22. Epub 2013/08/10.
298. Curran JM, Fawcett S, Hamilton L, Rhodes NP, Rahman CV, Alexander M, Et Al. The Osteogenic Response Of Mesenchymal Stem Cells To An Injectable PLGA Bone Regeneration System. Biomaterials. 2013;34(37):9352-64. Epub 2013/09/21.
299. Wang W, Cao B, Cui L, Cai J, Yin J. Adipose Tissue Engineering With Human Adipose Tissue-Derived Adult Stem Cells And A Novel Porous Scaffold. Journal Of Biomedical Materials Research Part B, Applied Biomaterials. 2013;101(1):68-75. Epub 2012/10/24.
300. Athanassopoulos A, Tsaknakis G, Newey SE, Harris AL, Kean J, Tyler MP, Et Al. Microvessel Networks [Corrected] Pre-Formed In Artificial Clinical Grade Dermal Substitutes In Vitro Using Cells From Haematopoietic Tissues. Burns. 2012;38(5):691-701. Epub 2012/03/01.
301. Zhang X, Yang J, Li Y, Liu S, Long K, Zhao Q, Et Al. Functional Neovascularization In Tissue Engineering With Porcine Acellular Dermal Matrix And Human Umbilical Vein Endothelial Cells. Tissue Engineering Part C, Methods. 2011;17(4):423-33. Epub 2010/11/11.
302. Greaves NS, Benatar B, Baguneid M, Bayat A. Single-Stage Application Of A Novel Decellularized Dermis For Treatment-Resistant Lower Limb Ulcers: Positive Outcomes Assessed By Siascopy, Laser Perfusion, And 3D Imaging, With Sequential Timed Histological Analysis. Wound Repair And Regeneration : Official Publication Of The Wound Healing Society [And] The European Tissue Repair Society. 2013. Epub 2013/10/19.
303. Bauer SM. Angiogenesis, Vasculogenesis, And Induction Of Healing In Chronic Wounds. Vascular And Endovascular Surgery. 2005;39(4):293-306.
304. Watt SM, Gullo F, Van Der Garde M, Markeson D, Camicia R, Khoo CP, Et Al. The Angiogenic Properties Of Mesenchymal Stem/Stromal Cells And Their Therapeutic Potential. British Medical Bulletin. 2013;108:25-53. Epub 2013/10/25.
305. Carretero M, Guerrero-Aspizua S, Del Rio M. Applicability Of Bioengineered Human Skin: From Preclinical Skin Humanized Mouse Models To Clinical Regenerative Therapies. Bioengineered Bugs. 2011;2(4):203-7.
306. Gauvin R, Chen YC, Lee JW, Soman P, Zorlutuna P, Nichol JW, Et Al. Microfabrication Of Complex Porous Tissue Engineering Scaffolds Using 3D Projection Stereolithography. Biomaterials. 2012;33(15):3824-34. Epub 2012/03/01.

307. Grogan SP, Chung PH, Soman P, Chen P, Lotz MK, Chen S, Et Al. Digital Micromirror Device Projection Printing System For Meniscus Tissue Engineering. Acta Biomaterialia. 2013;9(7):7218-26. Epub 2013/03/26.
308. Sheridan WS, Grant OB, Duffy GP, Murphy BP. The Application Of A Thermoresponsive Chitosan/Beta-GP Gel To Enhance Cell Repopulation Of Decellularized Vascular Scaffolds. Journal Of Biomedical Materials Research Part B, Applied Biomaterials. 2014. Epub 2014/03/26.

Appendix 1

Stoke Mandeville Hospital
Mandeville Road
Aylesbury
Buckinghamshire
HP21 8AL
Tel: 01296 315 000
www.buckinghamshirehospitals.nhs.uk

Patient Information Sheet B

Research Study – Stem and Progenitor Cells in Wound Healing

We would like to invite you to take part in our research study. Before you decide we would like you to understand why the research is being done and what it would involve for you.

At your next hospital visit, one of our team will go through the information sheet with you in person and answer any questions you have. We'd suggest this should take about 10 minutes.

Talk to others about the study if you wish.

Part 1 tells you the purpose of this study and what will happen to you if you take part.

Part 2 gives you more detailed information about the conduct of the study.

Ask us if there is anything that is not clear.

Part 1

What is the purpose of the study?

The purpose of the study is to find out if cells capable of building new blood vessels (stem and progenitor cells) can be grown from fat. We would like to compare these to similar cells grown from blood. In the future these cells could be used in treatments to improve wound healing and scarring.

Why have I been invited?

You have been selected as a potential participant because you are having a breast reconstruction operation, during which some of your body fat will be removed and discarded.

Do I have to take part?

No. It is up to you to decide to join the study. We will describe the study and go through this information sheet. If you agree to take part, we will then ask you to sign a consent form. You are free to withdraw at any time, without giving a reason. This would not affect the standard of care you receive.

What will happen to me if I take part?

When your tummy tissue is harvested to make your new breast a corner of fat is normally discarded. This is because we know it does not have as good a blood flow as the rest of the tissue. If you agree to take part in the study, your operation will proceed as normal, but instead of disposing of the discarded corner of fat removed during your operation as waste, it will be collected in a sample container and taken to the stem cell research laboratory in Oxford.

Whilst you are under anaesthetic, a 50ml blood sample would be taken from a vein. This is approximately one tenth of the amount of blood given in a routine blood bank donation and should not cause you any potential harm, although you may notice a small bruise as with any blood test. This blood sample would also be taken to the stem cell research laboratory in Oxford.

You do not need to do anything else, and there is no change to your recovery or post operative follow up.

The clinical researcher is a plastic surgery doctor who will have access to your medical records at the time of sample

collection for the purpose of obtaining general information about your health and operation.

What are the possible disadvantages and risks of taking part?

The blood test may cause a small bruise as with any blood sample taken.

What are the possible benefits of taking part?

There are no direct benefits to you by taking part in the study, but information from the study may be used to develop treatments to improve wound healing and scarring in the future.

What happens when the research study stops?

At the end of the study, processed samples will be stored in the stem cell research laboratory in case there is any need to recheck results in the future.

What if there is a problem?

Any complaint about the way you have been dealt with during the study will be addressed. The detailed information on this is given in Part 2.

Will my taking part in the study be kept confidential?

Yes. We will follow ethical and legal practice and all information about you will be handled in confidence. The details are included in Part 2.

If the information in Part 1 has interested you and you are considering participation, please read the additional information in Part 2 before making any decision.

Part 2

What will happen if I don't want to carry on with the study?

If you change your mind about taking part in the study once the fat and blood samples have been collected, you can choose to withdraw your consent within two weeks of your operation and the samples will be disposed of as waste in the manner usually undertaken at operation. After this time the samples will have completed the first stage of processing and results will have already been generated. If you wish to withdraw consent please call 01865387916 to speak to Miss Jennifer Kean.

What if there is a problem?

If you have a concern about any aspect of this study, you should ask to speak to the researchers who will do their best to answer your questions [Tel: 01865387916, Miss Jennifer Kean]. If you remain unhappy and wish to make a complaint, you can do this via the Patient Advice and Liaison Service (PALS). Details can be obtained from www.pals.nhs.uk or you can telephone the Stoke Mandeville Hospital PALS on 01494 425882.

Will my taking part in this study be kept confidential?

When the fat and blood samples are collected they will be labelled with an identification number as there is no need for anyone outside the hospital team to identify you. The clinical researcher will keep a list of sample numbers and the corresponding participant details in a separate

password protected file on an NHS computer. All information which is collected about you during the course of the research will be kept strictly confidential, and any information about you which leaves the hospital will have your name and address removed so that you cannot be recognised.

What will happen to any samples I give?

In the lab, the fat and blood samples will be processed by mechanical and chemical breakdown to obtain cellular samples. There will then be a selective growth of progenitor cells from the cellular samples in a specific growth medium. The resulting cells will then be examined and characterised by appearance and behaviour to confirm they have potential to grow blood vessels. A comparison of these cells from fat and blood will be made with those sourced from umbilical cord blood, which is known to grow a large number of potentially useful cells.

The progenitor cells from these sources will be grown with other support cells from bone marrow, blood, skin or fat in a scaffold, and these will be examined to look for the best source of cells for blood vessel formation. If successful, the next stage will be to add specialised skin cells to the structure, to examine whether or not a functional skin barrier can be created in the lab.

Will any genetic tests be done?

No.

What will happen to the results of the research study?

The study will be reported in a thesis submitted for a DPhil in Clinical Laboratory Sciences at Oxford University by the clinical researcher. The results may be published in

scientific journals and presented at scientific meetings and conferences. You will not be identified in any future results or presentation of the research findings.

Who is organising and funding the research?

The research is funded by the charity Restore – Burn and Wound Research (Registered Charity Number 1003899, http://www.restore-research.org.uk).

Who has reviewed the study?

All research in the NHS is looked at by an independent group of people, called a Research Ethics Committee, to protect your interests. This study has been reviewed by Southampton and South West Hampshire Research Ethics Committee A and given a favourable opinion.

Further information and contact details

1. For general information about research: www.nres.npsa.nhs.uk

2. For specific information about this research project: Miss Jennifer Kean (01865 387916)

3. For advice as to whether you should participate: Family, friends, anyone in the plastic surgery team at Stoke Mandeville Hospital or Miss Jennifer Kean (01865 387916)

4. Who you should approach if you are unhappy with the study: The Stoke Mandeville Hospital PALS (**01494 425882** or www.pals.nhs.uk)

Appendix 2

CONSENT FORM

Stoke Mandeville Hospital
Mandeville Road
Aylesbury
Buckinghamshire
HP21 8AL
Tel: 01296 315 000
www.buckinghamshirehospitals.nhs.uk

Title of Project: Stem and Progenitor Cells in Wound Healing

Name of Researcher:
Miss Jennifer Kean

Please initial the boxes.

1. I confirm that I have read and understand Patient Information Sheet B (version 2, dated 17/12/09) for the above study. I have had the opportunity to consider the information, ask questions and have had these answered satisfactorily. ☐

2. I understand that my participation is voluntary and that I am free to withdraw at any time without giving any reason, without my medical care or legal rights being affected. ☐

3. I understand that relevant sections of my medical notes and data collected during the study, may be looked at by the clinical researcher, by individuals from regulatory authorities or from the NHS Trust, where it is relevant to my taking part in this research. I give permission for these individuals to have access to my records. ☐

4. I agree to take part in the above study. ☐

……	……	……..
Name of Patient	Date	Signature
……	……	……..
Name of Person taking consent	Date	Signature

Consent Form B- Stem and Progenitor Cells in Wound Healing v1: 17/09/09

Appendix 3

DSRed Immunofluorescent transductions

In order to prepare cells for better visualisation in three-dimensional cultures, Green Fluorescent Protein (GFP) and DS Red lentiviral particles were created for transduction of MSCs and UCB ECFC derived cells. The sourcing of these cells is described in Chapters 3 and 4 and the method of particle preparation and transduction is described in Chapter 2 section 2.11. The results of GFP transductions are shown in Chapter 6 section 6.3.1.

DS Red lentiviral transductions required a much higher MOI and also addition of Polybrene®, a cationic polymer which decreases electrostatic repulsion of the viral particles from the cell surface (200), in order to achieve adequate fluorescence. DS Red transductions achieved in HEK293T cells initially at 6.2x104 TU/ml, again calculated following titration of viral particles at 10^{-3}, 10^{-4}, 10^{-5} and 10^{-6} particles/ml applied in triplicate to wells containing $4x10^4$ and $8x10^4$ cells/well, are shown in Figure A3.1 (Image A). Image B shows a representative image of AT MSCs at day 1 post transduction with DS Red lentiviral particles at MOI 5 with 1µl Polybrene® (1µl/ml). This was the lowest MOI which achieved approximately 70% transduction of cells (Table A3.1). Representative images of the DS Red transduced MSCs at passage 5 are shown in Figure A3.1 (Images C and D).

Table A3.1: DS Red lentiviral transductions to determine optimal multiplicity of infection.

Multiplicity of Infection (MOI)	Percent transduction		Percent viability	
	No Polybrene®	1µl Polybrene®	No Polybrene®	1µl Polybrene®
5	0%	70%	95%	75%
10	0%	80%	95%	80%

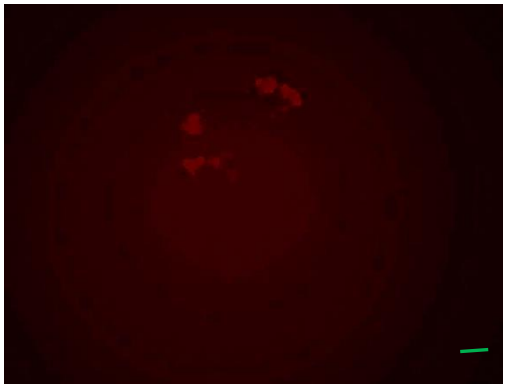

A DS Red transduced HEK293T

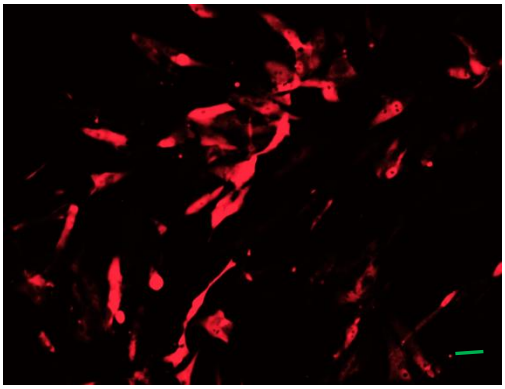

B DS Red transduced AT MSC at day 1

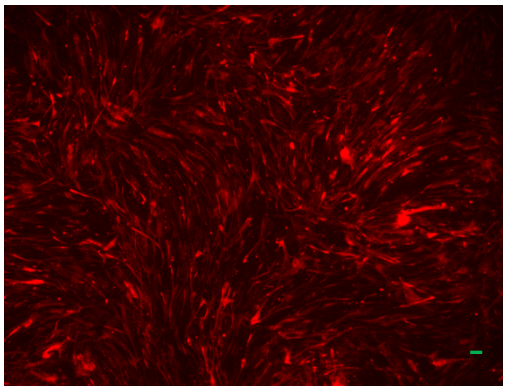

C DS Red transduced AT MSC at p5

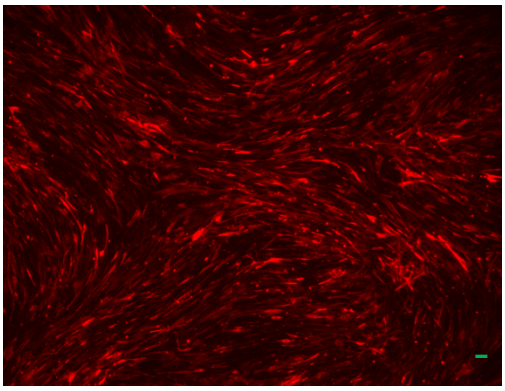

D DS Red transduced MV MSC at p5

Figure A3.1: DS Red lentiviral transductions. A- Transduction of HEK293T cells at 6.2 x10⁴ transducing units per ml. Titration of DS Red determined the MOI for subsequent transductions. B- Appearance of AT MSCs transduced with DS Red lentiviral particles at an MOI of 5 with 1µl Polybrene® at day 1 post transduction. C- AT MSC and D- MV MSC at passage 5. These cells were brought out of liquid nitrogen storage into culture having been frozen in aliquots at 14 days post transduction. (Fluorescent microscopy, 100µm scale bars)

Fluorescent labelled UCB ECFC derived cells and MSCs were initially used in the three-dimensional sandwich assay to assess tubule formation. Figure 6.2 (Image A) is representative of the results of a two-dimensional sandwich assay with co-culture of 10^4 DS Red labelled MV MSC and 10^3 GFP labelled UCB ECFC derived cells. Apart from one well which showed evidence of scanty tubule formation among clusters of GFP labelled UCB ECFC derived cells (Image B), there was no evidence of any microvasculature formation in three sets of assays repeated in triplicate. Expansion of DS Red transduced MSCs was slow compared with GFP MSCs and this was thought to be due to the high MOI of the DS Red transduction and the need for Polybrene® addition. This is in keeping with findings of Lin *et al.* (200), who showed a

decrease in human MSC proliferation following lentiviral transductions in the presence of Polybrene®, and so due to project time constraints this poor proliferation was not investigated further. Subsequent assays used GFP labelled MSCs for monocultures or unlabelled MSCs when in co-culture with GFP labelled UCB ECFC derived cells or HUVECs. A representative image of the tubule formation achieved when 10^3 GFP labelled UCB ECFC derived cells are cultured with 10^4 unlabelled MV MSC in the two-dimensional sandwich assay is shown in Figure A3.3.

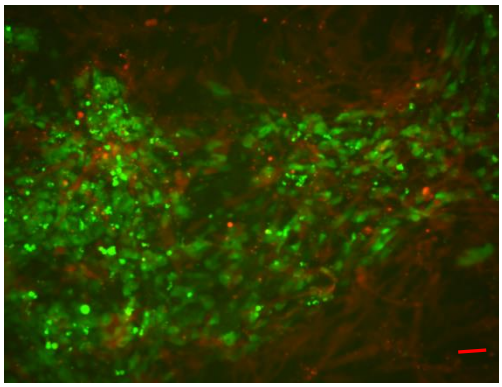

A Representative image of co-culture of 10^3 GFP labelled UCB ECFC derived cells and 10^4 DsRed labelled MV MSC

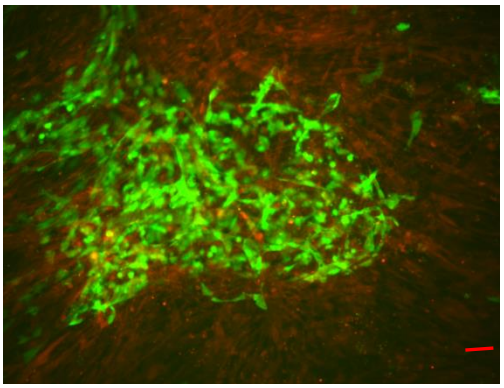

B Unique image of co-culture of 10^3 GFP labelled UCB ECFC derived cells and 10^4 DsRed labelled MV MSC

Figure A3.2: Co-culture of GFP labelled UCB ECFC derived cells and DsRed labelled MV MSC in the two-dimensional sandwich assay. A- Representative image of co-culture wells showing clusters of GFP labelled UCB ECFC derived cells on the DsRed labelled MV MSC layer. B- Unique image with some scanty tubule formation visible among the clumps of GFP labelled UCB ECFC derived cells. Images were taken at day 14 in culture. (Fluorescent microscopy, 100µm scale bars)

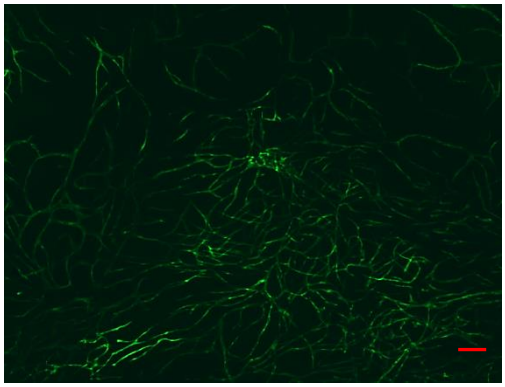

Figure A3.3: Representative image of co-culture of 10^3 GFP labelled UCB ECFC derived cells and 10^4 unlabelled MV MSC in the two-dimensional sandwich assay. Images were taken at day 14 in culture. (Fluorescent microscopy, 100µm scale bar)